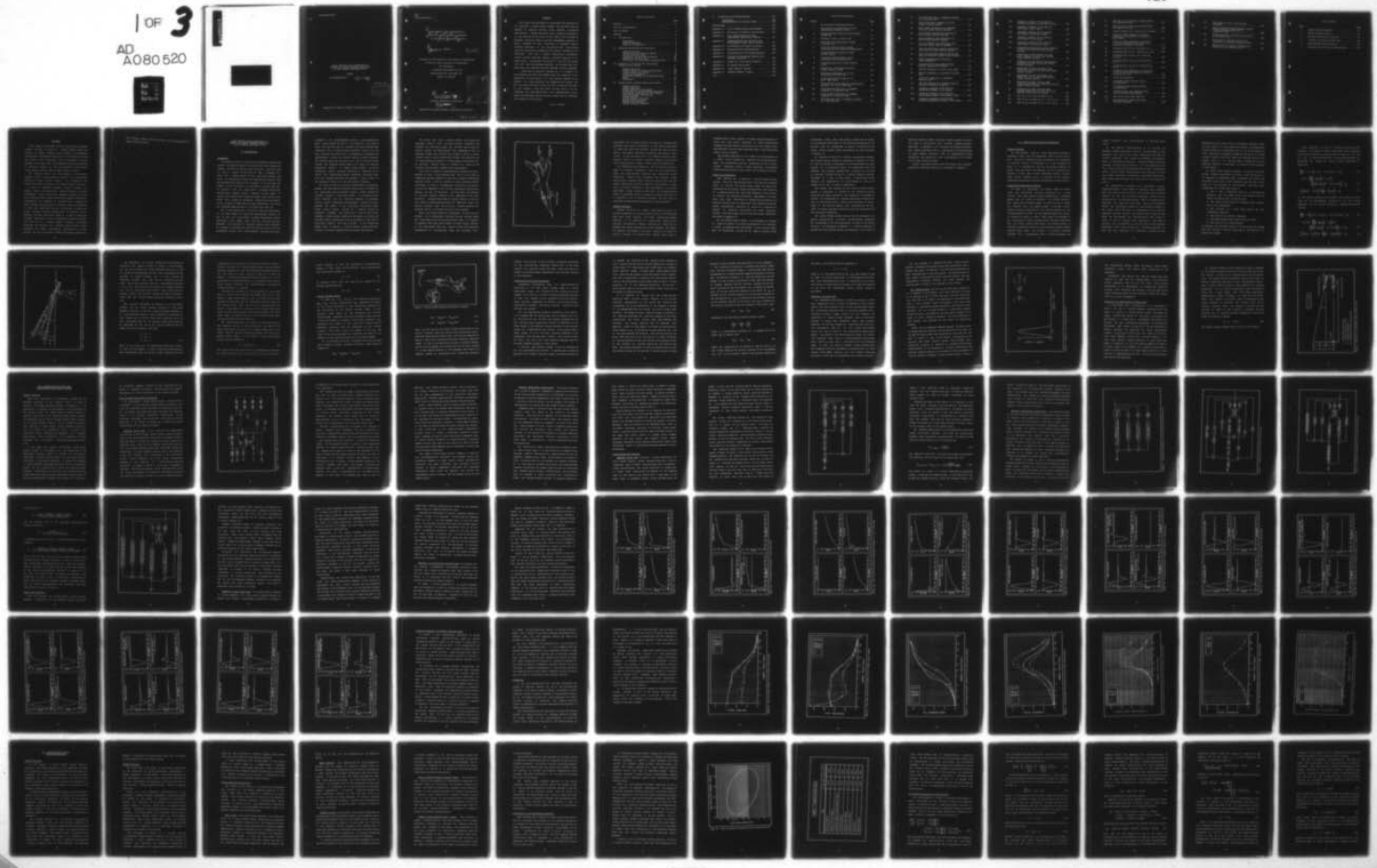
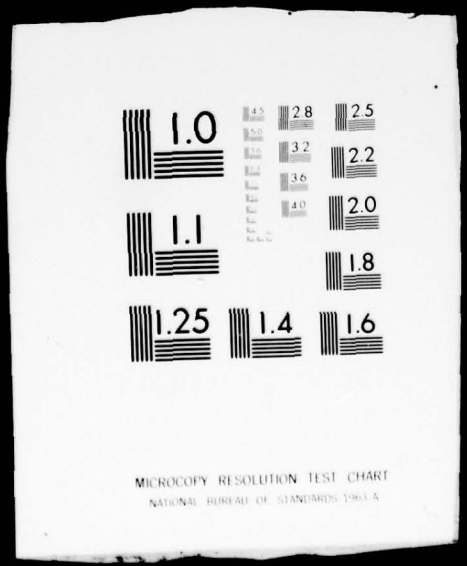
AD-A080 520 AIR FORCE INST OF TECH WRIGHT-PATTERSON AFB OH SCHOO--ETC F/G 1/3
USING VERTICAL GUST ALLEVIATION TO IMPROVE THE TARGET TRACKING --ETC(U)
AUG 79 E R MOLNER
UNCLASSIFIED AFIT/GGC/EE/79-5 NI

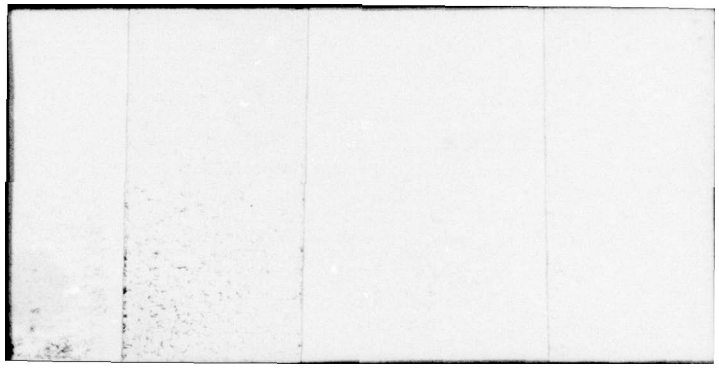
1 OF 3
AD A080520



1 OF 3

AD
A080520





AFIT/GGC/EE/79-5

USING VERTICAL GUST ALLEVIATION TO IMPROVE THE TARGET TRACKING CAPABILITY OF THE CONTROL CONFIGURED YF-16

THESIS

AFIT/GGC/EE/79-5 Eric R. Molner
1 Lt USAF

DDC
RECEIVED
FEB 11 1980
A

Approved for public release; distribution unlimited

(14) AFIT/GGC/EE/79-5

(6) USING VERTICAL GUST ALLEVIATION TO IMPROVE THE TARGET TRACKING CAPABILITY OF THE CONTROL CONFIGURED YF-16

(9) Master's THESIS

(12) 292

Presented to the Faculty of the School of Engineering

of the Air Force Institute of Technology

Air University

in Partial Fulfillment of the

Requirements for the Degree of

Master of Science

Accession For
NTIS GRA&I
DDC TAB
Unannounced
Justification
By
Distribution/
Availability Codes
Dist | Avail and/or special
A

(10) Eric R. Molner
1st Lieutenant USAF

Graduate Electrical Engineering

(11) August 1979

Approved for public release; distribution unlimited

012 225

Preface

This thesis was undertaken to investigate the possibility of designing a flight control system for the YF-16 that is capable of reducing aircraft pitch response to unwanted disturbances, thereby improving target tracking performance. It was realized at the start of this effort that a system so designed generally tends to provide underdamped responses to pilot commands as well, resulting in degraded overall handling qualities. It was anticipated that this problem could be eliminated by augmenting the control afforded by the horizontal tail with a second longitudinal aerodynamic control surface. This was, indeed, a workable approach. As is demonstrated, coordinated deflection of both the horizontal tail and the trailing-edge flaperons can provide both gust alleviation and improved aircraft response to pilot commands.

I would like to thank my advisor, Dr. C. H. Houpis, for his continued patience and guidance from the inception to the completion of this thesis. I am also greatly indebted to my sponsor, Mr. Finley Barfield, who suggested the project, and who was never too busy to take the time to help me find some of the answers. I must also thank my wife, Debra, for her unceasing and much appreciated love, understanding, assistance, and tolerance during the many months that my attention was focused on this project.

Eric R. Molner

Table of Contents

	Page
Preface	ii
List of Illustrations	v
List of Tables	x
Abstract	xi
I. Introduction	1
Background	1
Problem Statement	5
Order of Presentation	6
II. Modeling and Simulation Techniques	9
Chapter Overview	9
Longitudinal Equations of Motion	9
Control Surface Inputs	16
Simulation of Vertical Turbulence	18
Modeling a Vertical Gust	21
Definition of Longitudinal Tracking Error	24
III. Analysis of the YF-16 CCV Longitudinal Flight Control System	27
Chapter Overview	27
Control System Functional Description	28
Linearization for Analysis	33
System Time Responses	41
Frequency Response to Discrete Vertical Gusts	59
Discussion	60
IV. Flight Control System Design and Analysis	69
Chapter Overview	69
Design Objective	70
Design Approach Alternatives	71
Limitation of the Rigid-Body Assumption	74
State Space Equations for the Aircraft	78
Selected System Configuration	84
System Equation	87
System Transfer Functions	89
System Design Solutions	94
System Time Responses	99
System Frequency Response	106

V. Conclusions and Recommendations 136

Conclusions 136
Recommendations for Further Study 137

Bibliography 140

Appendix A: List of Abbreviations and Symbols 142

Appendix B: Derivation of Stability Derivatives . . . 151

Appendix C: State Space Modeling of the Longitudinal Equations of Motion 171

Appendix D: Scheduled Gains for the YF-16 CCV Longitudinal Flight Control System . . . 175

Appendix E: Determination of Sensor Locations 185

Appendix F: Rejected System Configurations 189

Appendix G: Determination of the System Equation . . 197

Appendix H: Solution of the System Equation for Transfer Functions 206

Appendix I: Design of a First-Order Observer 212

Appendix J: C* Control Derivation 219

Appendix K: YFCCV Computer Program 224

Appendix L: YFSOLVE Computer Program 245

Vita 263

List of Illustrations

Figure		Page
1	YF-16 Control Configured Vehicle	4
2	Equilibrium and disturbed aircraft longitudinal stability axes	13
3	Control surface deflection directional convention	17
4	Discrete (1-cos) vertical gust	23
5	Definition of longitudinal target tracking error	26
6	YF-16 CCV flight control system (baseline FCS with Maneuver Enhancement) . .	29
7	Linearized YF-16 baseline flight control system	35
8	Simulation configuration of the linearized YF-16 baseline FCS	38
9	Linearized YF-16 CCV flight control system	39
10	Simplified, linearized YF-16 CCV flight control system	40
11	Simulation configuration of the linearized YF-16 CCV FCS	42
12	YF-16 baseline FCS response to a pilot step input	47
13	YF-16 CCV FCS (with Maneuver Enhancement) response to a pilot step input	49
14	YF-16 baseline FCS with $'\alpha$ feedback response to a discrete gust	51
15	YF-16 baseline FCS with α_m feedback response to a discrete gust	53
16	YF-16 CCV FCS with $'\alpha$ feedback response to a discrete gust	55

17	YF-16 CCV FCS with α_m feedback response to a discrete gust	57
18	Peak pitch angle response of YF-16 flight control systems	62
19	Peak target tracking error response of YF-16 flight control systems	63
20	Peak normal acceleration response of YF-16 flight control systems	64
21	Peak horizontal tail deflection of YF-16 flight control systems	65
22	Peak horizontal tail deflection rate of YF-16 flight control systems	66
23	Peak trailing-edge flaperon deflection of YF-16 CCV flight control system	67
24	Peak trailing-edge flaperon deflection rate of YF-16 CCV flight control system . . .	68
25	Cornell Aeronautical Laboratory (CAL) Thumbprint	76
26	Selected pitch rate command flight control system configuration	85
27	PPE FCS response to a pilot step input . . .	110
28	PPE FCS response to a discrete vertical gust	113
29	YFF57 FCS response to a discrete vertical gust	116
30	PPE FCS response to a discrete gust at the pitch resonant frequency	118
31a	Frequency response of the PPE FCS (Pitch Rate Output, Pilot Input)	121
31b	Frequency response of the PPE FCS (Pitch Angle Output, Disturbance Input) . . .	122
32a	Frequency response of the PPE FCS (Normal Acceleration Output, Pilot Input) . .	123

32b	Frequency response of the PPE FCS (Normal Acc Output, Disturbance Input) . . .	124
33a	Frequency response of the PPE FCS (HT Output, Pilot Input)	125
33b	Frequency response of the PPE FCS (HT Output, Disturbance Input)	126
34a	Frequency response of the PPE FCS (TEF Output, Pilot Input)	127
34b	Frequency response of the PPE FCS (TEF Output, Disturbance Input)	128
35	Comparison of peak pitch angle response of YF-16 CCV and PPE flight control systems	129
36	Comparison of peak target tracking error response of YF-16 CCV and PPE flight control systems	130
37	Comparison of peak normal acceleration response of YF-16 CCV and PPE flight control systems	131
38	Comparison of peak horizontal tail deflection of YF-16 CCV and PPE flight control systems	132
39	Comparison of peak horizontal tail deflection rate of YF-16 CCV and PPE flight control systems	133
40	Comparison of peak trailing-edge flaperon deflection of YF-16 CCV and PPE flight control systems	134
41	Comparison of peak trailing-edge flaperon deflection rate of YF-16 CCV and PPE flight control systems	135
42	Plot of C_L vs α for 0.8 Mach at SL	155
43	Plot of C_{m_q} vs Mach for $\alpha_t = 0.8^\circ$ at SL . . .	156
44	Plot of $C_{m_{\dot{\alpha}}}$ vs Mach for $\alpha_t = 0.8^\circ$ at SL . . .	156

45	Plot of C_L as a function of Mach Number and angle-of-attack	164
46	Plot of C_D as a function of Mach Number and angle-of-attack	166
47	Impact pressure as a function of airspeed	176
48	Ratio of impact pressure to static pressure at altitude as a function of Mach Number	177
49	Ratio of static pressure at altitude to static pressure at Sea Level as a function of pressure altitude	178
50	Scheduled gain F3 as a function of q_c	179
51	Scheduled gain F4 as a function of q_c/P_s	180
52	Scheduled gain δ_f/G_{err} as a function of q_c/P_s	181
53	Scheduled gain δ_e/δ_f as a function of q_c/P_s	182
54	Scheduled gain δ_f/G_{DL} as a function of q_c/P_s	183
55	Scheduled gain $1845/a_{fps}$ as a function of P_s/P_o and determination of 1/M as a function of q_c/P_s	184
56	YF-16 wing planform	186
57	G-command flight control system configuration	190
58	C* command flight control system configuration	191
59	Selected pitch rate command flight control system configuration	198
60	Servo and first-order observer	217
61	Servo/observer system with state variable feedback	218

62 Definition of the C* time history envelopes 223

63 Basic functional YFCCV Computer Program diagram showing propagation of subsystem states 228

64 Simplified pitch rate FCS for the YF-16 at 0.8 Mach at SL 230

65 Continuous vs discrete system time responses for selected iteration rates . . . 231

66 General form of the FCS configuration simulated by the GENSIM option 235

List of Tables

Table		Page
1	Symmetric Aircraft Modes	77
2	System Variable Values	96
3	Transfer Functions For PPE FCS	97
4	Transfer Functions For YFF57 FCS	98
5	Time Response Characteristics	102
6	Stability Derivatives and Coefficients	170

Abstract

This thesis investigates the use of multiple aerodynamic control surfaces as a part of a flight control system configured to reduce aircraft pitch response to atmospheric disturbances. Coordinated deflection of two surfaces provides the desired gust alleviation with no decrease in system damping. At the same time, the commanded aircraft performance is improved relative to the performance of the baseline flight control system using a single control surface.

The aircraft chosen for this analysis is the General Dynamics YF-16. This particular aircraft has a fly-by-wire electronic flight control system - an arrangement that permits the control surfaces to be electronically activated.

A means of applying discrete vertical gusting to a modeled system is presented to permit evaluation of system performance. Using a simulation computer program, the YF-16 with baseline flight control system and Maneuver Enhancement augmentation are examined to determine gust response and pilot response characteristics. With this analysis completed, a basis for comparison has been established. To begin the design process, a system configuration is selected, and its equation derived. This matrix equation is used to solve for transfer functions in terms of unspecified system variables. With the aid of a second computer program, two design solutions are derived in an iterative manner, each of which satisfies the design requirements. Simulations of these systems are run to determine actual performance relative to

the defined target tracking criteria and the current YF-16 flight control systems.

USING VERTICAL GUST ALLEVIATION TO IMPROVE THE TARGET TRACKING CAPABILITY OF THE CONTROL CONFIGURED YF-16

I. Introduction

Background

In January of 1975, a full-scale development contract was awarded to General Dynamics to produce the first lightweight fighter aircraft in the Air Force inventory - the YF-16 (Ref 3). With a length of just over 46 feet, a wingspan of 31 feet, and a combat weight of less than 16,600 pounds, the YF-16 is considerably lighter and substantially smaller than most present-day fighters. As an example, it is only half the weight of the F-4E which it is destined to replace (Ref 17). In addition, with its single Pratt & Whitney F100-PW-100 afterburning turbofan engine producing 25,000 pounds of thrust, the aircraft has a power-to-weight ratio greater than unity. This results in incredible acceleration and takeoff rolls as short as 1000 feet with full afterburner. The YF-16 has a maximum speed of Mach 2+ at 40,000 feet (Ref 21).

One of the reasons for the YF-16's superior performance is its light weight. Its supersonic performance, however, is due to what has been called "relaxed longitudinal static stability". This simply means that the aircraft has been designed to be unstable in sub-sonic flight. This situation is created by locating the center of gravity (CG) aft of the aerodynamic center (AC). Traditionally, aircraft have been

designed to be aerodynamically stable in the longitudinal mode. This provides not only a trim condition, but tends to bring the aircraft back to straight and level attitude when disturbed from a trimmed flight condition. Were it not for this feature, the pilot would continuously be adjusting and compensating to keep the aircraft flying; in many instances, the aircraft could not be flown at all. As an aircraft breaks through the transonic region (Mach 0.9 to Mach 1.1) and goes supersonic, however, it becomes "super stable", as the AC effectively shifts rearward. Stability is increased to the extent that maneuvering becomes difficult. Generally, only slow and gradual maneuvers are possible - due, in part, to the supersonic flow of air over the control surfaces.

In order to make an aircraft maneuverable at supersonic speeds, the longitudinal stability margin must be reduced. No net improvement can be obtained, however, without making the aircraft unstable in sub-sonic flight - a situation which, until recently, was not tolerable. Advances in automatic control system technology have provided a solution to this problem. The answer is the electronic fly-by-wire (FBW) flight control system. Instead of a complex network of mechanical linkages, this system uses wires to relay pilot commands. Using various transducers and gyros, all pilot and aircraft control information is made available in the form of electrical signals. With such a system, it is a relatively simple task to design a control system using electronic circuits to provide compensation and closed-loop control.

The YF-16 uses such a control system for primary and secondary control. With its basic airframe designed to be unstable for sub-sonic flight, the aircraft relies upon the control system for stabilization. The advantage is that in sub-sonic flight, the aircraft can be made to fly in a normal (stable) manner, and in super-sonic flight, the stability can be electronically relaxed to allow greater maneuverability. In addition, overall drag is reduced as a result of the unstable airframe which reduces fuel requirements.

The YF-16 is clearly a technologically advanced aircraft. Because of this, it was selected over the F-4 to be used in conducting further research in the area of Control Configured Vehicles (CCVs). A CCV is a vehicle in which advanced control technology as well as aerodynamics, structures, and propulsion are all employed in the initial configuration definition process (Ref 10). To the YF-16, this has meant the addition of vertical canards mounted to the underside of the inlet structure, isolated fuel tanks for manual control of the CG, and control system modifications and additions. Under a $6 million contract from the Air Force, General Dynamics has modified the No. 1 prototype YF-16 for this purpose.

There are several potential advantages to the YF-16 CCV concept. As it incorporates multiple control surfaces about the longitudinal and lateral-directional axes, it is capable of maneuvers that most other fighter aircraft cannot achieve. In the longitudinal mode, the control system uses flaperons (combination of trailing-edge flaps and ailerons) and a

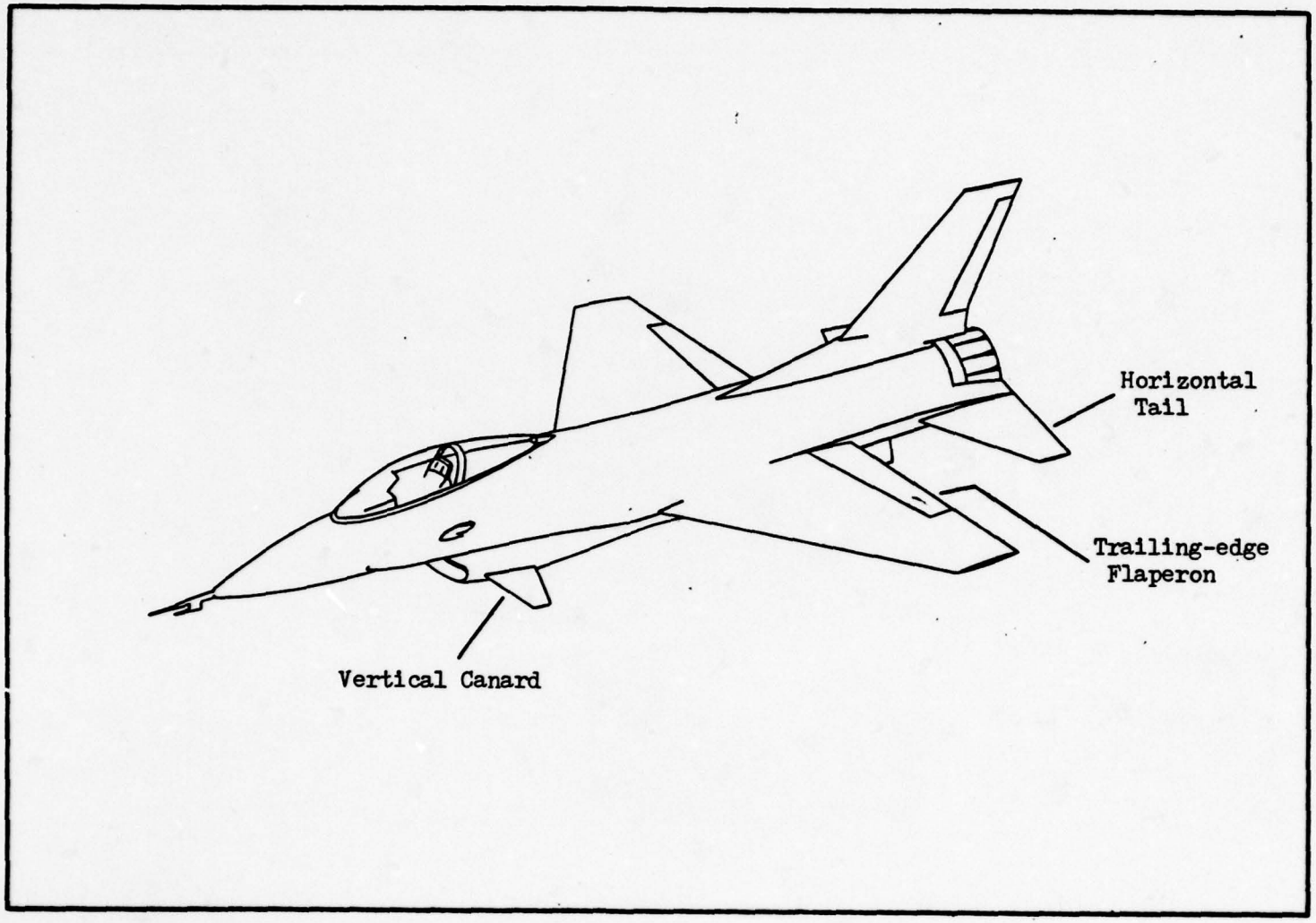


Figure 1. YF-16 Control Configured Vehicle.

horizontal tail to enable direct lift control, fuselage pitch pointing, and vertical translation. In the lateral-directional mode, the rudder and vertical canards are used to enable direct side force, fuselage yaw pointing, and lateral translation. It has been shown that in a combat situation, these features serve to improve tracking ability and increase firing opportunities. Figure 1 shows the CCV configuration.

An additional mode offered by the CCV control system is known as Maneuver Enhancement (ME). In this longitudinal mode, the trailing-edge flaperons are controlled by the difference between pilot G-command and aircraft normal acceleration response. This results in faster pitch rate and normal acceleration transient response, and provides a reduction in aircraft response to gust disturbances. It has been determined through flight testing that the ME augmentation makes it noticeably easier to perform precision tasks such as a constant-G turn at constant altitude. The end result is increased maneuverability and improved tracking ability.

Problem Statement

Because the YF-16 is a small, light weight aircraft, it is more susceptible to the perturbing effects of wind gusting than most other fighters. For target tracking and weapon delivery, it is essential to minimize the effect of any external disturbances. General Dynamics has shown that by feeding back normal acceleration to the flaperons, the amount of unwanted G-response at the pilot station as a result of vertical gusting is substantially reduced. This type of

feedback does little, however, to reduce the perturbations in pitch that also occur. Reduction of normal acceleration response provides mostly ride control. For the tracking task, perturbations in pitch angle generally have a more disturbing effect on the aircraft.

The problem addressed in this study is the development of a flight control system that improves the tracking performance and disturbance rejection properties of the aircraft, without degrading overall flying qualities. Disturbance induced perturbations in pitch angle are of primary interest.

Order of Presentation

When setting out to design an aircraft flight control system, there are many prerequisites that must be satisfied prior to starting the actual design phase. To begin with, regardless of the control system configuration, the objective is to somehow modify the open-loop dynamics of the aircraft to provide the required performance improvement. To accomplish this task, some means of mathmatically modeling the physical aircraft must be determined. The required non-dimensional longitudinal equations of motion are presented in Chapter II. Stability derivatives for these equations, derived from wind tunnel data for various flight conditions, are given in Appendix B.

As the flight control system to be designed is intended to reduce the effect of a given disturbance on the aircraft, a means of applying that disturbance to the aircraft model must be determined, as well as the shape or nature of the

disturbance itself. Also, some means of measuring the effect of the unwanted disturbance on the desired performance of the aircraft must be established to permit evaluation of the flight control system. These requirements are also satisfied in Chapter II.

An analysis of the YF-16 baseline and Maneuver Enhancement flight control systems is presented in Chapter III. This is done to provide an assessment of the performance of these systems and to establish a basis for comparison. Both time response and frequency response data is given, all of which is obtained through the use of a digital computer program, developed as a part of this thesis. A description of the features and capabilities of this program, as well as an example of its use, is given in Appendix K.

The design and analysis of the desired flight control system is presented in Chapter IV. The chapter begins by restating the design objective. This objective is expanded to include the elimination of several undesirable characteristics of the current YF-16 flight control systems, as determined in the previous chapter. Also addressed are the subjects of design approach alternatives and the limitations of the rigid-body assumption.

The actual design process begins with the selection of a system configuration. Alternate configurations, considered but determined to be less appropriate in light of the design criteria, are presented in Appendix F. A matrix equation is derived for the selected system configuration, and is used to

determine system transfer functions. These transfer functions are used in conjunction with a second computer program, described in Appendix L, to determine two design solutions. The chapter concludes with an evaluation of the performance of those design solutions. This is accomplished through simulation and comparison to the performance of the current YF-16 flight control systems.

Lastly, conclusions drawn from this effort and recommendations for continued research are presented in Chapter V.

II. Modeling and Simulation Techniques

Chapter Overview

In this chapter, a set of linear equations of motion is presented along with the assumptions used in their derivation. The use of angle-of-attack perturbation for simulation of vertical gusting is discussed, as is the technique for using it in conjunction with the particular equations of motion that are chosen. The modeling of air turbulence as a discrete "1-cos" gust is then addressed. Finally, longitudinal target tracking error is defined as the means of evaluating disturbance rejection performance in this thesis.

Longitudinal Equations of Motion

In order to investigate how various types of control affect the disturbance rejection properties of a given aircraft and flight control system configuration, a modeling scheme must be chosen to replicate the aircraft dynamics. This model must be simple enough to allow its use in design and analysis work, but complex enough to provide a sufficiently realistic simulation of the aircraft dynamics for the intended purpose. By far, the most popular models for analytic design are linear. A linear model allows the designer to use the myriad of linear systems design techniques developed over the years, greatly simplifying the design process. In addition to assuming linearity, many modeling schemes neglect flexible body modes, and perform a so-called rigid-body analysis. For a longitudinal study of high performance jet

fighter aircraft, this simplification is generally quite valid.

As the dynamic characteristics of an aircraft are actually highly non-linear, a linear aircraft model is only acccurate and valid over a small operating range about an initial condition. This method of modeling and analysis, known as perturbation analysis, usually provides sufficient accuracy for most design purposes if the perturbations from the initial (trimmed) flight condition are kept "reasonably" small. In most cases, depending upon the particular aircraft and flight condition in question, reasonably small means that angular perturbations are restricted to a few degrees or less.

For longitudinal analysis, as in this report, a three-degree-of-freedom linear model is generally used. Depending upon the intent of the analysis, the aircraft can be modeled relative to any one of several reference frames, such as stability-axis or wind-axis systems (Ref 7). Stability-axis equations are chosen for this study. This set of equations models the longitudinal motion of the aircraft relative to the earth, where the earth is considered to be an inertial reference. The two standard, and equally valid, forms of this model are dimensional and non-dimensional. The choice of which to use is usually made according to what type of aircraft data is available, as one form may be more directly applicable. Both forms produce the same model dynamics, as only the gain constants are affected to account for the

dimensions of the states. Thus, the modeling technique chosen for this report is a three-degree-of-freedom, non-dimensional stability-axis set of equations (Ref 1). As the derivation of these equations is somewhat lengthy and involved, no attempt is made to derive them here. There are excellent books on the subject (Refs 1, 7), and the reader unfamiliar with this modeling practice is enccuraged to consult the bibliography of this thesis.

As these linear equations attempt to model a non-linear system, several assumptions are made in their derivation. It is important to understand these assumptions to ensure that the model is valid for a given analysis, and that the limitations on the accuracy of that analysis are known. These assumptions are listed below (Ref 1):

1. The X and Z (stability) axes lie in the plane of symmetry, and the origin of the axis system is at the center of gravity (CG) of the aircraft.
2. The mass of the aircraft is constant (fuel consumption is not considered).
3. The aircraft is a rigid body (hence the term "rigid-body analysis").
4. The earth is an inertial reference.
5. The perturbations from equilibrium are small.
6. The flow of air is quasi-steady.

In addition, the equations require that the X-axis be aligned with the aircraft velocity vector while the vehicle is in equilibrium flight.

These equations, in terms of stability derivatives and constants (the values of which depend upon flight condition and aircraft structure) are given below in Eqns (1), (2), and (3) (Ref 1). The non-dimensional stability derivatives are determined and listed for various flight conditions in Appendix B.

$$\left[\frac{mU}{Sq}\,'\dot{u} - C_{x_u}\,'u\right] - C_{x_\alpha}\,'\alpha - C_w(\cos\theta_o)\,\theta = C_{F_{x_a}} \tag{1}$$

$$-C_{z_u}\,'u + \left[\left[\frac{mU}{Sq} - \frac{c}{2U}C_{z_{\dot{\alpha}}}\right]'\dot{\alpha} - C_{z_\alpha}\,'\alpha\right] + \left[\left[-\frac{mU}{Sq} - \frac{c}{2U}C_{z_q}\right]\dot{\theta} - C_w(\sin\theta_o)\,\theta\right] = C_{F_{z_a}} \tag{2}$$

$$\left[-\frac{c}{2U}C_{m_{\dot{\alpha}}}\,'\dot{\alpha} - C_{m_\alpha}\,'\alpha\right] + \left[\frac{I_y}{Sqc}\ddot{\theta} - \frac{c}{2U}C_{m_q}\dot{\theta}\right] = C_{m_a} \tag{3}$$

If the initial conditions are assumed to be zero, as is the case for the perturbation variables 'u, 'α, and θ, these equations can be written directly in Laplace notation as follows:

$$\left[\frac{mU}{Sq}s - C_{x_u}\right]'u(s) - C_{x_\alpha}\,'\alpha(s) - C_w(\cos\theta_o)\,\theta(s) = C_{F_{x_a}} \tag{4}$$

$$-C_{z_u}\,'u(s) + \left[\left[\frac{mU}{Sq} - \frac{c}{2U}C_{z_{\dot{\alpha}}}\right]s - C_{z_\alpha}\right]\alpha(s) + \left[\left[-\frac{mU}{Sq} - \frac{c}{2U}C_{z_q}\right]s - C_w(\sin\theta_o)\right]\theta(s) = C_{F_{z_a}} \tag{5}$$

$$\left[-\frac{c}{2U}C_{m_{\dot{\alpha}}}s - C_{m_\alpha}\right]'\alpha(s) + \left[\frac{I_y}{Sqc}s^2 - \frac{c}{2U}C_{m_q}s\right]\theta(s) = C_{m_a} \tag{6}$$

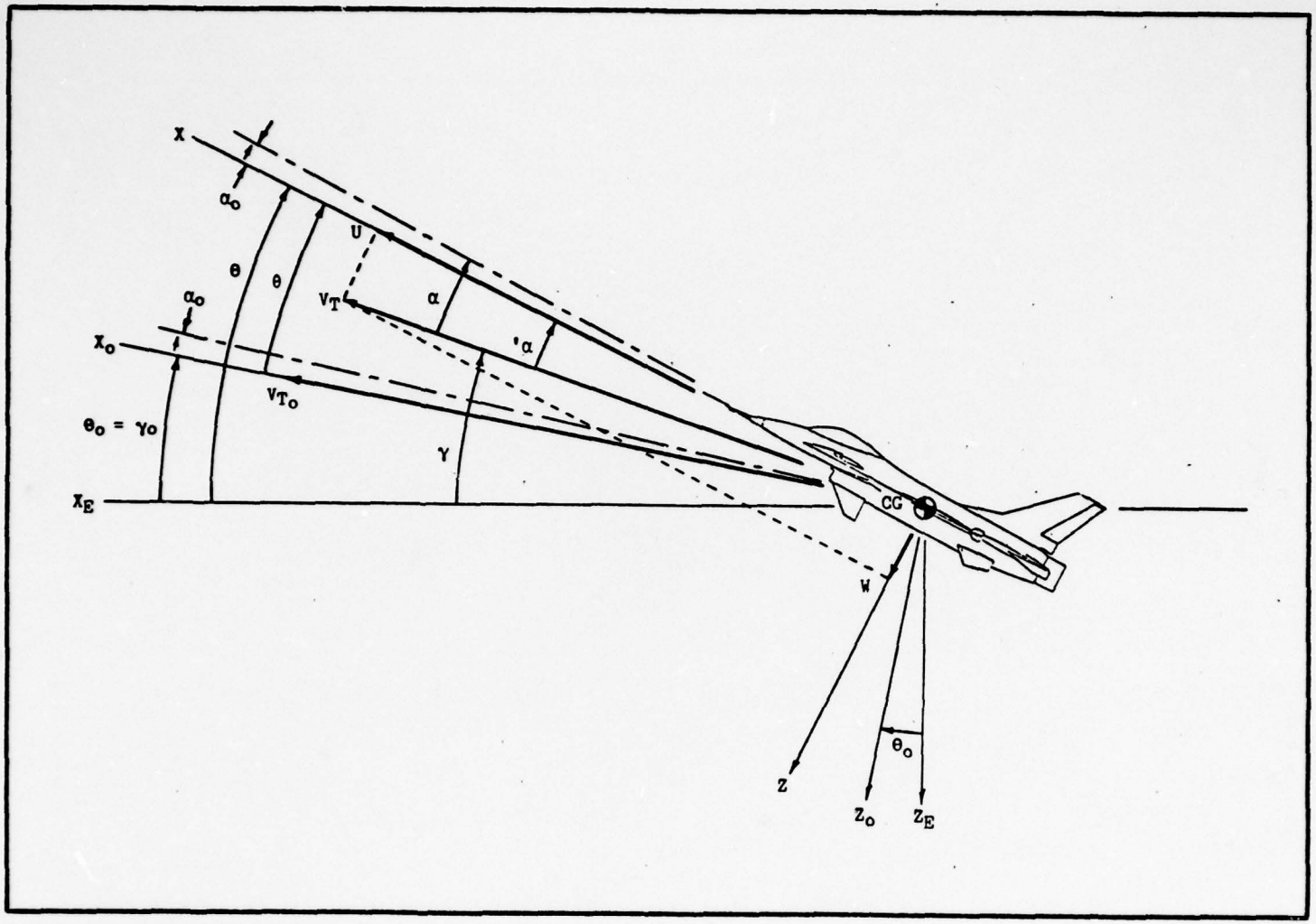


Figure 2. Equilibrium and disturbed aircraft longitudinal stability axes (Ref 1).

The definition of the axis system and the perturbation velocities and angles is shown in Figure 2. In the figure, X_E, Y_E, and Z_E define the earth reference axes, X_o, Y_o, and Z_o define the equilibrium aircraft axes (orientation of the aircraft in trimmed flight), and X, Y, and Z define the disturbed aircraft axes. The Y axis is defined out of the right wing of the aircraft, and for a longitudinal analysis, $Y = Y_o = Y_E$. The X axis of the aircraft is initially aligned with the X_o axis (into the relative wind), after which it remains fixed to the aircraft during the study of perturbations from the initial flight condition defined by the X_o axis.

The aircraft velocities of interest in a longitudinal analysis are the linear forward velocity, U, the linear downward velocity, W, and the angular pitching velocity, Q. In a perturbation analysis, these velocities are observed as they change from an initial steady state condition. As it is only the changes that are of interest, these velocities can be expressed as the sum of the initial condition and the change from that condition, such that

$$\begin{aligned} U &= U_o + u \\ W &= W_o + w \\ Q &= Q_o + q \end{aligned} \tag{7}$$

where U_o, W_o, and Q_o are the equilibrium velocities, and u, w, and q are the changes in these velocities resulting from some disturbance. Once the initial flight condition has been

established, U_o, W_o, and Q_o are taken as constants. Because a trimmed aircraft is in unaccelerated flight, the equilibrium pitching velocity, Q_o, and the equilibrium downward velocity, W_o, are equal to zero; thus $Q = q$, and $W = w$. There is, however, a non-zero equilibrium forward velocity, U_o. If the perturbation forward velocity, u, is divided by this equilibrium forward velocity, the non-dimensional perturbation forward velocity, $'u$, results.

The angles of interest are the pitch angle, θ, the attack angle, α, and in some instances the flight path angle, γ. The initial flight path angle, γ_o, may be defined as the angle between the horizontal and the equilibrium velocity vector of the aircraft, V_{T_o}. Note that in using stability axes, the initial pitch angle, θ_o, is equal to the initial flight path angle. As with the velocities previously described, the total pitch angle is equal to the sum of the initial pitch angle and the perturbation pitch angle, θ.

The angle-of-attack, α, is defined as the angle between the velocity vector of the aircraft and the chord of the wing. This angle is the sum of the trimmed attack angle, (the attack angle in initial equilibrium flight), and the perturbation attack angle, $'\alpha$. From Figure 2, this perturbation attack angle is defined as

$$'\alpha = \tan^{-1}(w/U) \qquad (8)$$

The ratio of the two velocities is a dimensionless quantity, or radian measure. Since an underlying assumption of pertur-

bation analysis is that the variation in velocities and angles is kept small, this definition can be approximated with sufficient accuracy as

$$'\alpha = w/U \tag{9}$$

It follows, then, that the time rate of change of $'\alpha$ is defined approximately by

$$'\dot{\alpha} = \dot{w}/U \tag{10}$$

Control Surface Inputs

In Eqns (4), (5), and (6), the inputs are defined as $C_{F_{x_a}}$, $C_{F_{z_a}}$, and C_{m_a}, respectively. $C_{F_{x_a}}$ represents the effect of the sum of the forces in the X direction resulting from the deflections of all control surface inputs. In this analysis, these inputs are the horizontal tail and the trailing-edge flaperons. The force created by these surfaces in the X direction is a change in total drag. Similarly, $C_{F_{z_a}}$ represents the effect of the sum of the forces in the Z direction resulting from the deflection of the control surfaces. This total force is a change in lift. C_{m_a}, the input to the remaining equation, represents the effect of the movement of the control surfaces on the pitching moment.

For an aircraft with both horizontal tail and trailing-edge flaperon control surfaces, the above input terms are defined as

$$C_{F_{x_a}} = C_{x_{\delta_{ht}}} \delta_{ht} + C_{x_{\delta_{tef}}} \delta_{tef} \tag{11}$$

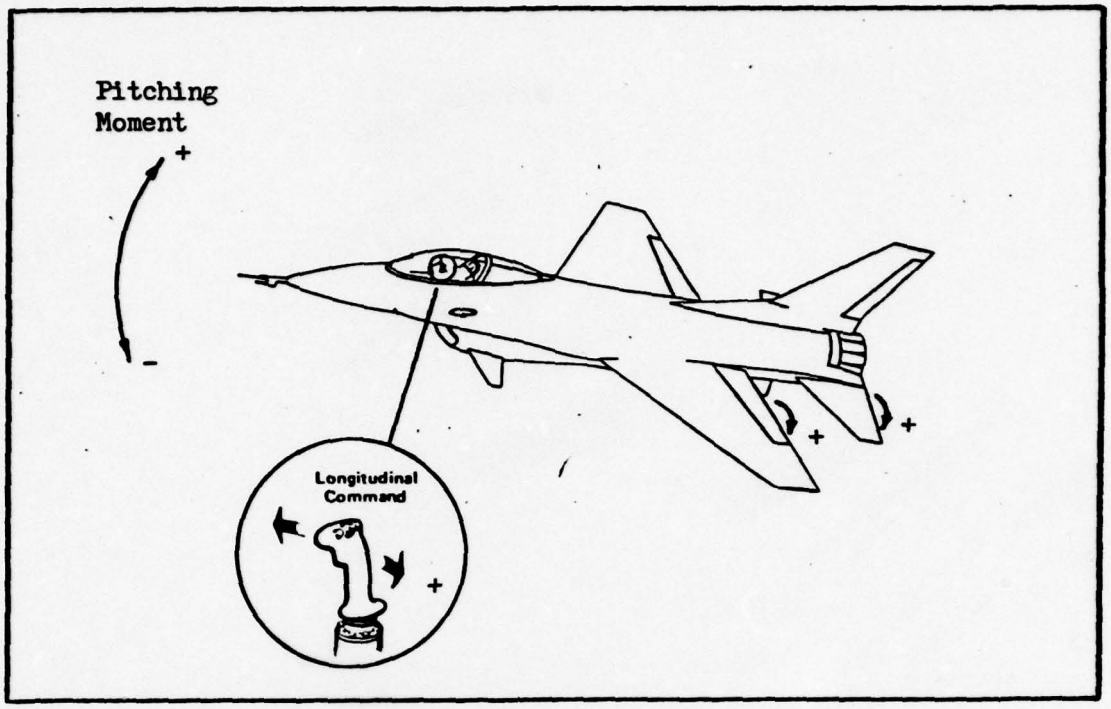


Figure 3. Control surface deflection directional convention.

$$C_{F_{z_a}} = C_{z_{\delta_{ht}}} \delta_{ht} + C_{z_{\delta_{tef}}} \delta_{tef} \quad (12)$$

$$C_{m_a} = C_{m_{\delta_{ht}}} \delta_{ht} + C_{m_{\delta_{tef}}} \delta_{tef} \quad (13)$$

where δ_{ht} and δ_{tef} are the actual angular deflections of the control surfaces. There are certain sign conventions associated with these angular deflections, and they are depicted in Figure 3. Note that a positive deflection produces a positive change in lift on the deflecting surface. A positive deflection of the horizontal tail creates lift on the tail, causing it to move upward relative to the fuselage. The result is a negative change in pitch angle, and a nose down attitude,

causing the aircraft to lose altitude. A positive deflection of the trailing-edge flaperons creates lift on the wing, causing the aircraft to gain altitude. There may also be a change in pitching moment, depending on the size and location of the flaperons.

Simulation of Vertical Turbulence

Atmospheric disturbances occur in a random fashion as quantities of air move about through space. In a three dimensional world, the velocity of this moving air can be thought of as the sum of three velocity components relative to some axis system. In the analysis of aircraft control, these velocity components are defined as vertical gusting, longitudinal gusting, and lateral gusting, relative to the aircraft axis system.

For the longitudinal analysis performed in this report, it is assumed that the lateral gust can be ignored, as it is, by the nature of the aircraft axis system, perpendicular to the vertical plane (wings-level flight). In addition, as the small change in the relative forward velocity of the aircraft caused by a longitudinal gust results in an assumed negligible change in lift, this gust velocity component is not considered. The vertical gust, however, has a direct effect on total lift, and is the gust velocity component used for the gust response analyses in this thesis.

A vertical gust causes a change in the net velocity of the air surrounding the aircraft. An upward gust, producing positive lift, causes a positive change in angle-of-attack as

it changes the direction of the relative wind. Because of this, vertical gusting can be directly modeled as a change in attack angle. If a step upward gust could occur, an instantaneous positive change in attack angle would result before there could be any change in aircraft motion. Note, however, that this is apparently in conflict with the previous definition of the perturbation attack angle given in Eqn 9. In this equation, "w" is the downward velocity of the aircraft - which implies that if the aircraft doesn't move, there can be no change in angle-of-attack.

It is important to realize that the stability-axis equations model aircraft motion relative to an inertial reference (approximated as the earth). The motion of the surrounding air is not considered. If the analysis or design to be accomplished does not include the use of attack angle feedback, the manner by which angle-of-attack is modeled is not important providing the resulting response is correctly interpretted. The YF-16, however, uses such feedback, and therefore the correct quantity must be employed. This quantity, which, in this report, is called true perturbation attack angle, or α_m, is defined as the perturbation from trim in the angle between the relative wind and the chord of the wing. Note that this is not the same as $'\alpha$, which is defined as the perturbation in the angle between the velocity vector of the aircraft (in inertial space) and the chord of the wing. The subtle difference in these two definitions is that the velocity vector of the aircraft in inertial space is only

parallel to the relative wind when there is no air movement.

The velocity of moving air is perhaps most easily viewed from the earth reference frame. A vertical gust can then be represented as a single velocity component parallel to the Z_E axis as defined in Figure 2. If both the moving air and the motion of the aircraft are defined in this same axis system, it becomes apparent that the vertical velocity of the aircraft relative to the surrounding air is simply the difference of the two velocities relative to the earth. If $w_{a/A}$ is defined as the vertical velocity of the aircraft relative to the surrounding air, $w_{a/E}$ is defined as the vertical velocity of the aircraft relative to the earth, and $w_{A/E}$ is defined as the vertical velocity of the air relative to the earth, then

$$w_{a/A} = w_{a/E} - w_{A/E} \tag{14}$$

Dividing by the equilibrium forward velocity yields

$$\frac{w_{a/A}}{U_o} = \frac{w_{a/E}}{U_o} - \frac{w_{A/E}}{U_o} \tag{15}$$

Since in a perturbation analysis, U_o is assumed to be constant, Eqn 15 implies that

$$\alpha_{a/A} = \alpha_{a/E} - \alpha_{A/E} \tag{16}$$

where the subscripts are as defined in Eqn 14. Since α_m is the attack angle of the aircraft relative to the surrounding air, and $'\alpha$ is the attack angle of the aircraft relative to

the earth, this equation may be expressed as

$$\alpha_m = {}'\alpha + \alpha_g \tag{17}$$

where α_g is a shorthand notation for $-\alpha_{A/E}$. The change of sign is made to allow an upward gust to be defined as positive. The error associated with using ${}'\alpha$ instead of α_m as a feedback source is demonstrated in Chapter III, where an analysis of the YF-16 CCV longitudinal flight control system is performed.

Modeling a Vertical Gust

As atmospheric disturbance is random in nature, it would seem appropriate that it should be modeled as such. Several models have been proposed, most of them statistically based. The disturbance velocity field is generally assumed to be a zero-mean Gaussian random process for the analysis and simulation of linear systems. Although there is sufficient evidence to prove this assumption false, most analyses conducted on aircraft systems are concerned only with relative performance (Ref 13). For this reason, MIL-F-8785B allows the use of either of two statistically based random models - the Dryden or von Karmam spectral forms. For simulation purposes, many times a filtered Gaussian distributed noise source is used, and is considered to be an acceptable model. It does not, however, produce enough extreme gusts when compared to actual atmospheric turbulence data. For this reason, MIL-F-8785B requires that the random turbulence generated in this way be supplemented with discrete gusting.

For the purpose of comparing aircraft flight control systems, a discrete gust model may be more appropriate than a random gust model. In addition to permitting measurement of peak perturbations in aircraft motion, the discrete gust is very useful in determining control surface actuator rate and displacement saturation effects. For these reasons, the discrete gust is used in the analyses in this thesis.

The Discrete Gust. The form of discrete gust selected is as it appears in MIL-F-8785B. This form, depicted in Figure 4, is referred to as a "1-cos" type gust. Its name comes from the fact that it is formed by displacing an inverted cosine wave a unit distance above the distance axis. This model provides a continuous waveform beginning and ending at zero velocity. For an aircraft flying at a relatively constant forward velocity, the length of the gust may be thought of in terms of time instead of distance. For the simulations in this thesis, the duration of all gusts is measured in seconds.

There are two important shaping factors: the peak value, or maximum gusting velocity, and the duration of the gust. It is required that several gust durations be used such that the gust is tuned to each of the natural frequencies of the aircraft and flight control system. This provides for a worst-case analysis in addition to allowing control power effectiveness to be evaluated at critical frequencies. The maximum gusting velocity is an equally critical parameter in such an analysis. Although a linear system insures a one-to-

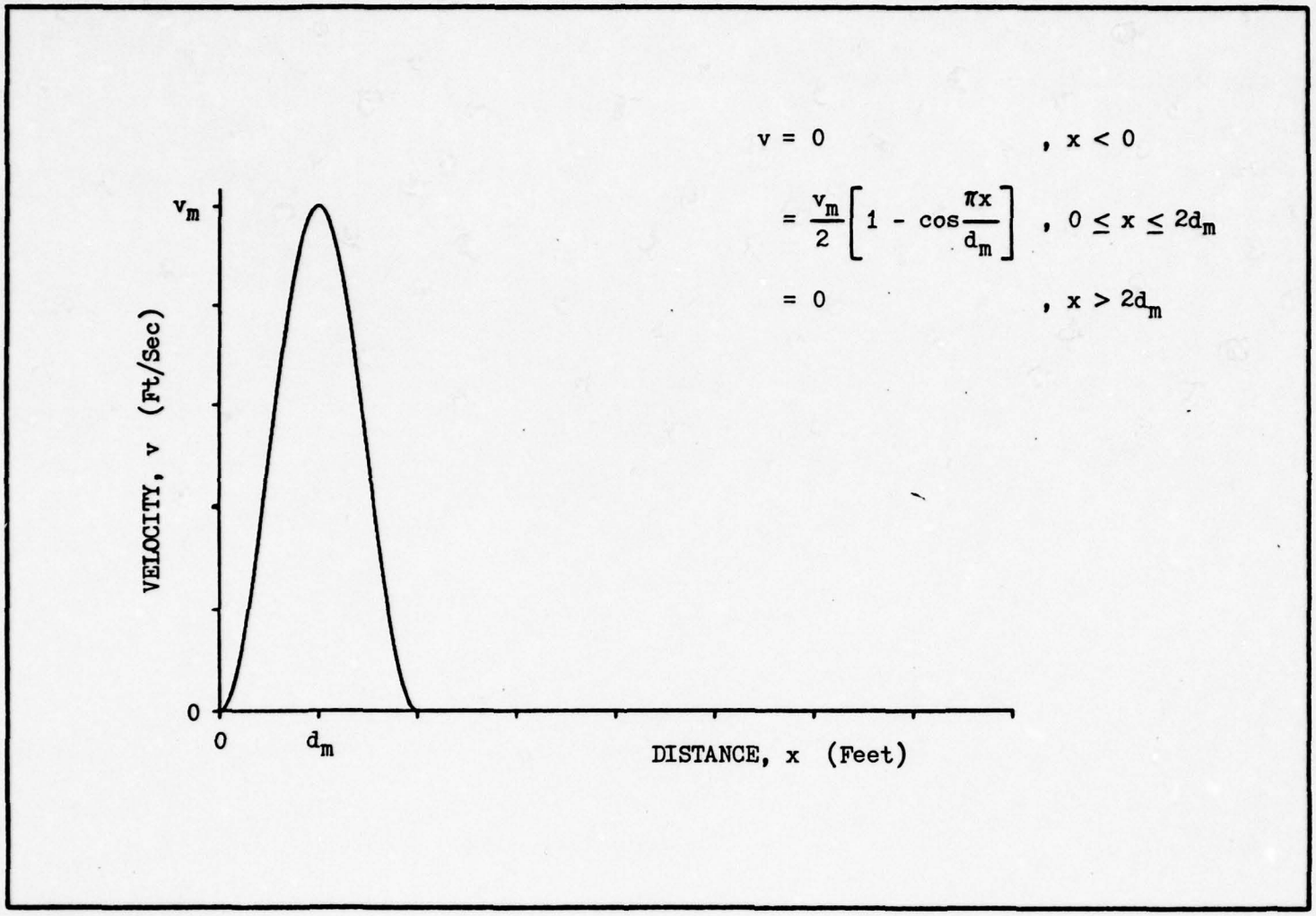


Figure 4. Discrete (1 - cos) vertical gust (Ref 13).

one relationship between input and output, larger inputs eventually cause rate and/or limit saturation of the actuators.

Throughout this report, a 50 feet per second (fps) peak velocity is used for the discrete gust. At the selected flight condition, Mach 0.8 at Sea Level, this velocity corresponds to an approximate 3.2 degree peak change in relative wind direction. The standard duration used is one second (one-half second to peak velocity), except for simulations at critical frequencies.

Definition of Longitudinal Tracking Error

In performing this investigation, it is necessary to examine the use of various feedback configurations in an effort to produce a flight control system that makes the target tracking task easier for the pilot. To determine the performance of a given FCS, a measurement tool needs to be devised. The gust alleviation performance of the Maneuver Enhancement (ME) system of the YF-16 CCV was evaluated by General Dynamics by measuring the normal acceleration response at the pilot station (Ref 10). There was no attention given, however, to the effect on pitch response. It is clear that aircraft angular rotation, or pitch angle response, is important if a gun (non-seeking weapon) is fired at a distant target. As an example, for a target at 6000 feet, a change in pitch attitude of a single degree results in a miss distance of approximately 105 feet if inertia and acceleration factors are neglected.

An accurate tracking error measurement would be composed of all factors defining the motion of both target and tracking vehicle, as well as the characteristics of the projectile. The target tracking measurement used in this report is greatly simplified compared to such a comprehensive definition. It does, however, provide a good indication of tracking performance for an aircraft undergoing minor acceleration firing at a fixed target. This first-order longitudinal approximation, shown in Figure 5, is made up of two components. The tangent of the pitch angle is multiplied by the target distance to calculate the tracking error due to aircraft rotation. Then, the change in aircraft vertical position is added to this quantity to provide for miss distance due to aircraft vertical translation. The sum of these two components yields

$$T_E = h + d\tan\theta \tag{18}$$

and defines target tracking error as used in this report.

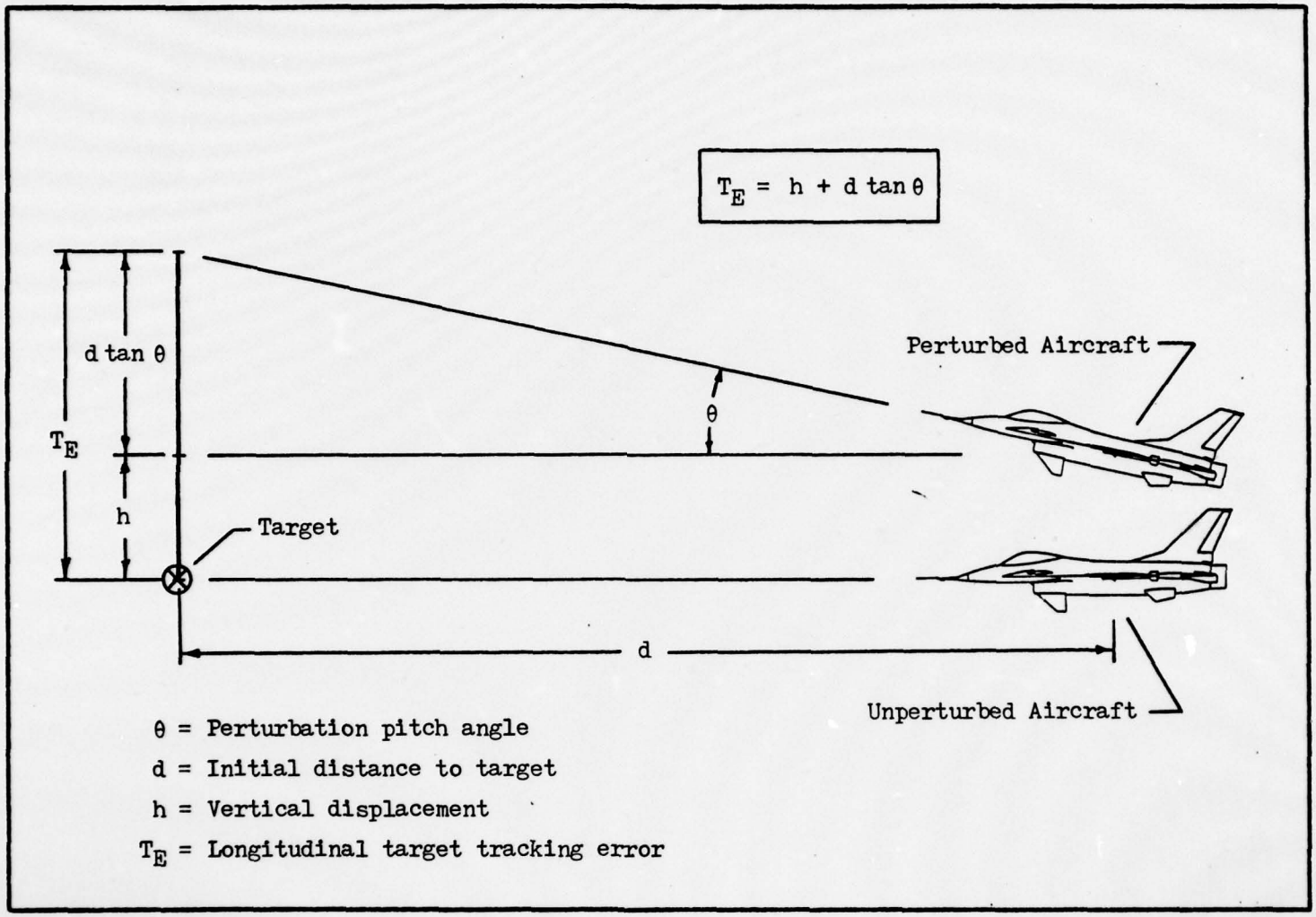


Figure 5. Definition of longitudinal target tracking error.

III. Analysis of the YF-16 CCV Longitudinal Flight Control System

Chapter Overview

There are essentially two significant reasons for the analysis performed in this chapter. First, in order to evaluate the design solution presented in Chapter IV, it is appropriate to compare its performance to the performance of the current YF-16 CCV flight control systems. Second, by running simulations on the existing flight control systems, the simulation results can be checked against those documented by General Dynamics (Refs 9, 10) to validate the simulation approach. A rather lengthy digital computer program is used to perform the simulations using a multiple state transition matrix technique (see Appendix K for a complete description), and a verification of its capability provides assurance that it performs a sufficiently accurate simulation.

In the pages that follow, the baseline YF-16 flight control system is described, as is the integration of the additional circuitry needed to provide the CCV Maneuver Enhancement function. These systems are then simplified and linearized to facilitate simulation. A system time response is then performed, employing both pilot and gust disturbance inputs. As the flight control system uses angle-of-attack feedback, simulations are run using both true perturbation attack angle and stability-axis perturbation attack angle, so that the results may be compared (see Chapter II). An empiri-

cal frequency response analysis is also performed for the system in response to discrete vertical gusts. The chapter concludes with a brief discussion of the results obtained.

Control System Functional Description

The longitudinal flight control system of the YF-16 is illustrated in the functional block diagram of Figure 6. The solid line connecting paths represent the baseline YF-16 FCS, and the dashed line connecting paths represent the implementation of the Maneuver Enhancement augmentation. In the following paragraphs, the function of each block is briefly described in an effort to provide the reader with a basic understanding of the design philosophy.

Baseline YF-16 FCS. In the design of the longitudinal axis portion of YF-16 flight control system, General Dynamics chose to use three measurable quantities as feedback signals: angle-of-attack to allow for variance of static stability by scheduled gain, pitch rate for damping, and normal acceleration to provide g-command capability. Electrical signals are transmitted from the redundant sensors, gyros, and accelerometers that measure these quantities to the analog Basic Flight Control Computer. The pilot inputs longitudinal commands to this computer via a force-sensing sidestick controller. As shown in Figure 6, this input is reshaped by nonlinear stick force gradients. These nonlinearities tailor the force-stick output by allowing for mechanical preloading and electrical breakout, as well as a pitch command gradient.

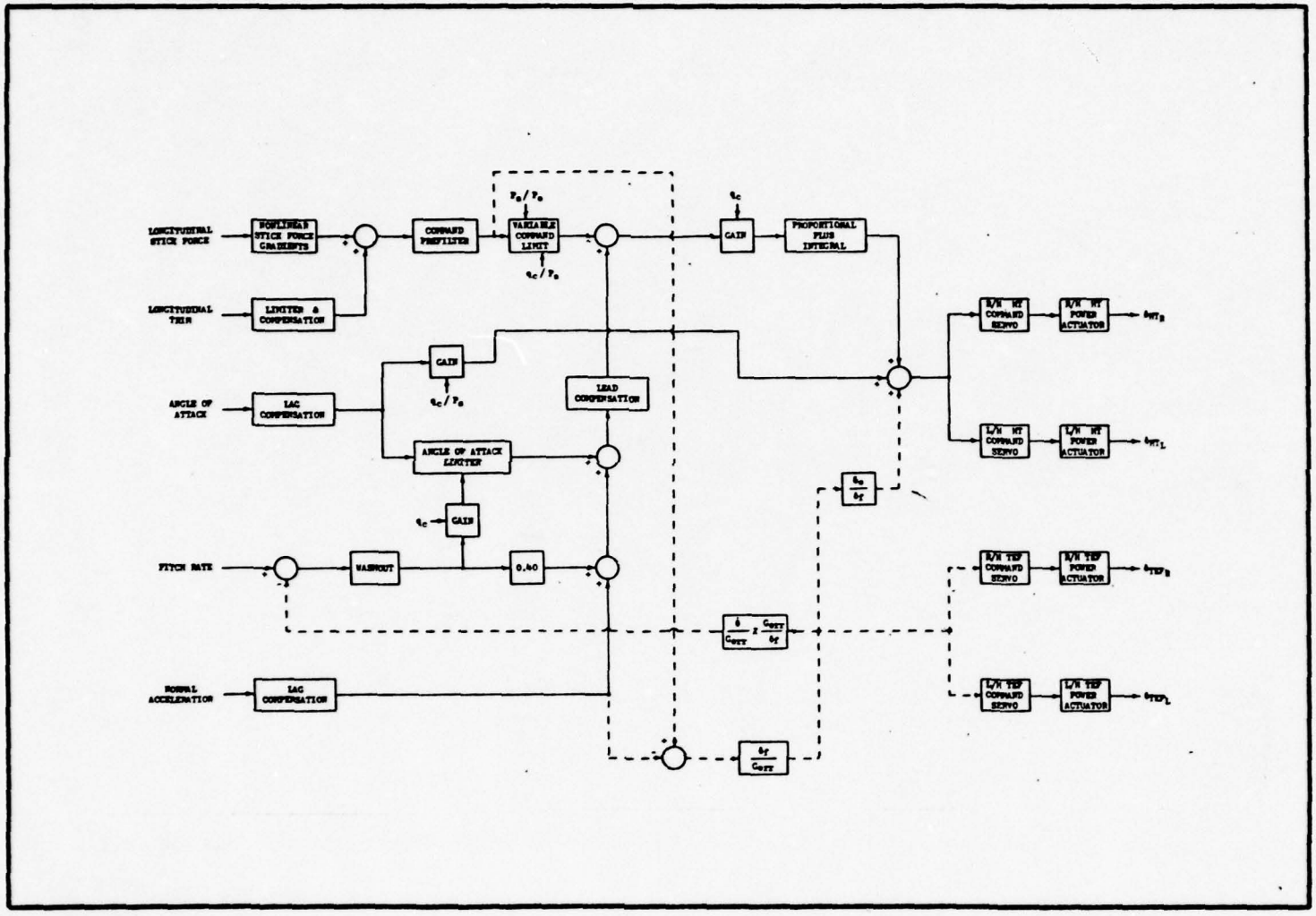


Figure 6. YF-16 CCV flight control system (baseline FCS with Maneuver Enhancement).

In addition to the force-stick, the pilot is also permitted a trim adjustment.

The command prefilter is simply a unity-gain first-order lag that is used to filter pilot command transients to a desired rate. The variable command limit, a nonlinear gain computed as a function of ratios of static and impact pressures, safeguards the aircraft from control inputs that would result in exceeding the permissible wing-root bending moment at critical flight conditions. Depending on the flight condition, this command limit varies from a minimum of approximately 5.5 Gs to a maximum of 8 Gs. The output of this limiter may be considered as the effective system input.

Variable forward-loop gain is provided as a function of impact pressure which schedules the gain according to airspeed. A proportional forward-loop path provides for quick response to commanded inputs, while an integrated path forces a zero steady-state error condition to exist for those same inputs. As the feedback summed in prior to that integration consists of normal acceleration and washed-out pitch rate, the steady-state response is equal to the commanded Gs. This type of flight control system provides the pilot with what is essentially a C* command aircraft (see Appendix J for a discussion of the C* concept). During command transients, the aircraft responds with pitch rate changes not unlike the response from a pitch rate commanded FCS. In steady-state, however, the pilot is commanding Gs, as the output of the washout in the pitch rate feedback loop goes to zero. In

addition, this design provides a series trim to maintain a 1-G trimmed condition in the absence of a pilot input. The lag and lead compensation in the pitch rate and normal acceleration feedback paths provide the phase relationships which result in desired system performance characteristics.

Attack angle feedback, used to control static stability, is summed in after the forward-loop integration. The gain in this feedback path is scheduled according to Mach number. It is this gain that allows the longitudinal static stability to be increased for sub-sonic flight, and decreased for super-sonic flight as discussed in Chapter I. Attack angle feedback is also used to provide angle-of-attack limiting for automatic spin prevention. As the angle-of-attack approaches a critical point in flight, a nonlinear multiple of attack angle feedback is used to reduce the pilot's commanded input to prevent further increases in angle-of-attack. A variable amount of pitch rate input to this limiter is used to provide the additional system damping that is desirable at these high angle-of-attack conditions.

The output of the flight control computer is routed to the electromechanical horizontal tail command servos. The mechanical outputs of these servos drives the hydraulic horizontal tail power actuators. The horizontal tail is designed to permit independent left-hand and right-hand deflections, which allow for smoother roll control. For longitudinal control, however, the two command servos are fed symmetrically.

Maneuver Enhancement Augmentation. The Maneuver Enhancement system is based on commanding a symmetrical deflection of the trailing-edge flaperons as a consequence of a non-zero differential between commanded Gs and normal acceleration. As a portion of the CCV flight control package, this system is implemented in an analog Auxiliary Flight Control Computer.

Commanded input is obtained from the Basic Flight Control Computer using the signal at the output of the command prefilter. This quantity is compared to the measured normal acceleration to provide an error signal. The algebraic signs of the comparator inputs are opposite to those in the basic FCS, which produces an error signal of opposite polarity to that driving the horizontal tail. Recall that positive rotation of the aircraft is obtained by an upward (negative) horizontal tail deflection. Positive translation, on the other hand, is acquired as a result of downward (positive) flap deflection.

The flap G-error signal, multiplied by a scheduled gain, is used in three ways. It is used directly to command trailing-edge flaperon deflections by symmetrically driving the flaperon command servos. These servos operate the hydraulic power actuators which in turn deflect the flaperon surfaces. It is also used to provide a horizontal tail/trailing-edge flaperon interconnect by symmetrically driving the horizontal tail command servos through a scheduled gain. This interconnect is intended to allow sufficient tail deflection to offset the pitching moment created by flaperon deflection.

This allows a direct lift effect with no change in attack angle during the early transient period following a commanded stick input. Finally, the error signal is used to provide a pitch rate bias. This bias signal, summed in with the pitch rate feedback to the basic FCS, is intended to negate this feedback and prevent an opposing horizontal tail deflection during the early transient period (Ref 9).

Before leaving this subject, it is important to note that since the horizontal tail/trailing-edge flaperon interconnect and pitch rate bias signals are generated in an open-loop manner, the intended function of these two signals is clearly dependent upon the accuracy of the scheduled gains. Also, as previously mentioned, operation at critical attack angles causes a non-zero output from the angle-of-attack limiter in the basic FCS, which results in reduced pilot command authority. As this occurs, the flaperon G-error signal increases, commanding large flaperon deflections. These large deflections result in increased drag which degrades aircraft performance.

Linearization for Analysis

Baseline YF-16 FCS. To permit a linear simulation, the YF-16 flight control system nonlinearities must first be simplified. Most of these nonlinearities have a piecewise-linear characteristic, that allows reduction to a simple gain if signal level restrictions are adhered to. The simplest case is the hard or soft limiter with a dead zone. If the input level is assumed to remain within the dead zone, the

output is zero, and the function may be removed completely. Scheduled gains, on the other hand, may be easily determined by chosing a flight condition. These gains are defined in Appendix D. Finally, as the trimmed angle-of-attack at the selected flight condition is relatively small (see Appendix B), it is assumed that the angle-of-attack limiter output is negligible. General Dynamics apparently makes a similar assumption in their linear analysis performed in Reference 10.

The flight condition selected for the analyses in this chapter, as well as in Chapter IV, is 0.8 Mach at Sea Level. This FC is chosen for two reasons. First, it is near the transonic region, and is a condition quite sensitive to terrain-induced and atmospheric turbulence. Second, it is the flight condition chosen for the disturbance analysis accomplished by General Dynamics (Ref 10). Use of this identical flight condition enables a comparison of results, and permits verification of the simulation technique.

The linearized model of the basic YF-16 flight control system is shown in Figure 7. The forward loop consists of the command prefilter, the scheduled gain F3 and P+I network, and the command servo and power actuator. There are, as shown in Figure 6, actually two command servos and two power actuators. However, as they are driven and operate symmetrically and both sides of the tail must move to constitute a horizontal tail deflection, modeling them as a single servo and actuator is valid. Note also in comparing this figure to

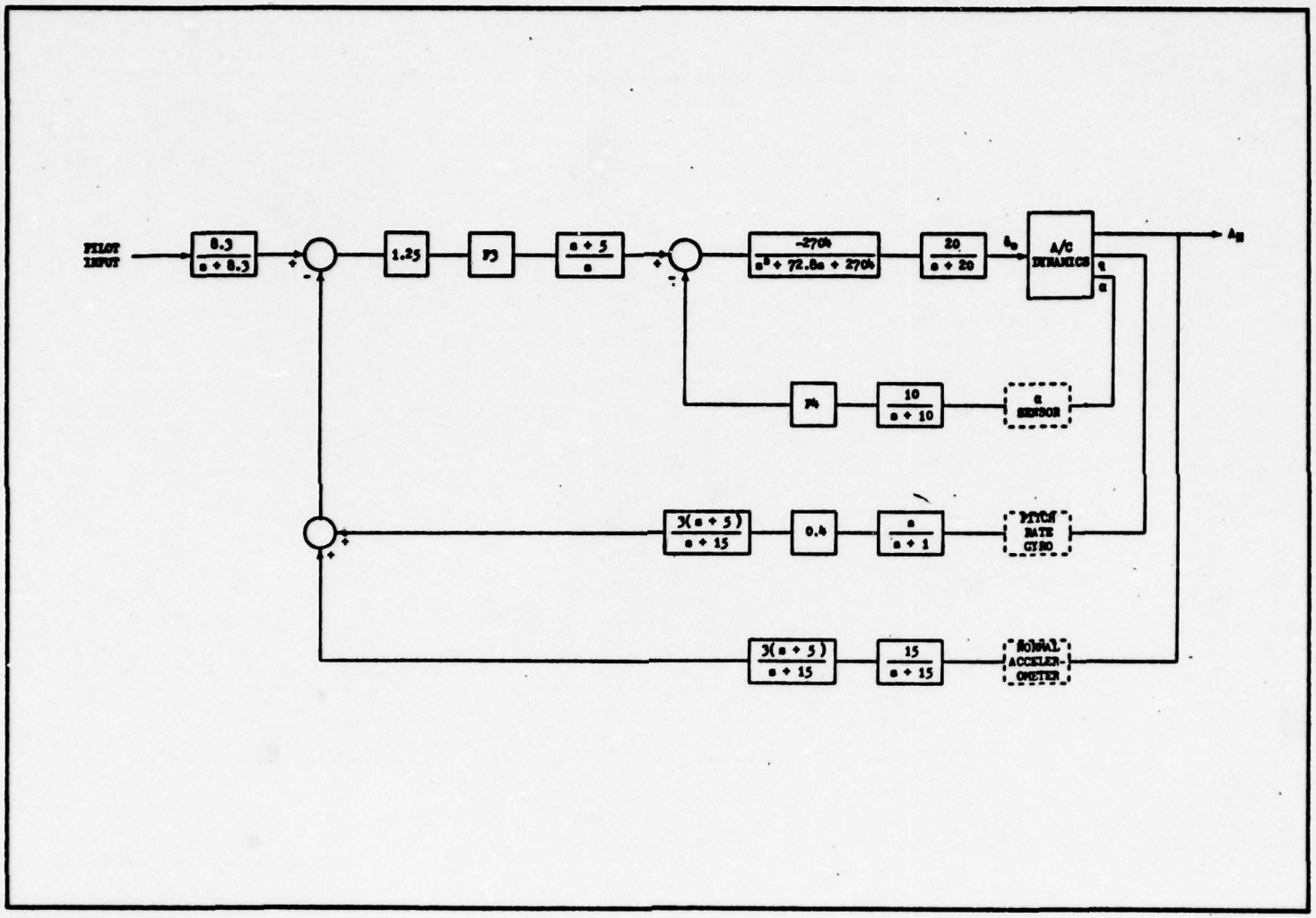


Figure 7. Linearized YF-16 baseline flight control system.

Figure 6 that algebraic signs at comparator inputs are changed, and the command servo gain is shown as negative. These changes are made to present the system in a more familiar form.

Although not shown in the figure, it is important to note that the power actuator rate saturates at 60 degrees per second with a maximum displacement of 25 degrees in either direction. Also of interest is the fact that an electrical resistance proportional to displacement is available from both the command servo and the power actuator. Appendix I details the design of a first-order observer to permit access to the internal state of the command servo.

The feedback paths consist of the appropriate sensor and simple first-order networks, with only the attack angle feedback path containing a scheduled gain. The model for the angle-of-attack sensor is the first-order lag

$$TF_{(\alpha\ \text{Sens})} = \frac{66.7}{s + 66.7} \tag{19}$$

The models for the pitch rate gyro and normal accelerometer are identical, and are given as the second-order lag

$$TF_{(q\ \text{Gyro})} = TF_{(A_N\ \text{Acc})} = \frac{98596}{s^2 + 376.8s + 98596} \tag{20}$$

The system of Figure 7 is further simplified by combining blocks, returning all feedback paths to the same point, and moving the command prefilter inside the feedback closure. The

result is shown in Figure 8. The only minor complication is the occurance of an unrealizable transfer function in the pitch rate feedback path. For simulation purposes, the free differentiator was removed and pitch acceleration feedback used instead of pitch rate. This option in the simulation program allows a more general case FCS to be simulated (see Appendix K for further discussion).

Maneuver Enhancement Augmentation. The linearized model of the YF-16 FCS with the Maneuver Enhancement system engaged is somewhat more complicated as indicated in Figure 9. The upper portion of this figure is identical to Figure 7, with the lower portion showing the Maneuver Enhancement augmentation. Although the models of the flaperon channel command servo and power actuator are dynamically identical to those in the horizontal tail channel, there are a few minor differences that should be addressed. As indicated in the figure, the sign of the servo gain in the flaperon channel is positive, and is modeled as such to reflect the described sign convention (Chapter II). Also, the power actuator rate saturates at 56 degrees per second, and is displacement limited to 20 degrees in either direction.

The system of Figure 9 may be greatly simplified by combining blocks and moving feedback and feedforward paths to common nodes. Leaving out the details, this reduction is given in Figure 10. The system may be further simplified by moving the resultant fourth-order "prefilter" inside the horizontal tail feedback loop closure. The factored form of

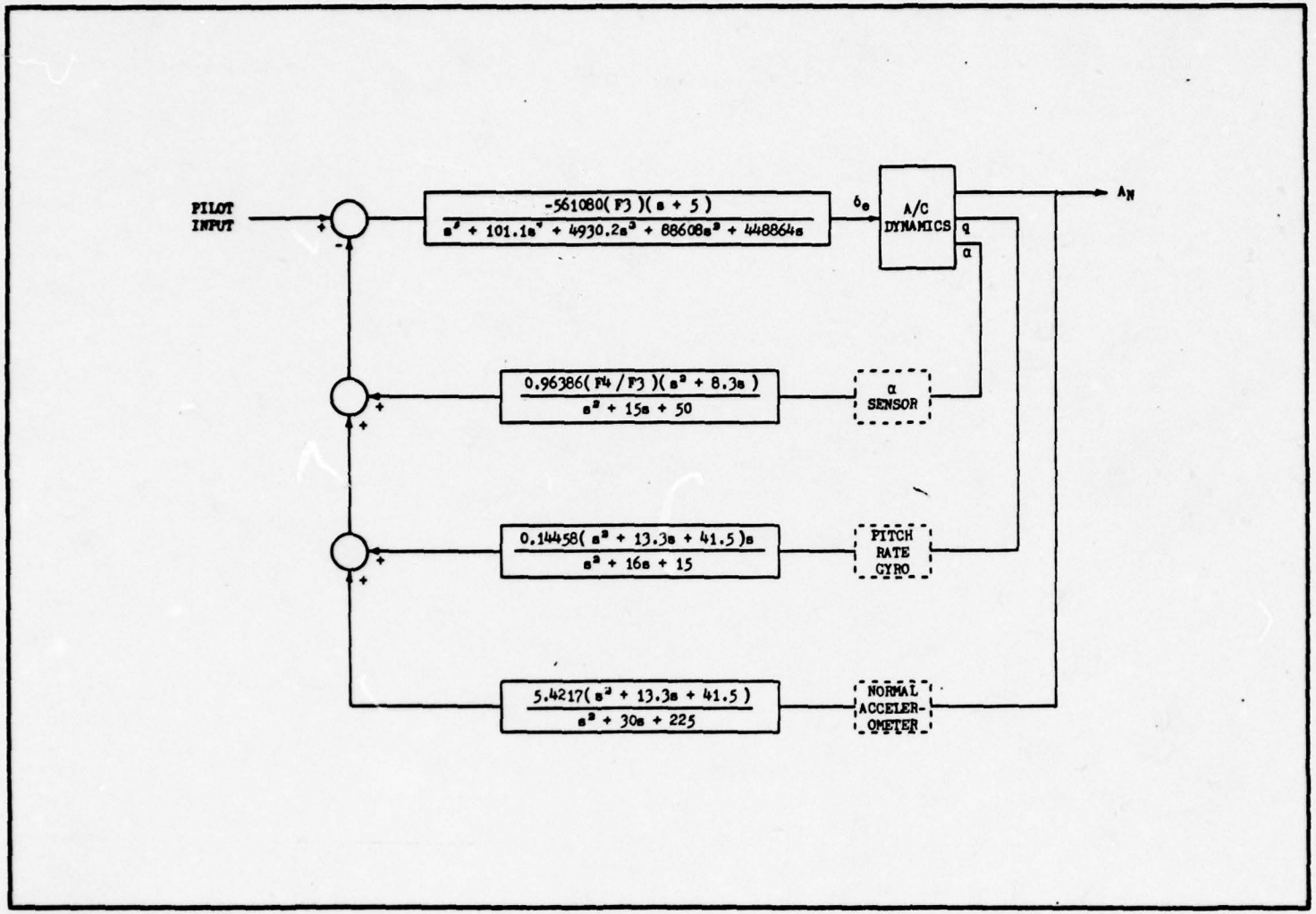


Figure 8. Simulation configuration of the linearized YF-16 baseline FCS.

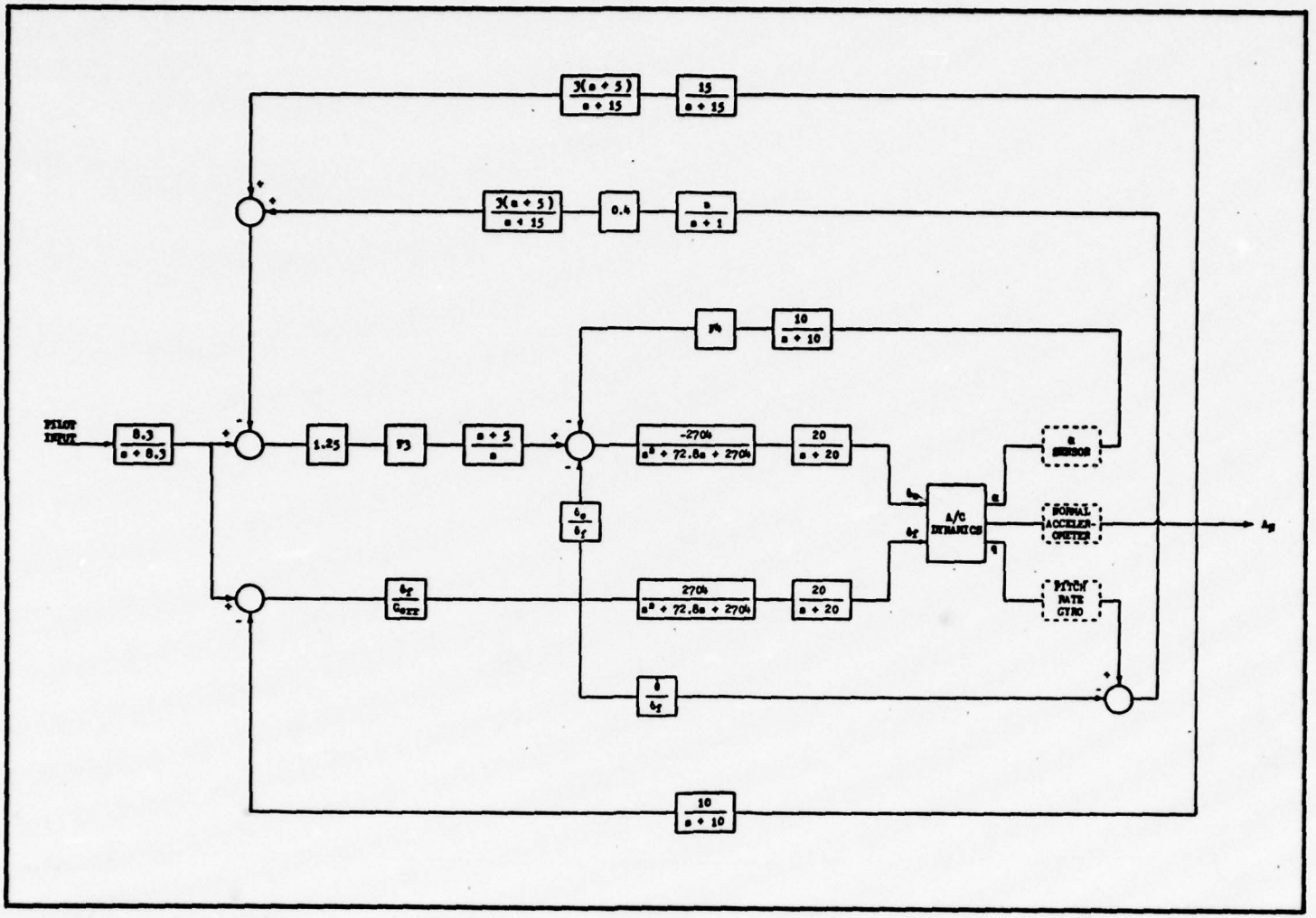


Figure 9. Linearized YF-16 CCV flight control system.

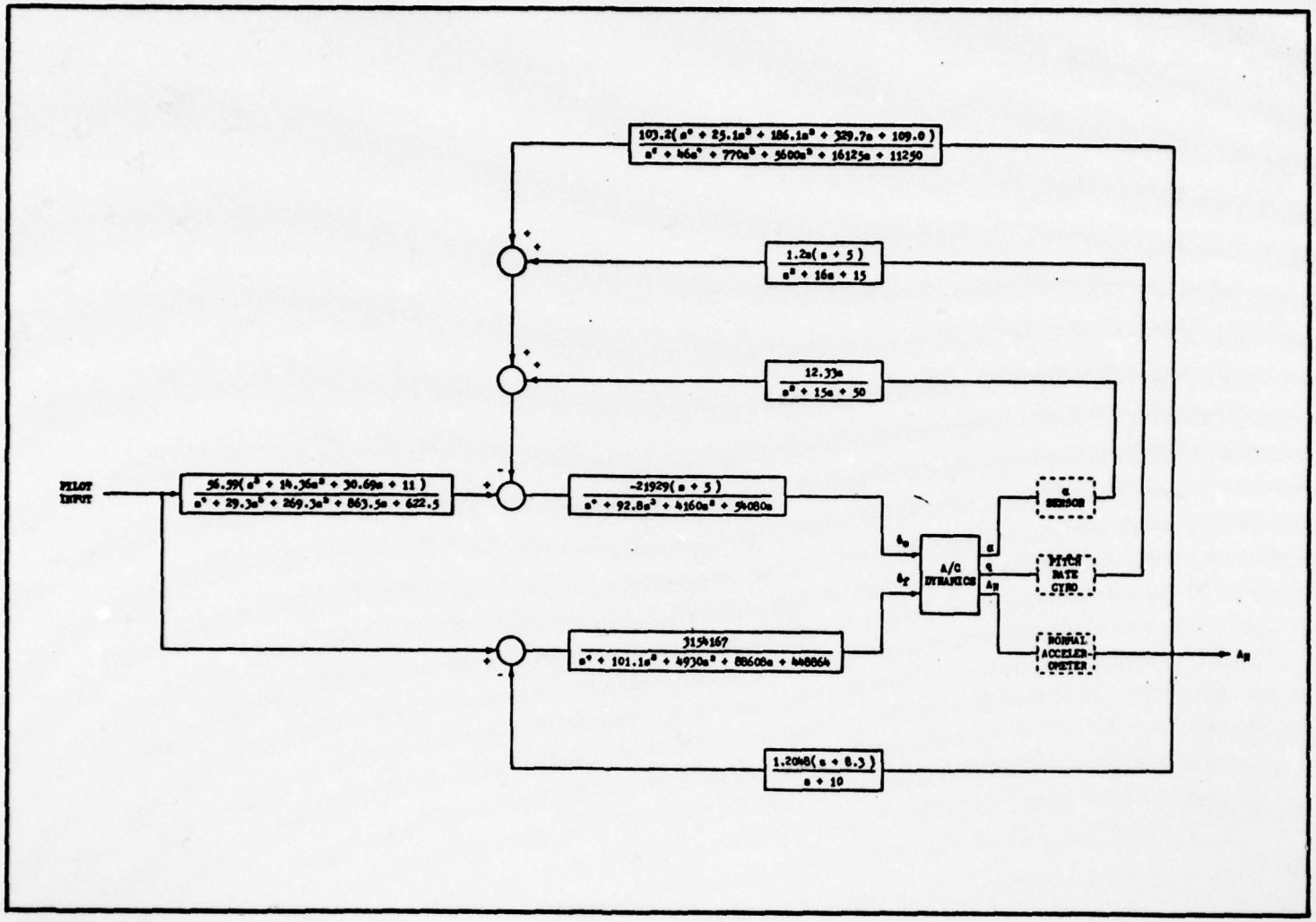


Figure 10. Simplified, linearized YF-16 CCV flight control system.

this prefliter is

$$TF = \frac{56.59(s + .4504)(s + 2.062)(s + 11.85)}{(s + 1)(s + 5)(s + 8.3)(s + 15)} \quad (21)$$

and the factored form of the remaining horizontal tail forward loop block is

$$TF = \frac{-21929(s + 5)}{(s + 20)(s + 36.4 \pm j37.14)s} \quad (22)$$

In combining these two blocks, a single cancellation is made, yielding

$$TF = \frac{-1240962(s + .4504)(s + 2.062)(s + 11.85)}{(s + 1)(s + 8.3)(s + 15)(s + 20)(s + 36.4 \pm j37.14)s} \quad (23)$$

Due to the fact that the simulation computer program cannot currently handle transfer functions in excess of fifth order, some simplifying approximation must be made. One straightforward approach is to assume that the second order dynamics of the servo are non-dominant. As there is a pole at -1 on the real axis with no zero nullifying its dominance, this assumption is valid. There is sufficient cancellation of poles and zeros for the feedback transfer functions, therefore no similar approximations are necessary. The final system model is given in Figure 11.

System Time Responses

With the aircraft and flight control system suitably modeled, a simulation of the composite system can now be

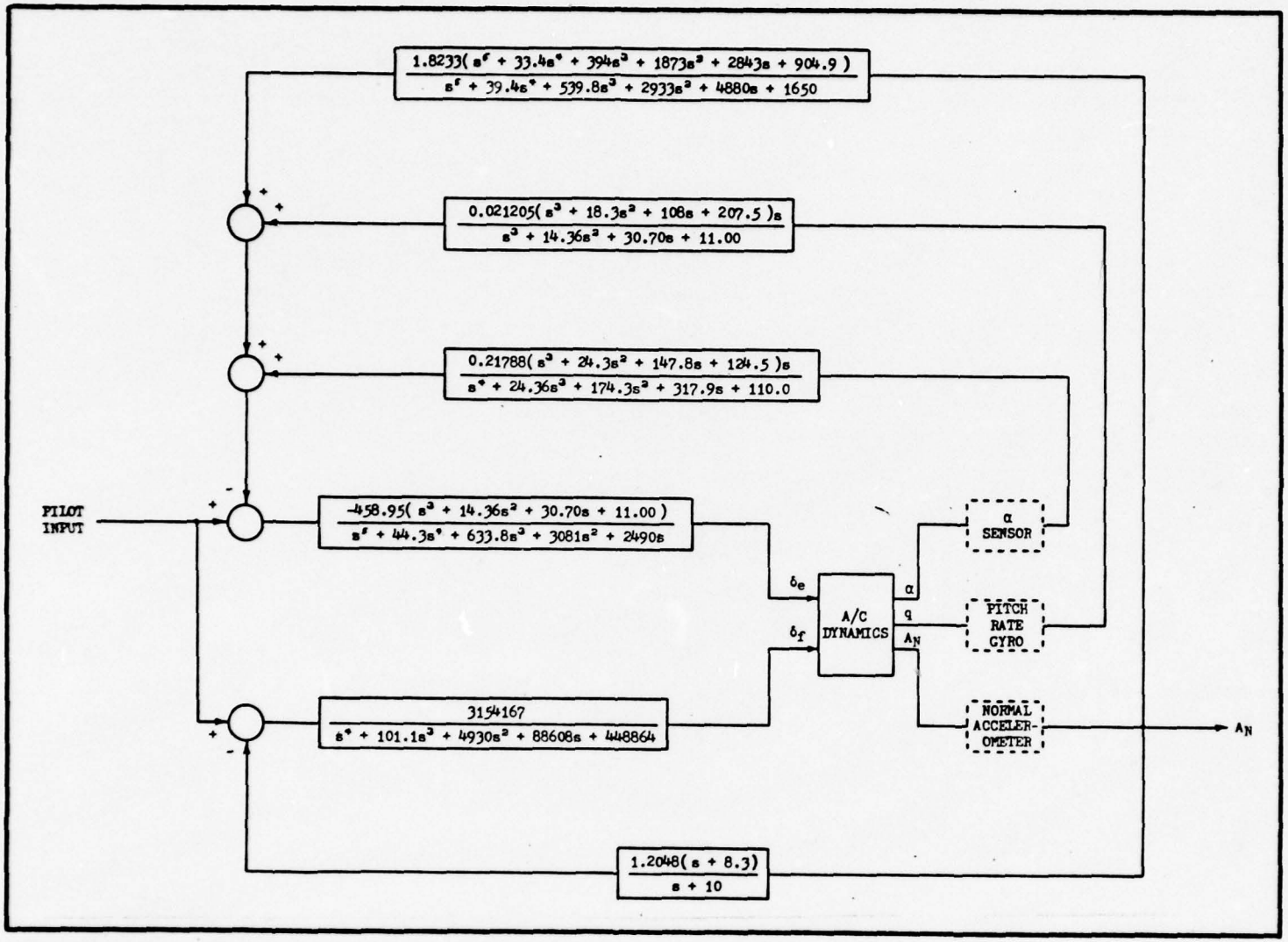


Figure 11. Simulation configuration of the linearized YF-16 CCV FCS.

effected for the selected flight condition (0.8 Mach @ SL). The simulation includes system state responses to pilot and disturbance inputs for the YF-16 FCS with the Maneuver Enhancement augmentation both out of circuit (Figure 8) and in circuit (Figure 11).

Computer generated plots of selected quantities are presented as simulation output. Angle-of-attack is shown in two ways, since two forms of this quantity have been identified. Those plots labeled "ANGLE OF ATTACK" show the stability-axis perturbation attack angle response. Plots labeled "OUTPUT OF ATTACK ANGLE SENSOR" reflect the form of attack angle that is being used as feedback, modified by the specified dynamics of the attack angle sensor.

Horizontal tail deflection and trailing-edge flaperon deflection are also among the quantities plotted. In addition to the plotted response, maximum achieved rate of deflection and rate limiter disposition are printed on these plots. If a rate saturation limit for the actuator is specified, the flag "LIMIT,ON" is printed. If no limit is defined, the flag "LIMIT,OFF" is printed. Recall that rate saturation of the horizontal tail actuators occurs at 60 degrees per second, and for the trailing-edge flaperon actuators, at 56 degrees per second. For those simulations wnere a rate limit is specified, these values are utilized.

Response to Pilot Step Input. To simulate system response to a pilot command, a 1-G step input is applied. System response with Maneuver Enhancement switched off is shown in

Figure 12, while response with Maneuver Enhancement switched on is shown in Figure 13. The input dimensionality is given in volts. This is done for convenience only, since, depending on the system being simulated, the commanded response can be any state or a linear combination of states. As the actual input to the FCS is a voltage, the label "volts" is chosen as a representative dimensionality.

Examination of the system response characteristics portrayed in these figures reveals the intended function of Maneuver Enhancement - to improve transient performance. Note that the onset of both pitch rate and normal acceleration are substantially quickened relative to the basic YF-16 FCS responses. This initial transient improvement is due to the deflection of the trailing-edge flaperons. With horizontal tail control only, changes in normal acceleration are accomplished by rotation of the aircraft. The rate of response is, therefore, dependent on the rate of aircraft rotation. The trailing-edge flaperons, however, directly increase lift on the wing, and permit a more rapid increase in normal acceleration.

Approximately one second after application of the step input, the normal acceleration response of both systems is essentially the same - a slow increase over the succeeding few seconds to the commanded level. For the Maneuver Enhancement system, the transition from flaperon induced translation to horizontal tail induced rotation is clearly defined at the 0.3 second point. This interim pause in G-onset is a somewhat

undesirable handling characteristic caused by the extremely sudden change in flaperon deflection rate.

Although the improvement in initial transient response is clearly visible, it is important to note that the responses shown are for a 1-G step command. Even at this low input level, trailing-edge flaperon deflection rate reaches approximately one-half the actuator saturation rate. As the aircraft is capable of pulling in excess of 7 Gs over straight and level flight, an actuator rate of close to 200 degrees per second would be required to obtain the same transient response characteristics shown in Figure 13. As the flaperons are clearly responsible for the improvement in transient response obtained with Maneuver Enhancement, a flaperon deflection rate limit of 56 degrees per second decidedly impacts the amount of improvement available during high-performance maneuvers.

Response to the Discrete Vertical Gust. To simulate system response to atmospheric disturbances, discrete (1-cos) vertical gust inputs are applied. Peak gust velocity is 50 feet per second, with a duration of one second. This gust was chosen to be consistant with that used in the disturbance analysis performed by General Dynamics.

To enable a direct comparison of the system responses that are obtained as a result of feeding back each of the two previously defined forms of angle-of-attack, simulations are run for each case. In addition, responses are shown for the FCS with and without Maneuver Enhancement.

System response with ME off and $'\alpha$ feedback is shown in Figure 14. In this case, the measured angle-of-attack is assumed to be $'\alpha$ modified by the sensor dynamics. Therefore, the two traces are almost identical. System response with ME off and α_m feedback is shown in Figure 15. The difference between the measured attack angle and $'\alpha$ is apparent.

Comparing the two figures, the peak perturbation in aircraft pitch angle is actually almost 80% greater when using α_m feedback than that obtained by incorrectly using $'\alpha$ as the feedback quantity. This results in a corresponding increase in target tracking error. There is also a change in the number of negative Gs pulled as a result of the gust, as well as an increase in horizontal tail deflection.

Figures 16 and 17 show the system response with ME on, using $'\alpha$ and α_m feedback, respectively. As in the previous case for ME off, use of α_m as a feedback quantity provides a more accurate simulation of actual system performance.

The gust alleviation properties of Maneuver Enhancement can be recognized from a comparison of Figures 15 and 17. For a discrete gust of one second duration, pitch angle perturbation and peak target tracking error are reduced by about 10%, and normal acceleration perturbation is improved by more than 40%. The large improvement in normal acceleration response is the natural result of feeding back only normal acceleration to the trailing-edge flaperons. Any deviation from the commanded value forces a flaperon deflection that attempts to null only that error.

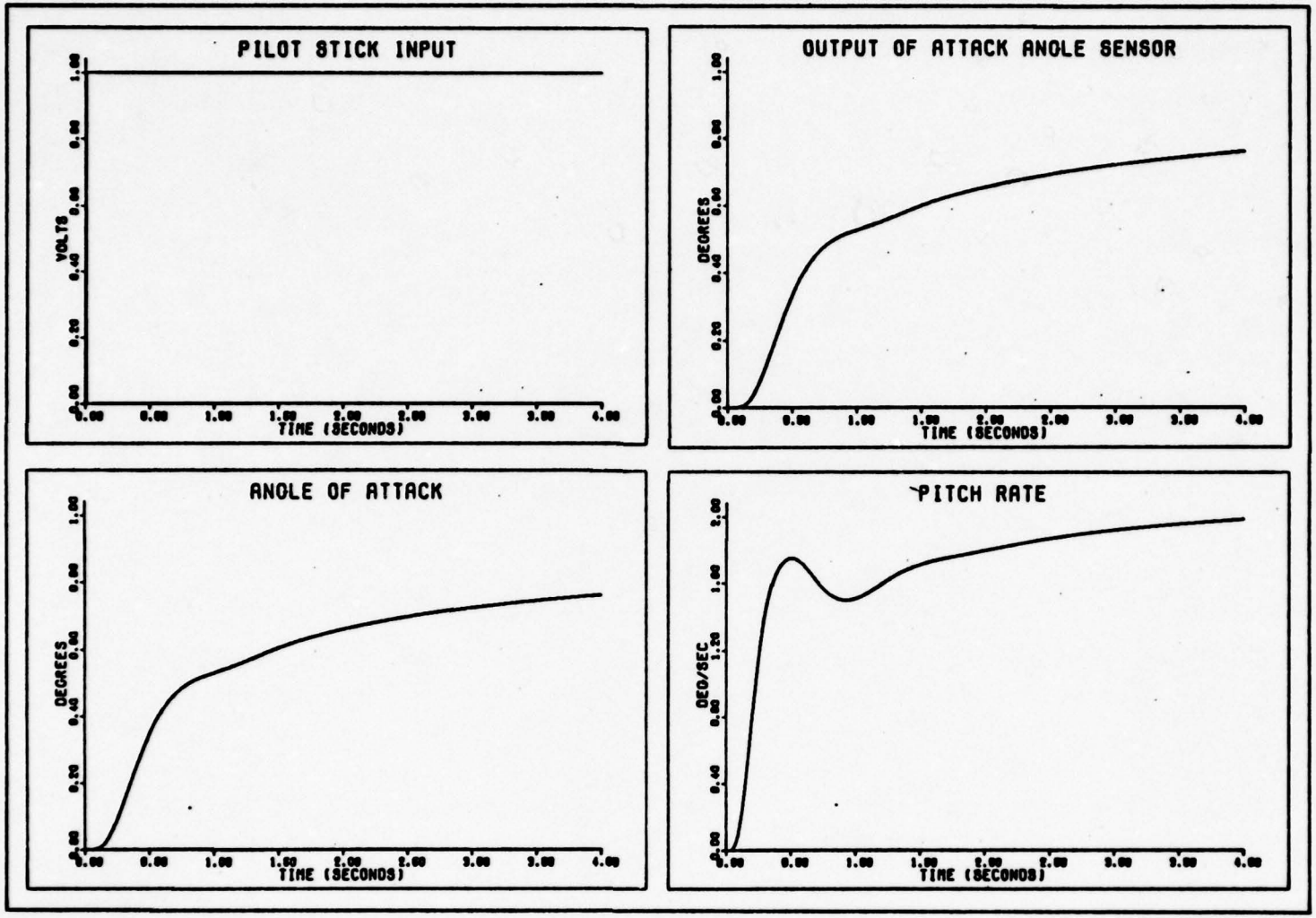


Figure 12a. YF-16 baseline FCS response to a pilot step input.

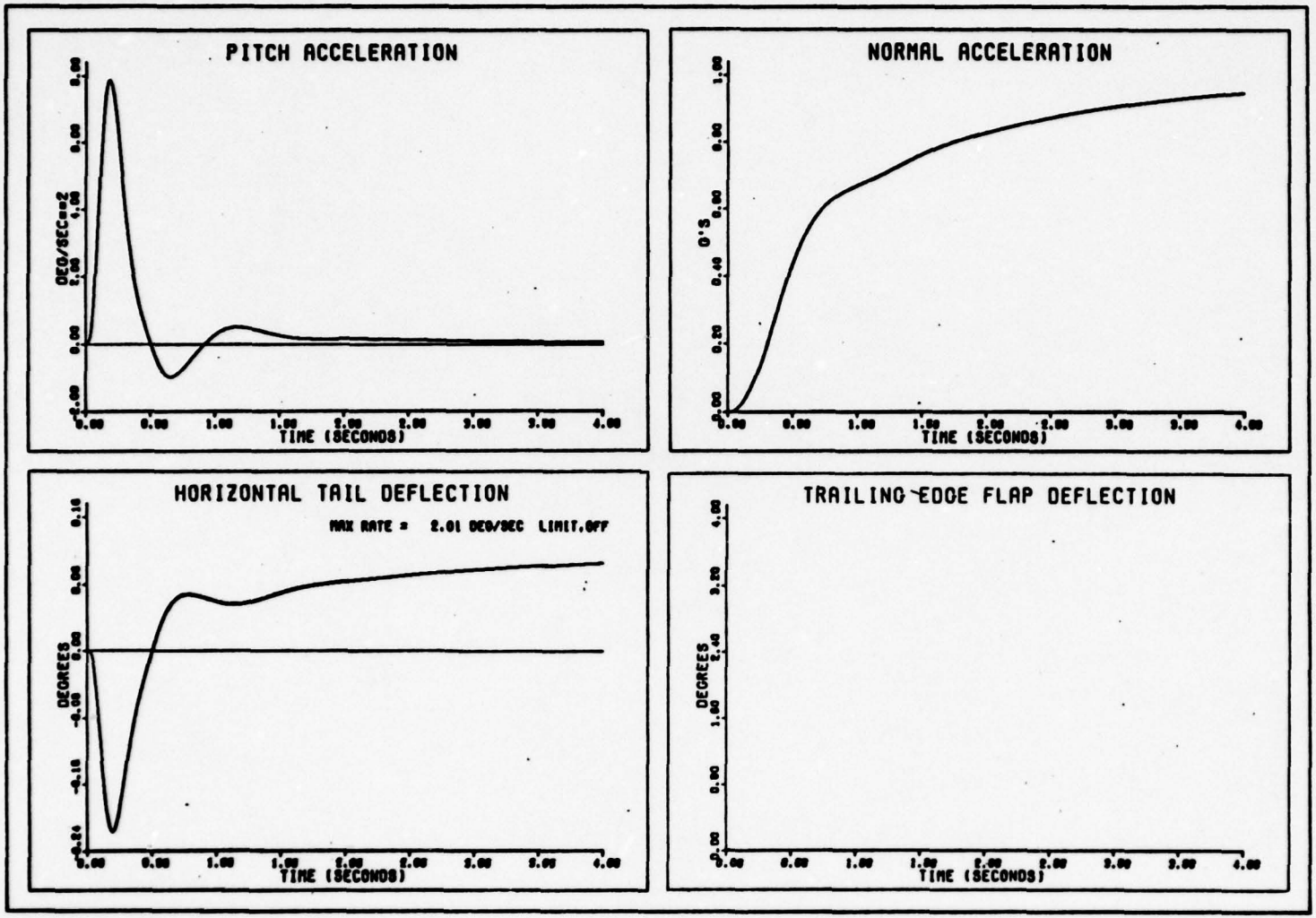


Figure 12b. YF-16 baseline FCS response to a pilot step input.

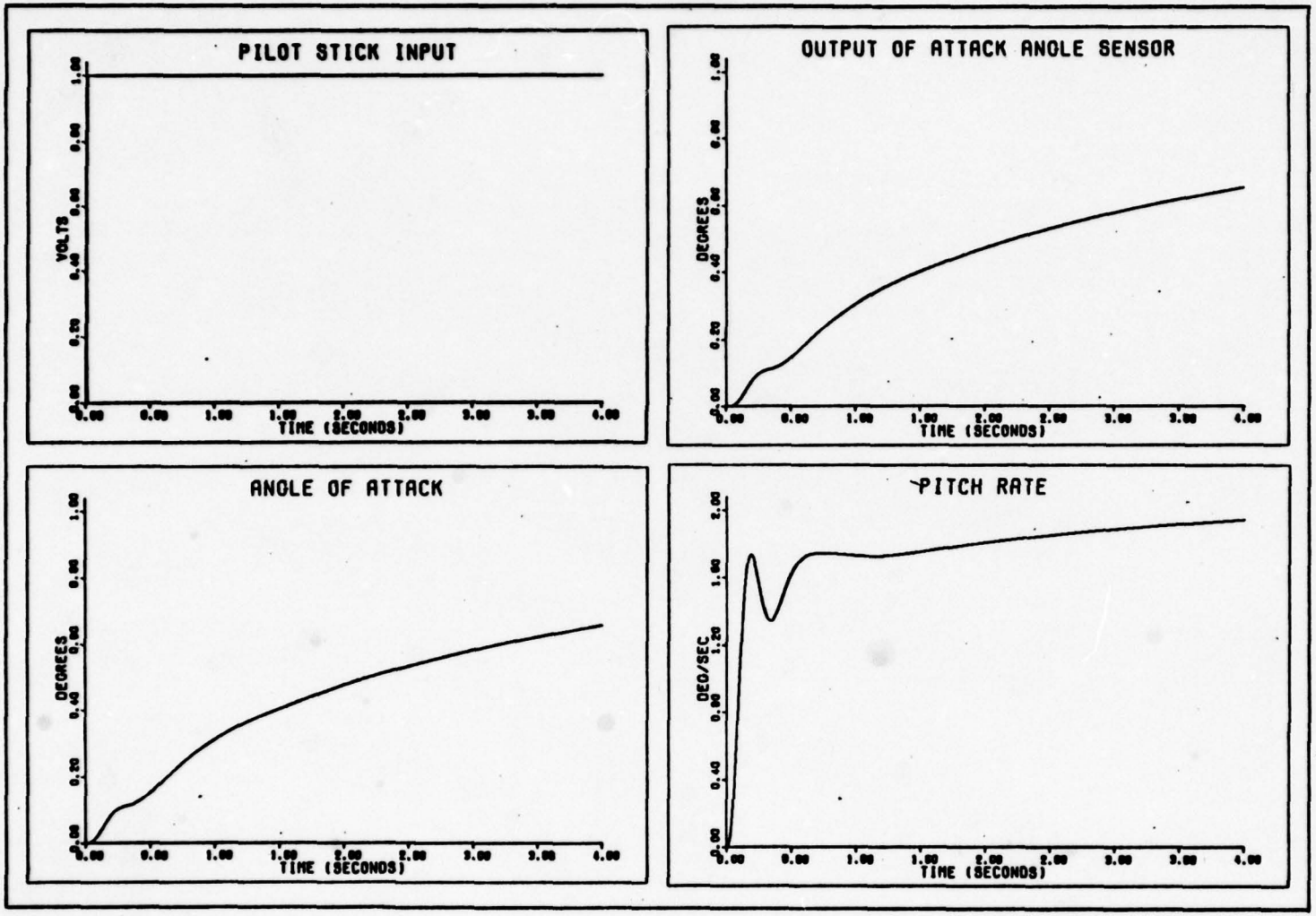


Figure 13a. YF-16 CCV FCS (with Maneuver Enhancement) response to a pilot step input.

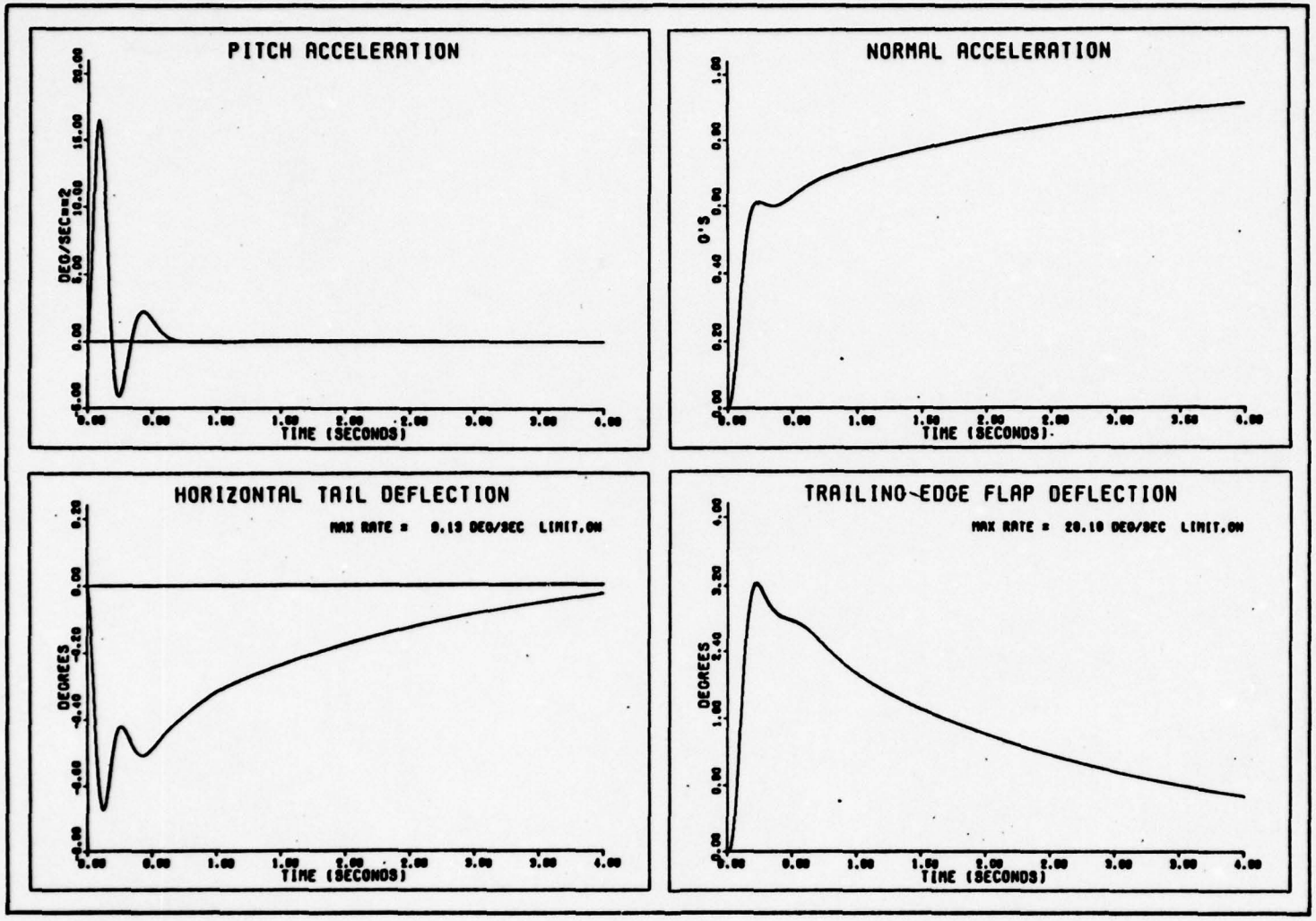


Figure 13b. YF-16 CCV FCS (with Maneuver Enhancement) response to a pilot step input.

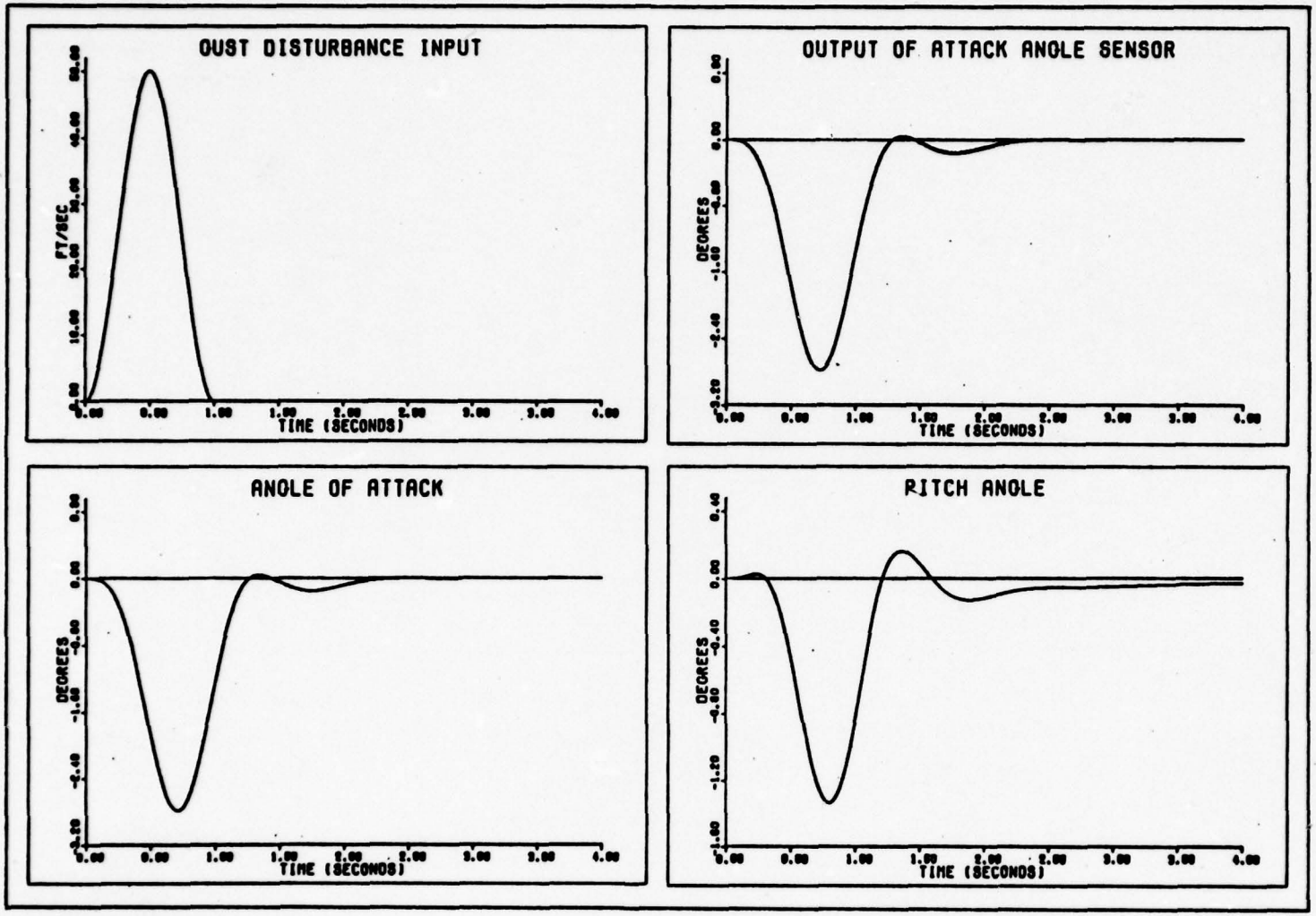


Figure 14a. YF-16 baseline FCS with 'α feedback response to a discrete gust.

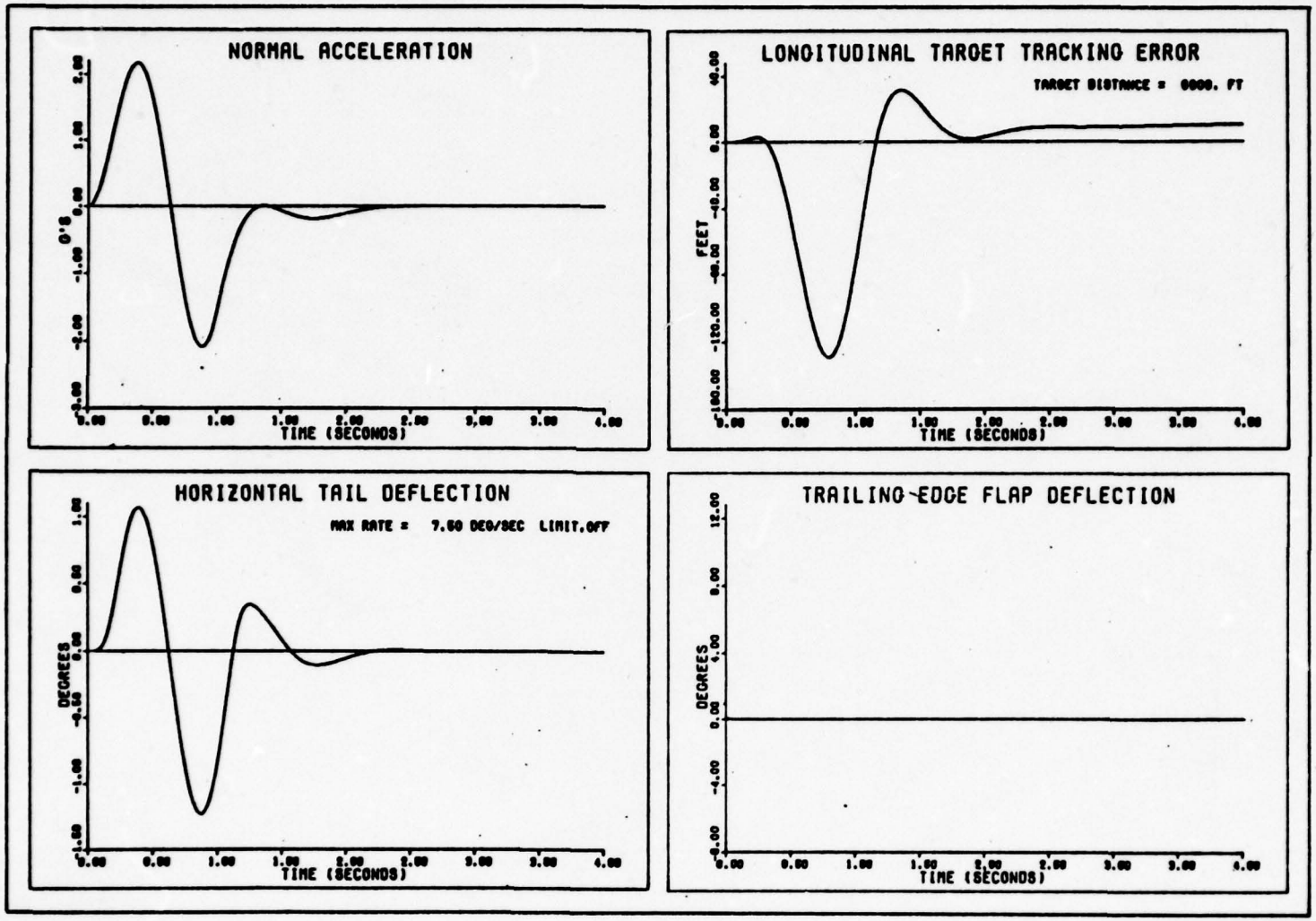


Figure 14b. YF-16 baseline FCS with 'α feedback response to a discrete gust.

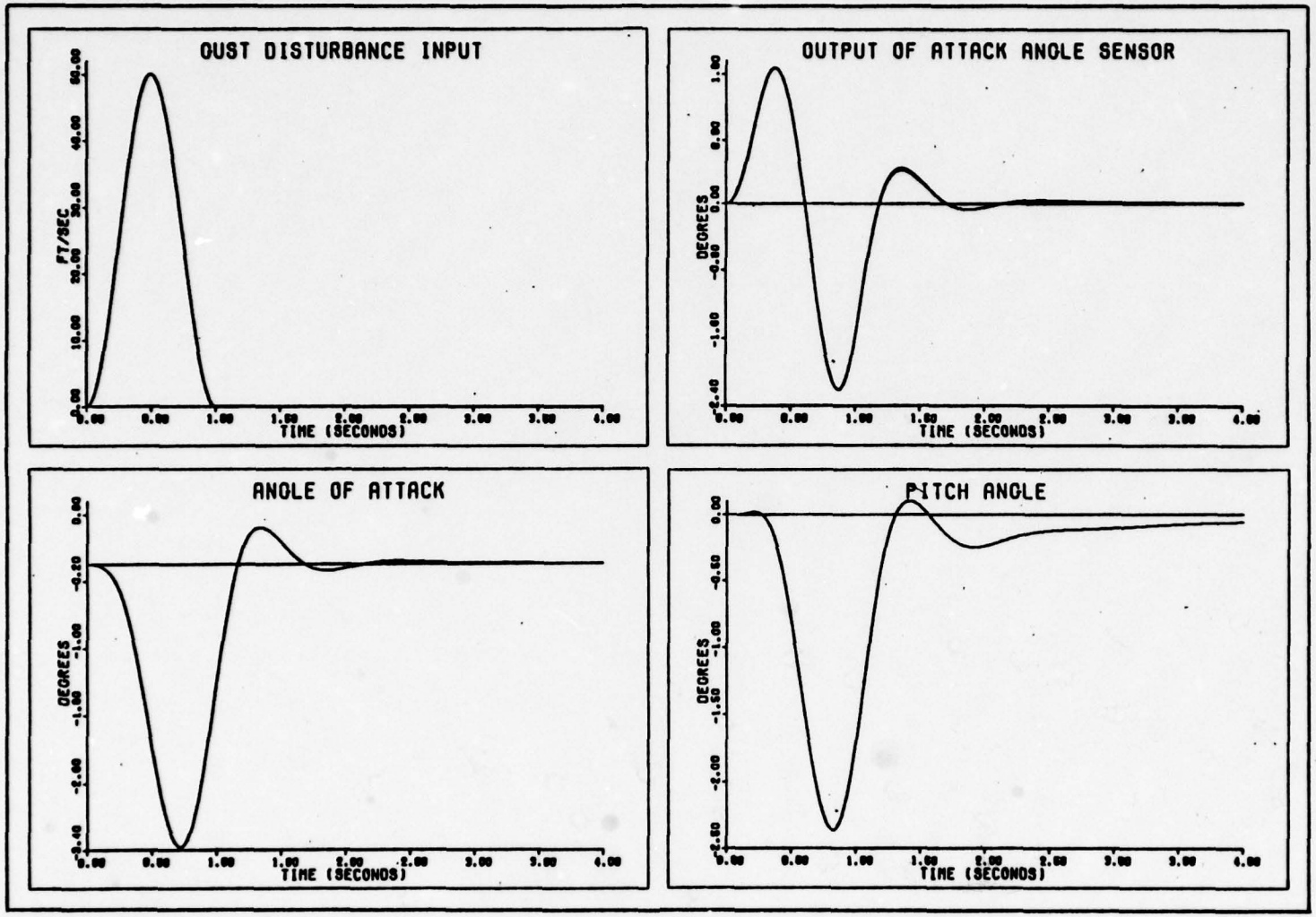


Figure 15a. YF-16 baseline FCS with α_m feedback response to a discrete gust.

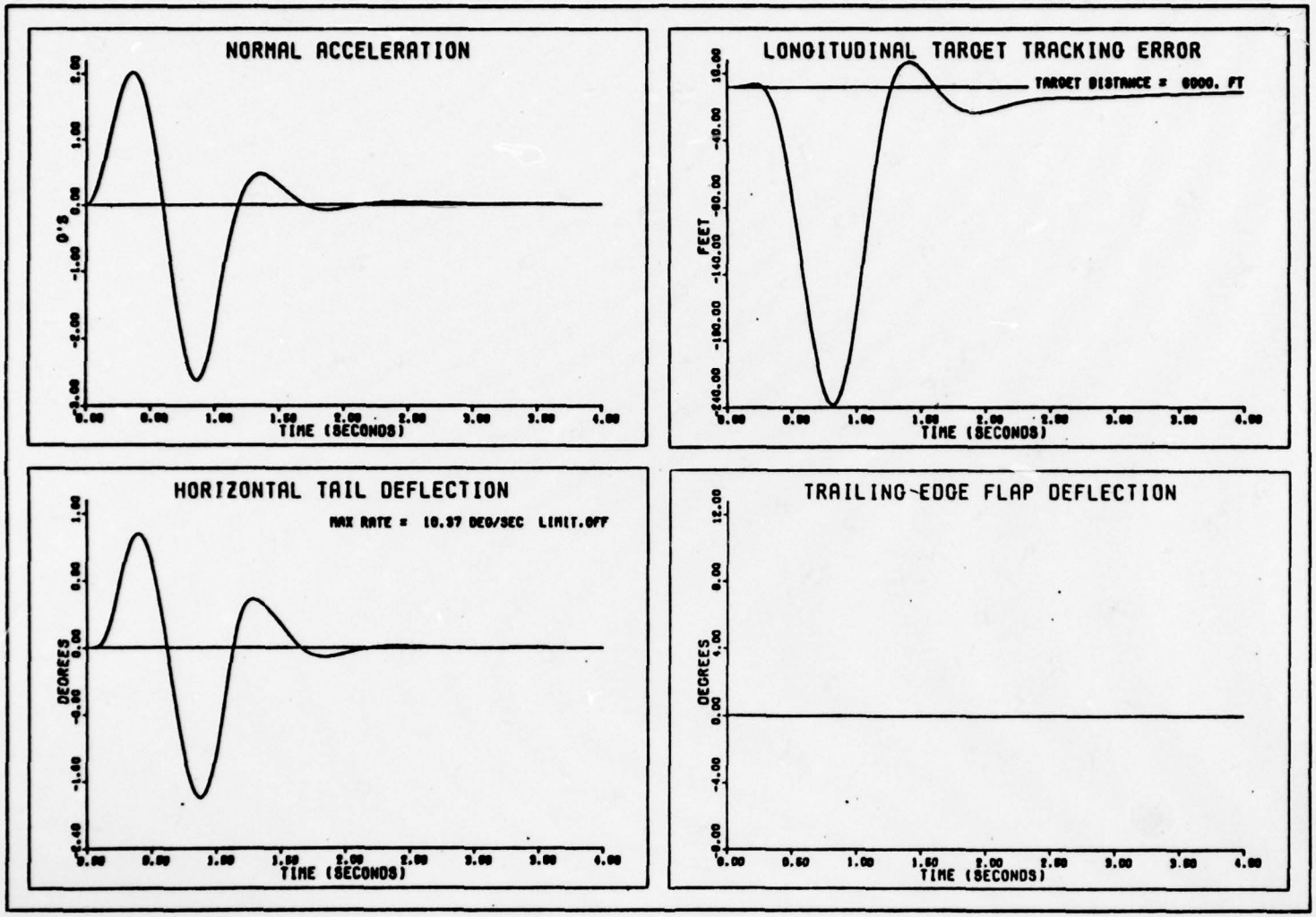


Figure 15b. YF-16 baseline FCS with α_m feedback response to a discrete gust.

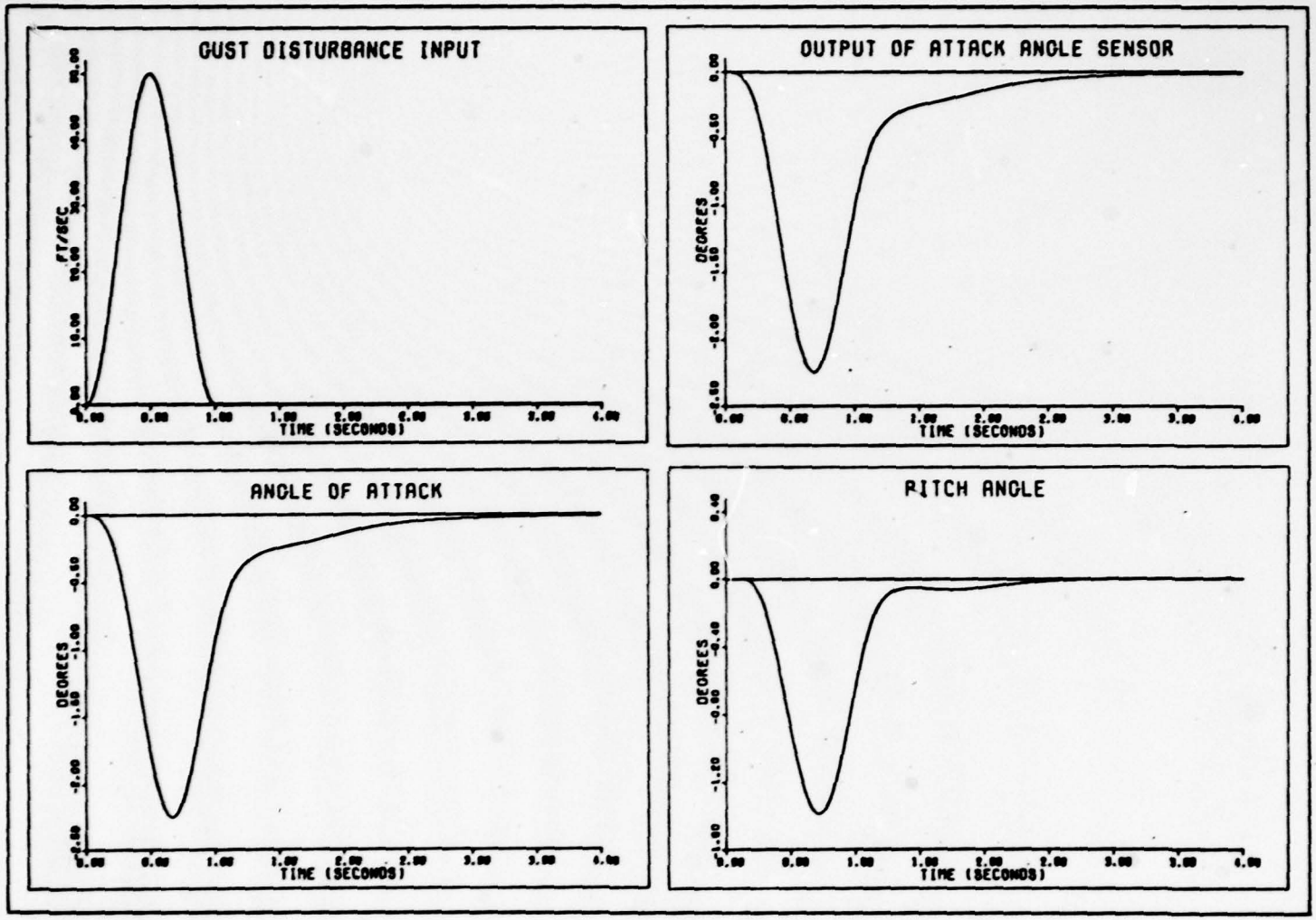


Figure 16a. YF-16 CCV FCS with 'α feedback response to a discrete gust.

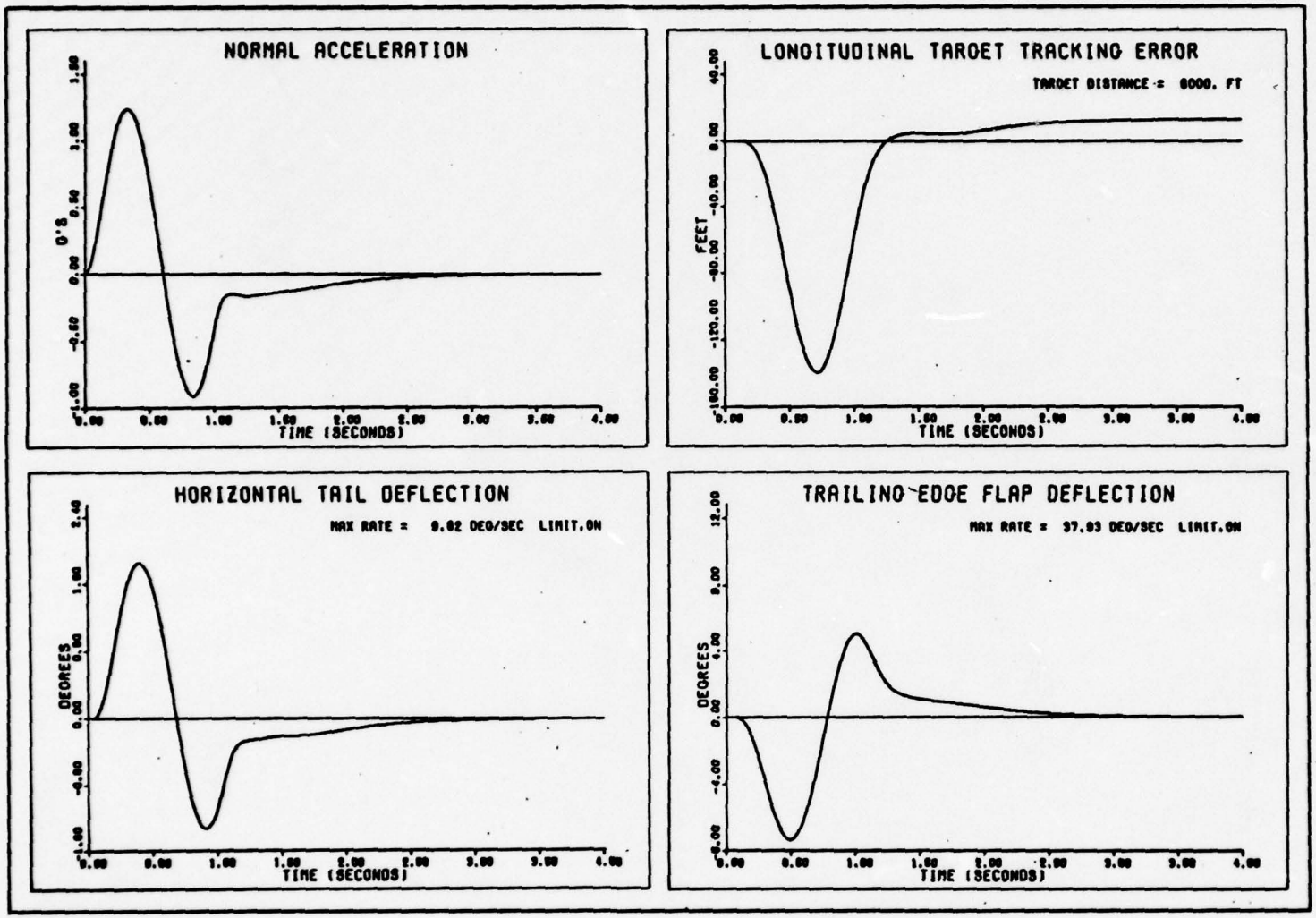


Figure 16b. YF-16 CCV FCS with 'α feedback response to a discrete gust.

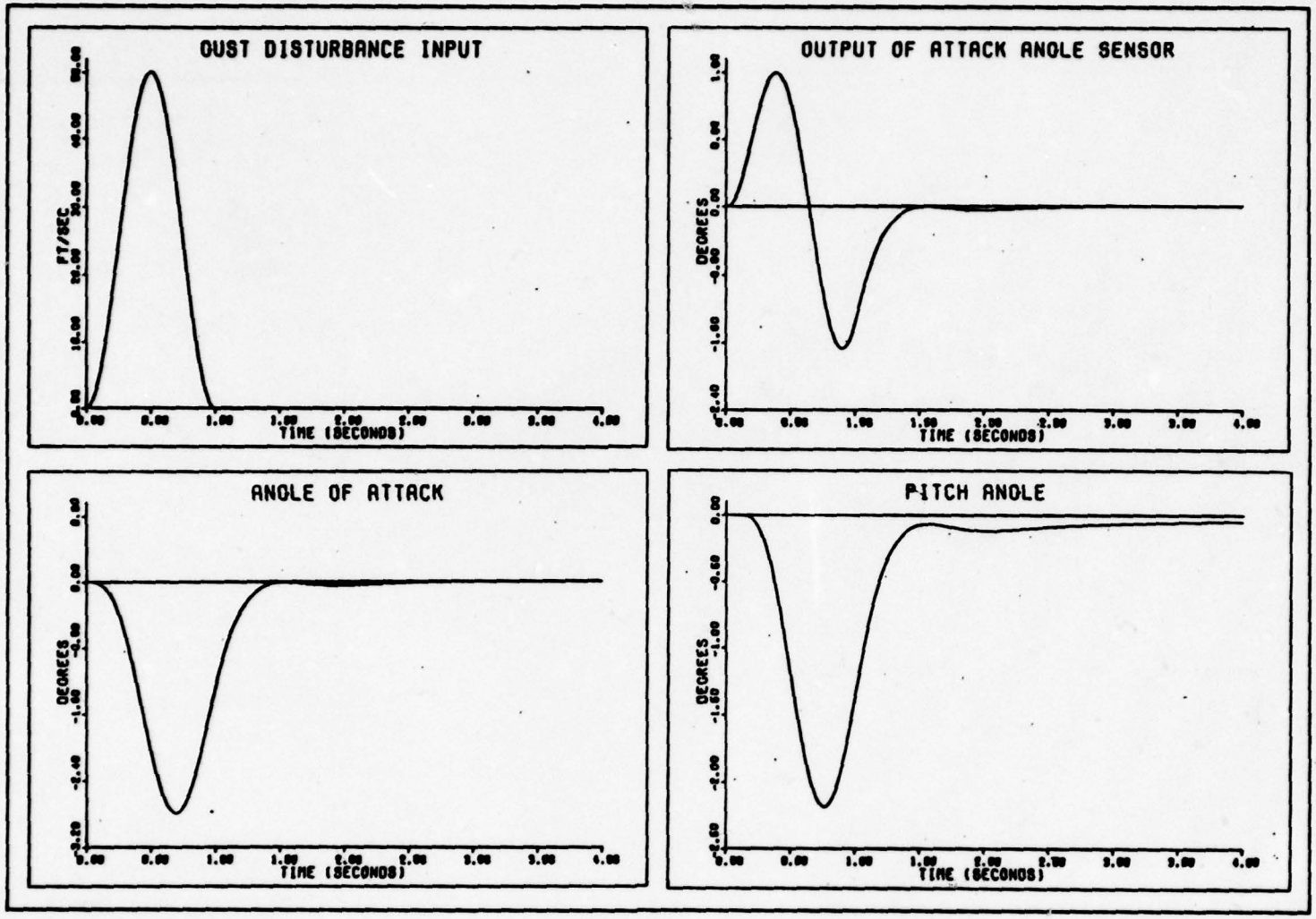


Figure 17a. YF-16 CCV FCS with α_m feedback response to a discrete gust.

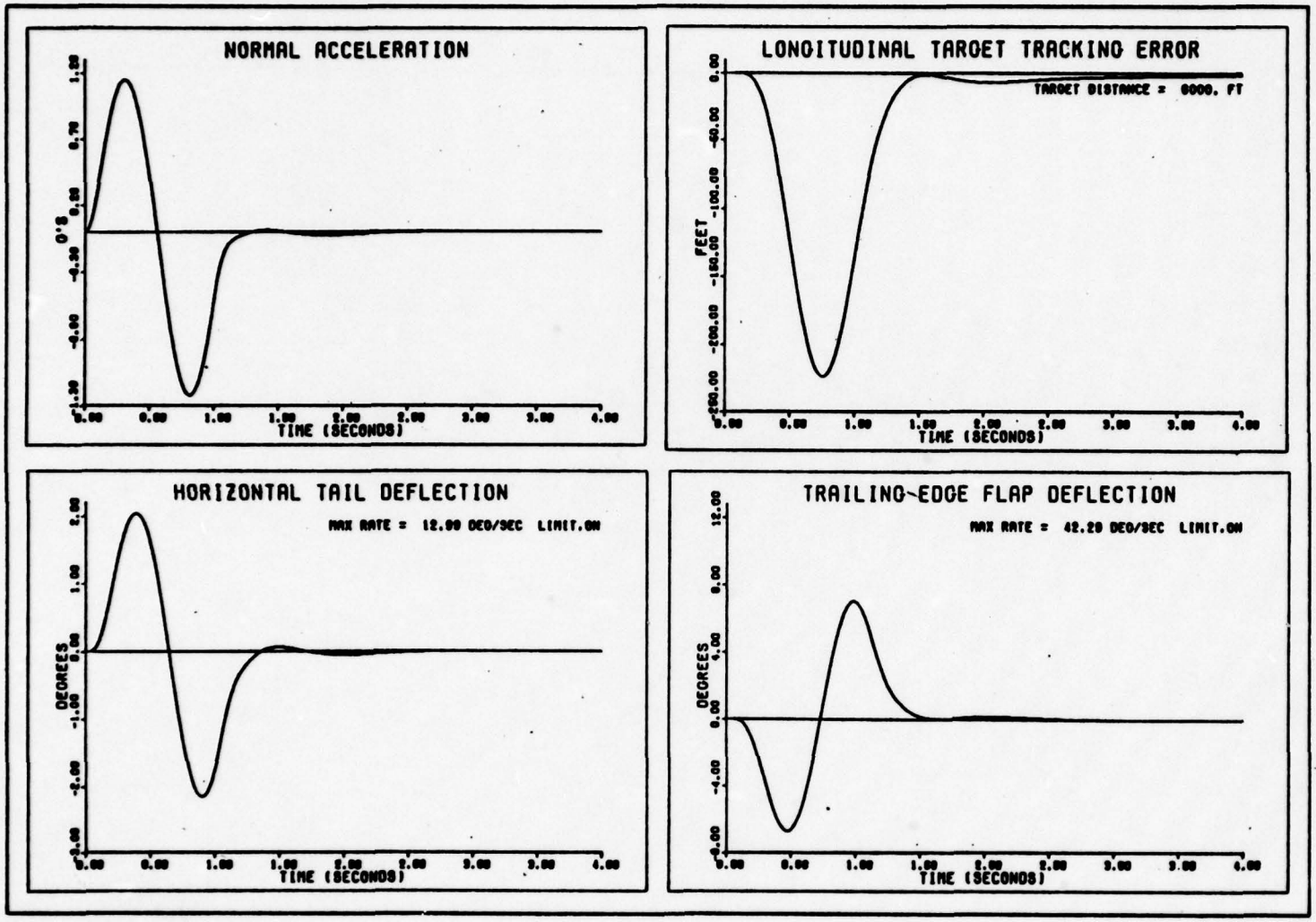


Figure 17b. YF-16 CCV FCS with α_m feedback response to a discrete gust.

Frequency Response to Discrete Vertical Gusts

To permit a more encompassing assessment of system disturbance response characteristics, gusts of various frequencies should be applied to the system. A single gust of one second duration does not give a true indication of the performance of the system in the presence of gusts that are of shorter or longer duration. Digesting page after page of simulation output to get that overall picture is, however, a formidable task. A type of frequency response analysis is the obvious answer.

To determine the frequency response analytically, the closed-loop system transfer functions must be known. Although the transfer function for the system without Maneuver Enhancement can be calculated with little difficulty, the same cannot be said about the system with Maneuver Enhancement. The added complication of running feedback loops to an additional input - when the measurable outputs are dependent on both inputs - increases the complexity by several orders of magnitude. Even if the transfer functions could be determined, it would perhaps be more informative to examine system response to discrete gusts of varying durations, as opposed to applying a sine wave input of varying frequency.

One way of obtaining such data is to first run several simulations applying discrete gusts of varying durations to the system. Then, for each run, the absolute value of the maximum perturbation of a given quantity can be plotted against the frequency of the gust applied. The gust frequency

is simply the multiplicative inverse of the gust duration. There is, of course, no periodic frequency associated with a discrete gust, but this approach permits the data to be plotted in a more familiar form.

For this analysis, ten simulations are run for each of the four system configurations - $'\alpha$ or α_m feedback with and without Maneuver Enhancement. Gust durations covering a range of .03 to 30 seconds are applied, and in each case, maximum gust velocity is 50 feet per second. The results are shown for seven quantities of interest in Figures 18 through 24. The effect of using $'\alpha$ feedback is clearly visible, as is the influence of Maneuver Enhancement. A small marker placed on the frequency axis in each figure indicates the gust duration that was used in the previous time response analysis.

Discussion

It has been demonstrated that aircraft performance can indeed be improved through the use of the trailing-edge flaperons as an active control surface. In response to pilot commands, initial transient response is significantly enhanced by the flaperon deflections which supplement the normal aircraft rotation. In turbulence, the flaperon movements result in substantially reducing undesirable perturbations in normal acceleration.

Also demonstrated was the importance of using the correct measure of angle-of-attack as a feedback quantity to model the actual system. In the case presented, $'\alpha$ is not the attack angle physically measured by the sensing device. As

demonstrated, $'\alpha$ is only correctly used when the analysis being performed excludes the effect of external disturbances on the aircraft (i.e., when determining aircraft response to pilot inputs). It is shown in Equation 17 that when there is no movement of surrounding air ($\alpha_g = 0$), then, and only then, is $'\alpha$ equal to α_m.

Although the Maneuver Enhancement augmentation designed by General Dynamics does function as a gust alleviation system which provides improvement in normal acceleration response, it provides little or no improvement in pitch response. As a result, it provides no appreciable reduction in target tracking error as defined herein. The major reason for this is that the system was designed primarily to enhance aircraft response to pilot commands - thus, Maneuver Enhancement. Its gust alleviation performance was essentially a fallout of the chosen configuration employing normal acceleration feedback to the flaperons.

It is likely that aircraft response to turbulence can be further reduced if that is the design objective. One possibility of interest might be the use of attack angle and/or pitch rate feedback to the flaperons. This is the subject of the next chapter.

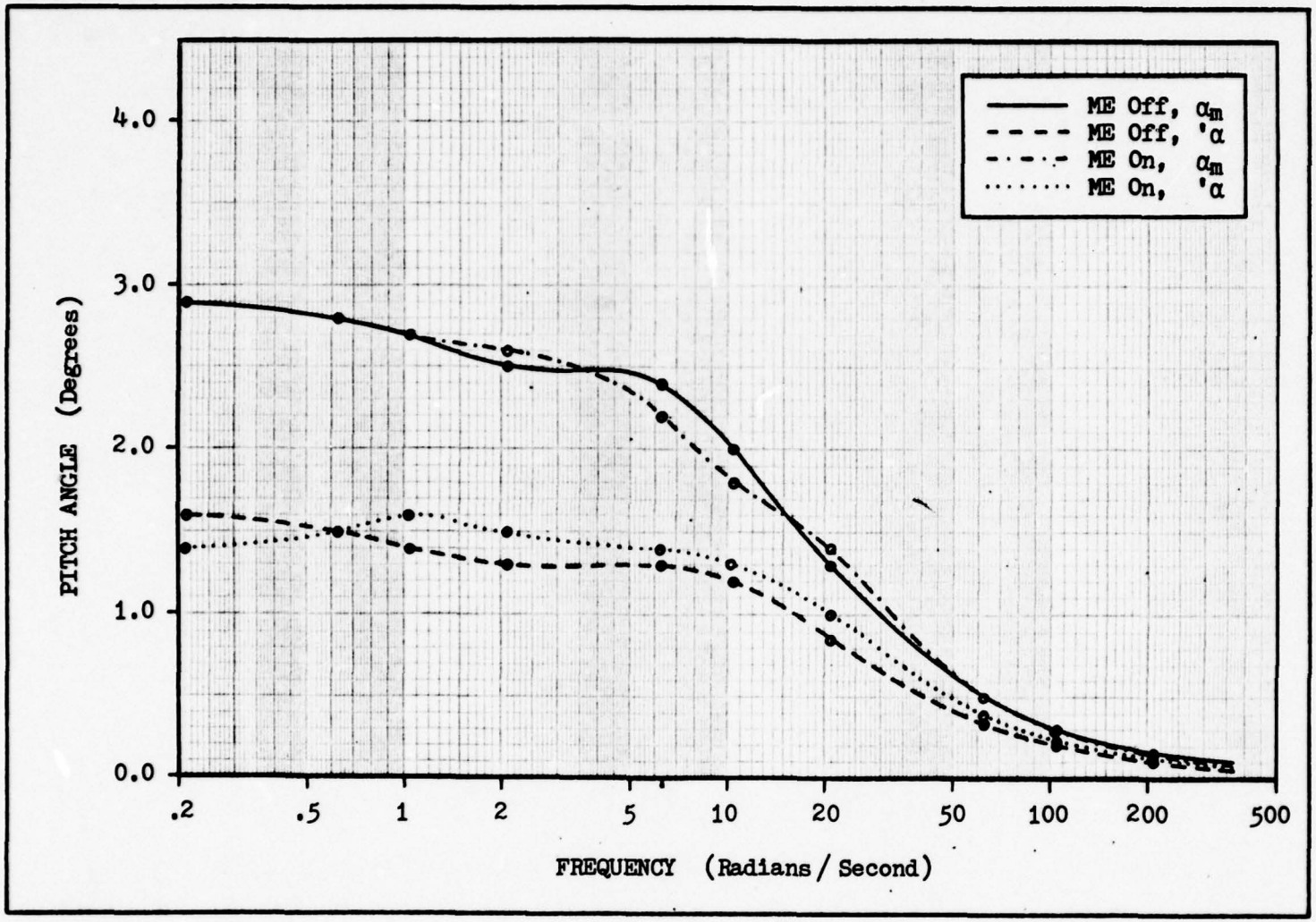


Figure 18. Peak pitch angle response of YF-16 flight control systems.

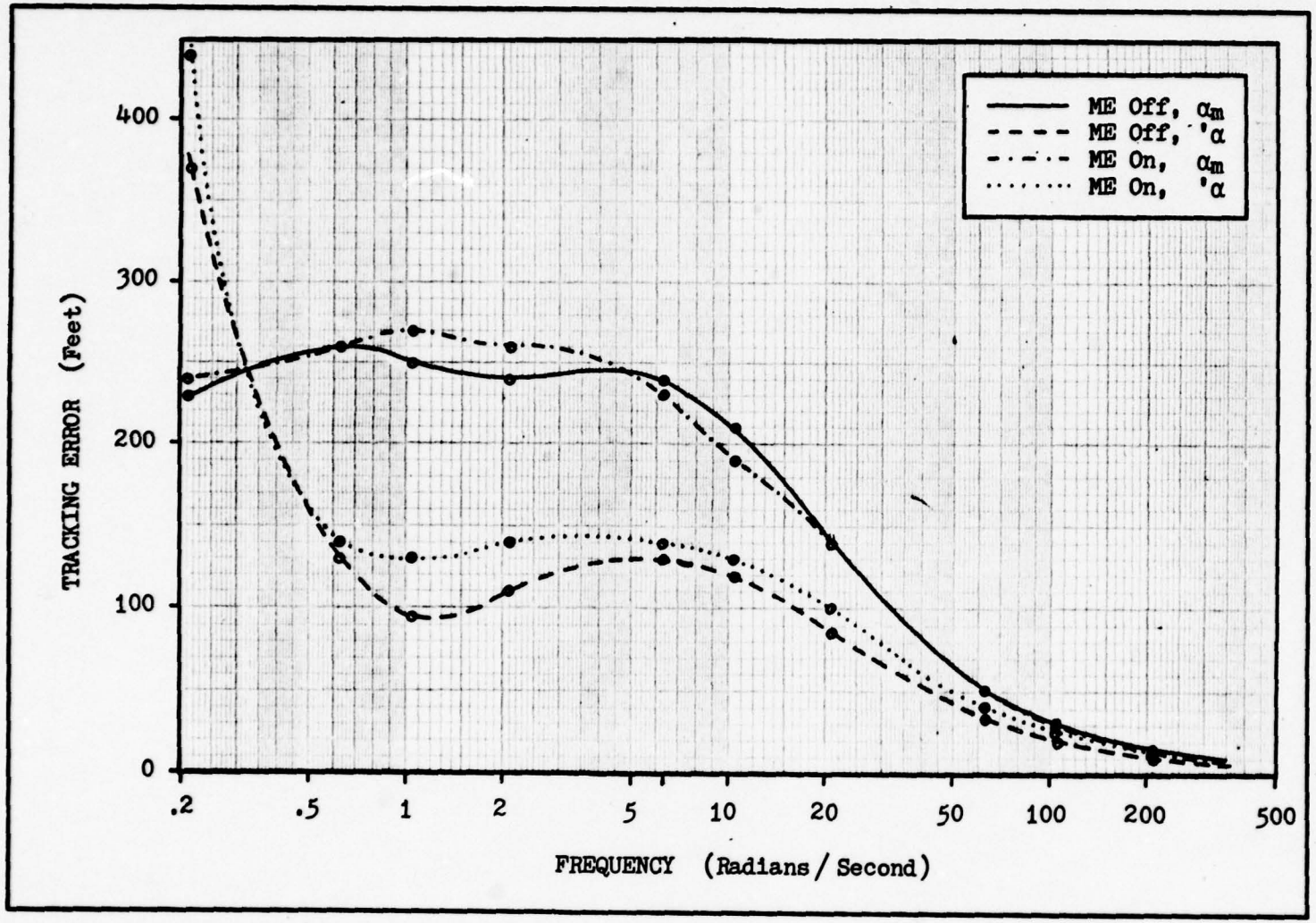


Figure 19. Peak target tracking error response of YF-16 flight control systems.

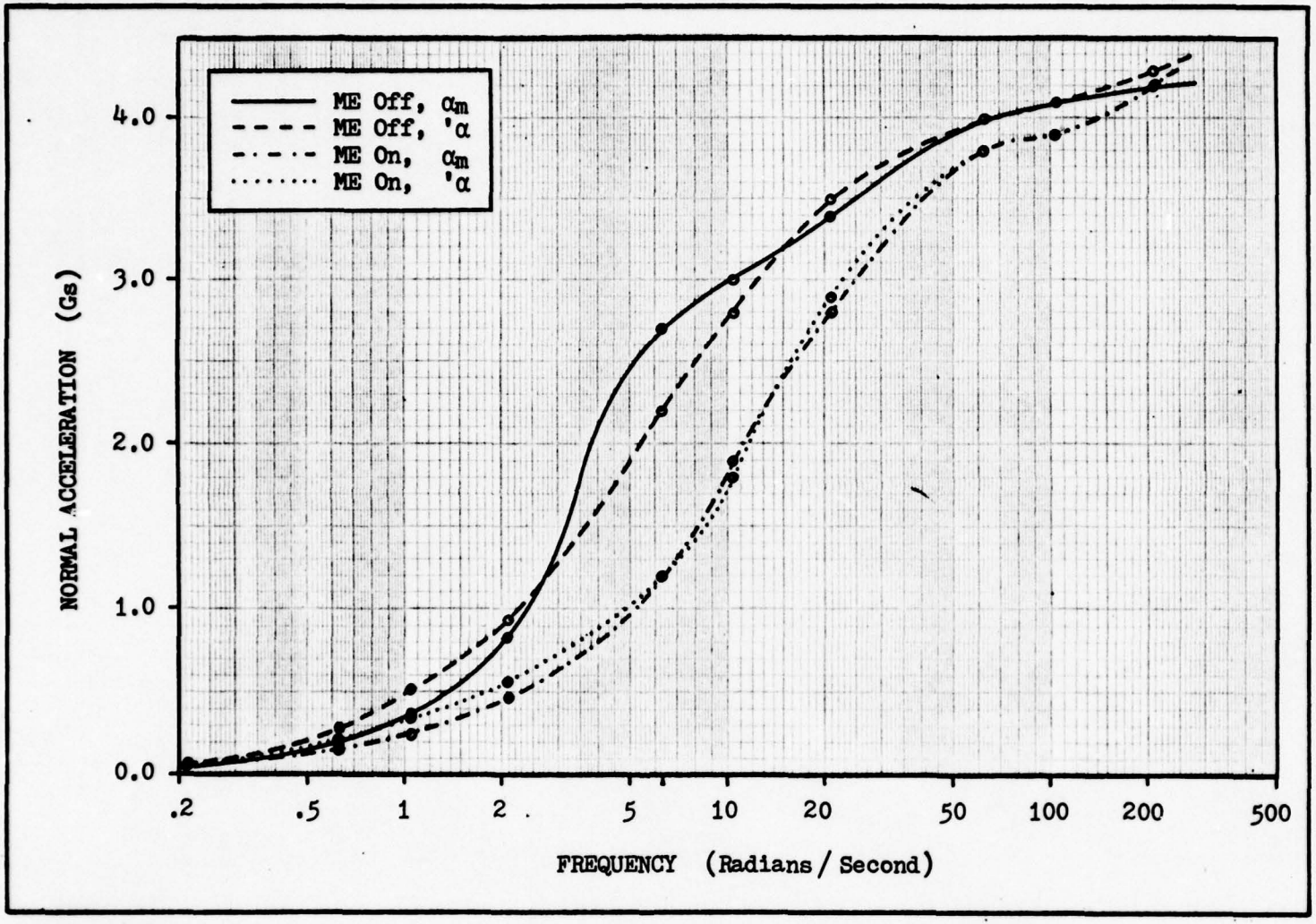


Figure 20. Peak normal acceleration response of YF-16 flight control systems.

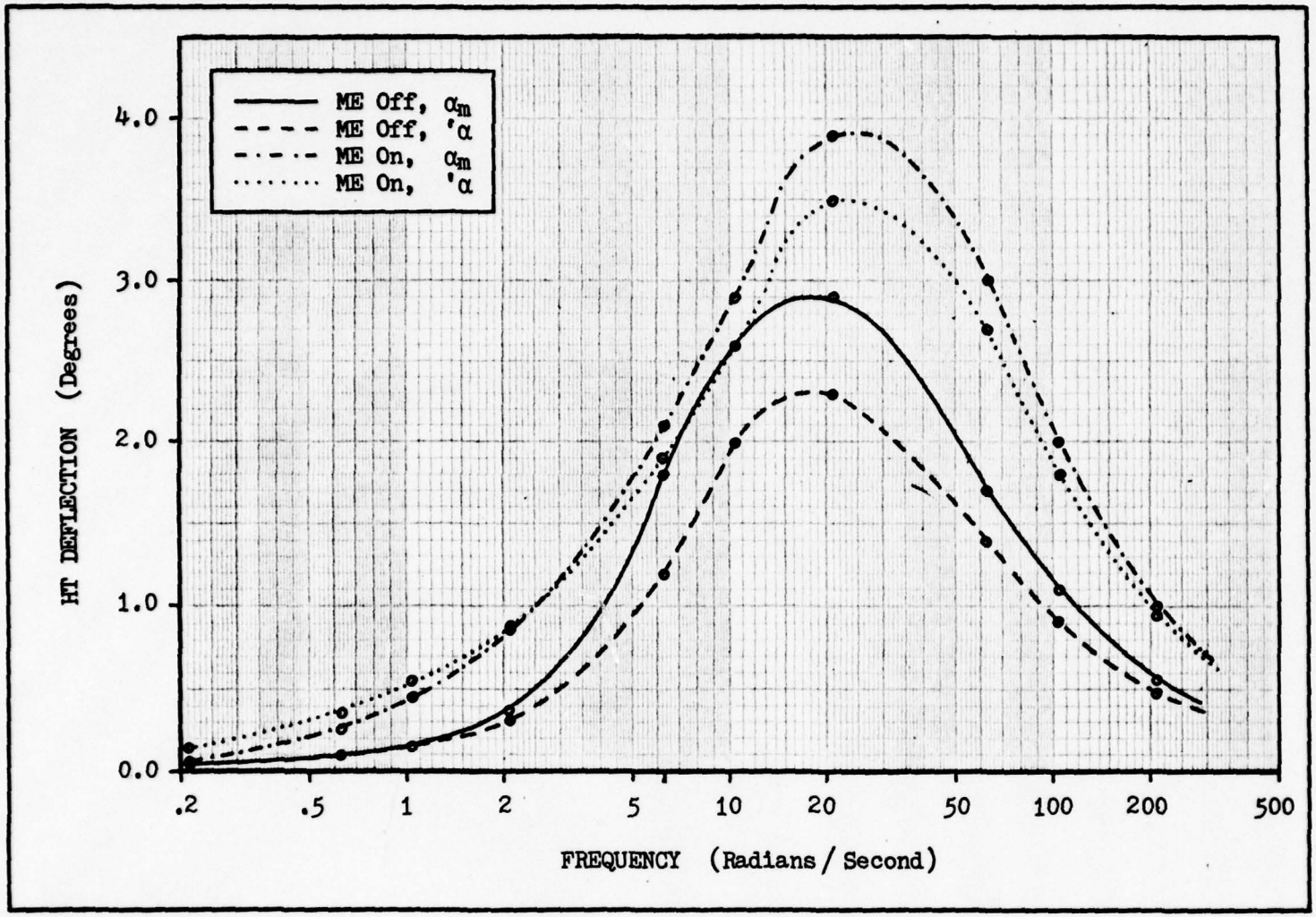


Figure 21. Peak horizontal tail deflection of YF-16 flight control systems.

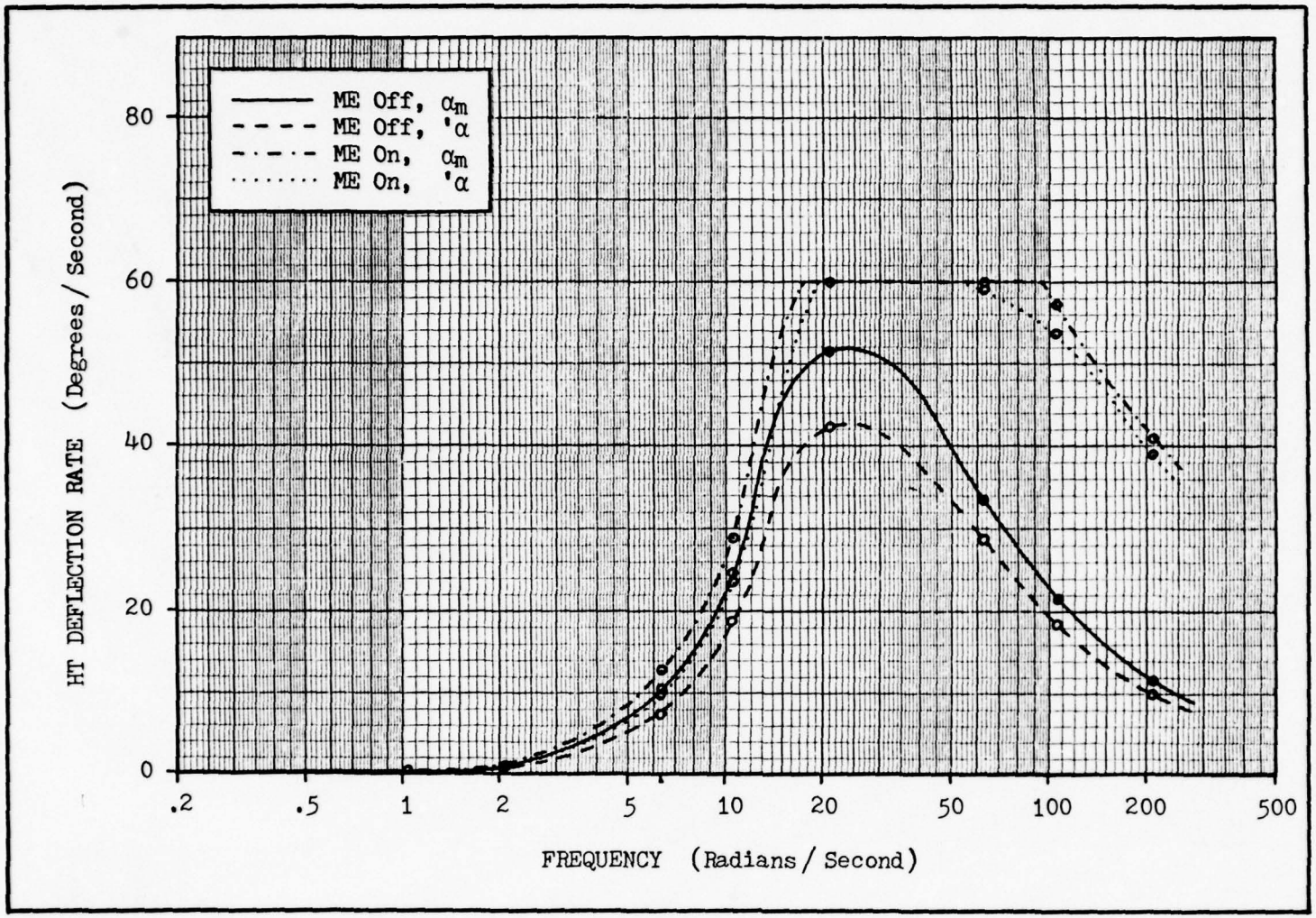


Figure 22. Peak horizontal tail deflection rate of YF-16 flight control systems.

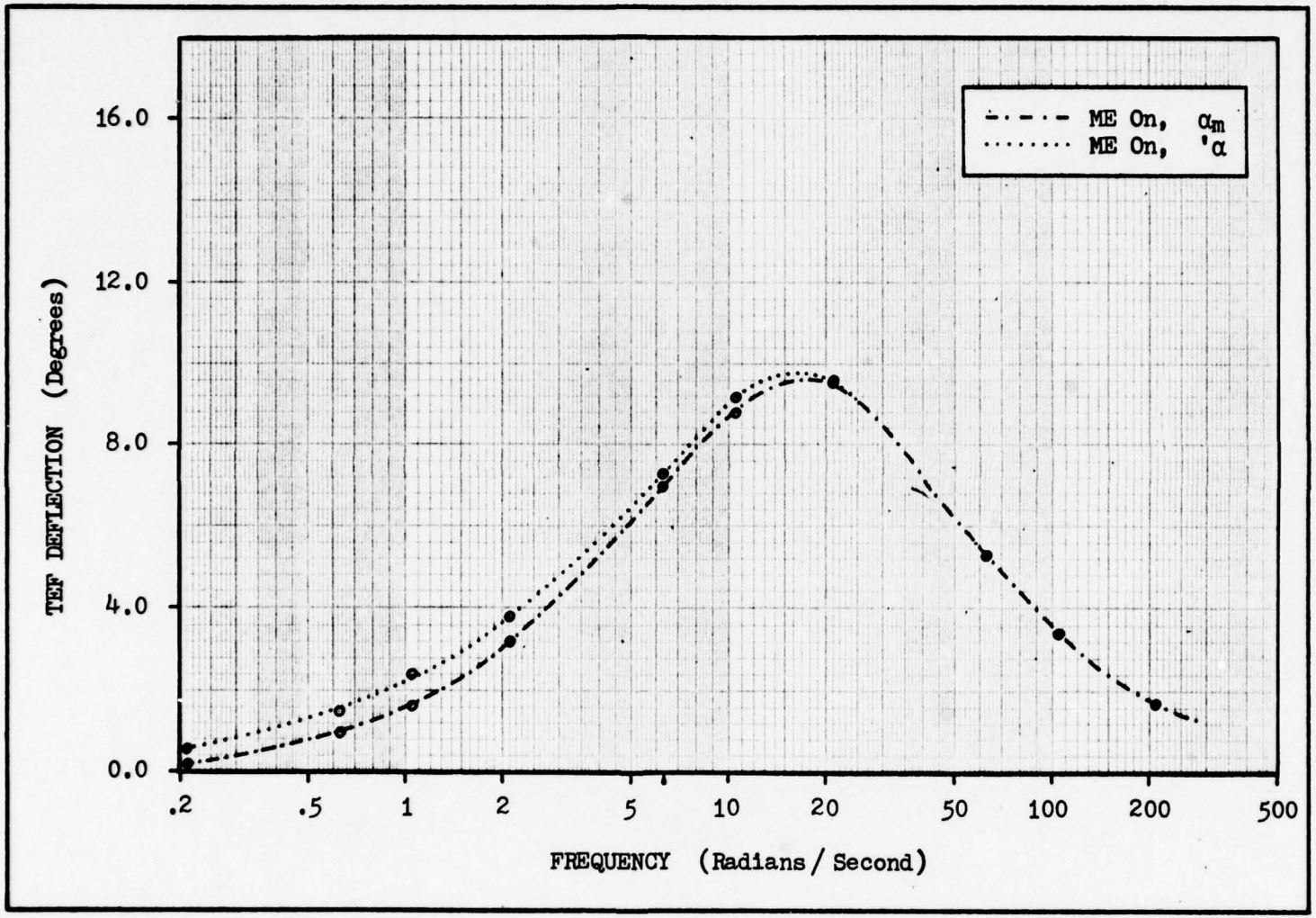


Figure 23. Peak trailing-edge flaperon deflection of YF-16 flight control systems.

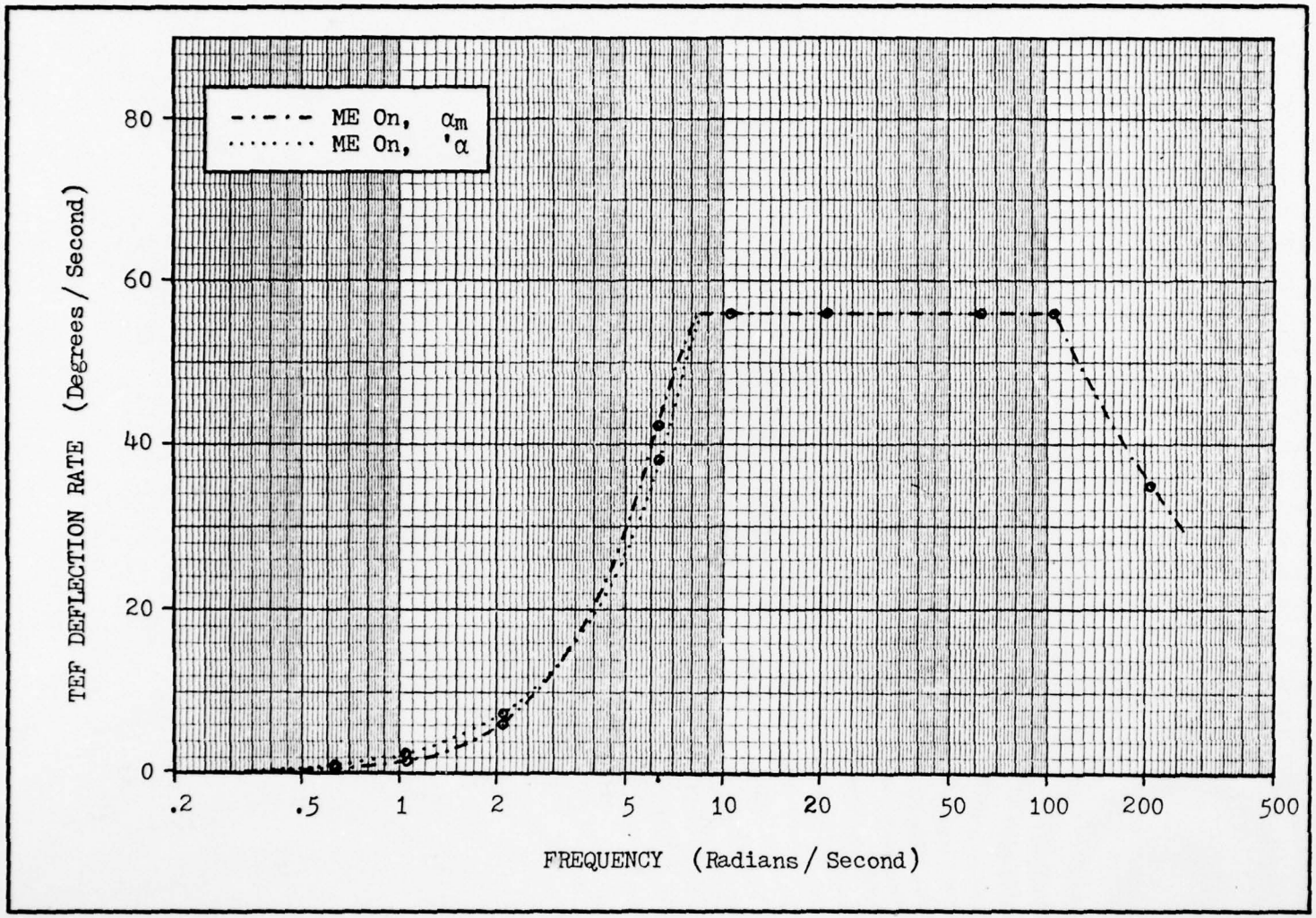


Figure 24. Peak trailing-edge flaperon deflection rate of YF-16 flight control systems.

IV. Flight Control System Design and Analysis

Chapter Overview

In this chapter, a flight control system design is presented. The design objective is first addressed, followed by a discussion of the design approach alternatives that were attempted. The range of applicability of the rigid-body assumption for the longitudinal axis of the YF-16 is then briefly discussed. This is done to provide some insight as to the limitations which must be imposed on selection of the dominant closed-loop eigenvalues.

The chosen design methodology utilizes a matrix representation of the aircraft equations of motion, and therefore a set of state-space equations - including all the required measurable outputs - is determined. Of the several possible feedback configurations that were examined, a pitch rate command system is selected and modeled in matrix format. Detailed modeling of the rejected systems is contained in Appendix F.

The transfer functions of interest are determined by employing Cramer's Rule, and then briefly analyzed. An iterative approach to finding acceptible solutions to these transfer functions is used to derive the required gains in two design examples. The primary design is simulated with both pilot and disturbance inputs, and compared to the simulations in Chapter III. Both analytical and empirical frequency response data is also presented. The secondary

design is simulated for discrete gust input only, to compare its performance with the primary design.

Design Objective

The first step in the design of any control system must be the definition of system performance requirements - a design objective. In this thesis, that design objective is the development of a flight control system that improves the tracking performance and disturbance rejection properties of the aircraft, without degrading overall flying or handling qualities.

There are a few undesirable characteristics of the previously examined Maneuver Enhancement system that should be avoided in the design, if possible. As mentioned in Chapter III, operation of the aircraft at critical attack angles causes a non-zero output from the angle-of-attack limiter, resulting in increasing reductions in pilot command authority. As the ME system is not affected by this limiter, increased pilot command levels result in large flaperon deflections. These large deflections result in increased overall drag at a flight condition where maximum aircraft performance is essential. It is therefore desirable to eliminate this problem in the design.

Also mentioned in Chapter III is the fact that the trailing-edge flaperon power actuators are too quickly rate saturated. A pilot command in excess of two Gs results in actuator rate saturation and subsequent degradation of aircraft performance with increased pilot command levels. It

would be most desirable to maintain flaperon effectiveness over the entire range of pilot command authority.

A third difficulty with the ME system is the interim pause in G-onset caused by a sudden change in flaperon deflection rate. As previously discussed, this is the point of transition from flaperon induced translation to horizontal tail induced rotation of the aircraft. A softening of this transition point is a desirable design feature.

Design Approach Alternatives

The intent of this section is to provide some background and rationale for the design approach presented in this thesis. Many hours were invested in attempts to use other methods - each attempt resulting in failure for one reason or another. The selected approach, straightforward though iterative in nature, was the only approach that produced an acceptable design. In the paragraphs that follow, each of the methods attempted is briefly discussed.

Root Locus. A classical design approach, this method was tried as a first attempt toward determining an acceptible design. It provides visibility into the locations of poles and zeros and permits easy incorporation of dynamic feedback compensation. However, although it can be applied to multiple-output systems by appropriate modeling and successive feedback loop closure, it does not lend itself well to multiple-input systems. For a two-input system, each half of the system must be designed separately, and the designer has

little or no feel for the performance of the composite system.

Modal Control. This approach can be easily applied to systems with any number of inputs or outputs. Also, the desired closed-loop eigenvalues can be selected according to a model system. One problem encountered with this method, however, is the need to make all states available for feedback. This requires the design of a first-order observer to "observe" the internal state of the second-order servos (see Appendix I). In addition, it is very difficult to implement dynamic compensation - if desired - using this method. The fatal difficulty, however, is the fact that there is no positive control over zero locations. As a result, although it was not difficult to design a system that responded well to pilot commands, no way was found to design a system to reject disturbances.

Optimal Control. This method, also directly applicable to multiple-input multiple-output systems, was attempted using a Quadratic Performance Index. As with modal control, access to all system states is required - in this case, for a solution to the algebraic Ricatti Equation. This method, also, is based upon feedback of fixed-gain multiples of system states, and therefore dynamic compensation to increase closed-loop system flexibility is extremely difficult to implement.

A frequent obstacle encountered when attacking the optimal servo problem is the selection of the weighting matrices.

A related drawback is the lack of positive control over placement of zeros, as well as the limited range of locations available. These problems, when combined perhaps with an insufficient knowledge of the design or application theory, prevented the design of a system that met the specified disturbance rejection requirements.

State Variable Feedback (Single Input). This method not only permits the assignment of eigenvalues by designing to a selected model, but also allows the designer to observe and predict the effect of system gain changes on zero locations. Analysis of the transfer functions of interest, when derived in general terms, indicates the relative influence of each gain on each factor of the characteristic and numerator equations. The obvious drawback of this approach, as with the root locus method, is the problem of designing each "half" of the two-input system separately - resulting in a composite system with unknown characteristics.

Limited State Feedback (Dual Input). This technique is simply a reduced form of full-state feedback with the added complexity introduced by modeling the complete two-input system with feedback to each input. This method may or may not allow assignment of eigenvalues, depending upon the feedback enployed. It does, however, generally allow sufficient flexibility to provide acceptable pole locations. In addition, transfer functions can be derived in general terms to permit the assessment of the impact of system gain values

on zero locations.

The primary drawback of this approach is the sheer volume of algebraic manipulations that are required to solve for the transfer functions - the extent of effort increasing exponentially with the system order. The method does, however, allow the addition of cascade and feedback compensation, which provides additional flexibility - at the cost of increasing the order of the system.

The limited state feedback approach is the design technique that produced the best results. No attempt is made to exactly specify eigenvalue locations; instead, a solution is sought in an iterative manner with the intent of determining the system gains that result in poles and zeros being placed in an acceptable envelope. The remaining portion of this chapter details how this approach is used in designing a flight control system that meets the performance requirements.

Limitation of the Rigid-Body Assumption

When deciding upon a desired or model closed-loop characteristic equation, the placement of the dominant eigenvalues is perhaps the most important consideration. The position of these eigenvalues largely determines the passband of the system - discounting the affect of zeros, of course. If dominant pole placement is such that this passband extends sufficiently high in frequency to allow sensitivity to unmodeled body bending modes, rigid-body simulation results are no longer valid.

In designing a flight control system for a high performance aircraft, there is a tendency to increase the open-loop natural frequency to permit a faster response time. The farther the dominant poles are moved from the origin, the faster the system responds to an input. There are several physical limits that must be observed, however, such as aircraft structure, control surface hinge moments, maximum actuator rates, handling quality, and sensitivity to body bending modes.

There are many generally accepted guidelines to aid in the selection of dominant eigenvalues for the purpose of attaining reasonable handling qualities. One method, expressed as a mapping of short period natural frequencies against damping ratio, is known as the Cornell Aeronautical Lab (CAL) "Thumbprint" (Ref 22). This envelope, shown in Figure 25, was derived from extensive handling quality data obtained with variable stability aircraft. It is intended for use in the design of flight control systems for fighter aircraft. Caution must be exercised in its use, however, for if a flight control system is designed such that it is inadvertently sensitive to a bending mode, the aircraft could become unstable under certain conditions. Therefore, it is important to ensure that the frequencies of the structural bending modes are well outside the proposed closed-loop system passband.

A partial list of structural bending modes for the YF-16 is given in Table I (Ref 8). Note that the frequency of the

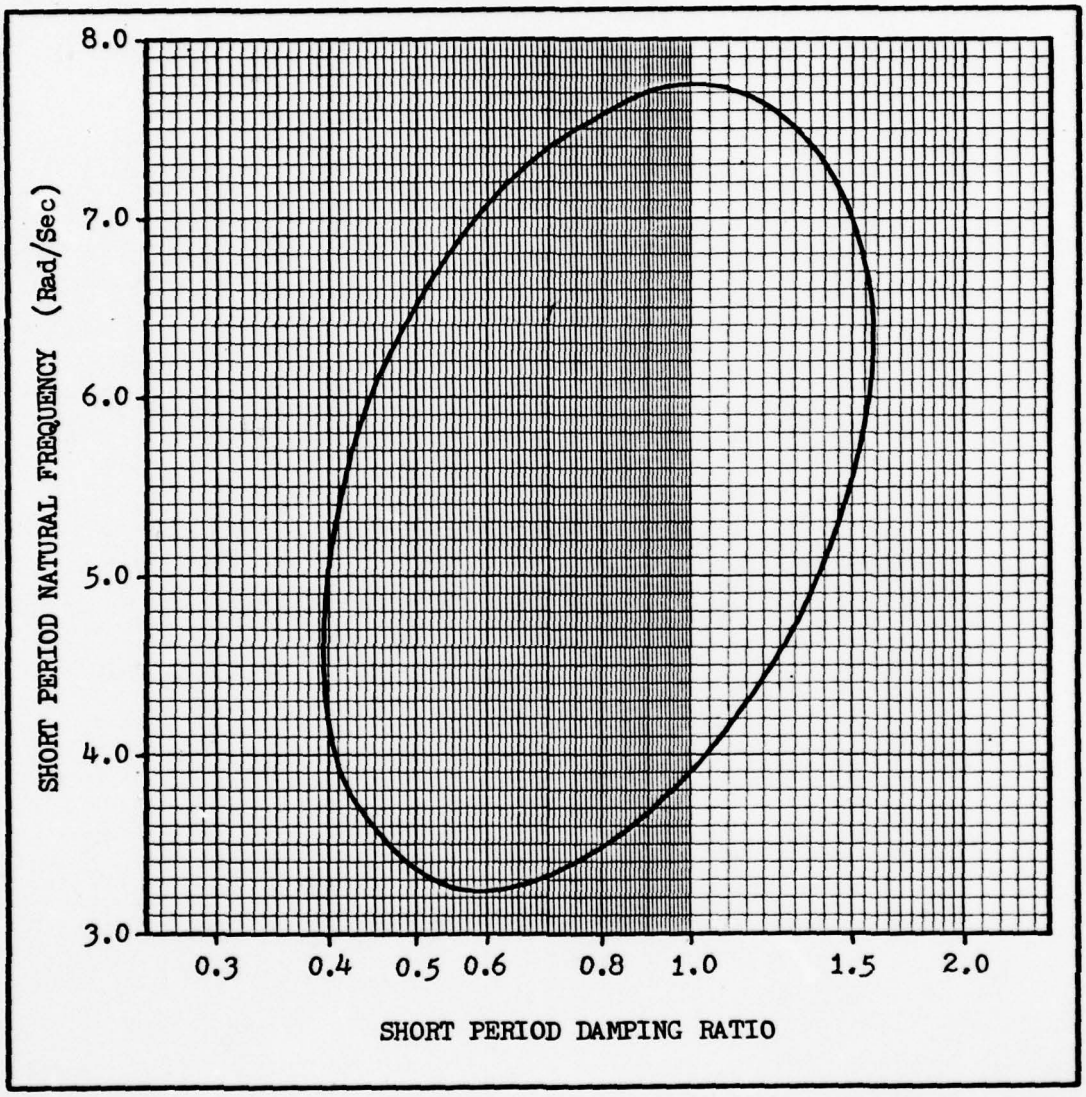


Figure 25. Cornell Aeronautical Laboratory (CAL) Thumbprint (Ref 22).

TABLE 1 - Symmetric Aircraft Modes

Mode	Freq (Hz)	Freq (r/s)
First Wing Bending	4.92	30.91
Fuselage Vertical Bending	12.33	77.47
Second Wing Bending & Second Fuselage Bending	20.77	130.5
Second Wing Bending	23.57	148.1
Horizontal Tail Bending	25.40	159.6
Horizontal Tail Bending	32.56	204.6
Wing Torsion	38.01	238.8
Flaperon Rotation	45.93	288.6

first wing bending mode is approximately 31 radians per second, and the frequency of the first fuselage bending mode is approximately 77 radians per second. For longitudinal analyses, the fuselage bending modes are generally of greatest interest, and, in many instances, the second structural modes may be dominant. For this aircraft, the second and third modes are dominant, indicating a relatively sound fuselage (Ref 8). From this data, it is assumed that placement of dominant eigenvalues within the CAL Thumbprint will not result in unacceptable sensitivity to any of the bending modes.

State-Space Equations for the Aircraft

For the purposes of design, a two-degree-of-freedom, or Short Period model for the aircraft is used. This simplification is valid for modern, high-speed fighter aircraft, as small pitch perturbations have a negligible effect on forward velocity (Ref 1). For the flight condition of interest, this model, derived in Appendix C, can be written as

$$\begin{bmatrix} \dot{\alpha} \\ \dot{q} \end{bmatrix} = \begin{bmatrix} -2.5194 & 0.98255 \\ 12.339 & -2.4853 \end{bmatrix} \begin{bmatrix} \alpha \\ q \end{bmatrix} + \begin{bmatrix} -.28115 & 0.3637 \\ -42.317 & 6.1322 \end{bmatrix} \begin{bmatrix} \delta_h \\ \delta_f \end{bmatrix} + \begin{bmatrix} -2.5194 \\ 12.339 \end{bmatrix} \alpha_g \qquad (24)$$

The longitudinal quantities that are measurable and available for feedback are angle-of-attack, pitch rate, and normal acceleration. These outputs must now be expressed in terms of

the two states and input quantities of Eqn 24. The simplest of the three is pitch rate, which is one of the two aircraft states. It may be written directly as

$$\begin{bmatrix} q_s \end{bmatrix} = \begin{bmatrix} 0 & 1 \end{bmatrix} \begin{bmatrix} \dot{\alpha} \\ q \end{bmatrix} + \begin{bmatrix} 0 & 0 \end{bmatrix} \begin{bmatrix} \delta_h \\ \delta_f \end{bmatrix} + \begin{bmatrix} 0 \end{bmatrix} \alpha_g \qquad (25)$$

Normal acceleration can be expressed as a linear combination of the aircraft states. Referring to Figure 2 in Chapter II, the sum of the forces in the Z-direction may be expressed as (Ref 1),

$$\sum \Delta F_Z = m(\dot{w} - U_o q) \qquad (26)$$

where 'm' is the mass of the aircraft. Recall that the force acting on an object is equal to the product of the mass of that object and its acceleration. If both sides of this equation are divided by the mass, an expression for acceleration in the Z-direction results. Setting 'A_Z' equal to the sum of these accelerations, the expression becomes

$$A_Z = \dot{w} - U_o q \qquad (27)$$

Referring to Eqn 10, if U_o is factored from the right side of the expression, then

$$A_Z = U_o(\dot{\alpha} - q) \qquad (28)$$

defines normal acceleration, positive downward, at the CG of the aircraft. The normal accelerometers in the YF-16, however, are not located at the CG, but rather 12.95 feet

further forward (see Appendix E for this calculation). As positive aircraft rotation results in an upward movement of these accelerometers, they sense pitching accelerations in addition to normal accelerations. The linear magnitude of these angular pitch accelerations at the accelerometer location is equal to the product of the acceleration, q, and the length of the moment arm, 12.95 feet. Reversing the terms on the right side of Eqn 28, this composite measurement - which is still referred to as normal acceleration - is now defined as

$$A_{N_S} = U_o(q - \dot{\alpha}) + 12.95\dot{q} \tag{29}$$

and the acceleration is positive upward.

Equation 29 may now be expanded in terms of the states and input quantities given in Eqn 24. With U_o = 893.5 ft/sec for this flight condition, this expansion results in

$$\begin{aligned} A_{N_S} = {} & 893.5q - 893.5(-2.5194\,\dot{\alpha} + .98255\,q - .28115\,\delta_h \\ & + .3637\,\delta_f - 2.5194\,\alpha_g) + 12.95(12.339\,\dot{\alpha} - 2.4853\,q \\ & - 42.317\,\delta_h + 6.1322\,\delta_f + 12.339\,\alpha_g) \end{aligned} \tag{30}$$

Performing the multiplications and summing like terms yields

$$A_{N_S} = 2410.9\,\dot{\alpha} - 16.595\,q - 296.80\,\delta_h - 245.56\,\delta_f + 2410.9\,\alpha_g \tag{31}$$

From Eqn 29, the dimension of A_{N_S} at this point is ft-deg/sec-sec, as all angles are in degrees, and the forward velocity is in feet per second. As the normal accelerometers sense A_{N_S} in Gs, it is appropriate to multiply Eqn 31 by some

conversion factor. Since one radian is equal to 57.296 degrees, and at sea level, g = 32.177 ft/sec-sec, the dimensional conversion factor is

$$CF\left[\frac{g}{\text{ft-deg}/\text{sec-sec}}\right] = (32.177)(57.296) = 1843.6 \qquad (32)$$

Dividing by this factor, normal acceleration (in Gs) may be written as

$$\begin{bmatrix} A_{N_s} \end{bmatrix} = \begin{bmatrix} 1.3077 & -.0090014 \end{bmatrix} \begin{bmatrix} {}'\alpha \\ q \end{bmatrix} + \begin{bmatrix} -.16099 & -.13320 \end{bmatrix} \begin{bmatrix} \delta_h \\ \delta_f \end{bmatrix} + \begin{bmatrix} 1.3077 \end{bmatrix} \alpha_g \qquad (33)$$

The third output to be derived is attack angle. As the aircraft is modeled to fly through other than still air, measurable angle-of-attack is not the equivalent of stability-axis perturbation attack angle as given in Eqn 24. The relationship between these angles, as previously derived, is

$$\alpha_m = {}'\alpha + \alpha_g \qquad (17)$$

There is an additional complication due to the affect of the location of the sensor itself. As with the normal acceleration defined in Eqn 28, attack angle has been defined as a measurement at the CG of the aircraft. The angle-of-attack sensors on the YF-16 are located on the nose, however, approximately 22.28 feet forward of the CG, as determined in Appendix E. Thus, these sensors, which measure the angle of

incidence of the moving air, are affected by the pitch rate (angular velocity) of the aircraft due to rotation.

One way to determine an expression for the effect of pitch rate on the sensor is to view that motion in terms of velocities. The linear vertical velocity contribution of the angular velocity at the sensor location resulting from aircraft rotation is simply the product of the magnitude of that velocity and the distance from the CG. The vertical velocity of the sensor, positive downward, relative to the earth, may now be given as

$$w_s = w - 22.28q \tag{34}$$

where pitch rate is measured in radians per second. Dividing each term in this expression by the equilibrium forward velocity, U_o, results in an equation defining the angular measurement of the sensor, relative to the earth. This may be written as

$$\alpha_s = '\alpha - 22.28(q/U_o) \tag{35}$$

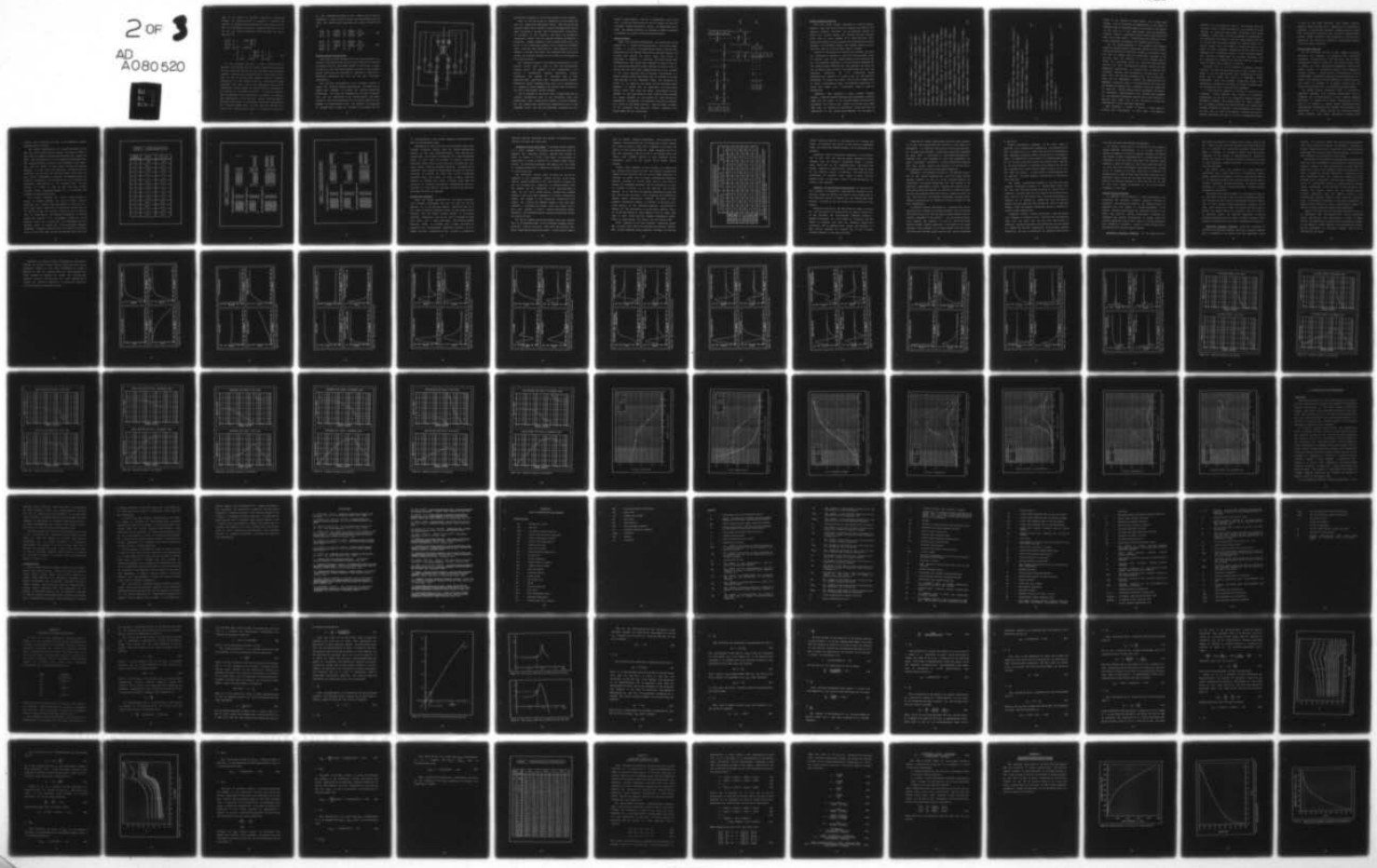
where attack angle is dimensioned in radians. In a manner analogous to the derivation of Eqn 17, the measurment of attack angle at the sensor location relative to the surrounding air can be expressed as

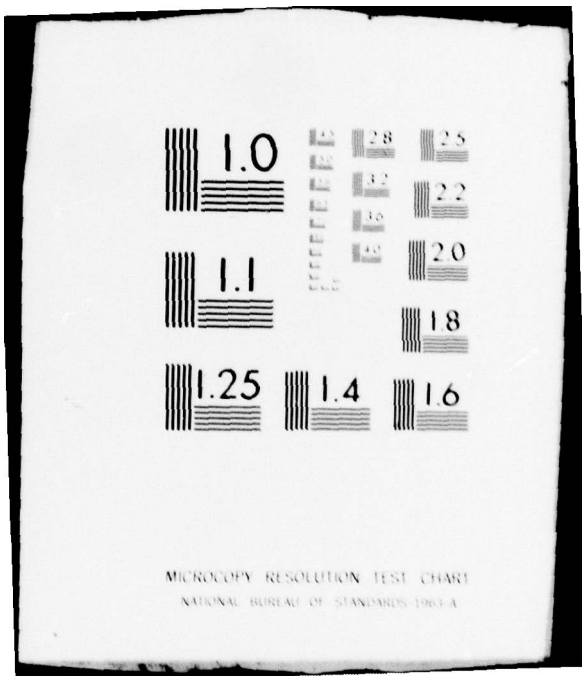
$$\alpha_s = '\alpha - .02494q + \alpha_g \tag{36}$$

where the velocity of the aircraft is substituted for U_o, and angle-of-attack is again dimensioned in radians. As pitch

AD-A080 520 AIR FORCE INST OF TECH WRIGHT-PATTERSON AFB OH SCHOO--ETC F/G 1/3
USING VERTICAL GUST ALLEVIATION TO IMPROVE THE TARGET TRACKING --ETC(U)
AUG 79 E R MOLNER
UNCLASSIFIED AFIT/GGC/EE/79-5 NI

2 OF 3
AD A080 520




1.0
1.1
1.25
1.4
1.6
2.8
2.5
2.2
2.0
1.8
MICROCOPY RESOLUTION TEST CHART
NATIONAL BUREAU OF STANDARDS 1963-A

rate in the system is actually measured in degrees per second, and angle-of-attack is measured in degrees, the equation is appropriately dimensioned for both states with no need for dimensional conversion. Combining Equations 25, 33, and 36, the system measurable output equation may now be expressed as

$$\begin{bmatrix} \alpha_s \\ q_s \\ A_{N_s} \end{bmatrix} = \begin{bmatrix} 1 & -.02494 \\ 0 & 1 \\ 1.3077 & -.0090014 \end{bmatrix} \begin{bmatrix} \alpha \\ q \end{bmatrix} + \begin{bmatrix} 0 & 0 \\ 0 & 0 \\ -.16099 & -.13320 \end{bmatrix} \begin{bmatrix} \delta_h \\ \delta_f \end{bmatrix} + \begin{bmatrix} 1 \\ 0 \\ 1.3077 \end{bmatrix} \alpha_g \qquad (37)$$

In the following sections, a system configuration is selected and modeled, and the transfer functions of interest for that system are derived. So that the model and associated transfer functions may be determined in a more general form, Eqns 24 and 37 are used with symbolic entries - requiring substitution of the actual values for the selected flight condition (0.8 Mach @ SL) at the appropriate time. Use of unspecified entries allows the derived transfer functions to be applied to any flight condition - or even any aircraft that is modeled in short period form. It permits, in general, the substitution of any two-state system, which includes a discrete state model. By converting a continuous system model to a discrete system model for some specified sampling rate (using the FORTRAN program YFCCV, as described in Appendix

K), the technique presented in this Chapter may be used to accomplish a direct digital design. The generalized aircraft state and output matrix equations are given in Eqns 38 and 39.

$$\begin{bmatrix} \dot{\alpha} \\ q \end{bmatrix} = \begin{bmatrix} a & b \\ c & d \end{bmatrix} \begin{bmatrix} \dot{\alpha} \\ q \end{bmatrix} + \begin{bmatrix} e & f \\ g & h \end{bmatrix} \begin{bmatrix} \delta_h \\ \delta_f \end{bmatrix} + \begin{bmatrix} i \\ m \end{bmatrix} \alpha_g \qquad (38)$$

$$\begin{bmatrix} \alpha_s \\ q_s \\ A_{N_s} \end{bmatrix} = \begin{bmatrix} 1 & -D \\ 0 & 1 \\ n & p \end{bmatrix} \begin{bmatrix} \dot{\alpha} \\ q \end{bmatrix} + \begin{bmatrix} 0 & 0 \\ 0 & 0 \\ u & v \end{bmatrix} \begin{bmatrix} \delta_h \\ \delta_f \end{bmatrix} + \begin{bmatrix} 1 \\ 0 \\ x \end{bmatrix} \alpha_g \qquad (39)$$

Selected System Configuration

Three basic system configurations were investigated in an attempt to determine which would be most effective in meeting the design criteria. The system chosen on that basis is shown in Figure 26. For reference purposes, details of the rejected system variations are contained in Appendix F, along with a discussion explaining why each did not meet the design requirements.

The selected configuration, the q-command system in Figure 26, contains cascade compensation, and makes use of simple gain feedback to produce the desired closed-loop performance. All gains and compensation are given in general form, and are determined in the design process. The power actuators have been eliminated from the system model for the purpose of simplification. They are, however, not forgotten or assumed away, as they are included in the system for all

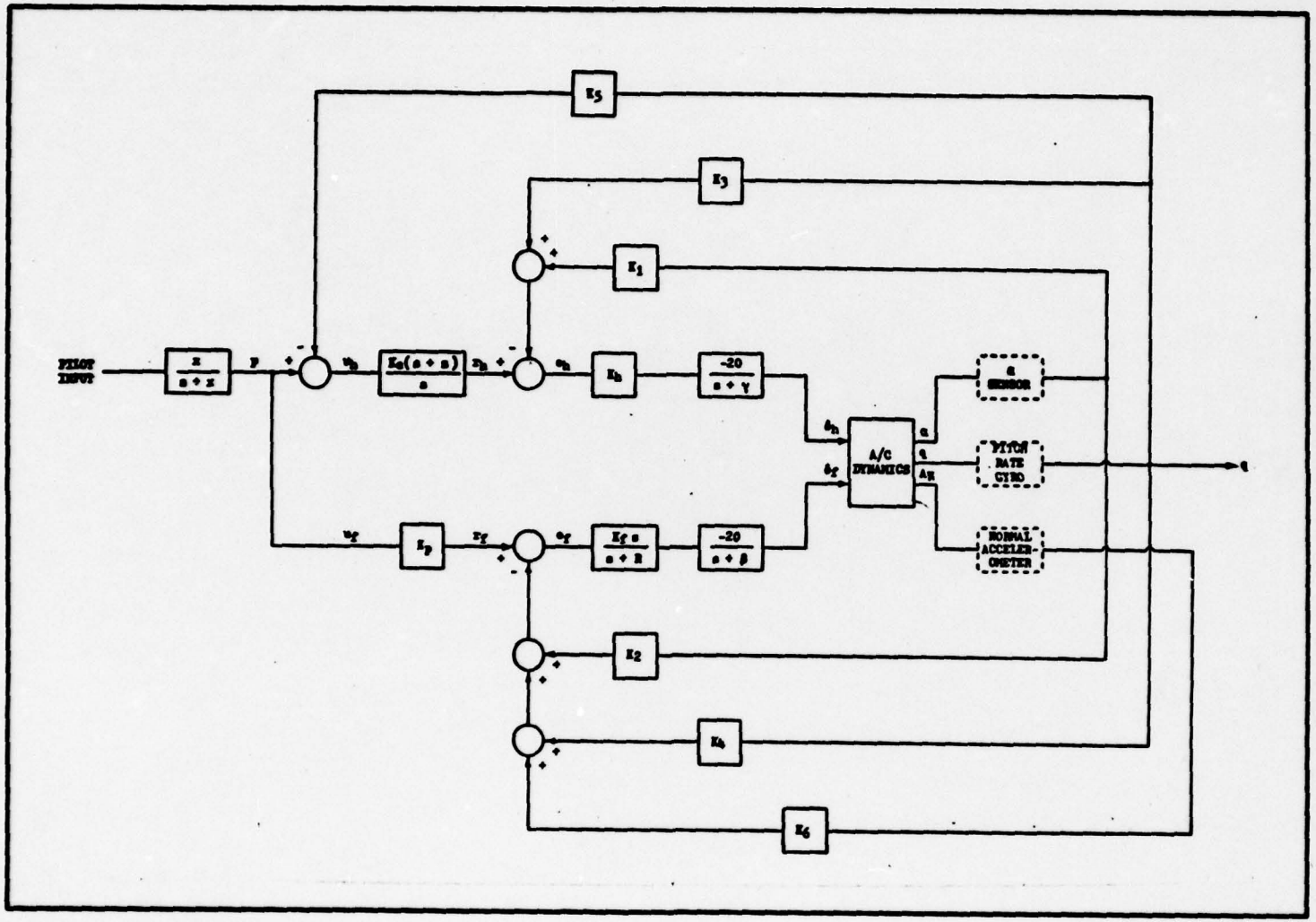


Figure 26. Selected pitch rate command flight control system configuration.

simulations presented in the latter portion of this chapter.

Each of the two servos is modeled as a first-order lag with an unspecified eigenvalue. Recall that the servos and actuators each have a resistive output available which can be used to produce a voltage that is proportional to position. As currently on the aircraft, each servo is actually an integrating device, with the required feedback provided by a mechanical linkage. Removal of this linkage would return the servo to its integrating posture, and an electrical feedback could close the loop, modifying the servo dynamics so as to produce a desired first-order lag. Although this flexibility exists, the original dynamics of the servos are maintained in the design solution.

One important feature of the system configuration is the washout circuit that is used to feed the trailing-edge flaperon servo. The purpose of this compensation is to prevent a steady-state flaperon deflection, thereby eliminating the problem of increased drag in high angle-of-attack conditions. This technique permits flaperon deflection during transients only, such as in turbulence or in response to pilot commands, but ensures that the horizontal tail is the primary control surface.

Also of interest is the use of both a proportional and an integral feed-forward path to the horizontal tail. The proportional path allows quick response to pilot commands, and the integral path ensures zero steady-state error in the commanded pitch rate. The trailing-edge flaperons are com-

manded proportionally, through an unspecified gain. Pitch rate is also fed back inside of the P+I network to allow for increased design flexibility. Lastly, an unspecified first-order lag command prefilter is included to smooth transients in commands and improve handling characteristics.

System Equation

Given the selected configuration, the system must now be modeled as a single matrix expression. This can be accomplished in a fairly straightforward fashion, step-by-step, beginning with the modeled short period aircraft dynamics and working back towards the system input. This effort is described in Appendix G, with only the final system model presented here. The system state equation is given in Eqn 40, and the system measurable output equation is given in Eqn 41. Notice that the first-order command prefilter is not included in the state equation. This is because the prefilter is a simple cascade signal conditioner that is intended to provide rate-limiting of the commanded input, and therefore has little or no impact on the design of the remaining system dynamics. It should also be noted that the attack angle sensor, pitch rate gyro, and normal accelerometer are not modeled in the state equation. They have not been included for design purposes as the dynamics of these devices are essentially non-dominant, and therefore they have a negligible affect on the design solution. They are shown in Figure 26 for reference only. They are, however, included in the system model for all simulations.

$$\begin{bmatrix} \dot{'\alpha} \\ \dot{q} \\ \dot{\delta}_h \\ \dot{x} \\ \dot{\delta}_f \\ \dot{y} \end{bmatrix} = \begin{bmatrix} a & b & e & 0 & f & 0 \\ c & d & g & 0 & h & 0 \\ 20K_1K_h & 20K_h(K_cK_5 + K_3 - .025K_1) & -\gamma & 0 & 0 & -20zK_hK_c \\ 0 & 0 & 0 & 0 & 1 & 0 \\ 20K_f(K_2 + nK_6) & 20K_f(K_4 - .025K_2 + pK_6) & 20uK_6K_f & -R\beta & (20vK_6K_f - R - \beta) & 0 \\ 0 & -K_5 & 0 & 0 & 0 & 0 \end{bmatrix} \begin{bmatrix} '\alpha \\ q \\ \delta_h \\ x \\ \delta_f \\ y \end{bmatrix}$$

$$+ \begin{bmatrix} 0 \\ 0 \\ -20K_hK_c \\ 0 \\ -20K_fK_p \\ 1 \end{bmatrix} p + \begin{bmatrix} i \\ m \\ 20K_1K_h \\ 0 \\ 20K_f(K_2 + xK_6) \\ 0 \end{bmatrix} \alpha_g \qquad (40)$$

$$\begin{bmatrix} \alpha_s \\ q_s \\ A_{N_s} \end{bmatrix} = \begin{bmatrix} 1 & -.025 & 0 & 0 & 0 & 0 \\ 0 & 1 & 0 & 0 & 0 & 0 \\ n & p & u & 0 & v & 0 \end{bmatrix} \begin{bmatrix} '\alpha \\ q \\ \delta_h \\ x \\ \delta_f \\ y \end{bmatrix} + \begin{bmatrix} 1 \\ 0 \\ x \end{bmatrix} \alpha_g \qquad (41)$$

System Transfer Functions

With the entire system expressed in a matrix format, Cramer's Rule may now be directly applied to solve for the required transfer functions. As the selected system is a pitch rate control system, the transfer function relating pitch rate to pilot command is of great interest. Also, because the design criteria require the minimization of pitch response to disturbance inputs, the transfer function relating pitch rate to a vertical gust input is needed.

Details of the process of deriving the transfer functions are contained in Appendix H, where the final product, given in general form, is the system characteristic equation and the two numerator equations. As the particular equations for the chosen flight condition are now required, the values of the entries in Eqns 24 and 37 are substituted into them. The resulting expression for the closed-loop system characteristic equation is given in Eqn 42. The numerator expression for pitch rate output with a pilot command input is given in Equation 43, and, the numerator expression for pitch rate output with a disturbance input is given in Equation 44.

Normally, when designing a state variable feedback system, a desired system characteristic polynomial is determined and set equal to the derived system characteristic polynomial on a term by term basis. In this way, each feedback gain is resolved to a particular value such that the eigenvalues of the system being designed are set equal to

$$s^6 + [5.0047 + (\beta + \gamma + R) + 2.664K_fK_6]s^5 + [-5.8622 + 5.0047(\beta + \gamma + R) +$$

$$(\beta\gamma + \beta R + \gamma R) + 4.9243K_fK_6 + 2.664\gamma K_fK_6 + 846.34K_hK_cK_5 - 122.64K_fK_4 + 846.34K_hK_3 -$$

$$7.274K_fK_2 + 122.64DK_fK_2 + 5.623K_hK_1 - 846.34DK_hK_1]s^4 + [-5.8622(\beta + \gamma + R) +$$

$$5.0047(\beta\gamma + \beta R + \gamma R) + R\beta\gamma - 193.25K_fK_6 + 4.9243\gamma K_fK_6 + 2201.7K_hK_cK_5 + 846.34zK_hK_cK_5 +$$

$$846.34(\beta + R)K_hK_cK_5 - 398.74K_fK_4 - 122.64\gamma K_fK_4 + 2201.7K_hK_3 + 846.34(\beta + R)K_hK_3 +$$

$$378.74DK_fK_2 - 138.58K_fK_2 - 7.274\gamma K_fK_2 + 122.64D\gamma K_fK_2 + 845.55K_hK_1 + 5.623(\beta + R)K_hK_1 -$$

$$2201.7DK_hK_1 - 846.34D(\beta + R)K_hK_1 + 2649.5K_hK_fK_cK_6K_5 + 2649.5K_hK_fK_6K_3 + 38.4K_hK_fK_6K_1 -$$

$$2649.5DK_hK_fK_6K_1]s^3 + [-5.8622(\beta\gamma + \beta R + \gamma R) + 5.0047R\beta\gamma - 193.25\gamma K_fK_6 + 2201.7zK_hK_cK_5 +$$

$$846.34(R\beta + z\beta + Rz)K_hK_cK_5 - 398.74\gamma K_fK_4 + 846.34R\beta K_hK_3 + 2201.7(\beta + R)K_hK_3 - 138.58\gamma K_fK_2 +$$

$$5.623R\beta K_hK_1 - 846.34DR\beta K_hK_1 + 398.74D\gamma K_fK_2 + 2201.7(\beta + R)K_hK_cK_5 + 845.55(\beta + R)K_hK_1 -$$

$$2201.7D(\beta + R)K_hK_1 + .33393K_hK_fK_cK_6K_5 + 2649.5zK_hK_fK_cK_6K_5 + .33393K_hK_fK_6K_3 + 2649.5K_hK_fK_6K_1 -$$

$$.33393DK_hK_fK_6K_1 - 5466.6K_hK_fK_cK_5K_2 + 5466.6K_hK_fK_4K_1 - 5466.6K_hK_fK_3K_2]s^2 +$$

$$[-5.8622R\beta\gamma + 2201.7(R\beta + z\beta + Rz)K_hK_cK_5 + 846.34R\beta zK_hK_cK_5 + 2201.7R\beta K_hK_3 + 845.55R\beta K_hK_1 -$$

$$2201.7DR\beta K_hK_1 + .33393zK_hK_fK_cK_6K_5 - 5466.6zK_hK_fK_cK_5K_2]s + [2201.7zR\beta K_hK_cK_5] \qquad (42)$$

$$[846.34K_hK_c - 122.64K_fK_p]s^4 +$$

$$[2201.7K_hK_c + 846.34zK_hK_c + 846.34(\beta + R)K_hK_c + 2649.5K_hK_fK_cK_6 - 398.74K_fK_p - 122.64\gamma K_fK_p]s^3 +$$

$$[2201.7zK_hK_c + 2201.7(\beta + R)K_hK_c + 846.34z(\beta + R)K_hK_c + 846.34R\beta K_hK_c + .33393K_hK_fK_cK_6 +$$

$$2649.5zK_hK_fK_cK_6 - 5466.6K_hK_fK_cK_2 + 5466.6K_hK_fK_pK_1 - 398.74\gamma K_fK_p]s^2 +$$

$$[2201.7(R\beta + \beta z + Rz)K_hK_c + 846.34zR\beta K_hK_c + .333393zK_hK_fK_cK_6 - 5466.6zK_hK_fK_cK_2]s +$$

$$[2201.7zR\beta K_hK_c] \qquad (43)$$

$$[12.339]s^5 +$$

$$[12.339(\beta + R + \gamma) + 193.25K_fK_6 + 122.64K_fK_2 - 846.34K_hK_1]s^4 +$$

$$[12.339(R\beta + \beta\gamma + \gamma R) + 193.25\gamma K_fK_6 + 122.64\gamma K_fK_2 - 2649.5K_hK_fK_6K_1 - 846.34(\beta + R)K_hK_1]s^3 +$$

$$[12.339R\beta\gamma - 846.34R\beta K_hK_1]s^2 +$$

$$[0]s + [0] \qquad (44)$$

those of the desired or model system. For a single input system, this is relatively straightforward, as the number of feedback loops is generally equal to the order of the system. In the case of a two input system with non-independent outputs, however, a multiple of each system state may be fed back two or more times - necessitating the solution of non-linear equations to determine the feedback gain values.

For the system proposed in this chapter, five feedback loops are closed around a fifth-order system. As three eigenvalues are modeled as completely variable, the feedback loops are used to modify only the second-order dynamics of the airframe. With the addition of a sixth feedback loop to define the controlled state, the resulting characteristic equation for this configuration contains highly nonlinear polynomial coefficients. A glance at Eqn 42 confirms this statement. Knowing that the equation is sixth order, and that there are thirteen variables, only six of these variables can be independent - leaving the remaining seven as dependent variables. There is the possibility that more than six degrees of freedom exist, implying a potential capability to solve for a desired characteristic polynomial and numerator polynomial simultaneously. This approach was attempted for the numerator polynomial relating pitch rate output to a vertical gust input, but no way was found to solve the resulting set of nine nonlinear equations.

When designing a system to reject a certain input (a vertical gust disturbance, in this case), the numerator

equation is very important. Even in this system, where the numerator gain is fixed (see Eqn 44), the placement of zeros relative to poles can cause large variations in the system response to that input. The mere placement of eigenvalues is not sufficient. The design is further complicated by the need to ensure that the system responds in a desired manner for a second (pilot) input. An attempt to assign locations for the zeros of both numerator polynomials and the poles of the characteristic polynomial, however, would certainly require more degrees of freedom than are available. Therefore, even if a technique for handling the resulting nonlinear equations could be found, there would be no solution.

Assuming that it is not possible to specify a desired location for both the poles and zeros of both transfer functions, it is still very possible that a combination of system gains can be found that results in acceptable system performance. Given the proposed closed-loop system, the flexibility afforded by the number of system variables makes the existence of such a solution quite probable.

A trial-and-error approach is utilized to search for an acceptable design solution. This process is simplified considerably by the use of an interactive computer program. Designated YFSOLVE, the program allows the user to input a set of system variables, and then calculates the closed-loop transfer functions of interest in both polynomial and factored form. One or more of the system variables can then be altered, permitting the user to note the corresponding change

in each of the three equations. This method, however, requires each resulting set of equations to be evaluated to determine if the current iteration produces a better system than the previous iteration. With the aid of program YFCCV, several system solutions were simulated in the process of developing the ability to recognize a good design solution from the transfer functions.

System Design Solutions

In the remaining portion of this chapter, two design solutions are analyzed to determine their respective performance characteristics. Both solutions use the system configuration shown in Figure 26. The primary design, which is called the Pitch Performance Enhancement (PPE) flight control system, is designed to minimize pitch response to vertical gusting - using both the horizontal tail and the trailing-edge flaperons to nullify pitch perturbations. As a result, the flaperons initially deflect in a positive direction (down) in response to an upward vertical gust, and assist the horizontal tail in controlling pitching moment.

The second design, designated YFF57, is included for comparison purposes. This alternate system makes use of a different set of system gains to allow a negative flaperon deflection in response to an upward vertical gust. This is done in an attempt to reduce normal acceleration while simultaneously minimizing pitch response with horizontal tail deflections. It is shown that for the pitch rate command system proposed, only a small improvement in normal accel-

eration can be realized, and only at the expense of largely degrading pitch response.

The values determined for the system variables for the PPE and YFF57 flight control systems are given in Table 2. Note that the feedback and feed-forward gains are largely the same. The differences lie in the flaperon forward-loop gain, the relative amount of attack angle feedback to the flaperons, and the amount of pilot input driving the flaperon channel. In each case, the eigenvalues of both servos are unchanged from those of the existing servos on the YF-16. As only slight improvement is obtained by modifying them, the original eigenvalues are retained so as not to require any mechanical modifications to the aircraft. Also, for both designs, an attempt is made to keep the value of each variable within reasonable bounds; i.e., no extremely high feedback or feed-forward gains.

The transfer functions for each of these systems, as output by program YFSOLVE, are given in Tables 3 and 4. Examining the transfer functions modeling pitch rate for a pilot input (Q/P), recall that the objective in each case is, of course, to make the aircraft flyable as well as insensitive to disturbances. The dominant eigenvalues of the PPE system are located to be overdamped, making use of two dominant zeros and a second pair of underdamped, but less dominant poles to enhance the initial transient response. Acceptable response characteristics are obtained with system YFF57, on the other hand, by placing dominant poles and zeros

TABLE 2 - System Variable Values

System Variable	PPE FCS	YFF57 FCS
K_1	0.28	0.28
K_2	-22.0	-15.0
K_3	-0.40	-0.40
K_4	-7.0	-7.0
K_5	1.0	1.0
K_6	15.0	15.0
K_p	0.10	1.0
K_c	1.0	1.0
K_h	1.0	1.0
K_f	0.50	2.0
γ	20.0	20.0
β	20.0	20.0
z	5.0	5.0
R	15.0	15.0

TABLE 3 - Transfer Functions For PPE FCS

THE Q/P NUMERATOR EQUATION IS:

.84020800E+03	S**4	(-.49487733E+01)	+J(0.)
.55783973E+05	S**3	(-.24509980E+01)	+J(0.)
.64924865E+06	S**2	(-.61301197E+01)	+J(0.)
.26159930E+07	S**1	(-.52863161E+02)	+J(0.)
.33025500E+07	S**0		

THE Q/W NUMERATOR EQUATION IS:

.12339000E+02	S**5	(0.)	+J(0.)
.54200480E+03	S**4	(0.)	+J(0.)
.48761800E+03	S**3	(-.39399384E+00)	+J(.23175125E+01)
.29414400E+04	S**2	(-.39399384E+00)	+J(-.23175125E+01)
0.	S**1	(-.43138165E+02)	+J(0.)
0.	S**0		

THE CHARACTERISTIC EQUATION IS:

.10000000E+01	S**6	(-.61672080E+01)	+J(.30821059E+01)
.79984700E+02	S**5	(-.61672080E+01)	+J(-.30821059E+01)
.26850058E+04	S**4	(-.24780938E+01)	+J(0.)
.57559908E+05	S**3	(-.11597144E+02)	+J(-.23095478E+02)
.55117652E+06	S**2	(-.11597144E+02)	+J(.23095478E+02)
.23830295E+07	S**1	(-.41977903E+02)	+J(0.)
.33025500E+07	S**0		

TABLE 4 - Transfer Functions For YFF57 FCS

THE Q/P NUMERATOR EQUATION IS:

.60106000E+03	S**4	(-.22686243E+01) +J(.93201832E+00)
.10983722E+06	S**3	(-.22686243E+01) +J(-.93201832E+00)
.10386242E+07	S**2	(-.52823733E+01) +J(0.)
.31353576E+07	S**1	(-.17291957E+03) +J(0.)
.33025500E+07	S**0	

THE Q/W NUMERATOR EQUATION IS:

.12339000E+02	S**5	(0.) +J(0.)
.25599698E+04	S**4	(0.) +J(0.)
.24155068E+05	S**3	(-.12338570E+00) +J(0.)
.29414400E+04	S**2	(-.97791294E+01) +J(0.)
0.	S**1	(-.19756728E+03) +J(0.)
0.	S**0	

THE CHARACTERISTIC EQUATION IS:

.10000000E+01	S**6	(-.25797123E+01) +J(.12288408E+01)
.13992470E+03	S**5	(-.25797123E+01) +J(-.12288408E+01)
.53624143E+04	S**4	(-.50850457E+01) +J(0.)
.12501815E+06	S**3	(-.16405481E+02) +J(.23494562E+02)
.95784338E+06	S**2	(-.16405481E+02) +J(-.23494562E+02)
.29023941E+07	S**1	(-.96869267E+02) +J(0.)
.33025500E+07	S**0	

in close proximity, with overall response also affected by a pair of less dominant poles.

Examination of the pitch rate for disturbance input (Q/W) transfer functions reveals that the system configuration results in two free differentiations. This permits zero steady-state pitch angle perturbation for a step disturbance input. In each case, an attempt is made to locate the remaining three zeros in such a way as to minimize the transient output from the transfer functions. It should not be forgotten that freedom to locate poles and zeros in specific locations is limited. As there are a total of thirteen alterable poles and zeros, at least an equal number of degrees of freedom must exist to freely place them. The selection of transfer functions is therefore not only constrained in this manner, but also by the trial-and-error technique that must be employed.

System Time Responses

Using the values determined for the system variables, time response simulations are run for each of the two designs. As in the previous chapter, simulation data is in the form of computer generated plots. As the primary design solution, the PPE flight control system, is of greater interest, simulations are run for both a discrete vertical gust input, and a pilot step input. The alternate design solution, YFF57, is included only to show the effect of requiring the trailing-edge flaperons to deflect so as to oppose vertical translation of the aircraft in response to

vertical gusting. Therefore, this system is simulated for a discrete vertical gust input only.

Response to Pilot Step Input. To simulate system response to a pilot command, a one degree per second step input is applied. The resulting aircraft response (PPE system) is shown in Figure 27. Pilot stick input, as indicated, is dimensioned in volts to account for a general flight control system, as previously discussed. The applied unit step input is actually dimensioned in degrees per second, as the system is a pitch rate FCS.

The simulation results shown in Figure 27 may now be compared to the simulation results for the YF-16 flight control systems presented in the last chapter in Figures 12 and 13. In making this comparison, it becomes apparent that the systems are not responding to the same magnitude of input. As the YF-16 flight control systems are G-command systems, a unit step input produces a 1-G normal acceleration output, and roughly a 2.05 degree per second pitch rate output. For a pitch rate command system, a unit step input produces a one degree per second pitch rate output, and in this case, roughly a 0.485 G normal acceleration output. Therefore, the commanded system responses essentially differ by a factor of two.

One way of judging system performance from time response data is to determine some of the classical response characteristics, such as rise time, peak time, and settling time. These measurements generally provide a good overall indica-

tion of system transient performance. The calculated time response characteristics for the measurable aircraft outputs are given in Table 5. Rise time is computed in two ways: the period of time during which the output increases from 5% to 80%, and, similarly, from 5% to 95% of its maximum value. The former, less standard measure is made necessary by the overdamped nature of the current YF-16 flight control systems.

Attack angle response, in this instance, is a measure of how quickly the aircraft attains the required attitude with respect to the relative wind. At a given flight condition, an increase in pitch rate or normal acceleration requires a specific increase in attack angle. This is only true, of course, for commanded maneuvers that are achieved as a result of aircraft rotation, as is the case for each of these systems. It is true that the Maneuver Enhancement system and the PPE FCS use the direct lift created by the flaperons to enhance normal acceleration response. The effect of such flaperon deflection, however, is limited to the early transient portion of the commanded response, as discussed in Chapter III. The improvement in attack angle response realized by the PPE design is quite apparent from the table. Rise time is much faster than the Maneuver Enhancement system, which is, surprisingly, even slower than the baseline FCS.

Pitch response is also much improved - especially beyond 80% of final value. While the baseline and Maneuver Enhancement system responses slowly approach a maximum, the PPE FCS

TABLE 5 - Time Response Characteristics

	YF-16 Baseline FCS			YF-16 FCS with ME			PPE FCS		
	α	q	A_N	α	q	A_N	α	q	A_N
Rise Time (5% - 95%)	3.57	3.21	3.93	unk	3.18	> 6.0	1.38	.122	1.20
Rise Time (5% - 80%)	1.56	.273	1.59	unk	.116	1.80	.665	.0964	.675
Peak Time	undef	undef	undef	undef	undef	undef	undef	.251	undef
Maximum Overshoot	undef	undef	undef	undef	undef	undef	undef	14 %	undef
Settling Time (5%)	3.75	3.30	4.10	> 6.0	3.24	> 6.0	1.50	.588	1.25
Settling Time (2%)	4.69	4.88	5.30	> 6.0	5.14	> 6.0	2.57	.742	1.62

Peak Time and Maximum Overshoot are undefined for overdamped responses.

Data for each simulation was measured for a maximum of six seconds. The attack angle response for the YF-16 FCS with Maneuver Enhancement was sufficiently overdamped to prevent measurement of rise time.

output settles within 2% in three-quarters of a second. The amount of overshoot that occurs is well within an acceptable range for pitch rate command systems, and is therefore not a problem.

Comparing normal acceleration responses, it is interesting to note that the baseline system generates a faster response than the Maneuver Enhancement system - at least above about 80% of the commanded value. The overall PPE system response is, however, more than three times as rapid as the baseline system. In addition, the transition from translation to rotation, which occurs at about the 0.25 second point, is much more subtle. Overall performance is, clearly, much improved.

Response to the Discrete Vertical Gust. To simulate system response to atmospheric disturbances, discrete (1-cos) vertical gusts are applied. To enable a direct comparison to the simulation results in Chapter III, the discrete gust peak velocity is again 50 feet per second, with a duration of one second.

Simulation results for the PPE system are shown in Figure 28, and the results for system YFF57 are shown in Figure 29. As was intended, the trailing-edge flaperons deflect in opposite directions for each system. As discussed, the PPE system is designed such that the flaperons augment the horizontal tail in opposing pitch moment, and therefore, as both control surfaces are located aft of the CG, both initially deflect in the same direction.

Comparing the normal acceleration plots for both systems, it is clear that system YFF57 has resulted in only about a 7% improvement - a reduction from 2.48 to 2.32 Gs perturbation. At the same time, however, pitch angle response is degraded by about 470% - from 0.017 to 0.08 degrees perturbation. Although this pitch response is still very acceptable, the small improvement afforded in normal acceleration response with this system leads to the selection of the PPE FCS as more appropriate relative to the design objective.

Comparing the simulation results of the PPE FCS (Figure 28) to the results obtained with the YF-16 flight control systems (Figures 15 and 17) in the previous chapter, the differences are readily determined. The most obvious is the desirable improvement in pitch response and tracking error. Peak pitch angle perturbation is reduced by a factor of about 140 over the baseline YF-16 FCS, and by a factor of about 130 over the YF-16 FCS with Maneuver Enhancement. Maximum longitudinal tracking error is reduced by factors of about 9.5 and 9.0, respectively.

A greater relative improvement in tracking error can be realized with a target at increased distance. This is because the tracking error for the PPE system results mostly from the vertical movement of the aircraft - not the pitch perturbation. Exactly the opposite is true for the YF-16 flight control systems. Equally important is the shape of the actual tracking error response. It is very probable that the tracking error with the PPE system could be more easily controlled

by the pilot.

Normal acceleration response, on the other hand, is improved less significantly compared to the baseline YF-16 FCS. In Figure 15, it is shown that the YF-16 with baseline FCS responds by pulling roughly 2.0 positive Gs, followed by about 2.7 negative Gs. This results in a peak-to-peak change of 4.7 Gs over a one-half second time period. Also, negative Gs are more difficult to withstand than positive Gs. The PPE FCS responds with a peak-to-peak change of about 4.2 Gs over the same time period - an improvement of approximately 10%. In addition, the peak negative perturbation is improved by more than 35%.

The normal acceleration response of the YF-16 FCS with Maneuver Enhancement, however, is substantially better than the PPE FCS. The peak-to-peak variation is only 2.4 Gs - a reduction of almost 50% over the baseline YF-16 FCS and more than 40% over the PPE system. Also, the peak perturbation in negative Gs is reduced by roughly 55% over the baseline system, and more than 30% over the PPE FCS. This is expected, however, since the Maneuver Enhancement system is designed to control normal acceleration.

Comparing control surface deflections, peak horizontal tail movement is reduced by more than 70% over the baseline YF-16 FCS, and about 75% over the YF-16 FCS with ME. In addition, maximum horizontal tail deflection rate is reduced by roughly 75% and 80%, respectively. Trailing-edge flaperon deflection and rate of deflection are reduced by 90% and 92%

over the YF-16 FCS with Maneuver Enhancement.

To ensure a valid test of the ability of this system to reject discrete disturbances, it is of some interest to excite the system at its pitch resonant frequency and observe the results. A gust of approximately 0.3 seconds duration was determined to be this worst case input. The resultant system response is shown in Figure 30. Peak pitch angle perturbation is still less than 0.06 degrees, and maximum target tracking error is reduced to less than eight feet. In addition, the probability of a gust of such short duration occurring with a magnitude equal to that of the longer duration discrete gust used for the previous analysis is quite low (Ref 4). In light of this fact, system performance at the pitch resonant frequency is very good.

System Frequency Response

To complete the assessment of system performance, both analytical and empirical frequency response analyses are presented. The analytical method is the standard process of applying sine wave inputs of various frequencies to the system, plotting output phase and magnitude relative to the input. The empirical method, as described in Chapter III, indicates the maximum perturbation of system states for constant magnitude discrete gust inputs of various durations. This analysis is included to permit a further comparison of the PPE and YF-16 flight control systems.

Analytical Frequency Response. In the design process,

the system was modeled in standard matrix format (Eqns 40 and 41). These matrices were used directly by program TOTAL (Ref 23) to calculate the analytical frequency response plots shown in Figures 31 through 34. Notice that the resonant frequency of the system is approximately 23 radians per second. The system is therefore maximally excited by an input of that frequency, roughly equivalent to a 0.3 second duration discrete gust.

The system pitch rate response to a pilot command is essentially flat (within 3dB) up to 50 radians per second. Normal acceleration response is fairly good (within 6dB) up to 30 radians per second. The required deflection of control surfaces decreases monotonically below the system resonant frequency to maintain system performance without actuator displacement saturation.

The system pitch angle response to a disturbance input is no less than 34 dB down over the entire frequency spectrum. This accounts for the excellent disturbance rejection properties of this system. Normal acceleration response, on the other hand, falls off at 20dB per decade only below about 3 radians per second. Above that frequency, there is little or no rejection. Again, the required deflection of control surfaces decreases below the system resonant frequency, which reduces the possibility of actuator displacement saturation.

Empirical Frequency Response. Using the technique described in the previous chapter, empirical frequency response data is compiled for the system. Peak gust magnitude is held

constant at 50 feet per second. The resulting peak perturbation data is plotted in Figures 35 through 41. To permit an instant comparison of this information with that previously determined for the YF-16 flight control systems, the data for those systems is also plotted in each figure.

The ability of the system to minimize pitch perturbations resulting from atmospheric disturbances is depicted quite clearly in Figure 35. Peak perturbation is no more than 0.06 degree for a gust of any frequency. Maximum tracking error is shown in Figure 36. A marked improvement is obtained for all gust frequencies above 0.6 radians per second. The large tracking error associated with the lower frequencies is a result of insufficient control of normal position. Because normal acceleration is not fed back to the horizontal tail channel, this control surface does not directly control vertical translation. Also, the washout circuit in the trailing-edge flaperon channel zeros flaperon deflection prior to subsidence of gusting at the lower frequencies. It should be well within the pilot's capabilities, however, to control vertical translation under these conditions.

Figure 37 verifies that the PPE system provides little or no improvement over the baseline YF-16 FCS in controlling normal acceleration peak perturbation. It does not show, however, the improvement in peak-to-peak acceleration change, or the reduction in peak negative Gs as discussed previously. Overall performance is, therefore, somewhat better than is indicated by the figure.

Reduction in control surface deflection is confirmed in Figures 38 and 40. Control surface deflection rate is also decreased, except at very high frequencies, as shown in Figures 39 and 41. Actuator rate for the horizontal tail never exceeds 18 degrees per second. The trailing-edge flaperon actuator rate-saturates at a gust frequency of 35 radians per second, as opposed to 8 radians per second for the YF-16 Maneuver Enhancement system.

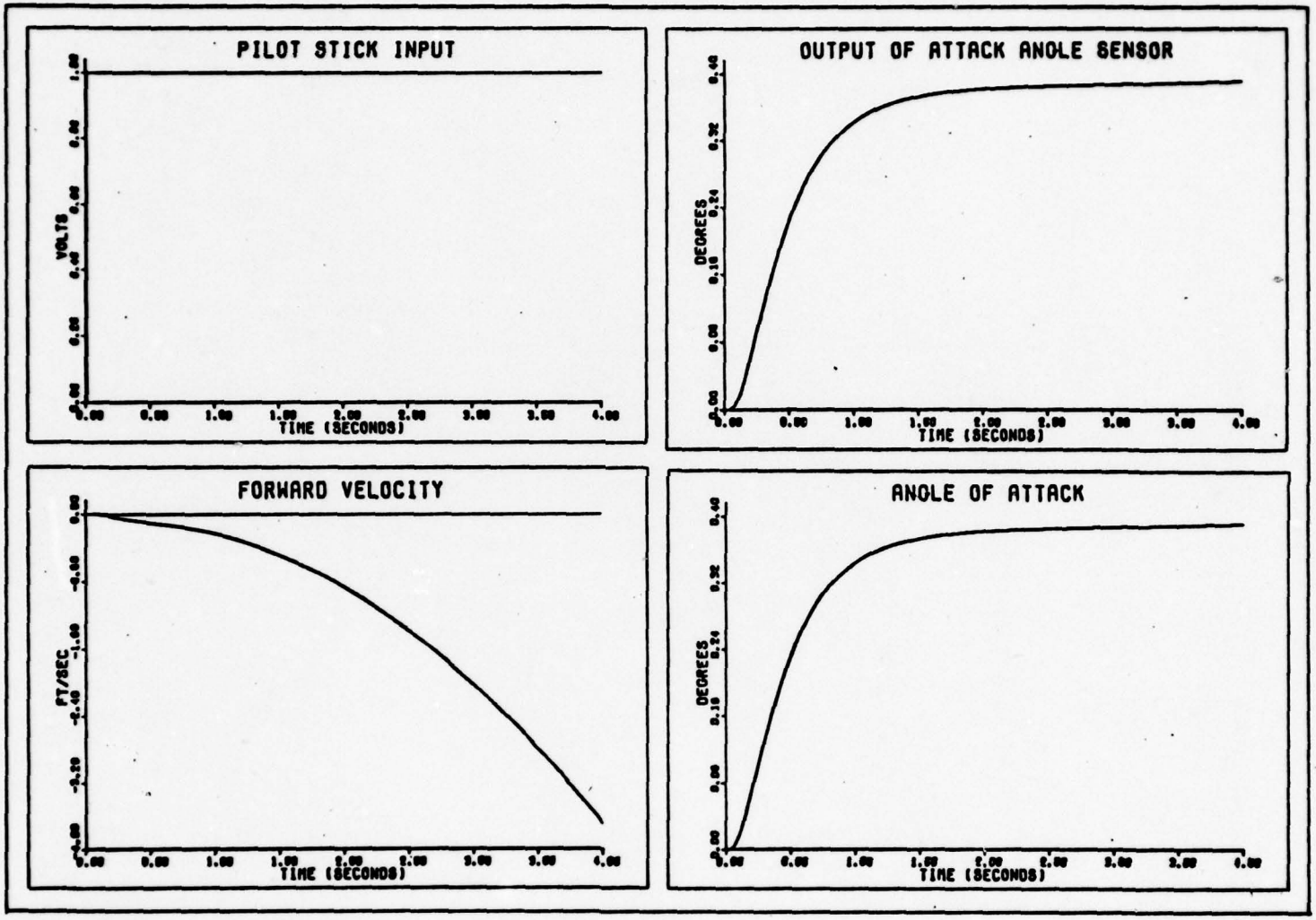


Figure 27a. PPE FCS response to a pilot step input.

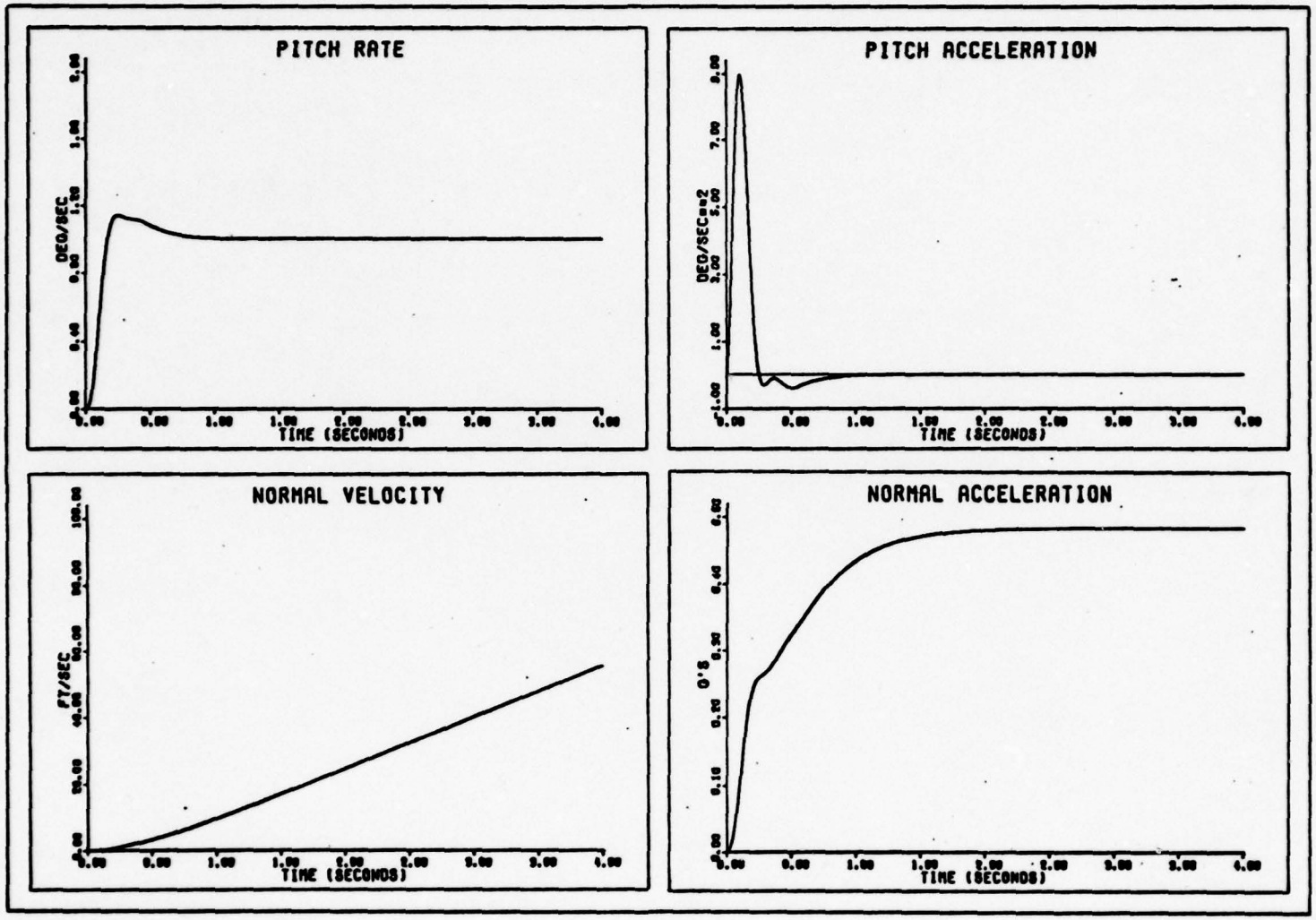


Figure 27b. PPE FCS response to a pilot step input.

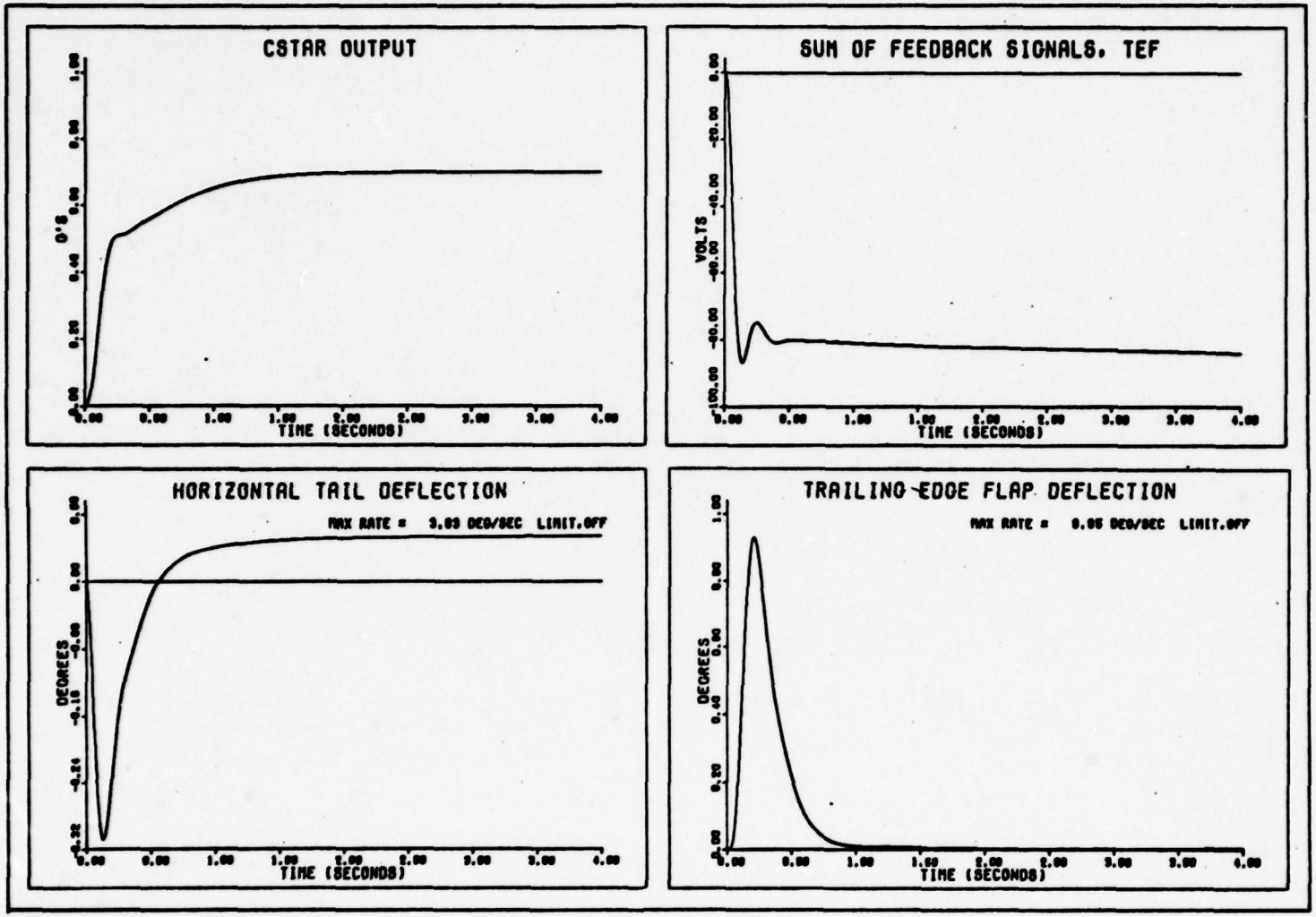


Figure 27c. PPE FCS response to a pilot step input.

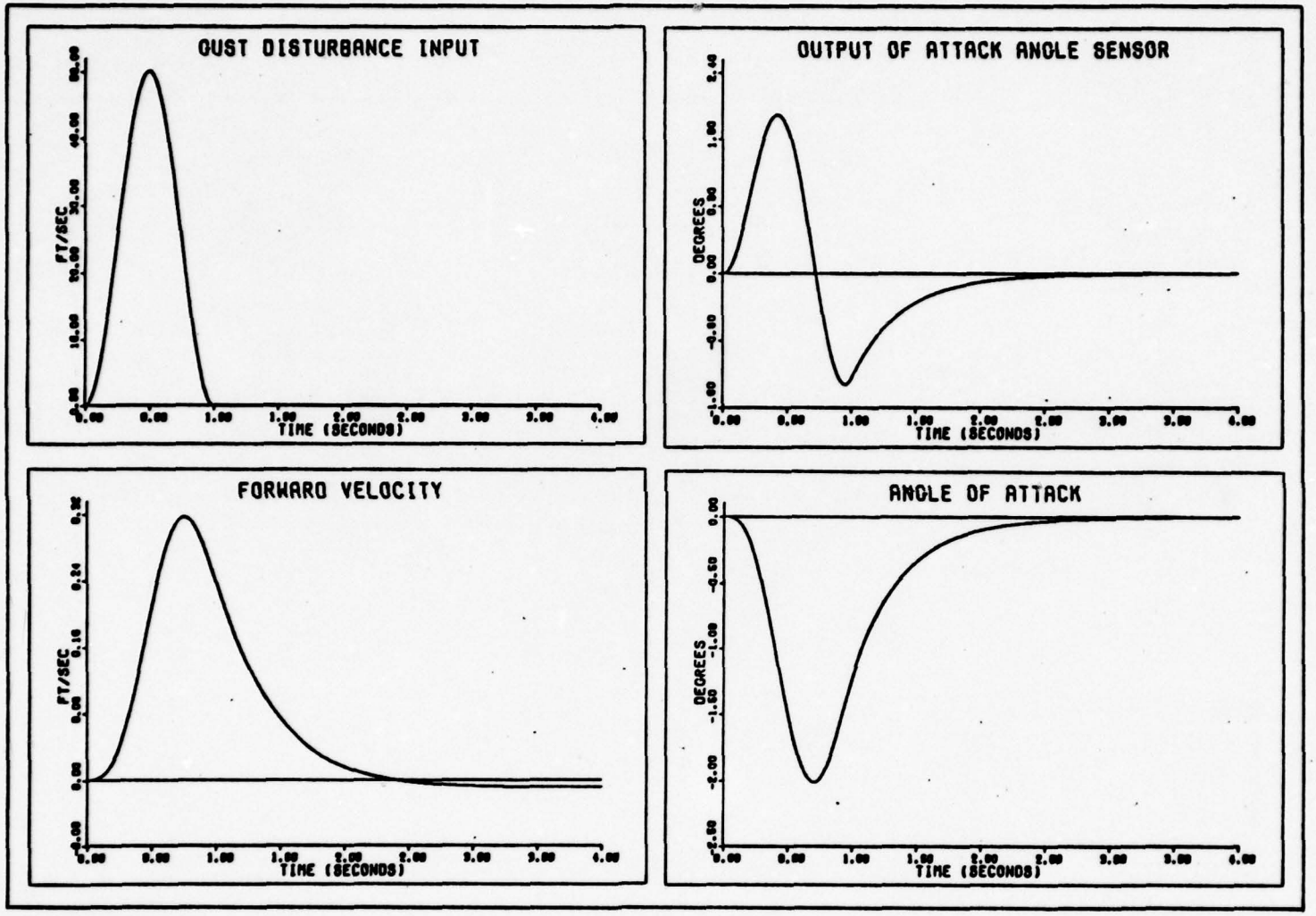


Figure 28a. PPE FCS response to a discrete vertical gust.

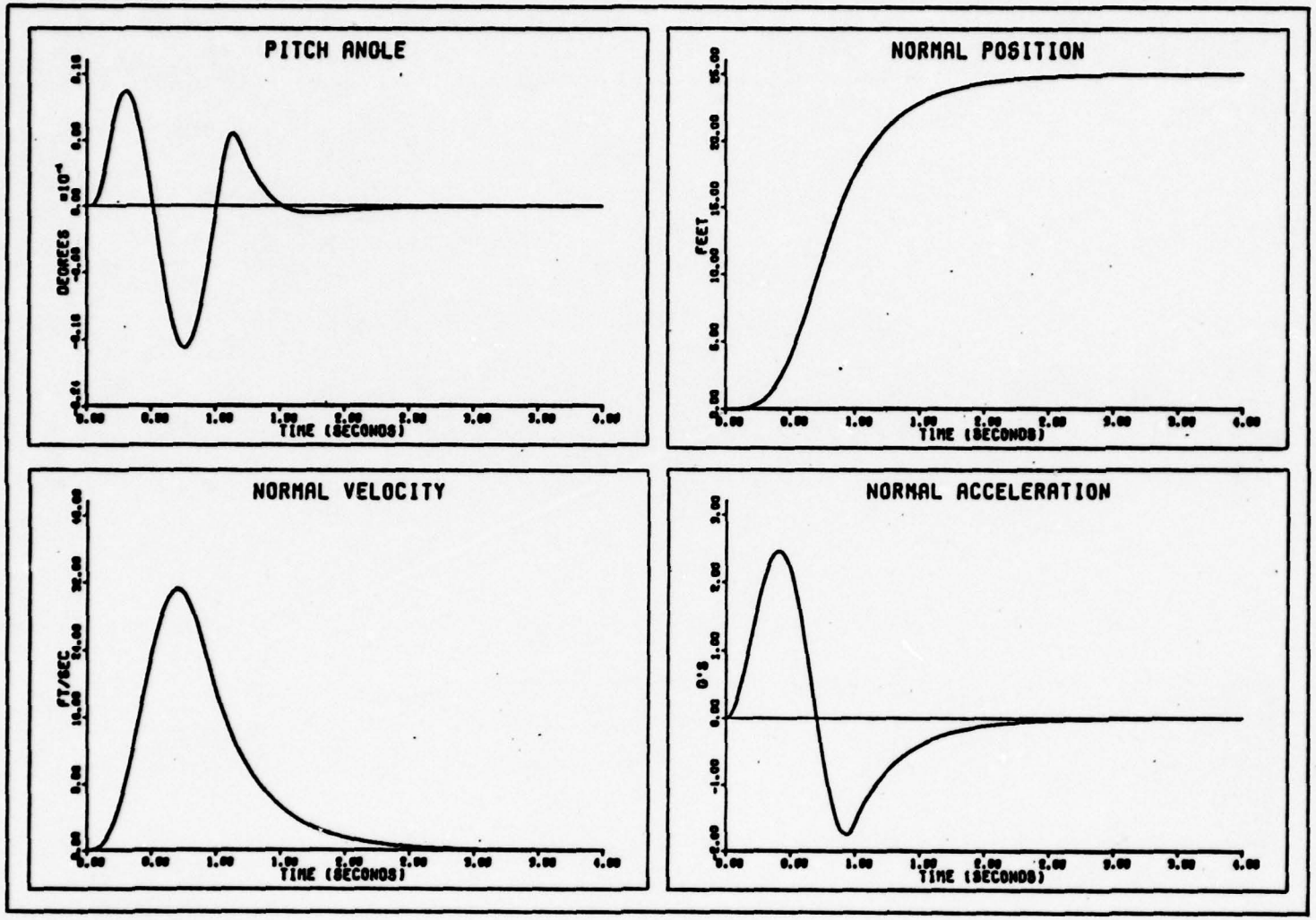


Figure 28b. PPE FCS response to a discrete vertical gust.

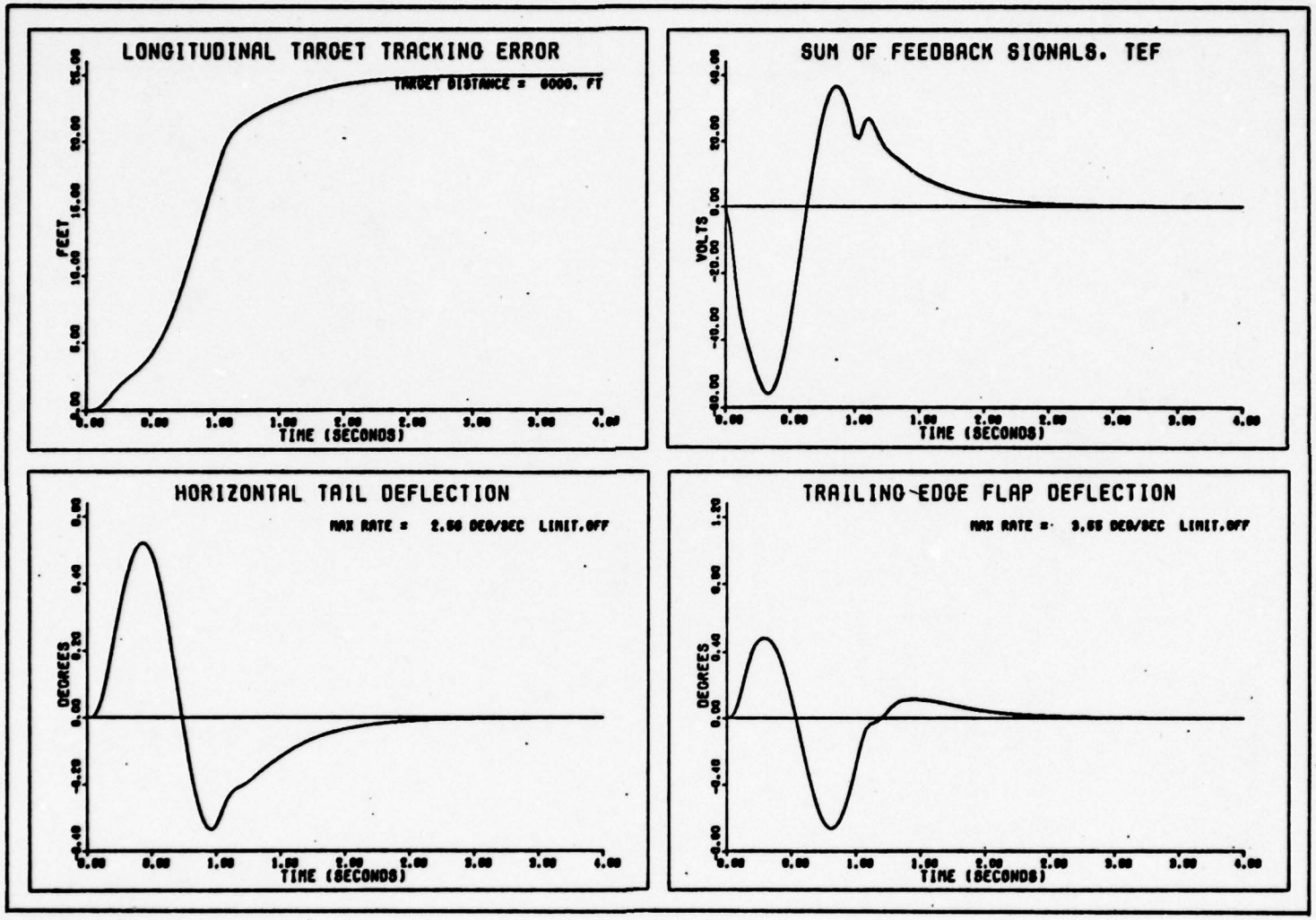


Figure 28c. PPE FCS response to a discrete vertical gust.

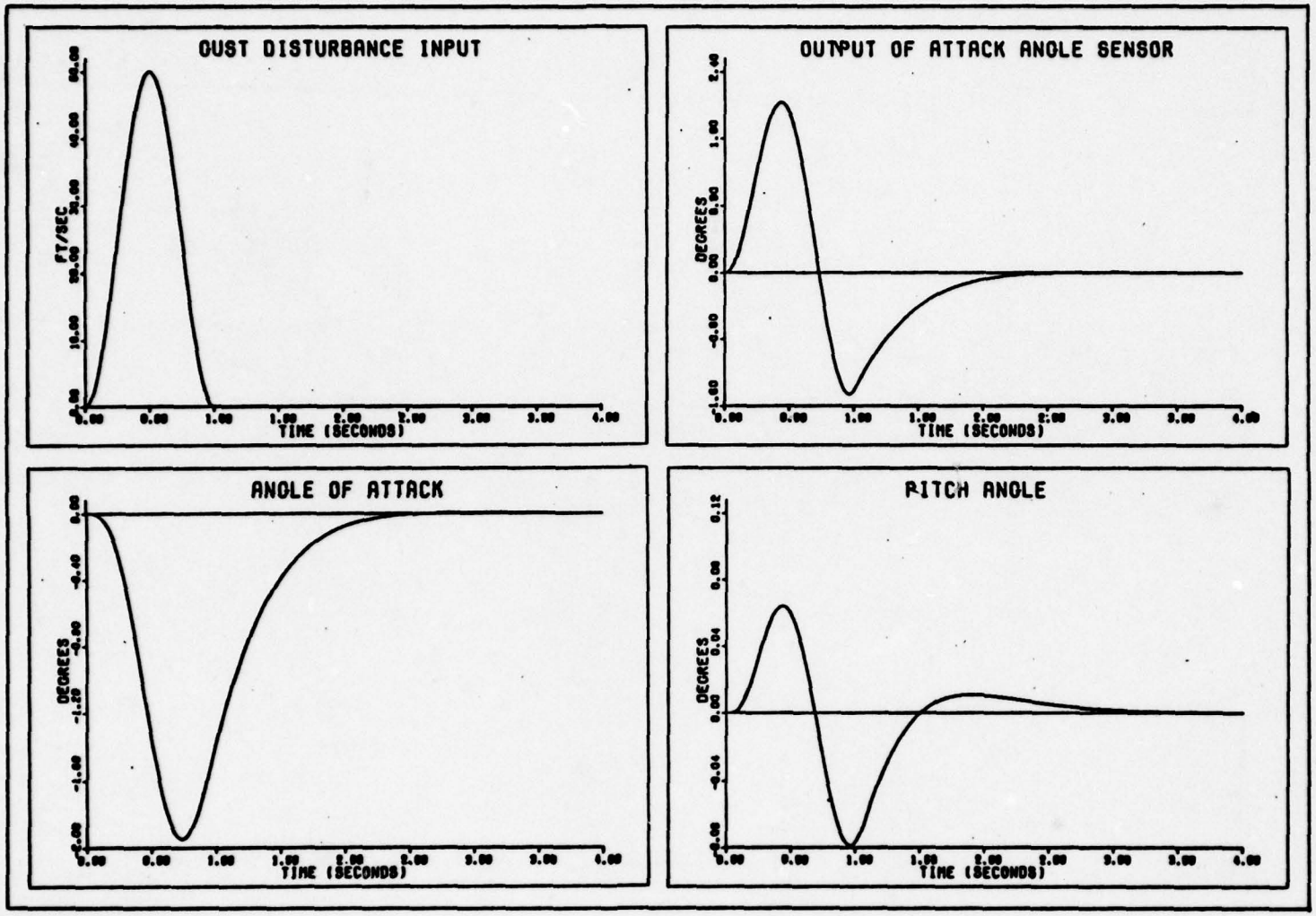


Figure 29a. YFF57 FCS response to a discrete vertical gust.

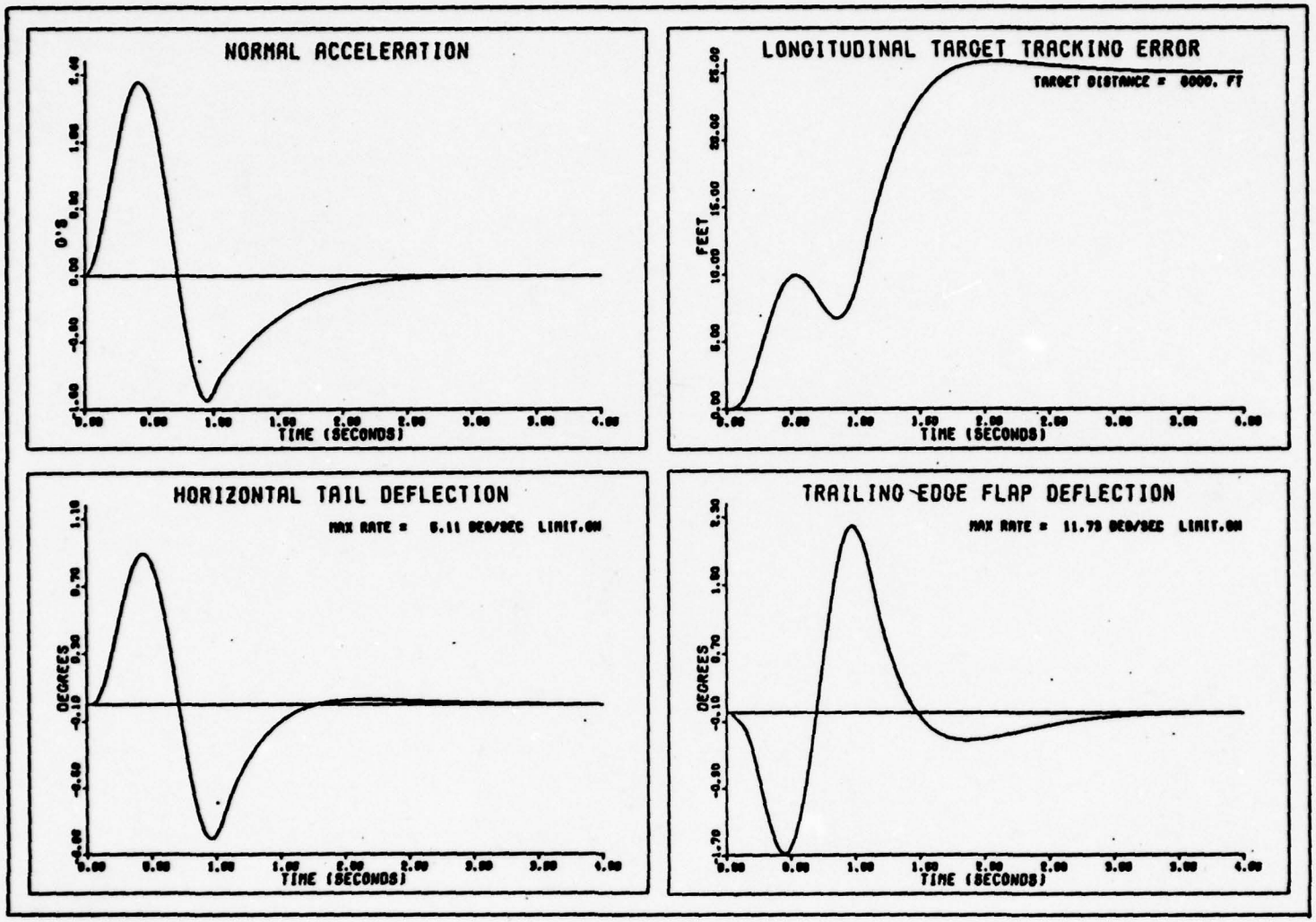


Figure 29b. YF57 FCS response to a discrete vertical gust.

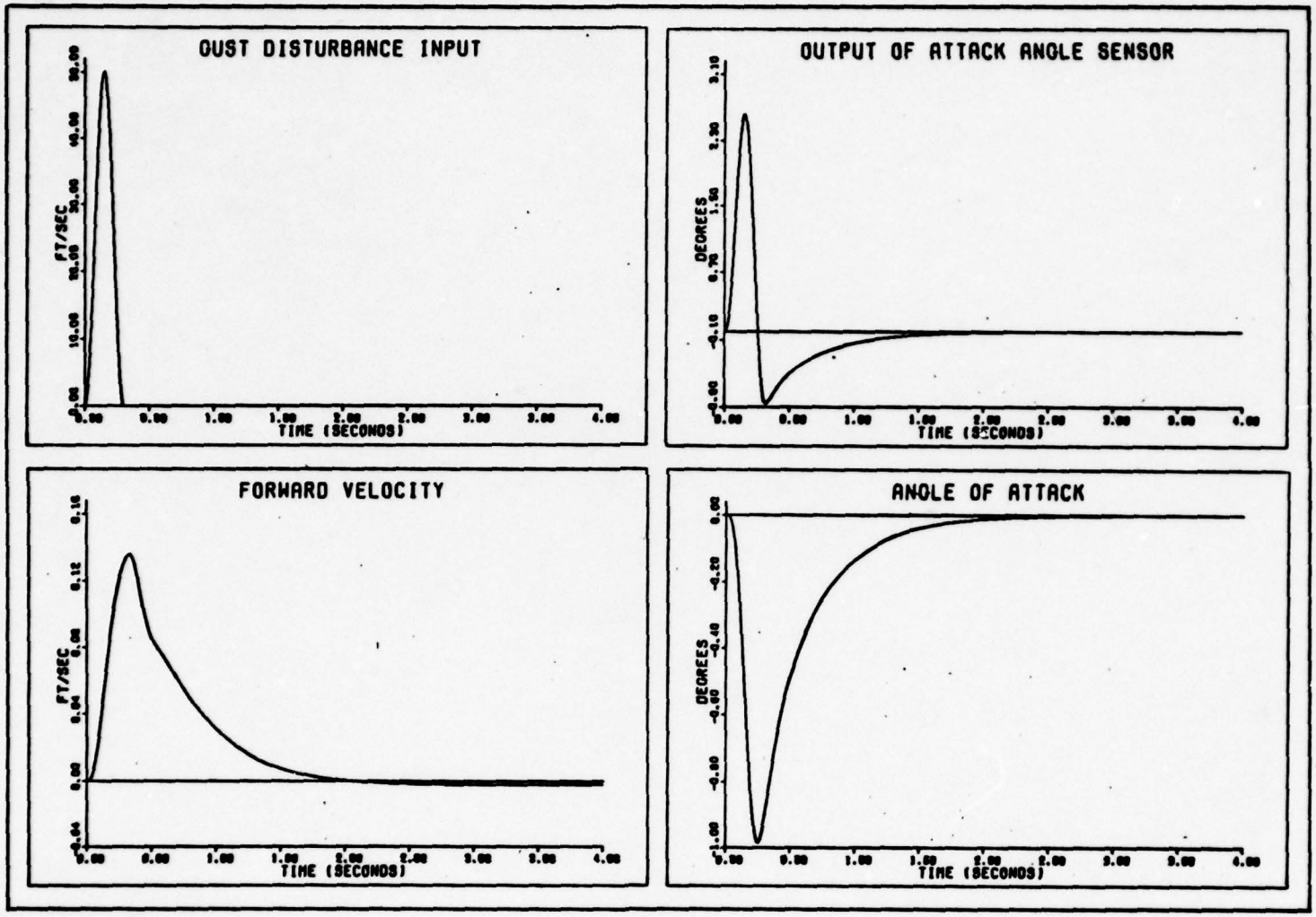


Figure 30a. PPE FCS response to a discrete gust at the pitch resonant frequency.

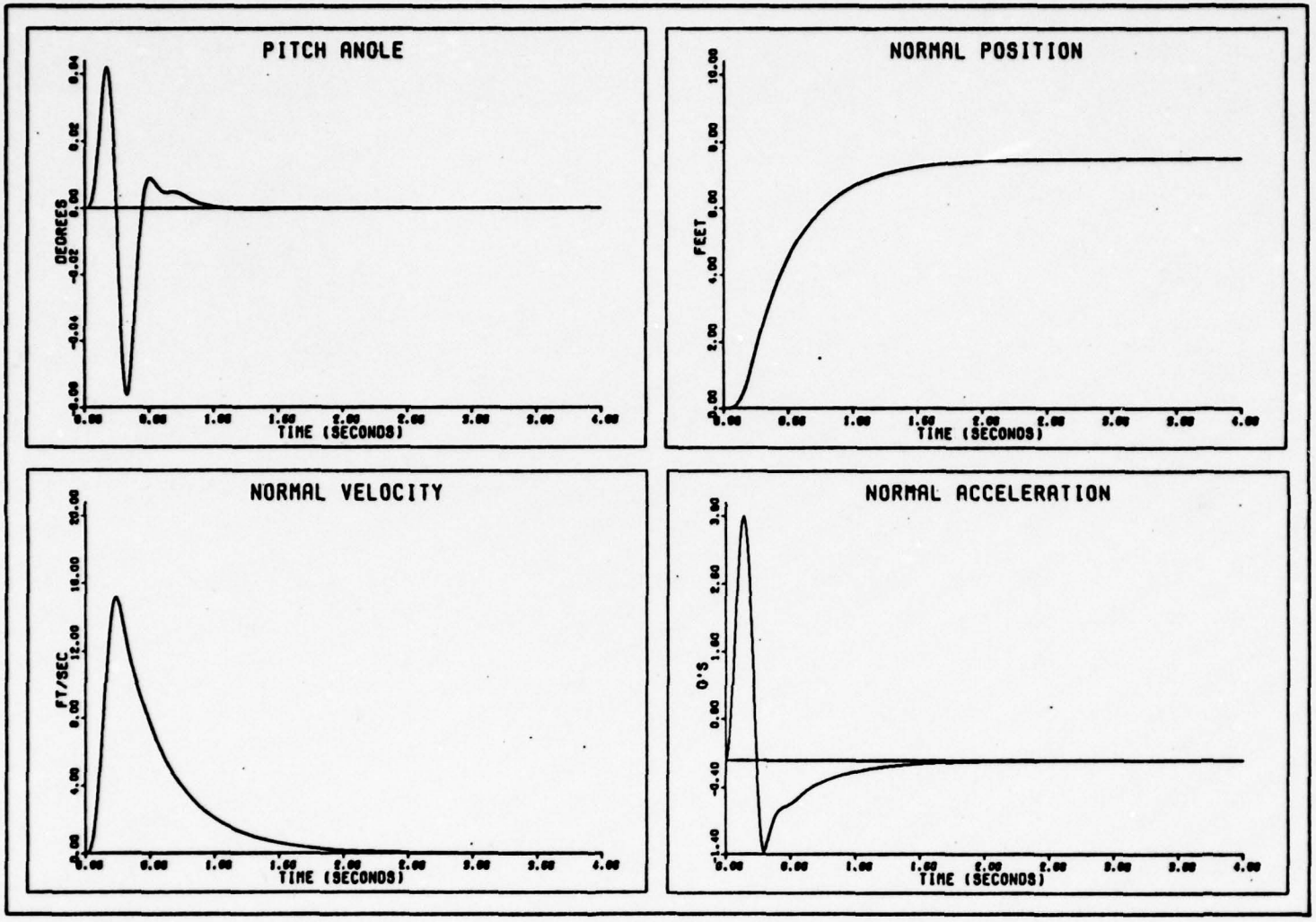


Figure 30b. PPE FCS response to a discrete gust at the pitch resonant frequency.

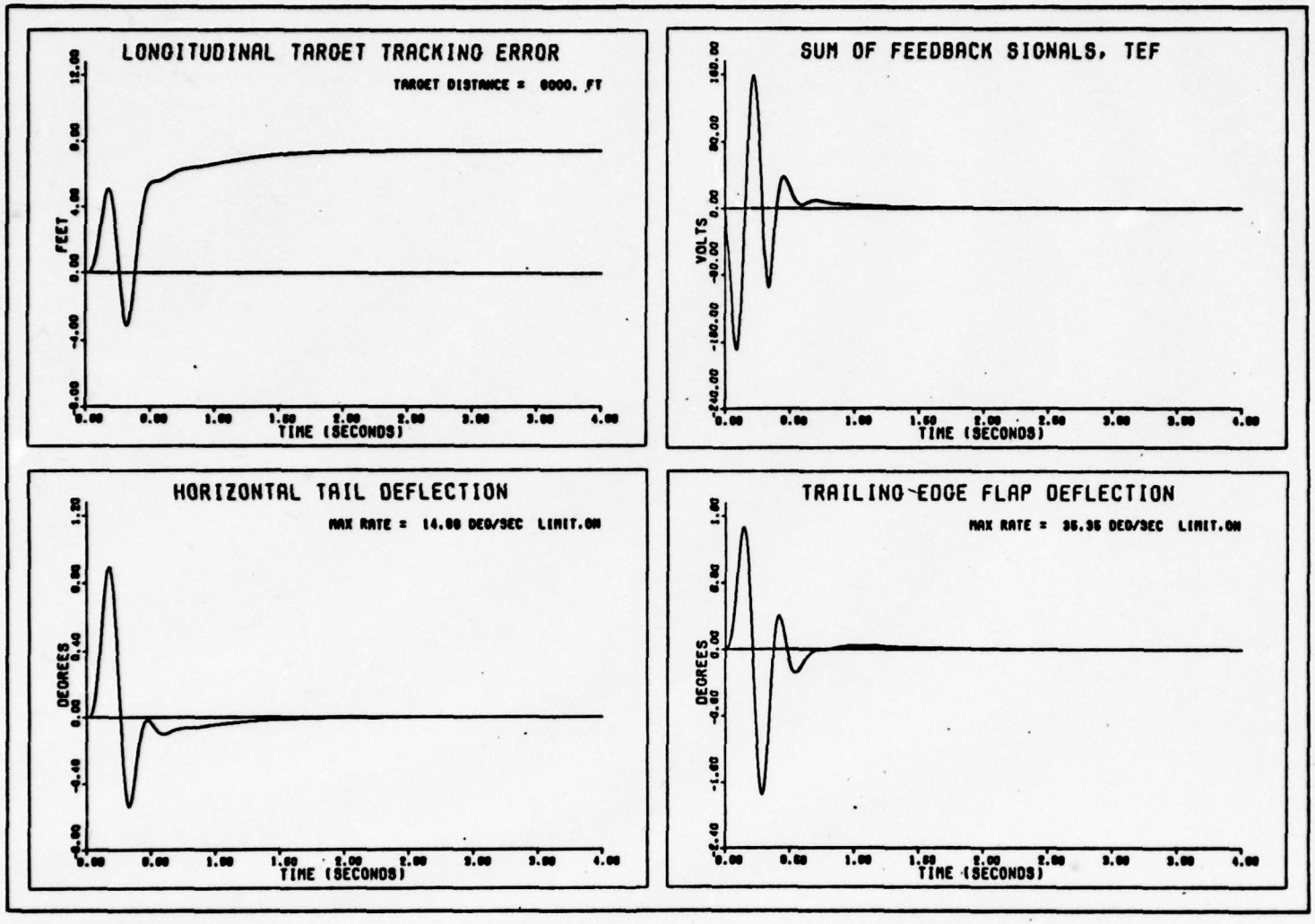


Figure 30c. PPE FCS response to a discrete gust at the pitch resonant frequency.

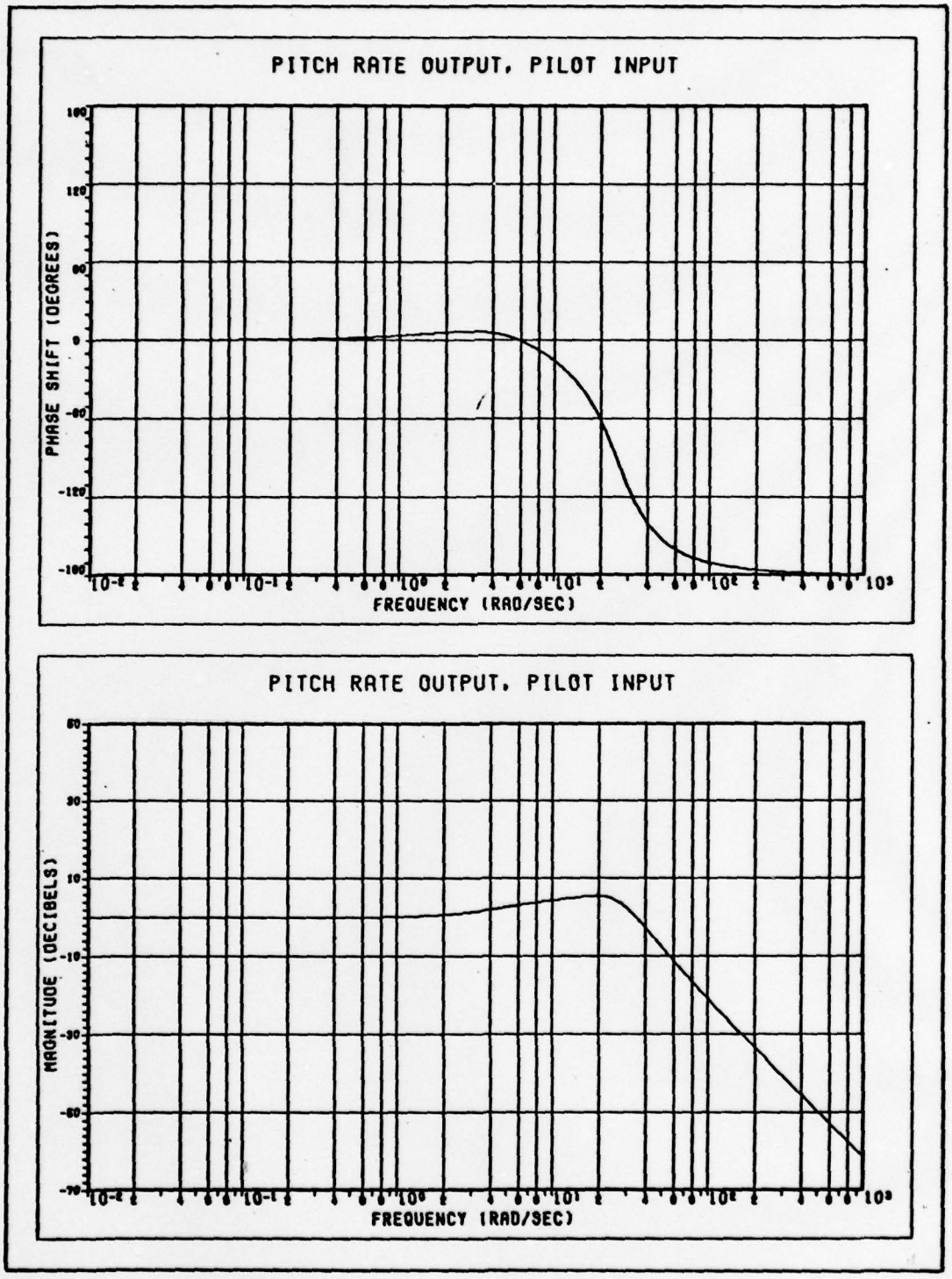


Figure 31a. Frequency response of the PPE FCS.

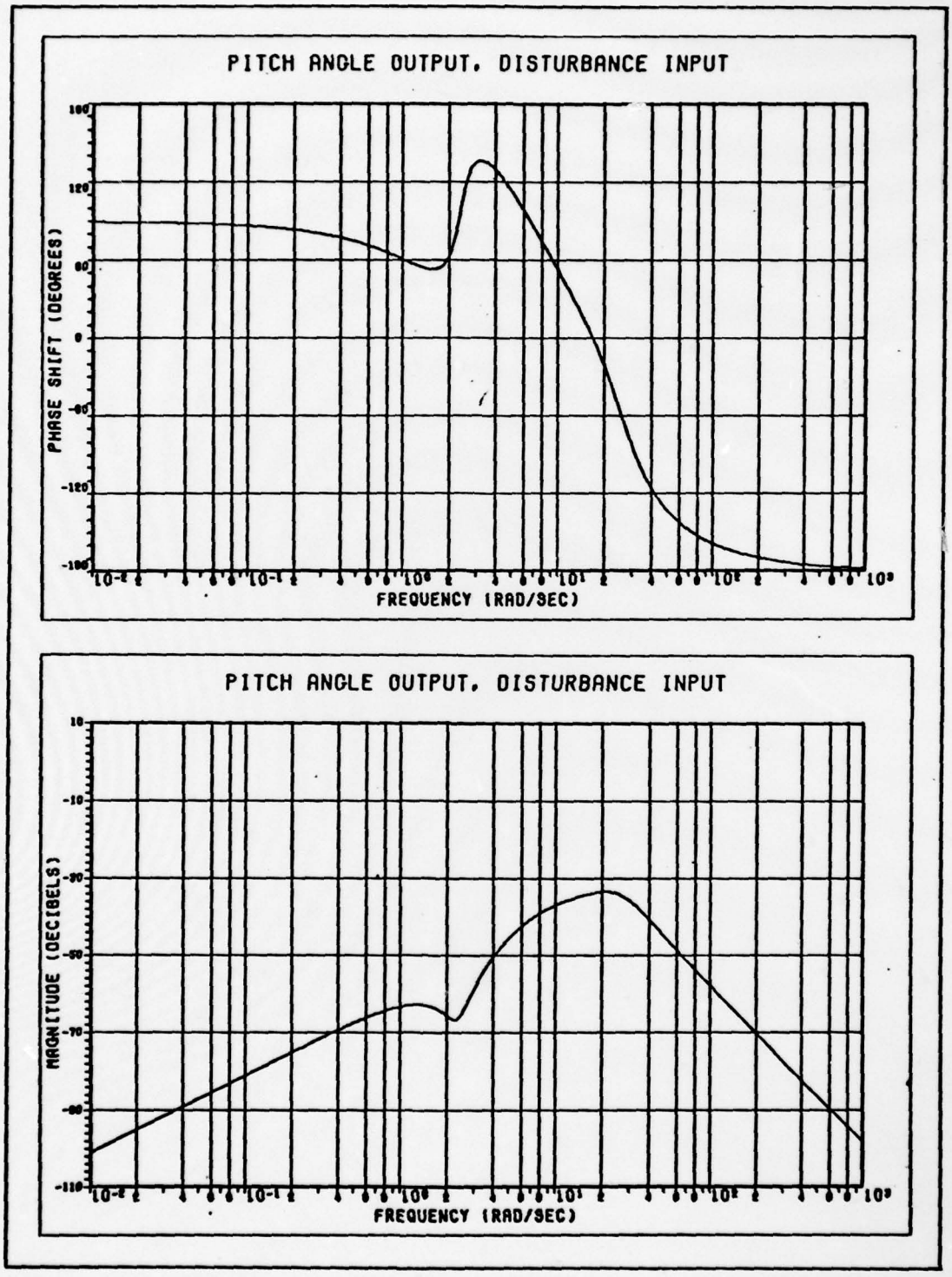


Figure 31b. Frequency response of the PPE FCS.

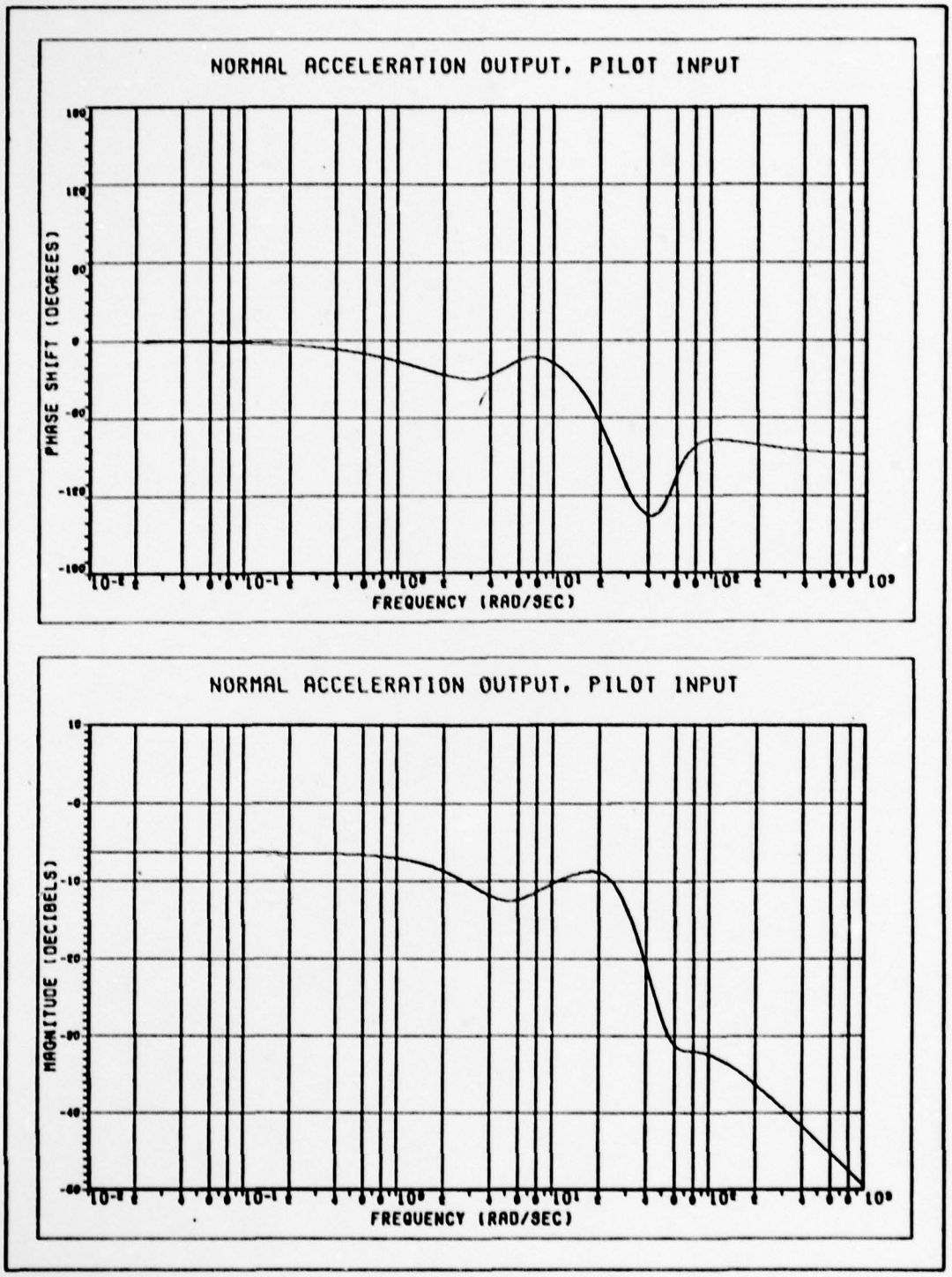


Figure 32a. Frequency response of the PPE FCS.

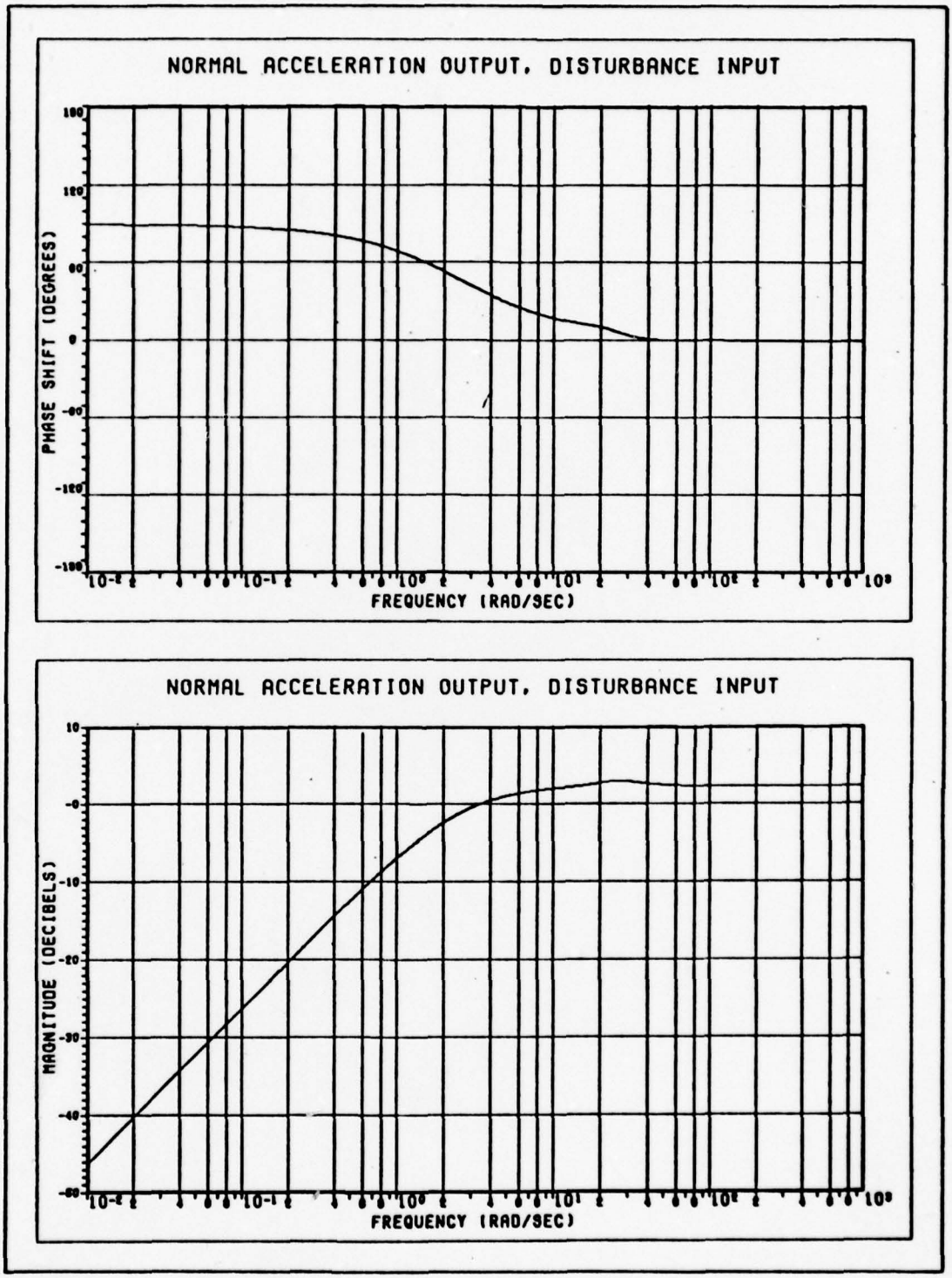


Figure 32b. Frequency response of the PPE FCS.

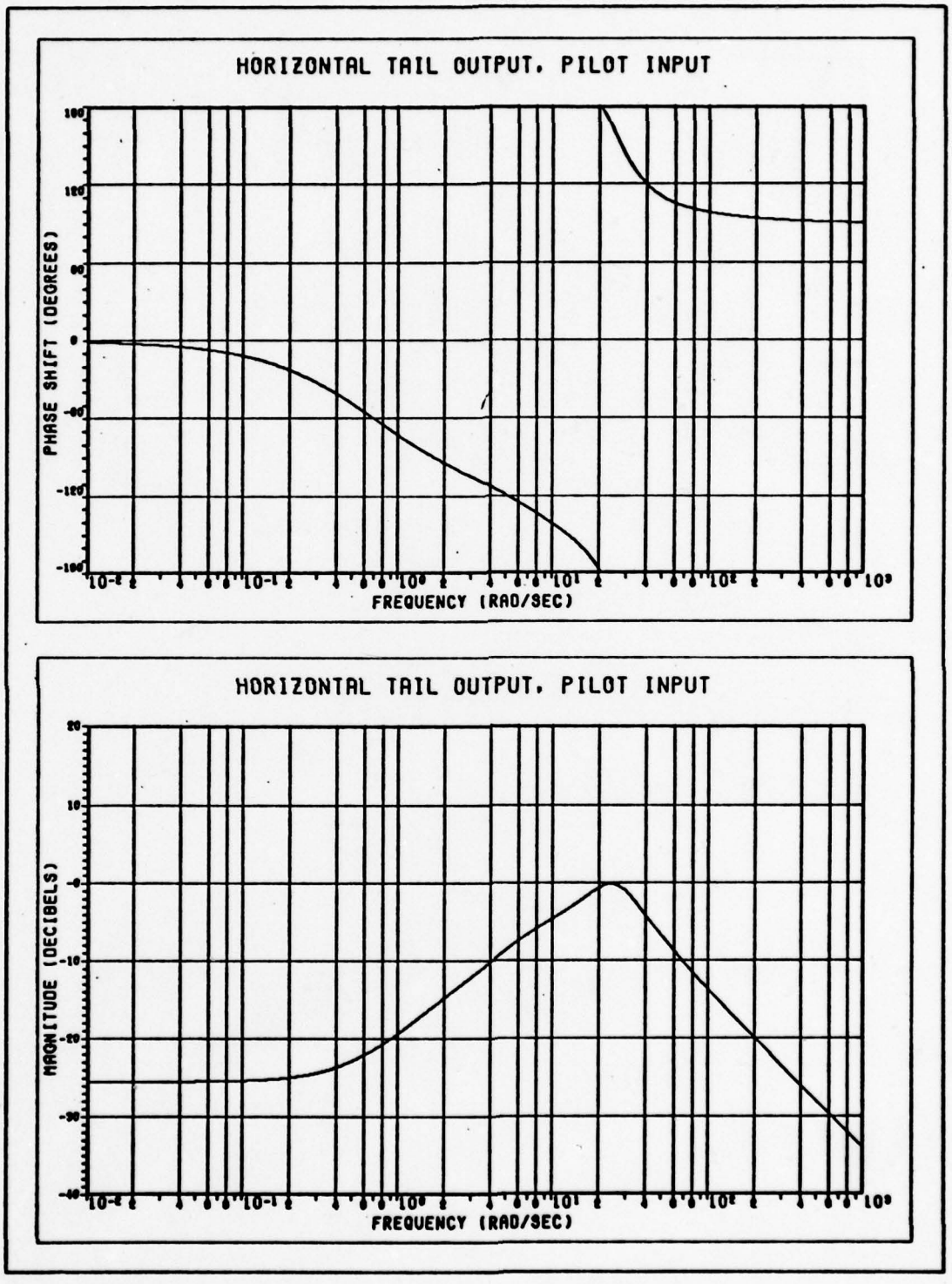


Figure 33a. Frequency response of the PPE FCS.

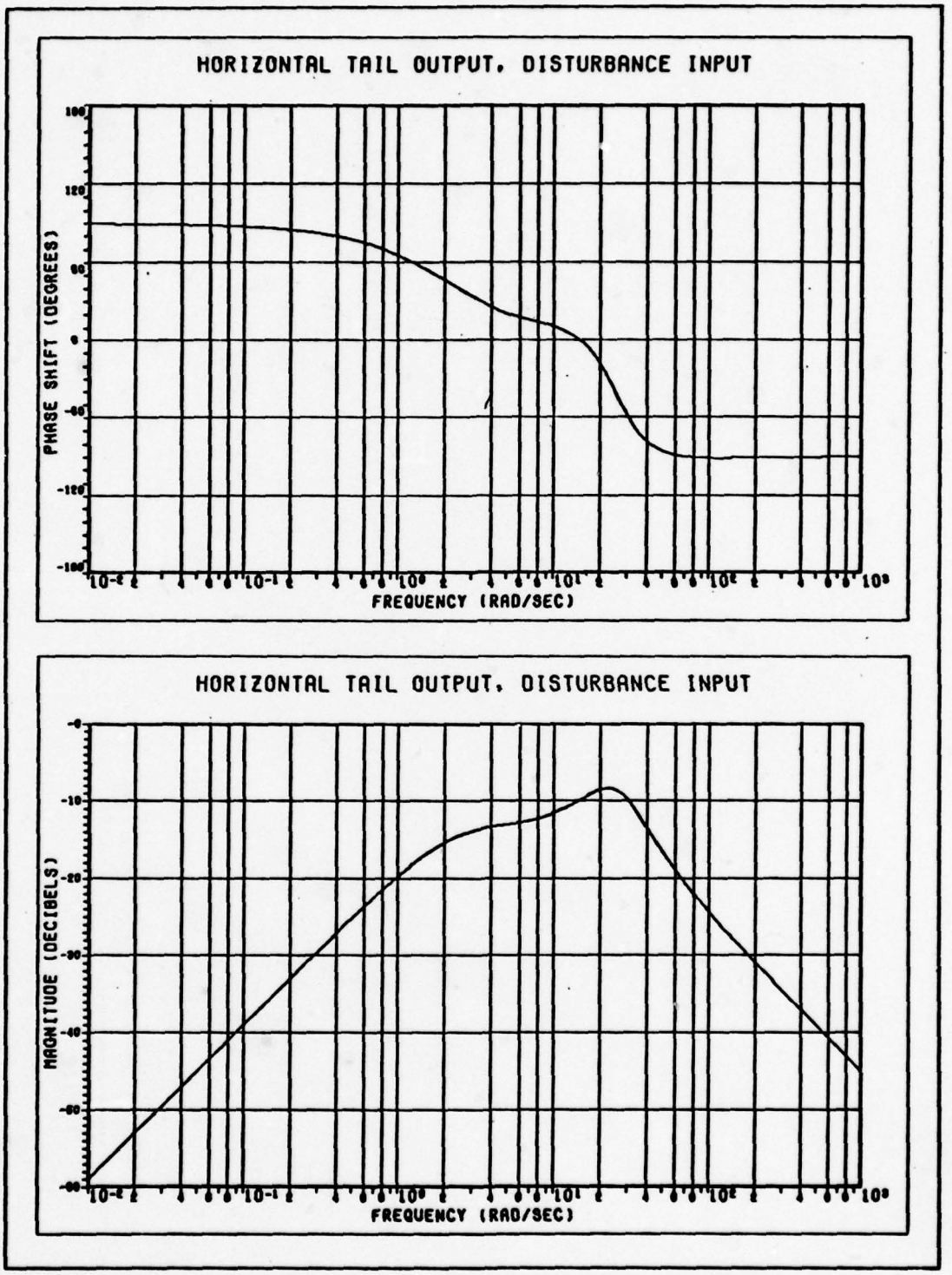


Figure 33b. Frequency response of the PPE FCS.

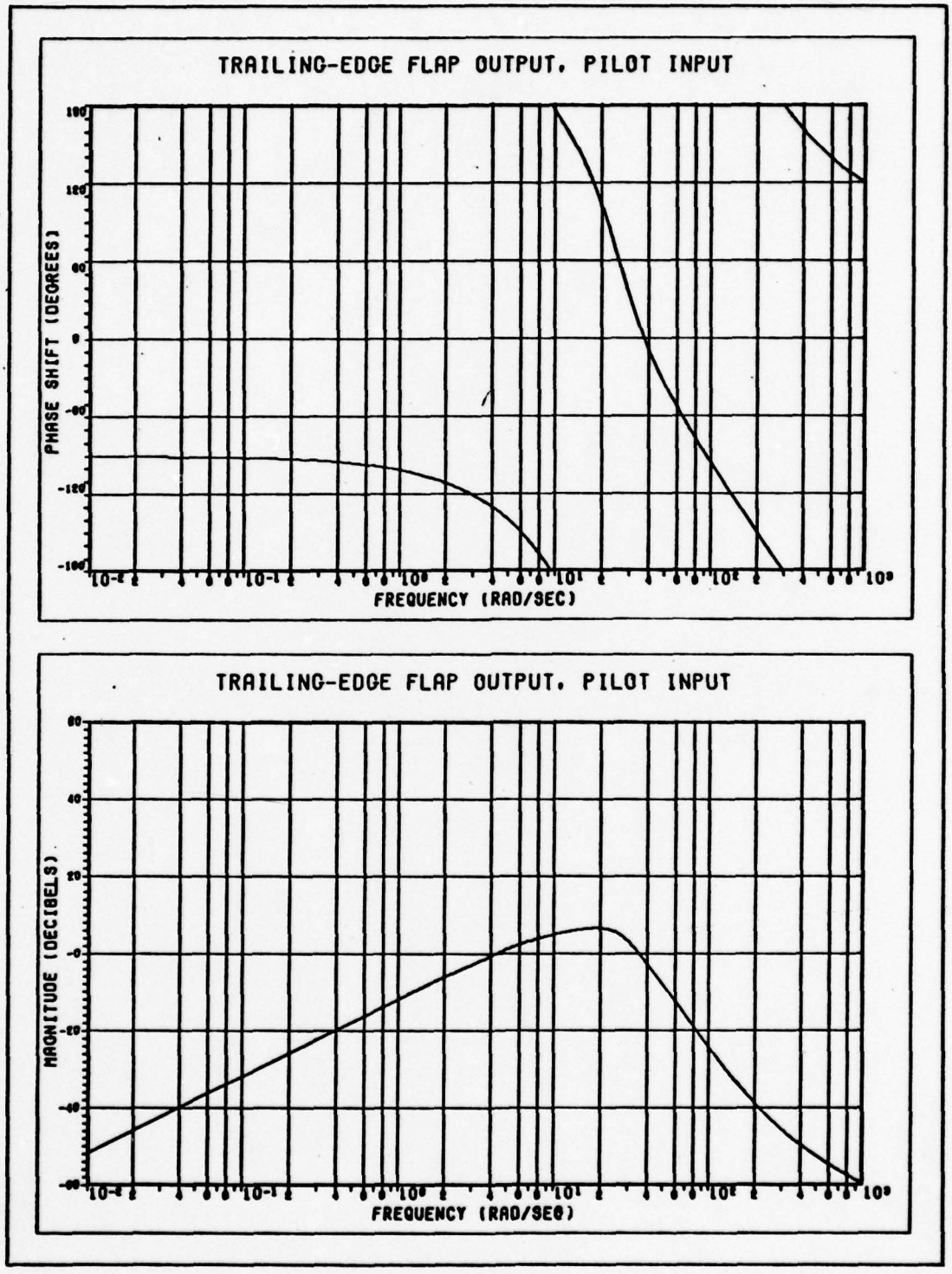


Figure 34a. Frequency response of the PPE FCS.

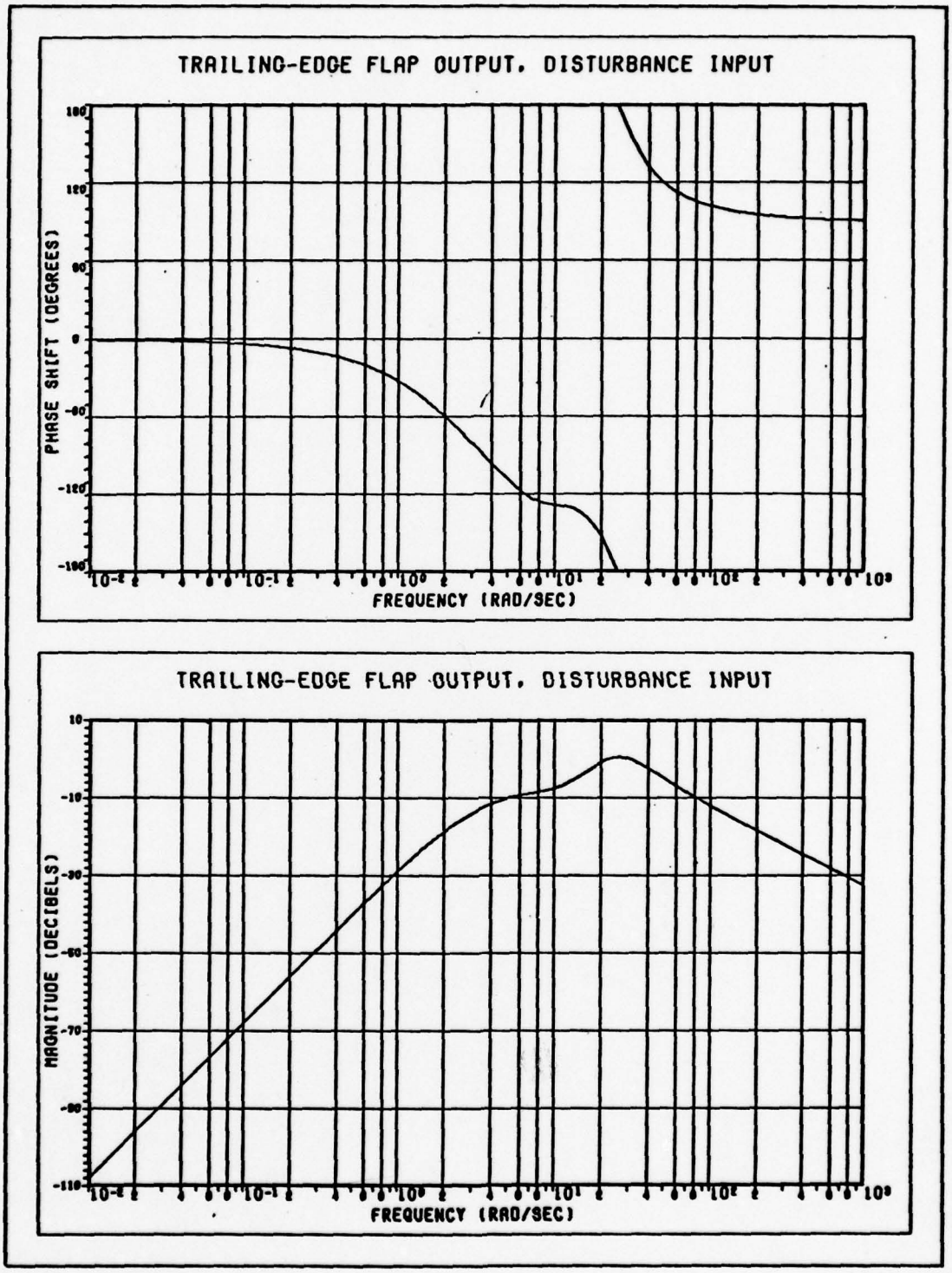


Figure 34b. Frequency response of the PPE FCS.

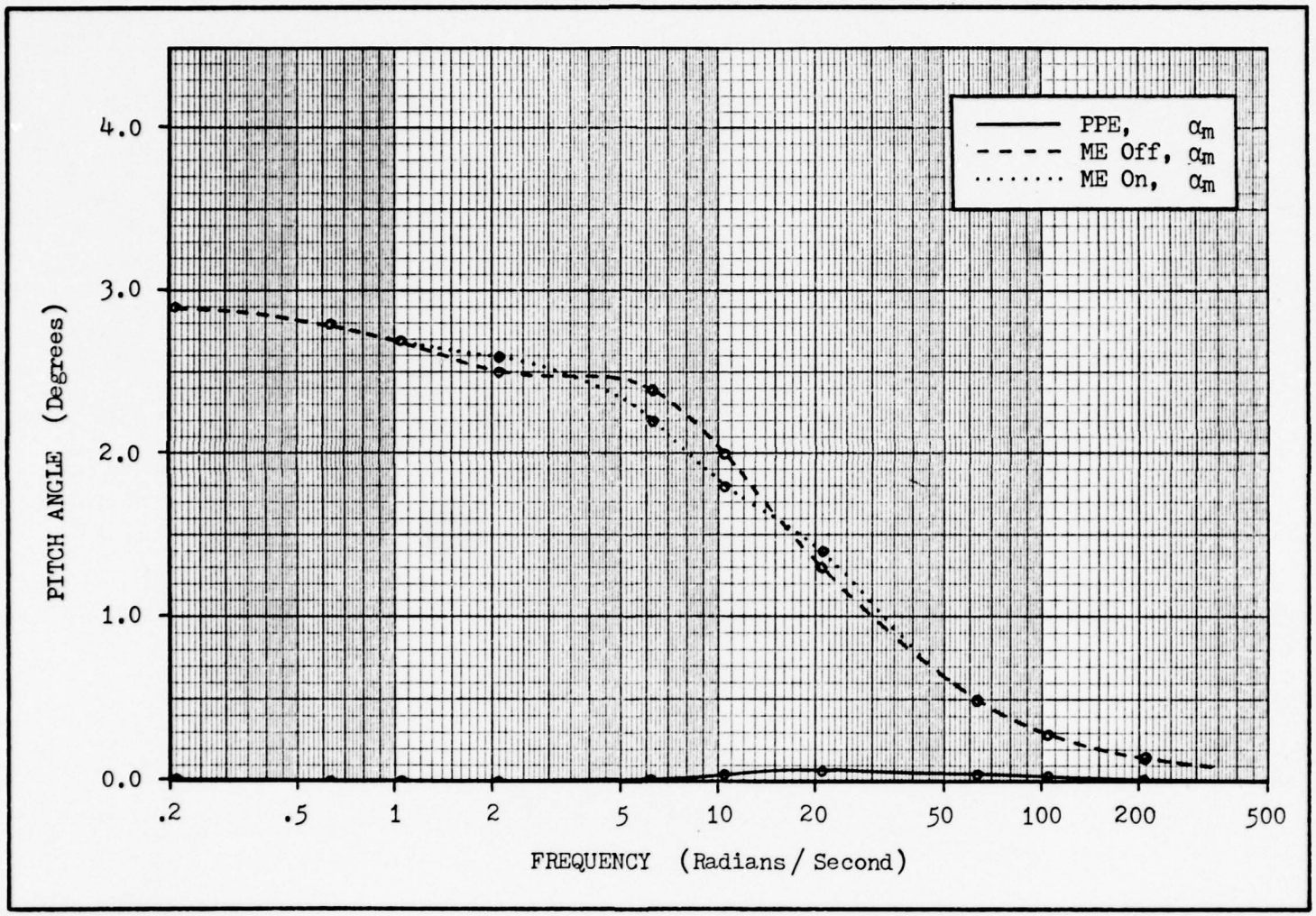


Figure 35. Comparison of peak pitch angle response of YF-16 CCV and PPE flight control systems.

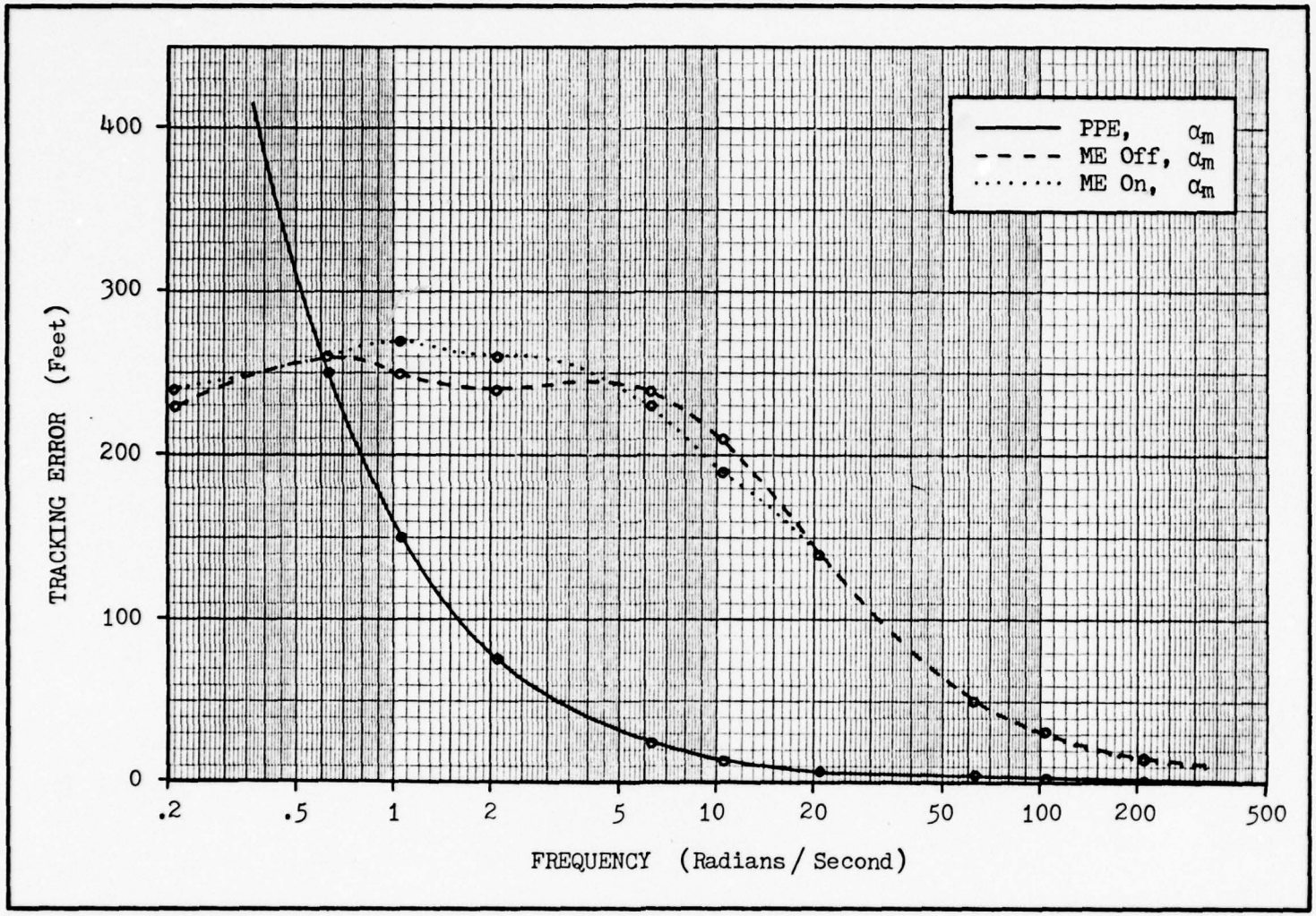


Figure 36. Comparison of peak target tracking error response of YF-16 CCV and PPE flight control systems.

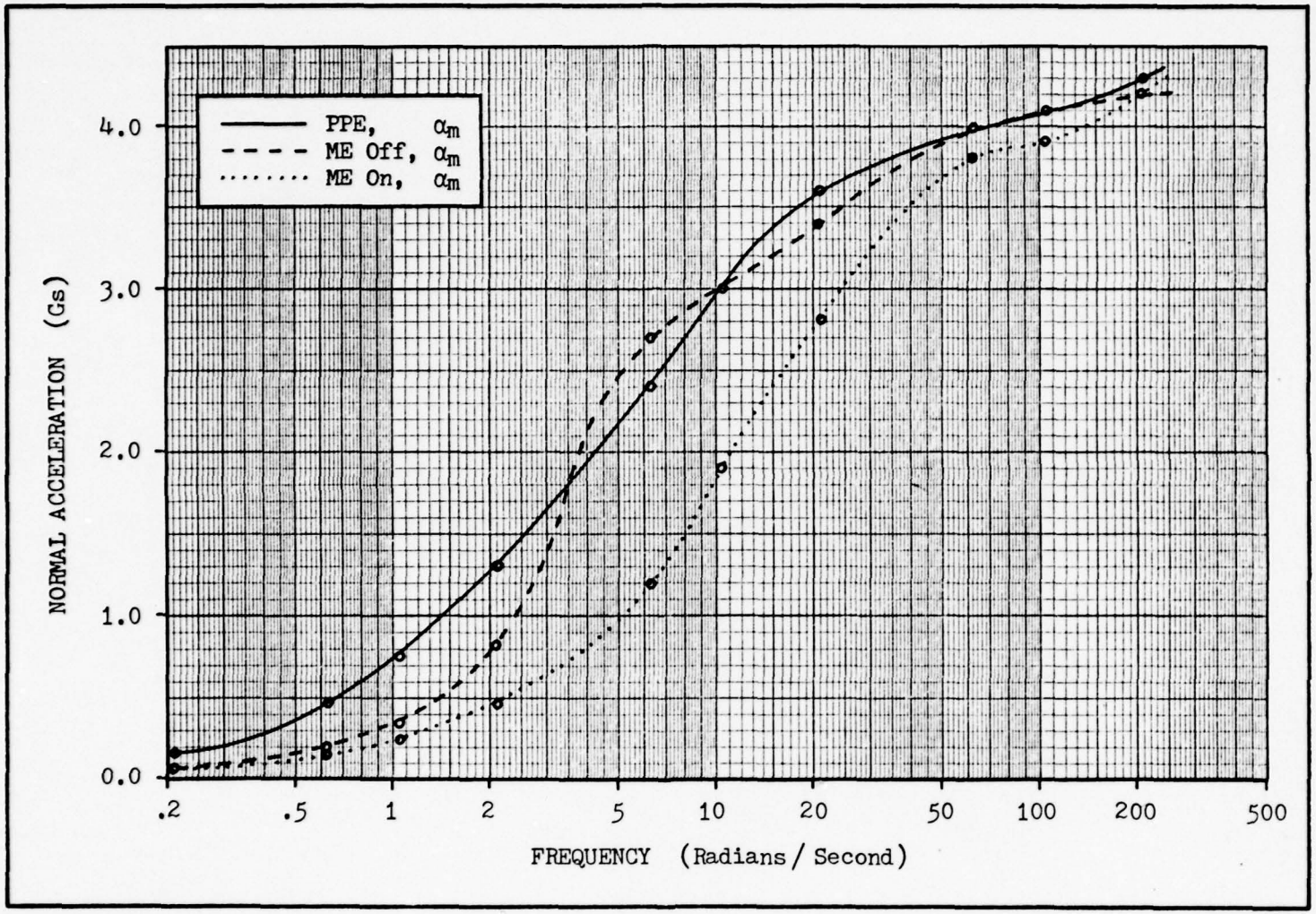


Figure 37. Comparison of peak normal acceleration response of YF-16 CCV and PPE flight control systems.

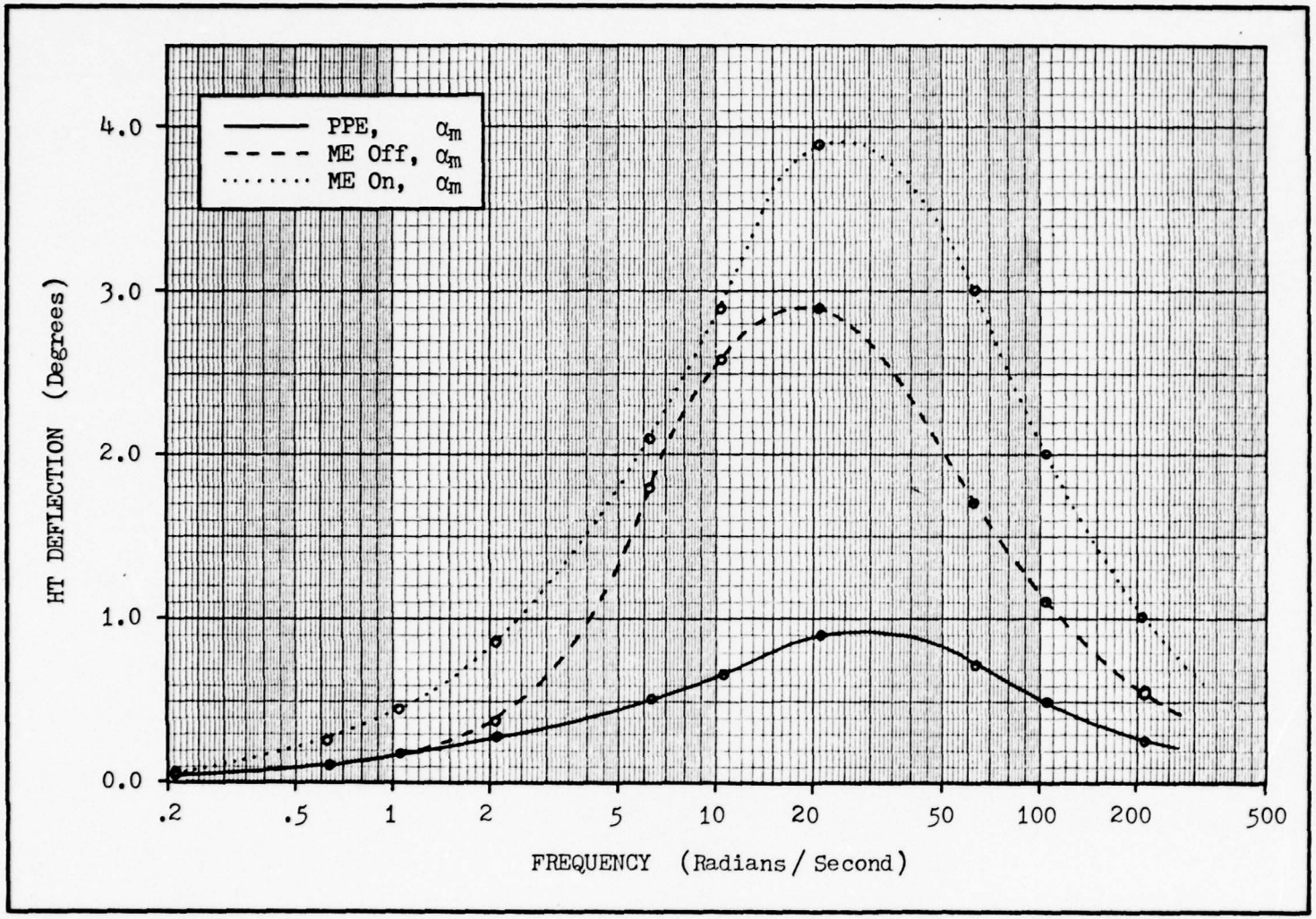


Figure 38. Comparison of peak horizontal tail deflection of YF-16 CCV and PPE flight control systems.

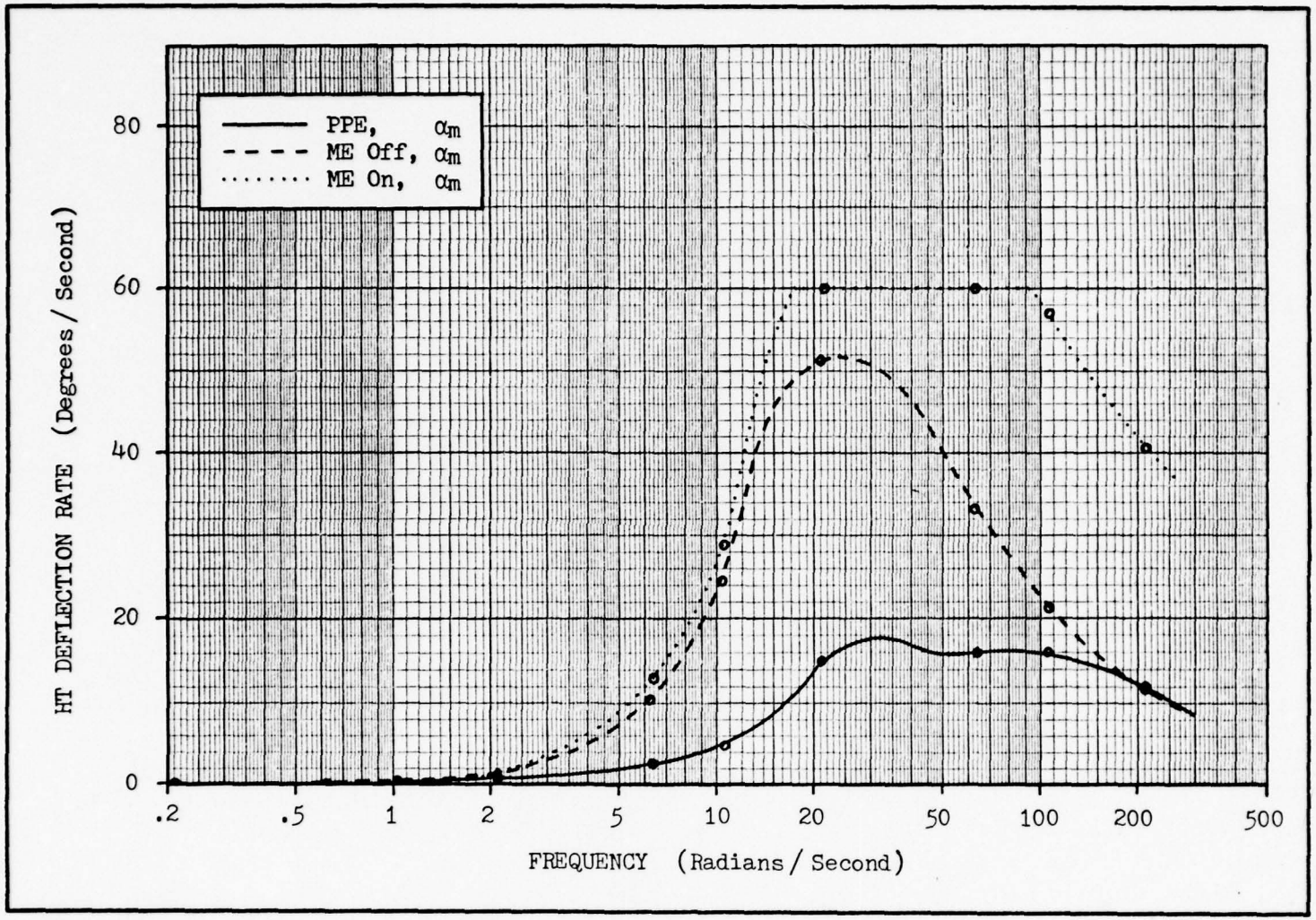


Figure 39. Comparison of peak horizontal tail deflection rate of YF-16 CCV and PPE flight control systems.

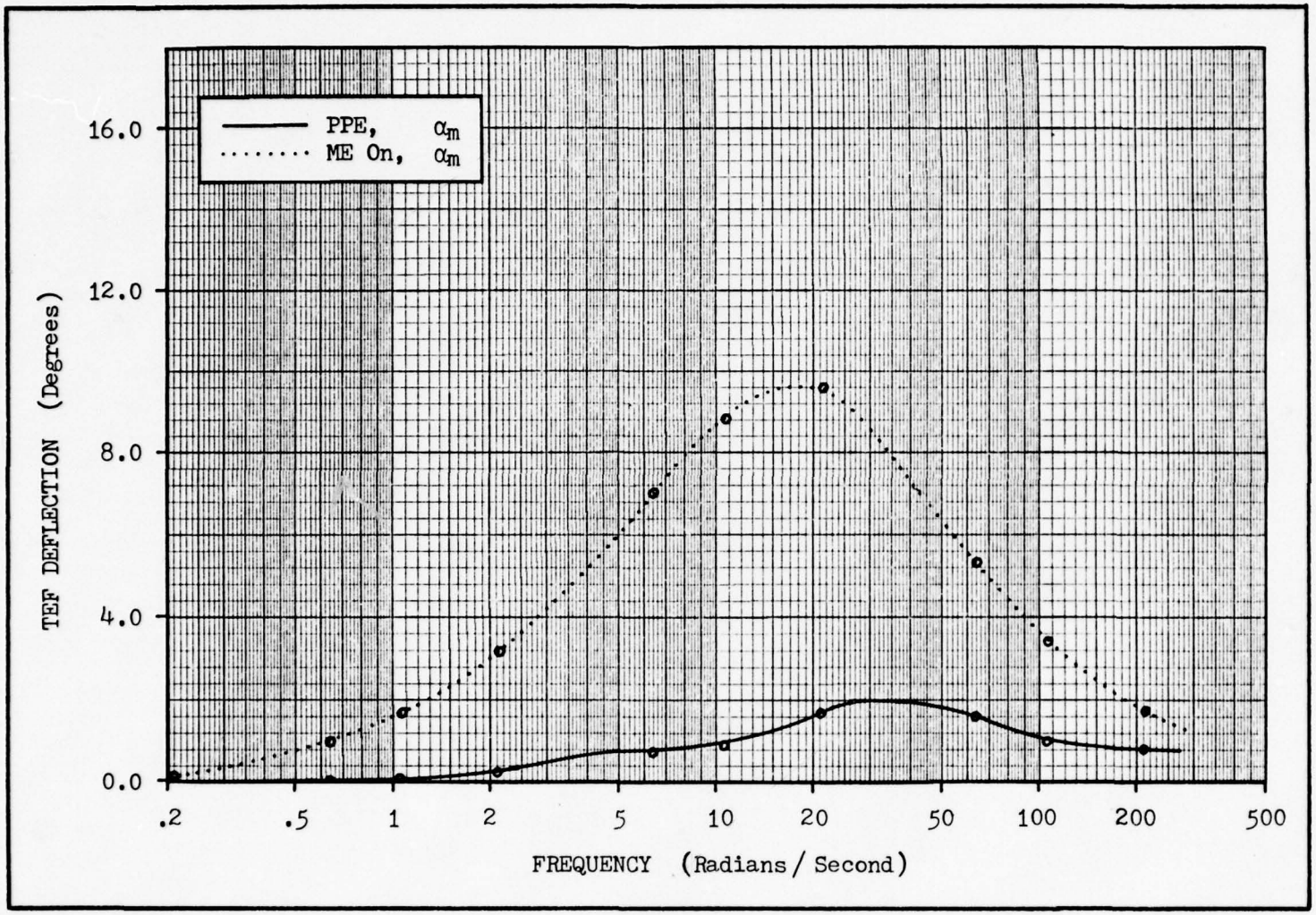


Figure 40. Comparison of peak trailing-edge flaperon deflection of YF-16 CCV and PPE flight control systems.

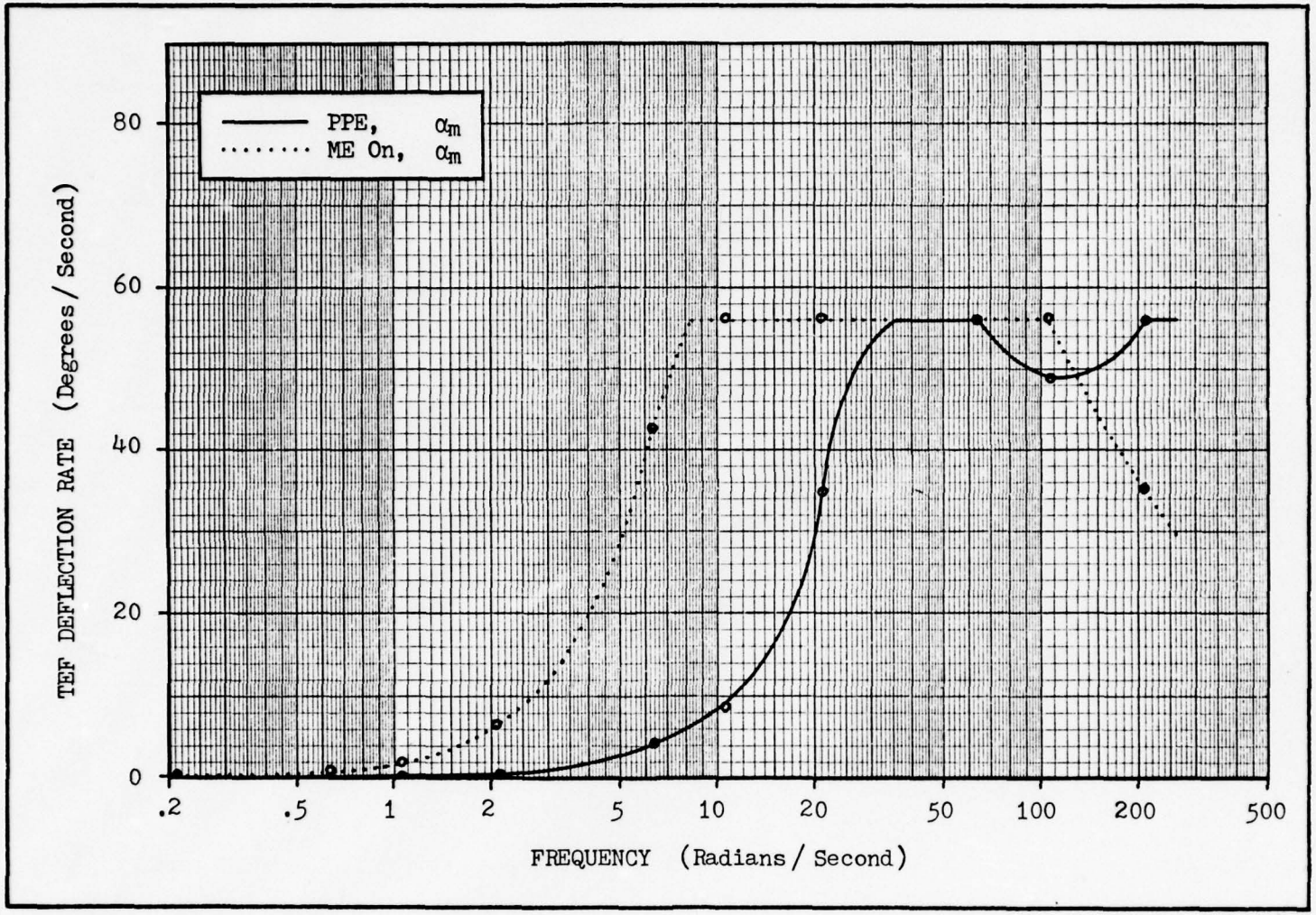


Figure 41. Comparison of peak trailing-edge flaperon deflection rate of YF-16 CCV and PPE flight control systems.

V. Conclusions and Recommendations

Conclusions

The primary objective of this investigation was to determine the possibility of reducing the magnitude of disturbance induced perturbations in the pitch response of the YF-16 through simultaneous and coordinated activation of the flaperons and horizontal tail. It has been clearly demonstrated that by careful selection of the system configuration, it is possible to both decrease aircraft response to disturbances and improve response to pilot commands.

An iterative approach using limited state feedback was found to produce the best results, as this method permitted the required control of zero locations by clearly modeling the effect of each of the system gains. Primary feedback to the horizontal tail consisted of pitch rate and angle-of-attack measurements. A secondary pitch rate feedback loop was closed around a proportional plus integral (P+I) compensator to form the desired pitch rate control system. The use of the cascaded P+I compensation resulted in an excellent system transient response to pilot commands, in addition to functioning as a series trim. Feedback to the trailing-edge flaperons consisted of pitch rate, normal accleration, and angle-of-attack. The problem of unnecessary drag induced by residual flaperon deflection was overcome by placing a washout circuit in the forward loop.

In the process of chosing a system configuration, it was

observed that in order to reduce the effect of disturbances on pitch response, a pitch rate command system is required. The use of normal acceleration feedback to the horizontal tail to permit a G-command system clearly degraded the pitch response to turbulence. As a possible compromise solution, a C* command configuration was attempted. The results, however, were no better than with the pure G-command system.

One other outcome of this thesis that should be mentioned is the recognition that stability-axis perturbation attack angle, $'\alpha$, only has meaning as an attack angle when the surrounding air is assumed motionless. If atmospheric disturbances are present, $'\alpha$ is not the attack angle that is measured by the angle-of-attack sensors. Since attack angle is used as a feedback quantity, system response is impacted by the manner in which it is defined. This was demonstrated clearly in Chapter III.

Recommendations

There is much follow-on research related to this investigation that can be of great interest to pursue. As with any flight control system design that has been examined at a single flight condition, it is important to determine if the desired performance can be achieved throughout the entire flight envelope. Non-dimensional stability derivatives for several flight conditions have been determined for the purpose of continued research, and are included in Appendix B. Such an analysis would additionally provide the necessary data to establish any required gain scheduling as a fuction

of flight condition. It may also reveal that a particular set of fixed system gains could be sufficient, with no need for gain scheduling.

A related area that should be investigated is the affect of changes in feedback and feed-forward gains on system stability and overall performance. A sensitivity analysis and failure modes and effects analysis could provide a good indication of the magnitude of performance degradation that can be anticipated as a result of unexpected gain changes. The results of such analyses might specify a requirement for certain components to be redundant with either simultaneous balanced feed or a voting capability.

For the purpose of reducing the amount of effort required to solve for the system transfer functions, the configuration of the PPE flight control system did not include the second-order power actuators. Although they were included for simulation purposes, thus validating the assumption that they can be removed for the design process, it may be interesting to determine if the dynamics of the actuators can be used to some advantage. To support such an effort, a first-order observer has been designed to access the actuator internal state, and is included in Appendix I.

One final area for continued research might be to investigate the use of the presented approach in the design of a discrete-time digital controller for the aircraft. In Chapter IV, the system equations were intentionally developed in a general form to support such an effort. It is assumed that a

digital design can be implemented in a manner analogous to that presented, by specifying a sampling rate and simply determining transfer functions in the z-plane instead of the s-plane. A successful design would have the advantage of permitting the use of a digital flight control computer. Such a system is not only generally smaller and lighter than its analogue counterpart, but more flexible and less failure prone as well. Control law implementation can be software derived, as opposed to hardwired, providing the capability for reprogramming.

Bibliography

1. Blakelock, John H. Automatic Control of Aircraft and Missiles. New York: John Wiley and Sons, Inc., 1965.

2. Cadzow, J.A. and H.R. Martens. Discrete-Time and Computer Control Systems. New Jersey: Prentice-Hall, Inc., 1970.

3. Carroll, Robert G.H. "F-16: Swing-Force Fighter For The '80s." Air Force Magazine, 59:30-35 (April 1976).

4. Chalk, C.R., T.P. Neal, T.M. Harris, F.E. Pritchard, and R.J. Woodcock. Background Information and User Guide For MIL-F-8785B. Tech Report AFFDL-TR-69-72. Ohio: Air Force Flight Dynamics Laboratory, August 1969.

5. D'Azzo, J.J. and C.H. Houpis. Feedback Control System Analysis and Synthesis. New York: McGraw-Hill Book Company, Inc., 1966.

6. D'Azzo, J.J. and C.H. Houpis. Linear Control System Analysis and Design. New York: McGraw-Hill Book Company, Inc., 1975.

7. Etkins, B. Dynamics of Flight: Stability and Control. New York: John Wiley and Sons, Inc., 1959.

8. Fighter CCV Gust Response Analysis. FZM-620-045. General Dynamics / Fort Worth Division, July 1976.

9. Fighter CCV Phase I Report - Configuration Selection and Control System Design. Tech Report AFFDL-TR-75-106. General Dynamics / Fort Worth Division, September 1975.

10. Fighter CCV Phase II Report - Detail Design. Tech Report AFFDL-TR-76-119. General Dynamics / Fort Worth Division, October 1976.

11. Lee, W.H., M. Athans, D. Costanon, and F. Bacchioloni. Tracking Systems With Applications To Aircraft Control System Design. Nasa Langley Research Grant No. ESL-R-720, MIT, January 1977.

12. Luenberger, David G. "An Introduction To Observers." Transactions, Institute of Electrical and Electronics Engineers, Vol AC-16, No. 6 (December 1971).

13. MIL-F-8785B. Military Specification - Flying Qualities of Piloted Airplanes. 7 August 1969, amended 16 Sep 1974.

14. Molner, E.R. Three-Degree-of-Freedom Longitudinal Simulation of the F-4E Fighter. Unpublished Laboratory Report. Ohio: Air Force Institute of Technology, Apr 1977.

15. Negro, James. EE6.60 Notes. Unpublished Class Notes. Ohio: Air Force Institute of Technology, Winter Quarter, 1977.

16. Porter, B. and T.R. Crossley. Modal Control - Theory and Applications. London: Taylor and Francis, 1972.

17. Rider, James G. "YF-16. Pilot Report." Air Force Magazine, 59:32-37 (October 1976).

18. Stability and Flight Control - Aft Center of Gravity Limit Determination. FZM-401-085. General Dynamics / Convair Aerospace Division, October 1973.

19. Stability and Flight Control - YF-16 Aerodynamic Data Summary, Volume 3 - Flexible Aerodynamic Data. FZM-401-041. General Dynamics, November 1973.

20. Stability and Flight Control - YF-16 System/Subsystem Summary Report, Volume 4. FZM-401-069-4. General Dynamics / Convair Aerospace Division, December 1973.

21. Taylor, John W.R. "Jane's - All the World's Aircraft Supplement." Air Force Magazine, 59:49-50 (August 1976).

22. Tobie, H.N. and E.M. Elliot. New Short Period Handling Qualities Criterion for Fighter Aircraft. Boeing Document No. DG-17841 T/N, September 1965.

23. TOTAL. Control System Analysis and Synthesis Computer Program. Unpublished User's Guide to Computer Program. OHIO: Air Force Institute of Technology, March 1978.

24. TRANFUN. Transfer Function Computer Program. Unpublished User's Guide to Computer Program. Ohio: Air Force Institute of Technology, 1974.

25. Wind Tunnel Tests of a 1/15 - Scale YF-16 Control Configured Vehicle at Mach Numbers From 0.6 to 1.2. AEDC-TR-74-91. Tennessee: Arnold Air Force Station, Sep 1974.

26. Wind Tunnel Tests of 1/9 - Scale YF-16 and F-16A/B Models at Mach Numbers From 0.6 to 2.0. AEDC-TR-76-166. Tennessee: Arnold Air Force Station, March 1977.

Appendix A

List of Abbreviations and Symbols

Abbreviations

AC	-	Aerodynamic Center
A/C	-	Aircraft
AFCC	-	Aux Flight Control Computer
CAL	-	Cornell Aeronautical Laboratory
CCV	-	Control Configured Vehicle
CDC	-	Control Data Corporation
CF	-	Conversion Factor
CG	-	Center of Gravity
CSA	-	Compensator/Servo/Actuator
FBW	-	Fly-by-wire
FC	-	Flight Condition
FCC	-	Flight Control Computer
FCS	-	Flight Control System
fps	-	Feet Per Second
FS	-	Fuselage Station
GW	-	Gross Weight
HT	-	Horizontal Tail
Hz	-	Hertz
IC	-	Initial Condition
L/H	-	Left Hand
MAC	-	Mean Aerodynamic Chord
ME	-	Maneuver Enhancement
P+I	-	Proportional Plus Integral

PPE	-	Pitch Performance Enhancement
R/H	-	Right Hand
r/s	-	Radians per Second
SL	-	Sea Level
SS	-	Span Station
TEF	-	Trailing-edge Flaperon
TF	-	Transfer Function (Laplace)
Undef	-	Undefined
Unk	-	Unknown
WL	-	Waterline

Symbols

$\underline{A}$	-	Continuous-time system dynamics matrix
A_N	-	Normal Acceleration, defined positive upward, measured at the normal accelerometer location
A_{N_s}	-	Normal Accelerometer output (positive upward)
A_z	-	Normal Acceleration, defined positive downward, at the center of gravity of the aircraft
$\underline{B}$	-	Continuous-time system control matrix
$\underline{C}$	-	System output matrix
c	-	Mean aerodynamic chord length
C_D	-	Coefficient of drag
$C_{F_{x_a}}$	-	The change in the forces in the X direction as a result of the sum of the deflections of all control surfaces
$C_{F_{z_a}}$	-	The change in the forces in the Z direction as a result of the sum of the deflections of all control surfaces
C_L	-	Coefficient of lift
C_{L_q}	-	The change in the coefficient of lift as a result of a pitching velocity
C_{L_α}	-	The change in the coefficient of lift as a result of a change in angle-of-attack caused by a change in w
C_{m_a}	-	The change in pitching moment as a result of the sum of the deflections of all control surfaces
C_{m_q}	-	The change in pitching moment as a result of a pitching velocity
C_{m_α}	-	The change in pitching moment as a result of a change in angle-of-attack caused by a change in w
$C_{m_{\dot{\alpha}}}$	-	The change in pitching moment as a result of the time rate of change of angle-of-attack caused by w

C_{m_δ} - The change in the pitching moment due to the deflection of a control surface

$C_{m_{\delta_{ht}}}$ - The change in the pitching moment due to the deflection of the horizontal tail

$C_{m_{\delta_{tef}}}$ - The change in the pitching moment due to the deflection of the trailing-edge flaperons

C_w - Coefficient due to the acceleration of gravity

C_{x_u} - The change in the force in the X direction as a result of a change in forward velocity

C_{x_α} - The change in the force in the X direction as a result of a change in angle-of-attack caused by a change in w

C_{x_δ} - The change in the force in the X direction due to a control surface deflection

$C_{x_{\delta_{ht}}}$ - The change in the force in the X direction due to a horizontal tail deflection

$C_{x_{\delta_{tef}}}$ - The change in the force in the X direction due to a trailing-edge flaperon deflection

C_{z_u} - The change in the force in the Z direction as a result of a change in forward velocity

C_{z_q} - The change in the force in the Z direction as a result of a pitching velocity

C_{z_α} - The change in the force in the Z direction as a result of a change in angle-of-attack caused by a change in w

$C_{z_{\dot{\alpha}}}$ - The change in the force in the Z direction as a result of the time rate of change of angle-of-attack caused by w

C_{z_δ} - The change in the force in the Z direction due to a control surface deflection

$C_{z_{\delta_{ht}}}$ - The change in the force in the Z direction due to a horizontal tail deflection

$C_{z_{\delta_{tef}}}$ - The change in the force in the Z direction due to a trailing-edge flaperon deflection

C^* - C-star longitudinal response criteria

$\underline{D}$ - System feedforward matrix

d	-	Initial distance from aircraft to target
D	-	Coefficient of pitching velocity specifying the amount that is sensed by the angle-of-attack sensor as a result of its position relative to the CG of the aircraft
dB	-	Decibel
d_m	-	Distance to peak vertical gust velocity (feet)
$\underline{F}$	-	Discrete-time system dynamics matrix
F_z	-	Force in the Z direction
F3	-	Forward-loop scheduled gain
F4	-	Attack angle feedback scheduled gain
g, G	-	Gravitational acceleration
		Vertical acceleration
$\underline{G}$	-	Discrete-time system control matrix
G_{err}	-	g error signal
h	-	Vertical displacement of the aircraft caused by an external disturbance
H	-	Altitude, in feet
I_y	-	Mass moment of inertia about the Y axis of the aircraft
$\underline{K}$	-	System feedback matrix
K_c	-	Horizontal tail command forward-loop gain
K_f	-	Trailing-edge flaperon forward-loop gain
K_h	-	Horizontal tail forward-loop gain
K_N	-	C* feedback gain of normal acceleration measured at the CG of the aircraft
K_p	-	Trailing-edge flaperon command forward-loop gain
K_q	-	C* feedback gain of pitch rate based upon crossover velocity
$K_{\dot{q}}$	-	C* feedback gain of pitch acceleration based upon the distance from the aircraft CG to the

pilot station

K_1 - Attack angle feedback gain to the HT channel

K_2 - Attack angle feedback gain to the TEF channel

K_3 - Pitch rate feedback gain to the HT channel

K_4 - Pitch rate feedback gain to the TEF channel

K_5 - Pitch rate command feedback gain to the HT channel

K_6 - Normal acceleration feedback gain to the TEF channel

L - Lift force

l_t - The distance, in feet, from the wing MAC to the horizontal tail MAC

m - Mass of the aircraft, in slugs

$\underline{M}$ - System disturbance feedforward matrix

$\underline{N}$ - System disturbance input matrix

P_o - Static pressure at Sea Level

P_s - Static pressure at altitude

q - The change in pitching velocity resulting from some disturbance

Dynamic pressure

Q - Total angular pitching velocity

Q_o - Equilibrium angular pitching velocity

q_c - Impact pressure

q_s - Pitch rate gyro output

R - TEF washout eigenvalue

s - Laplace variable

S - Planform area of the wing, in sq ft

T_E - Longitudinal target tracking error

u - The change in linear forward velocity resulting from some disturbance (perturbation forward

velocity)

$'u$	-	Non-dimensional perturbation forward velocity
U	-	Total linear forward velocity
U_o	-	Equilibrium forward velocity
v	-	Vertical gust velocity (ft/sec)
V	-	Aircraft velocity, in knots
v_m	-	Vertical gust peak magnitude (ft/sec)
V_s	-	Velocity of sound, in knots
$\underline{V}_T$	-	Aircraft velocity vector
$\underline{V}_{T_o}$	-	Equilibrium aircraft velocity vector
w	-	The change in linear vertical velocity resulting from some disturbance (perturbation vertical velocity)
W	-	Total linear vertical velocity, defined positive downward
W_o	-	Equilibrium vertical velocity, defined positive downward
w_g	-	Vertical gust velocity, defined positive downward
w_s	-	Vertical velocity of the angle-of-attack sensor, defined positive downward
$w_{a/A}$	-	Vertical velocity of the aircraft relative to the surrounding air
$w_{a/E}$	-	Vertical velocity of the aircraft relative to the Earth
$w_{A/E}$	-	Vertical velocity of the surrounding air relative to the Earth
x	-	Command prefilter eigenvalue
X, Y, Z	-	Orthogonal disturbed aircraft axes
X_o, Y_o, Z_o	-	Orthogonal equilibrium aircraft axes
X_E, Y_E, Z_E	-	Orthogonal Earth reference axes
z	-	HT P+I cascade compensator zero

1 - cos	-	Discrete vertical gust formed by displacing an inverted cosine wave a unit distance above the time axis
$'\alpha$	-	Perturbation attack angle ($\sim w/U$)
α	-	Angle-of-attack, defined as the angle between the velocity vector of the aircraft and the chord of the wing
α_o	-	Angle between the aircraft X axis and the chord of the wing
α_g	-	Effective attack angle generated as a result of the vertical velocity of the surrounding air relative to the Earth, defined positive for an upward gust ($-\alpha_{A/E}$)
α_m	-	True perturbation attack angle ($'\alpha + \alpha_g$)
α_s	-	Attack angle sensor output
α_t	-	Trim angle-of-attack (at equilibrium)
$\alpha_{a/A}$	-	Effective attack angle generated as a result of the vertical velocity of the aircraft relative to the surrounding air
$\alpha_{a/E}$	-	Effective attack angle generated as a result of the vertical velocity of the aircraft relative to the Earth
$\alpha_{A/E}$	-	Effective attack angle generated as a result of the vertical velocity of the surrounding air relative to the Earth
β	-	TEF servo eigenvalue
δ	-	Control surface angular deflection
δ_e	-	Elevator deflection (used interchangably with δ_h)
δ_f	-	Flaperon deflection (used interchangably with δ_{tef})
δ_h	-	Horizontal tail deflection
δ_{ht_L}	-	L/H horizontal tail deflection
δ_{ht_R}	-	R/H horizontal tail deflection
δ_{tef}	-	Trailing-edge flaperon deflection

δ_{tef_L}	-	L/H trailing-edge flaperon deflection
δ_{tef_R}	-	R/H trailing-edge flaperon deflection
γ	-	Air density ratio
		Flight path angle
		HT servo eigenvalue
γ_o	-	Initial (equilibrium) flight path angle
θ	-	Perturbation pitch angle
θ_o	-	Initial (equilibrium) pitch angle (angle between the horizontal and the aircraft axis)

Appendix B

Derivation of Stability Derivatives

To make use of the equations of motion presented in Chapter II, it is necessary to have certain aerodynamic data available on the aircraft to be modeled. Generally speaking, stability derivatives are usually not available, and they must be determined from lift, drag, and moment data. In the next several pages, non-dimensional stability derivatives for six flight conditions (FCs) are presented as derived from sources of corrected wind tunnel data (References 10,19,25,26). The six flight conditions are:

Mach	Altitude
0.6	Sea Level (SL)
0.6	30,000 ft
0.8	SL
0.8	30,000 ft
0.9	SL
0.9	30,000 ft

Since the YF-16 is unstable only in sub-sonic flight (Ref 9), no supersonic flight conditions are included. In addition, the aircraft is most susceptible to wind gust disturbances over the range of flight conditions chosen (Ref 8).

The procedure used for determining the derivatives and coefficients is illustrated for the flight condition used in

the analyses in Chapters III and IV (0.8 Mach at SL). Data for the remaining FCs was determined using the same methods. Data for all FCs is summarized in Table 6.

The first step in the process is to determine how much lift is necessary to maintain the aircraft in equilibrium flight. This occurs when the force generated by lift is exactly equal and opposite to the force of gravity. Lift is given by

$$L = C_L' S q \tag{45}$$

where S is the planform area of the wing, q is dynamic pressure, and C_L is the coefficient of lift. Setting lift equal to the force of gravity yields

$$C_L S q = mg \tag{46}$$

where m is the mass of the aircraft, and g is gravitational acceleration, defined positive downward. Solving this equation for C_L results in an expression that determines the necessary coefficient of lift to maintain equilibrium flight at any given altitude or airspeed. This expression is

$$C_L = \frac{mg}{Sq} \tag{47}$$

In this analysis, the GW (gross weight) of the aircraft is assumed to be 16,519 lbs at SL. As g = 32.81 at SL, the mass of the aircraft is determined to be

$$m = \frac{GW}{g} = 16,519/32.18 = 513.4 \text{ slugs} \tag{48}$$

For altitudes other than Sea Level, the weight (mg) will vary with g. A relation for gravitational acceleration as a function of altitude is (Ref 14),

$$g = 32.177 - (0.00009406)H \tag{49}$$

where H is the particular altitude, in feet.

The dynamic pressure, q, is a function of both altitude and airspeed. It can be determined from the expression

$$q = \frac{\gamma}{295}V^2 \tag{50}$$

where γ is the air density ratio at the altitude of interest, and V is the velocity of the aircraft, in knots. The air density ratio, defined as the ratio of air density at a specified altitude to air density at Sea Level, is a function of altitude only, and its value may be determined from a standard altitude table. To express q as a function of Mach Number, recall that Mach Number is defined as

$$\text{Mach Number} = M = \frac{V}{V_S} \tag{51}$$

where V_S is the velocity of sound, in knots. Combining Eqns 50 and 51, dynamic pressure can now be determined from the final expression

$$q = \frac{\gamma}{295}(MV_S)^2 \tag{52}$$

For the flight condition 0.8 Mach at SL, q = 949.9, since $\gamma = 1$ and $V_S = 661.7$ knots. The planform wing area of the YF-16 is S = 280 sq ft (Ref 10). The required lift coefficient can now

be readily determined as

$$C_L = \frac{mg}{Sq} = \frac{(32.18)(513.4)}{(280)(949.9)} \quad (53)$$

Given the value of C_L, the attack angle at which the aircraft will trim can be found. This establishes the equilibrium flight condition. Typical corrected wind tunnel data for this determination is shown in Figure 42 (Ref 26). The value of this trim angle-of-attack, $\alpha_t = 0.81$ degrees, can be read directly. Actually, the C_L vs α curve of Figure 42 is a family of curves, and the curve chosen depends upon the amount of horizontal tail deflection required to maintain equilibrium flight. Due to the aircraft velocity at this FC, however, the horizontal tail deflection is almost negligible, and therefore the $\delta_{ht} = 0$ curve is appropriate. With an established equilibrium condition, the required stability derivatives and coefficients may now be determined.

a. C_{m_q}

Given airspeed and α_t, this derivative can be determined directly from available data. A typical C_{m_q} vs Mach curve is shown in Figure 43 (Ref 19). For the FC of interest,

$$C_{m_q} = -4.05 \quad (54)$$

b. $C_{m_{\dot{\alpha}}}$

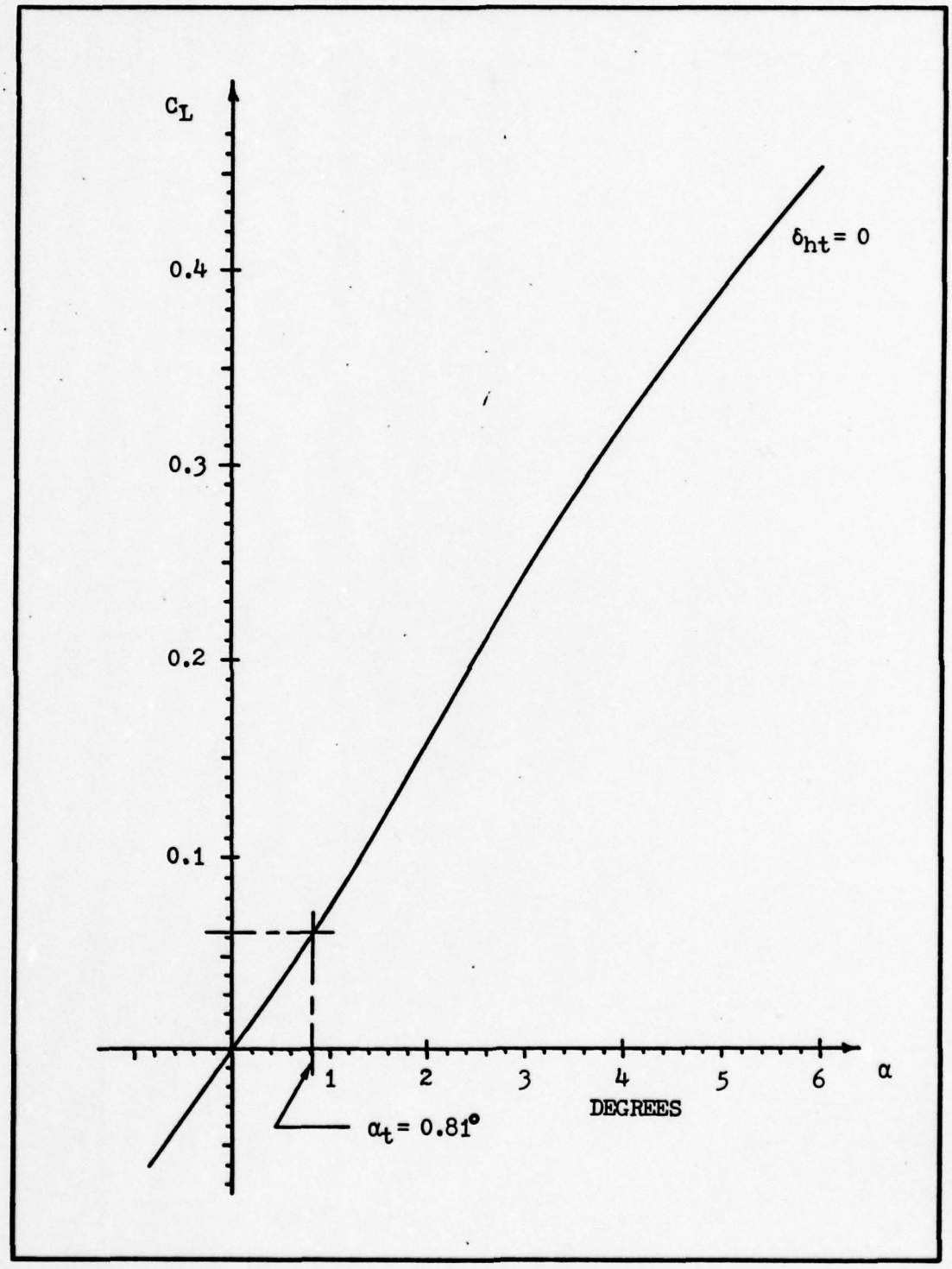


Figure 42. Plot of C_L vs α for 0.8 Mach at Sea Level (Ref 26).

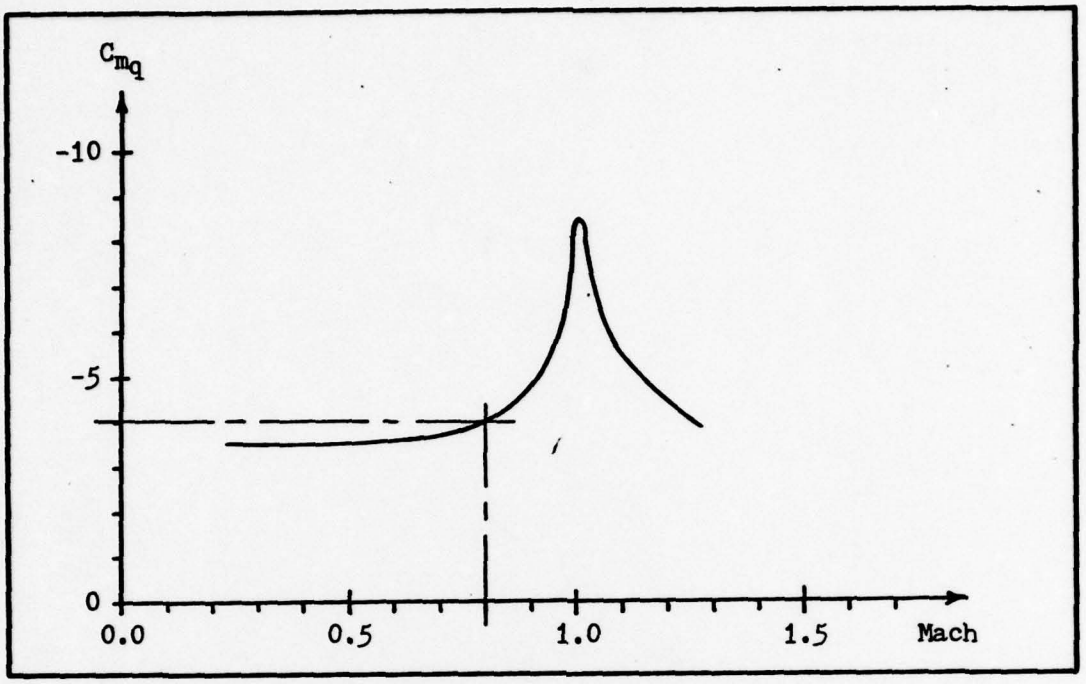


Figure 43. Plot of C_{m_q} vs Mach for $\alpha_t = 0.8°$ at Sea Level (Ref 19).

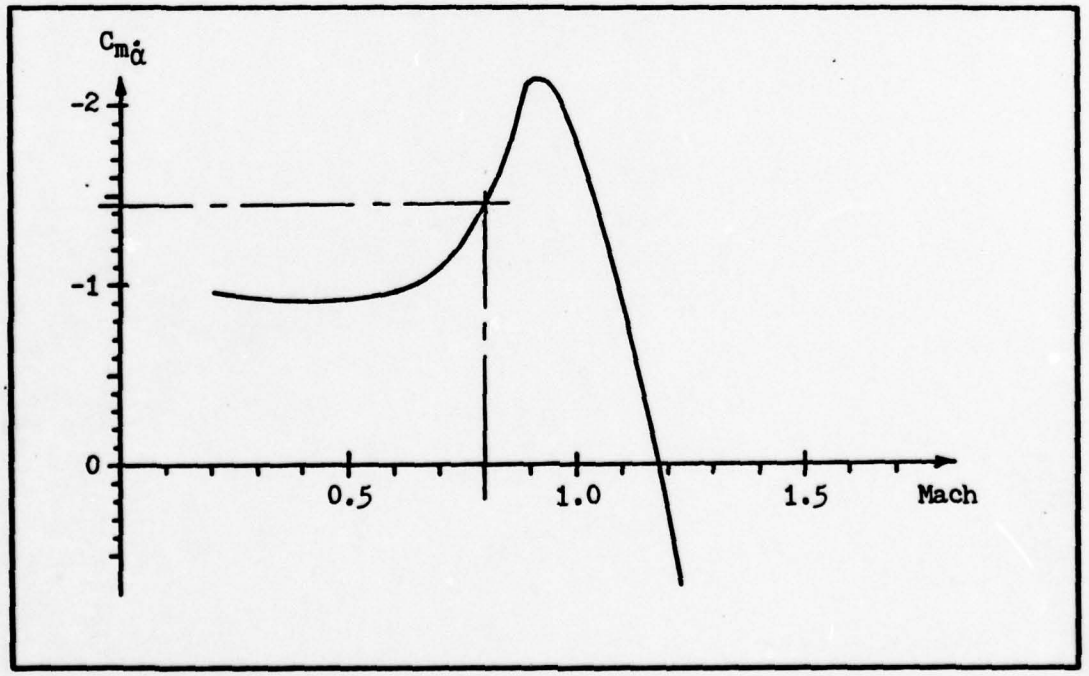


Figure 44. Plot of $C_{m_{\dot{\alpha}}}$ vs Mach for $\alpha_t = 0.8°$ at Sea Level (Ref 19).

Data for the determination of this derivative is also available plotted as a function of Mach Number for a given α_t. A typical curve is given in Figure 44 (Ref 19). For the FC of interest,

$$C_{m_{\dot{\alpha}}} = -1.45 \tag{55}$$

c. C_{z_q}

This derivative may sometimes be approximated by (Ref 1)

$$C_{z_q} = (c/l_t)C_{m_q} \tag{56}$$

where l_t is the distance from the wing MAC to the horizontal tail MAC. For the YF-16, l_t = 15.66 ft (Ref 10), and calculated in this way, $C_{z_q} = -2.83$. However, this expression is an approximation, and is generally valid only for conventional aircraft. Due to the placement of the horizontal tail relative to the wing of the YF-16, this method of determining C_{z_q} may not be as accurate as desired. It is assumed that a more accurate estimate can be made using the relation

$$C_{z_q} \simeq -C_{I_q} \tag{57}$$

Plots of C_{I_q} vs Mach Number are provided in Reference 19, and for the FC of interest, $C_{I_q} = 3.86$; therefore,

$$C_{z_q} \simeq -3.86 \tag{58}$$

d. $C_{z_{\dot{\alpha}}}$

This derivative may sometimes be approximated by (Ref 1):

$$C_{z_{\dot{\alpha}}} = (c/l_t) C_{m_{\dot{\alpha}}} \tag{59}$$

The relationship is the same as given in Eqn 56. Calculated in this manner, $C_{z_{\dot{\alpha}}} = -1.01$. Again, due to the design of the airframe, it is assumed that a more accurate estimate of this derivative can be made using the relation

$$C_{z_{\dot{\alpha}}} \simeq -C_{L_{\dot{\alpha}}} \tag{60}$$

From a plot of $C_{L_{\dot{\alpha}}}$ vs Mach Number (Ref 19), the value at the FC of interest is determined to be $C_{L_{\dot{\alpha}}} = 1.08$; therefore,

$$C_{z_{\dot{\alpha}}} \simeq -1.08 \tag{61}$$

In this case, the values obtained using both approximations are fairly close.

e. C_w

This term is simply a gravity term, and is equal to $-C_L$. For the FC of interest,

$$C_w = -C_L = -0.0621 \tag{62}$$

f. $\frac{mU}{Sq}$

The only unknown in this quantity is the forward velocity of the aircraft, U, in ft/sec. Knowing Mach Number, and given that the velocity of sound at SL is 661.7 knots, the velocity of the aircraft in knots can be determined from Eqn 51. As 1 knot is equal to 1.6878 ft/sec, the velocity of the aircraft, in ft/sec, is determined to be

$$U = (1.6878)(0.8)(661.7) = 893 \qquad (63)$$

and the value of the coefficient can now be found:

$$\frac{mU}{Sq} = \frac{(513.4)(893)}{(280)(949.9)} = 1.725 \qquad (64)$$

g. $\frac{c}{2U}$

Given the Mean Aerodynamic Chord length, c = 10.937 feet (see Appendix E), the value of this coefficient can be found:

$$\frac{c}{2U} = \frac{10.937}{2(893)} = 0.00612 \qquad (65)$$

h. $\frac{I_y}{Sqc}$

The unknown in this quantity is I_y, the mass moment of inertia about the Y axis. From Reference 19, $I_y = 39,199$; therefore,

upon the distance from the aircraft CG to the

$$\frac{I_y}{Sqc} = \frac{39199}{(280)(949.9)(10.937)} = 0.0135 \quad (66)$$

i. C_{L_α}

This derivative is simply the change in C_L as a result of a change in α. Therefore, its value can be determined by taking the slope of the curve in Figure 42 at the operating point. This slope is approximately 0.0758 per degree. Since the stability derivatives are non-dimensional, this figure must be multiplied by 57.296 degrees/radian. This multiplication results in

$$C_{L_\alpha} = (.0758)(57.296) = 4.34 \quad (67)$$

j. C_{m_α}

This derivative in the change in C_m (moment coefficient) as a result of a change in α. Unfortunately, a C_m vs α curve is not generally available. However, C_{m_α} can be broken down into two terms as follows:

$$C_{m_\alpha} = \frac{\partial C_m}{\partial \alpha} = \frac{\partial C_m}{\partial C_L}\frac{\partial C_L}{\partial \alpha} = \frac{\partial C_m}{\partial C_L} C_{L_\alpha} \quad (68)$$

There are C_m vs C_L curves available (Ref 26), and for the FC of interest, the slope of the curve is approximately 0.0331. Since both C_m and C_L are non-dimensional, there are no

u - The change in linear forward velocity resulting from some disturbance (perturbation forward

conversion factors to be concerned with. The product of this derivative and C_{L_α} is

$$C_{m_\alpha} = (0.0331)(4.34) = 0.144 \quad (69)$$

k. C_D

This term is the coefficient of drag, and is equal and opposite to the total thrust in equilibrium. Its value can be read directly from a drag polar (Ref 26), which is a family of C_D vs C_L curves that vary with Mach Number. For the FC of interest,

$$C_D = 0.024 \quad (70)$$

l. C_{z_α}

This derivative can be determined from the relationship (Ref 1):

$$C_{z_\alpha} = -C_D - C_{L_\alpha} \quad (71)$$

Since C_D and C_{L_α} have already been determined, the expression is useful, and this derivative is

$$C_{z_\alpha} = -0.024 - 4.34 = -4.364 \quad (72)$$

X_E, Y_E, Z_E - Orthogonal Earth reference axes

z - HT P+I cascade compensator zero

m. C_{x_α}

This derivative can be determined from the relationship (Ref 1):

$$C_{x_\alpha} = C_L - \frac{dC_D}{d\alpha} \tag{73}$$

As C_D vs α curves are not standard aerodynamic data, this expression must be broken down into

$$C_{x_\alpha} = C_L - \frac{\partial C_D}{\partial C_L}\frac{\partial C_L}{\partial \alpha} = C_L - \frac{\partial C_D}{\partial C_L} C_{L_\alpha} \tag{74}$$

The only unknown term is the change in C_D for a change in C_L. This information may be obtained from a drag polar (Ref 26), by finding the slope of the curve at the operating condition. This slope is determined to be approximately 0.0025, and is dimensionless. Substitution into Eqn 74 yields:

$$C_{x_\alpha} = 0.0621 - (.0025)(4.34) = 0.0513 \tag{75}$$

n. C_{z_u}

This derivative can be determined from the relationship (Ref 1):

$$C_{z_u} = -2C_L - V\frac{dC_L}{dV} \tag{76}$$

Since aerodynamic data expressing a change in C_L for a change in V is not generally available, one method that can be used to determine the derivative is to collect sufficient data points to make a plot of C_L vs V. From such a plot, the slope

δ_{ht_R} - R/H horizontal tail deflection

δ_{tef} - Trailing-edge flaperon deflection

of the curve at the operating point yields the required derivative. The available data is in the form of C_L vs α curves as a function of Mach Number (Ref 25). Equation 76, therefore, can not be used directly. However, since Mach Number is defined as vehicle velocity, V, divided by the velocity of sound, V_s, the following equivalence can be shown:

$$M\frac{dC_L}{dM} = (V/V_s)\frac{dC_L}{d(V/V_s)} = (V/V_s)\frac{dC_L}{(1/V_s)dU} = V\frac{dC_L}{dV} \qquad (77)$$

Therefore, Eqn 76 can be written as

$$C_{z_u} = -2C_L - M\frac{dC_L}{dM} \qquad (78)$$

which can be used directly with the available data.

Values of C_L as a function of both Mach Number and angle-of-attack are plotted in Figure 45. Since, for any flight condition, the values of Mach Number, C_L, and attack angle are all known, any two of the three will locate the operating point. The slope of the curve at that operating point is

$$\text{Slope} = \frac{dC_L}{dM} = \frac{.075}{1.2} = .0625 \qquad (79)$$

Substituting this value into Eqn 78 yields:

$$C_{z_u} = -2(.0621) - .8(.0625) = -.174 \qquad (80)$$

o. C_{x_u}

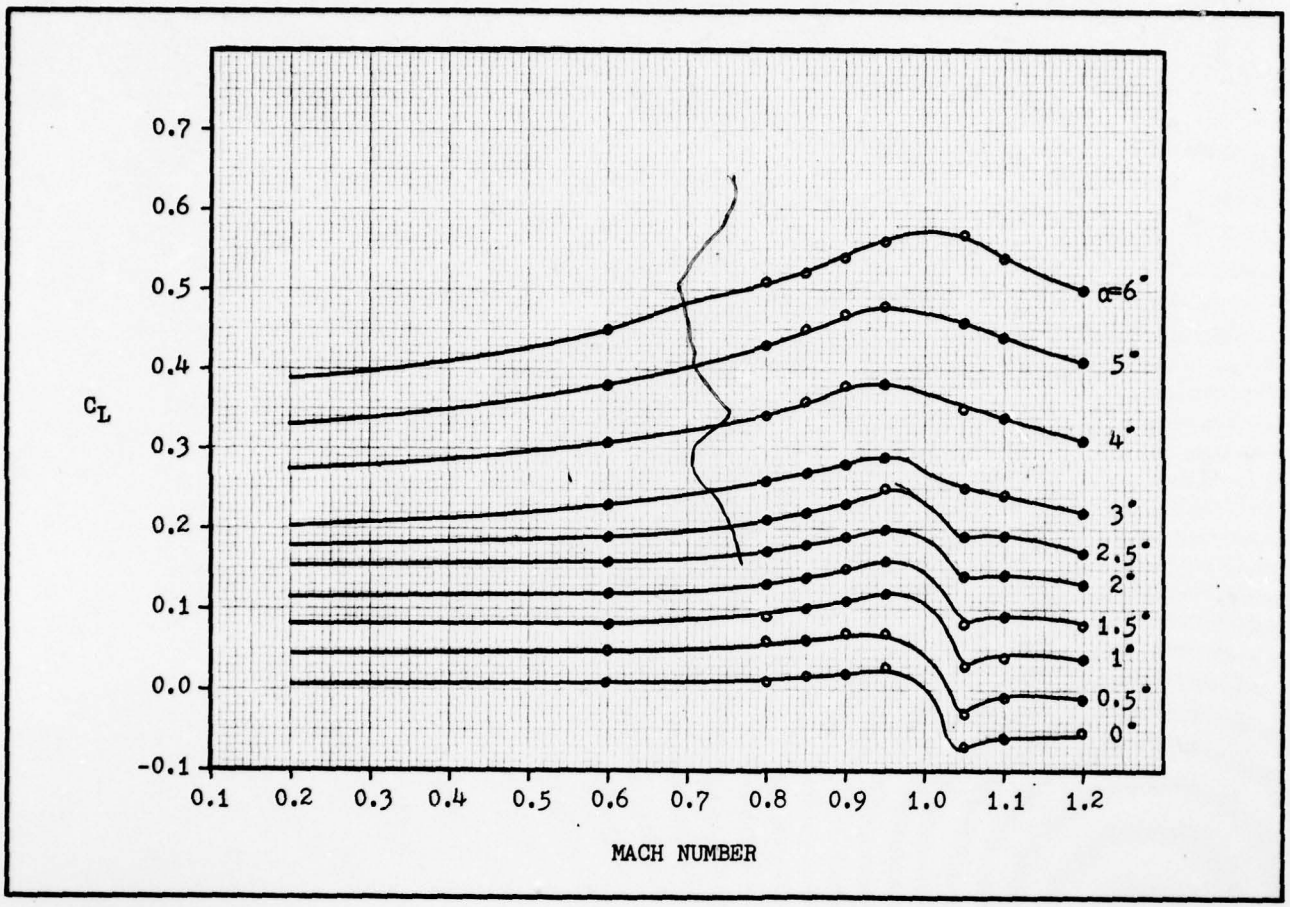


Figure 45. Plot of C_L as a function of Mach Number and angle-of-attack.

This derivative can be determined from the relationship (Ref 1):

$$C_{x_u} = -2C_D - V\frac{dC_D}{dV} \tag{81}$$

As in the previous case for C_{z_u}, data expressing a change in drag coefficient for a change in forward velocity is not generally available. Using the equivalence given in Eqn 77, it can be shown that Eqn 81 is equivalent to

$$C_{x_u} = -2C_D' - M\frac{dC_D}{dM} \tag{82}$$

Values of C_D as a function of both Mach Number and angle-of-attack are plotted in Figure 46. The slope of the curve at the operating point provides the required derivative. For the FC being considered,

$$\frac{dC_D}{dM} = \frac{.027}{1.2} = .0225 \tag{83}$$

Substituting this value into Eqn 82 yields:

$$C_{x_u} = -2(.024) - .8(.0225) = -.0660 \tag{84}$$

p. $C_{m_{\delta_{ht}}}$

This derivative is given as $C_{m_{\delta_{ht}}} = -.01$ per degree in Reference 10. Multiplying by 57.296 degrees/radian to put it in non-dimensional form,

$$C_{m_{\delta_{ht}}} = (-.01)(57.296) = -.573 \tag{85}$$

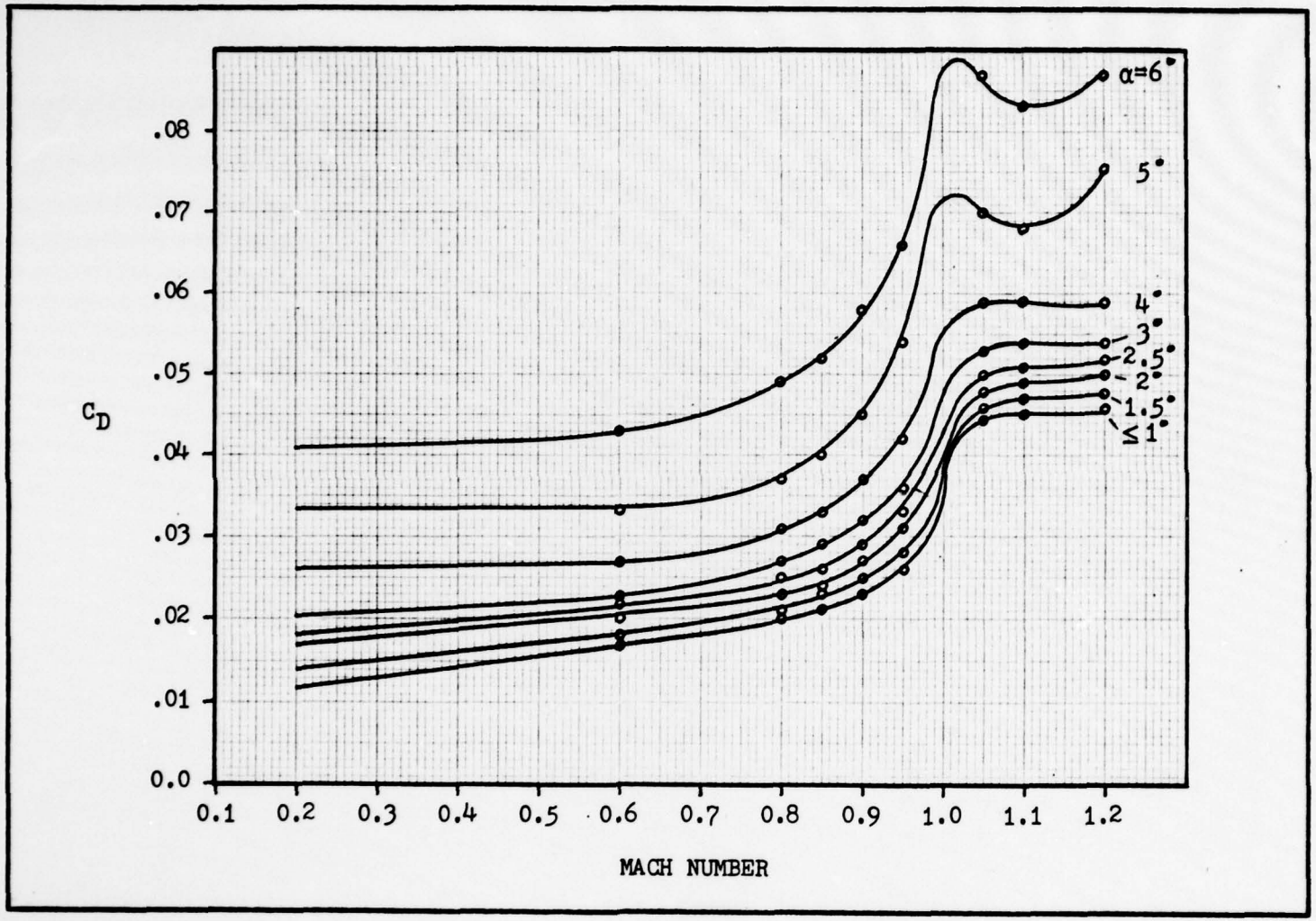


Figure 46. Plot of C_D as a function of Mach Number and angle-of-attack.

q. $C_{m_{\delta tef}}$

This derivative is given as $C_{m_{\delta tef}} = -.0015$ per degree in Reference 10. Multiplying by 57.296 degrees/radian to put it in non-dimensional form,

$$C_{m_{\delta tef}} = (-.0015)(57.296) = -.0859 \quad (86)$$

r. $C_{x_{\delta ht}}$

Reference 26 provides a family of curves that describe the changes in the coefficient of drag that result from various magnitudes of horizontal tail deflection for various Mach Numbers. The approximate change in total drag resulting from a horizontal tail deflection can be determined using linear estimation. Assuming that an average horizontal tail deflection at this flight condition is approximately 5 degrees or less for a perturbation analysis, two data points can be extracted from the given information:

ΔC_D	δ_{ht}
0	0
.00291	5

Assuming that $C_{x_{\delta ht}}$ changes linearly for horizontal tail deflections between 0 and 5 degrees, the slope of the line indicates the desired derivative. The non-dimensional form of the result is

$$C_{x_{\delta_{ht}}} = -\frac{\Delta C_D}{\delta_{ht}}(57.296) = -(.000581)(57.296) = -.0333 \qquad (87)$$

s. $C_{x_{\delta_{tef}}}$

Reference 25 provides a family of curves that describe the changes in the coefficient of drag that result from various magnitudes of trailing-edge flaperon deflection for various Mach Numbers. The same technique as in the previous case for $C_{x_{\delta_{ht}}}$ is used to determine this derivative. In non-dimensional form,

$$C_{x_{\delta_{tef}}} = -\frac{\Delta C_D}{\delta_{tef}}(57.296) = -(.000722)(57.296) = -.0414 \qquad (88)$$

t. $C_{z_{\delta_{ht}}}$

From Reference 10, it is given that $C_{L_{\delta_{ht}}} = 0.0085/\text{degree}$. If it is assumed that $C_{z_{\delta_{ht}}} \simeq -C_{L_{\delta_{ht}}}$, then, in non-dimensional form,

$$C_{z_{\delta_{ht}}} \simeq -(.0085)(57.296) = -.487 \qquad (89)$$

u. $C_{z_{\delta_{tef}}}$

From Reference 10, it is given that $C_{z_{\delta_{tef}}} = 0.011/\text{degree}$. If it is assumed that $C_{z_{\delta_{tef}}} \simeq -C_{L_{\delta_{tef}}}$, then, in non-dimensional form,

$$C_{z_{\delta_{tef}}} \simeq -(.011)(57.296) = -.630 \tag{90}$$

These stability derivatives and coefficients, and those for the remaining five flight conditions of interest, are summarized in Table 6.

TABLE 6 - Stability Derivatives and Coefficients

Mach	0.6		0.8		0.9	
Altitude	SL	30K	SL	30K	SL	30K
α_t	1.6	4.5	0.8	2.4	0.5	1.6
U (fps)	670	597	893	796	1005	895
C_L	.1104	.339	.0621	.191	.0491	.151
C_D	.026	.036	.024	.028	.026	.027
mU / Sq	2.300	6.899	1.725	5.175	1.533	4.600
I_y / Sqc	.0240	.0807	.0135	.0454	.0107	.0359
c / 2U	.00816	.00916	.00612	.00687	.00544	.00611
C_w	-.1104	-.339	-.0621	-.191	-.0491	-.151
C_{mq}	-3.60	-3.65	-4.05	-4.12	-4.80	-4.95
C_{zq}	-3.25	-3.27	-3.86	-3.92	-4.76	-4.91
$C_{L\alpha}$	4.27	4.41	4.34	4.55	4.86	4.92
$C_{m\alpha}$	.183	.135	.144	.0919	.153	.0974
$C_{m\dot{\alpha}}$	-.950	-1.15	-1.45	-1.47	-1.90	-2.20
$C_{x\alpha}$	.0216	-.113	.0513	-.0140	.0406	.0647
$C_{z\alpha}$	-4.30	-4.45	-4.36	-4.58	-4.89	-4.95
$C_{z\dot{\alpha}}$	-1.20	-1.22	-1.08	-1.04	-1.36	-1.35
C_{xu}	-.061	-.0811	-.0660	-.0767	-.112	-.108
C_{zu}	-.240	-.722	-.174	-.477	-.219	-.525
$C_{m\delta ht}$	-.590	-.607	-.573	-.602	-.573	-.619
$C_{m\delta tef}$	-.0544	-.0607	-.0859	-.100	-.118	-.154
$C_{x\delta ht}$	-.0305	-.0616	-.0333	-.0644	-.0362	-.0514
$C_{x\delta tef}$	-.0384	-.0688	-.0414	-.0722	-.0426	-.0593
$C_{z\delta ht}$	-.536	-.544	-.487	-.516	-.498	-.521
$C_{z\delta tef}$	-.688	-.802	-.630	-.802	-.544	-.796

Appendix C

State Space Modeling of the Longitudinal Equations of Motion

When analyzing or designing a system with state variable feedback, as in Chapter IV, it is most straightforward to model the system in matrix format. In this way, each state is readily identified as a feedback source, and the closed-loop system can be obtained with simple matrix manipulations. This technique becomes especially attractive when the added complexity of servos and dynamic compensation are considered. Modeling the equations of motion of the aircraft and all peripheral system dynamics individually in "state space" format permits the composite system to be obtained by matrix augmentation (see Appendix G).

The three-degree-of-freedom, non-dimensional, longitudinal, stability-axis equations of motion used in this investigation are presented in Chapter II as Eqns 1, 2, and 3. Assuming $\theta_o = 0$, and substituting a unique upper case letter for each coefficient of each state or input variable, the equations can be written in a more convenient form as follows:

$$A'\dot{u} - B'u - C'\alpha - D\theta = X\delta \tag{91}$$

$$-E'u + F'\dot{\alpha} - G'\alpha - H\theta = Z\delta \tag{92}$$

$$-I'\dot{\alpha} - J'\alpha + K\ddot{\theta} - L\dot{\theta} = M\delta \tag{93}$$

The states of this system of equations are perturbation in forward velocity, $'u$, perturbation in angle-of-attack, $'\alpha$,

perturbation in pitch angle, θ, and perturbation in pitch rate, $\dot{\theta}$ or q. The input, δ, is representative of any general input (horizontal tail or trailing-edge flaperons, or wind gust disturbances as used in this report). Equations 91, 92, and 93 can now be solved for the first derivative of each of the system states:

$$'\dot{u} = (B/A)'u + (C/A)'\alpha + (D/A)\theta + (X/A)\delta \quad (94)$$

$$'\dot{\alpha} = (E/F)'u + (G/F)'\alpha + (H/F)q + (Z/F)\delta \quad (95)$$

$$\dot{\theta} = q \quad (96)$$

$$\dot{q} = (J/K)'\alpha + (I/K)'\dot{\alpha} + (L/K)q + (M/K)\delta \quad (97)$$

Because Eqn 97 contains an "$\dot{\alpha}$" term, Eqn 95 must be substituted to allow the derivative term on the left of each equation to be expressed in terms of system states only. Performing this substitution, the new set of equations is

$$'\dot{u} = (B/A)'u + (C/A)'\alpha + (D/A)\theta + (X/A)\delta \quad (98)$$

$$'\dot{\alpha} = (E/F)'u + (G/F)'\alpha + (H/F)q + (Z/F)\delta \quad (99)$$

$$\dot{\theta} = q \quad (100)$$

$$\dot{q} = (IE/KF)'u + [(JF + IG)/KF]'\alpha + [(HI + LF)/KF]q + [(IZ + MF)/KF]\delta \quad (101)$$

These equations can now be put into matrix form

$$\begin{bmatrix} '\dot{u} \\ '\dot{\alpha} \\ \dot{\theta} \\ \dot{q} \end{bmatrix} = \begin{bmatrix} U1 & U2 & U3 & 0 \\ A1 & A2 & 0 & A4 \\ 0 & 0 & 0 & 1 \\ Q1 & Q2 & 0 & Q4 \end{bmatrix} \begin{bmatrix} 'u \\ '\alpha \\ \theta \\ q \end{bmatrix} + \begin{bmatrix} U_{in} \\ A_{in} \\ 0 \\ Q_{in} \end{bmatrix} \delta \quad (102)$$

where the terms U1, Q4, A_{in}, etc. represent the state and input variable coefficients in Eqns 98 through 101. Defined in terms of the original parameters in Equations 1, 2, and 3, the matrix entries of Eqn 102 are given in Eqns 103 through 114 as follows:

$$U1 = \frac{(C_{x_u})Sq}{mU} \tag{103}$$

$$U2 = \frac{(C_{x_\alpha})Sq}{mU} \tag{104}$$

$$U3 = \frac{(C_w)Sq}{mU} \tag{105}$$

$$U_{in} = \frac{(C_{x_\delta})Sq}{mU} \tag{106}$$

$$A1 = \frac{C_{z_u}}{(mU/Sq) - (c/2U)C_{z_{\dot\alpha}}} \tag{107}$$

$$A2 = \frac{C_{z_\alpha}}{(mU/Sq) - (c/2U)C_{z_{\dot\alpha}}} \tag{108}$$

$$A4 = \frac{(mU/Sq) + (c/2U)C_{z_q}}{(mU/Sq) - (c/2U)C_{z_{\dot\alpha}}} \tag{109}$$

$$A_{in} = \frac{C_{z_\delta}}{(mU/Sq) - (c/2U)C_{z_{\dot\alpha}}} \tag{110}$$

$$Q1 = \frac{\{(c/2U)C_{m_{\dot\alpha}}\}C_{z_u}}{(I_y/Sqc)\{mU/Sq - (c/2U)C_{z_{\dot\alpha}}\}} \tag{111}$$

$$Q2 = \frac{\{mU/Sq - (c/2U)C_{z_{\dot\alpha}}\}C_{m_\alpha} + (c/2U)(C_{m_{\dot\alpha}})C_{z_\alpha}}{(I_y/Sqc)\{mU/Sq - (c/2U)C_{z_{\dot\alpha}}\}} \tag{112}$$

$$Q4 = \frac{\{mU/Sq + (c/2U)C_{z_q}\}(c/2U)C_{m_{\dot\alpha}} + \{mU/Sq - (c/2U)C_{z_{\dot\alpha}}\}(c/2U)C_{m_q}}{(I_y/Sqc)\{mU/Sq - (c/2U)C_{z_{\dot\alpha}}\}} \tag{113}$$

$$Q_{in} = \frac{(c/2U)(C_{m_{\dot{\alpha}}})C_{z_\delta} + \{mU/Sq - (c/2U)C_{z_{\dot{\alpha}}}\}C_{m_\delta}}{(I_y/Sqc)\{mU/Sq - (c/2U)C_{z_{\dot{\alpha}}}\}} \qquad (114)$$

The "Short Period" model for the aircraft system is simply a reduced form of Eqn 102. It is obtained as a result of two basic assumptions:

1. Small perturbation in pitch have a negligible effect on aircraft forward velocity.

2. Control surface deflections introduce significantly small changes in total drag so as to cause negligible changes in aircraft forward velocity.

These assumptions permit the exclusion of the Eqn 98 from the system state matrix. Also, since neither Eqn 99 or Eqn 101 contain pitch angle terms, deletion of Eqn 100 does not result in the loss of any information. The two-state Short Period state space model may be expressed as

$$\begin{bmatrix} \dot{\alpha} \\ \dot{q} \end{bmatrix} = \begin{bmatrix} A2 & A4 \\ Q2 & Q4 \end{bmatrix} \begin{bmatrix} \alpha \\ q \end{bmatrix} + \begin{bmatrix} A_{in} \\ Q_{in} \end{bmatrix} \delta \qquad (115)$$

where each term is as defined in Eqns 108, 109, 110, 112, 113 and 114.

Appendix D

Scheduled Gains for the YF-16 CCV Longitudinal Flight Control System

The scheduled gains used in the YF-16 CCV longitudinal FCS are functions of impact pressure (q_c), the ratio of impact pressure to static pressure at altitude (q_c/P_s), or the ratio of static pressure at altitude to static pressure at sea level (P_s/P_o). To permit evaluation of these gains, Figures 47, 48, and 49 provide values of q_c, q_c/P_s, and P_s/P_o, respectively, as functions of known flight condition parameters. Graphs and equations for the scheduled gains are given in Figures 50 through 55.

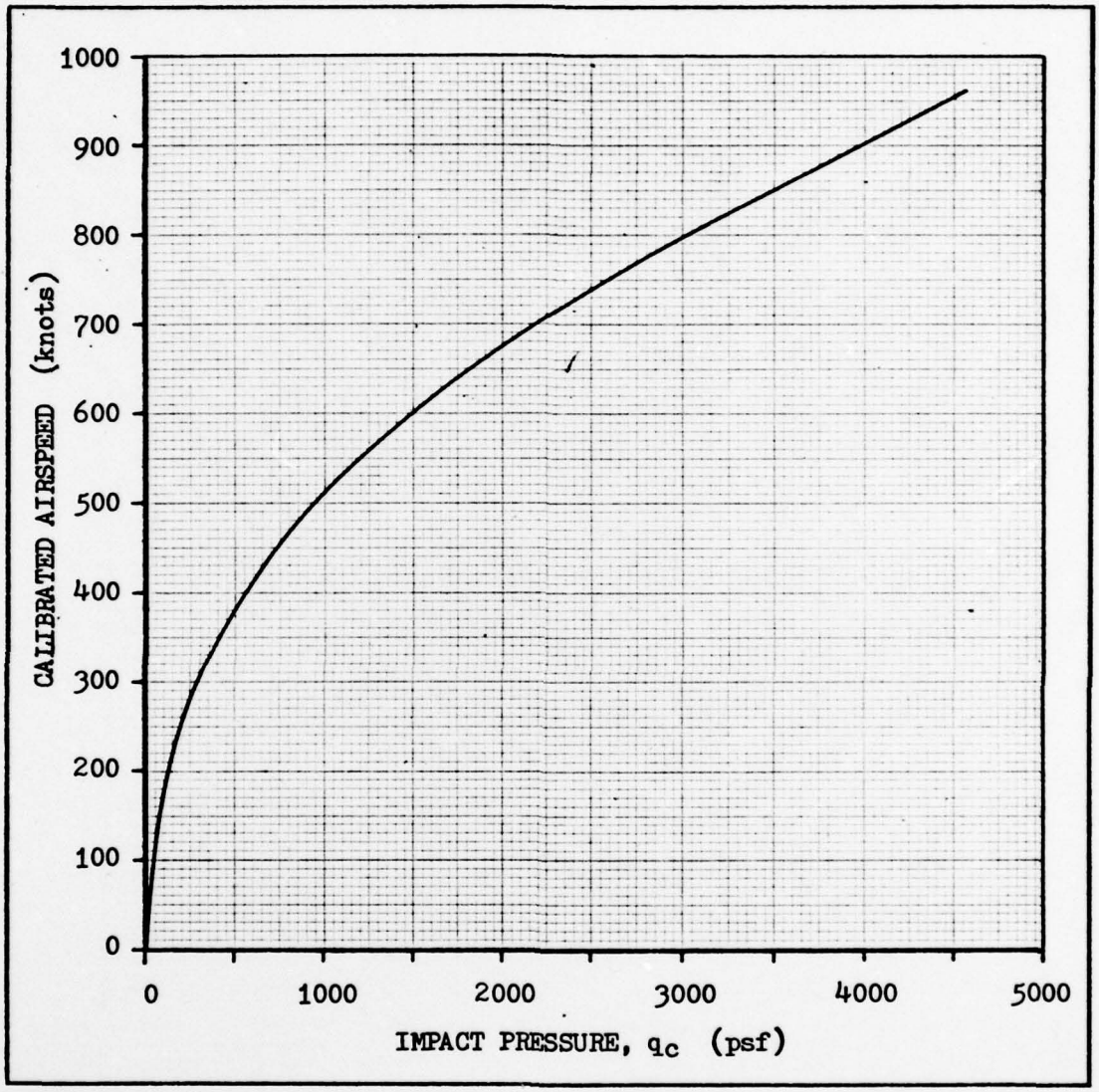


Figure 47. Impact pressure as a function of airspeed (Ref 10).

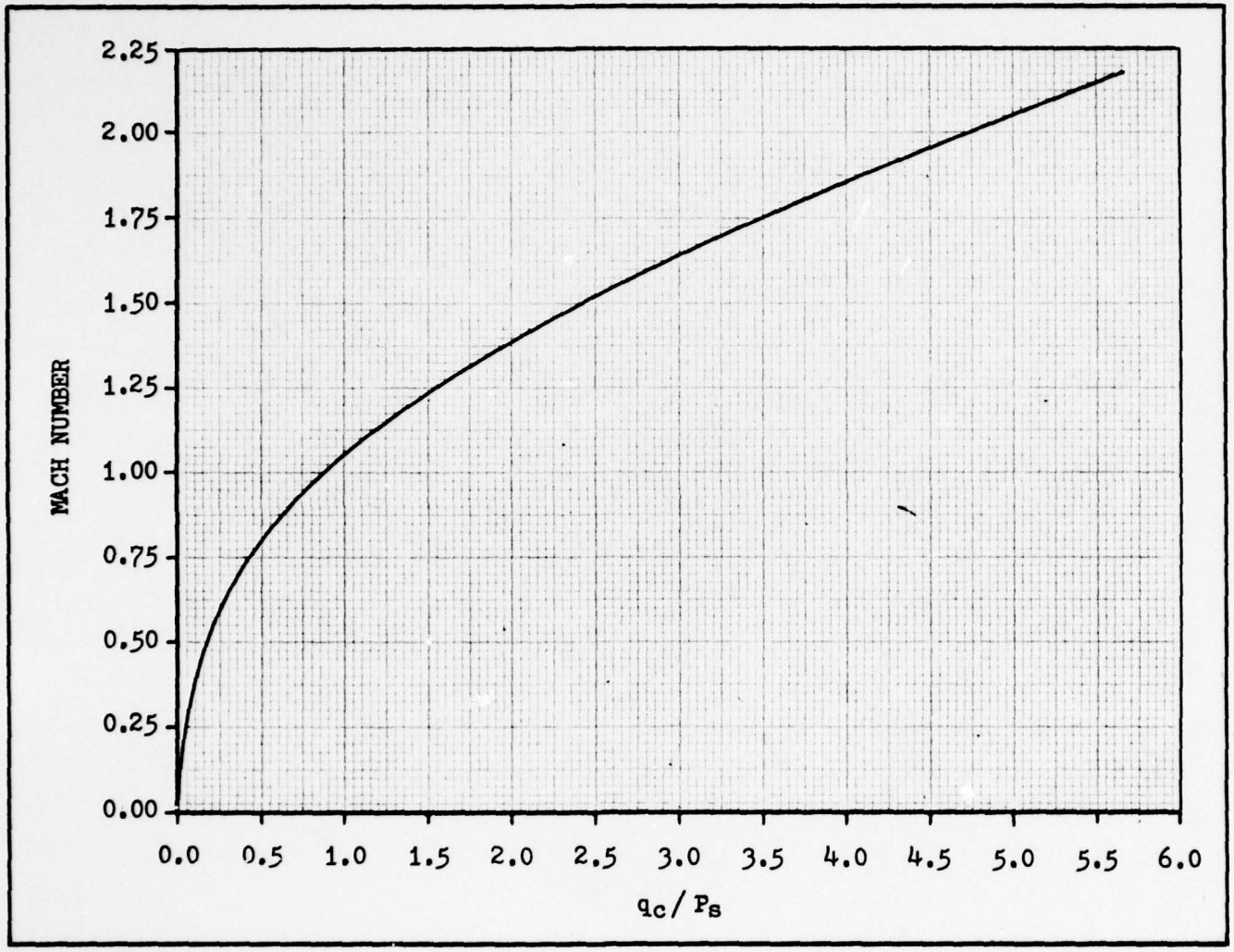


Figure 48. Ratio of impact pressure to static pressure at altitude as a function of Mach Number (Ref 10).

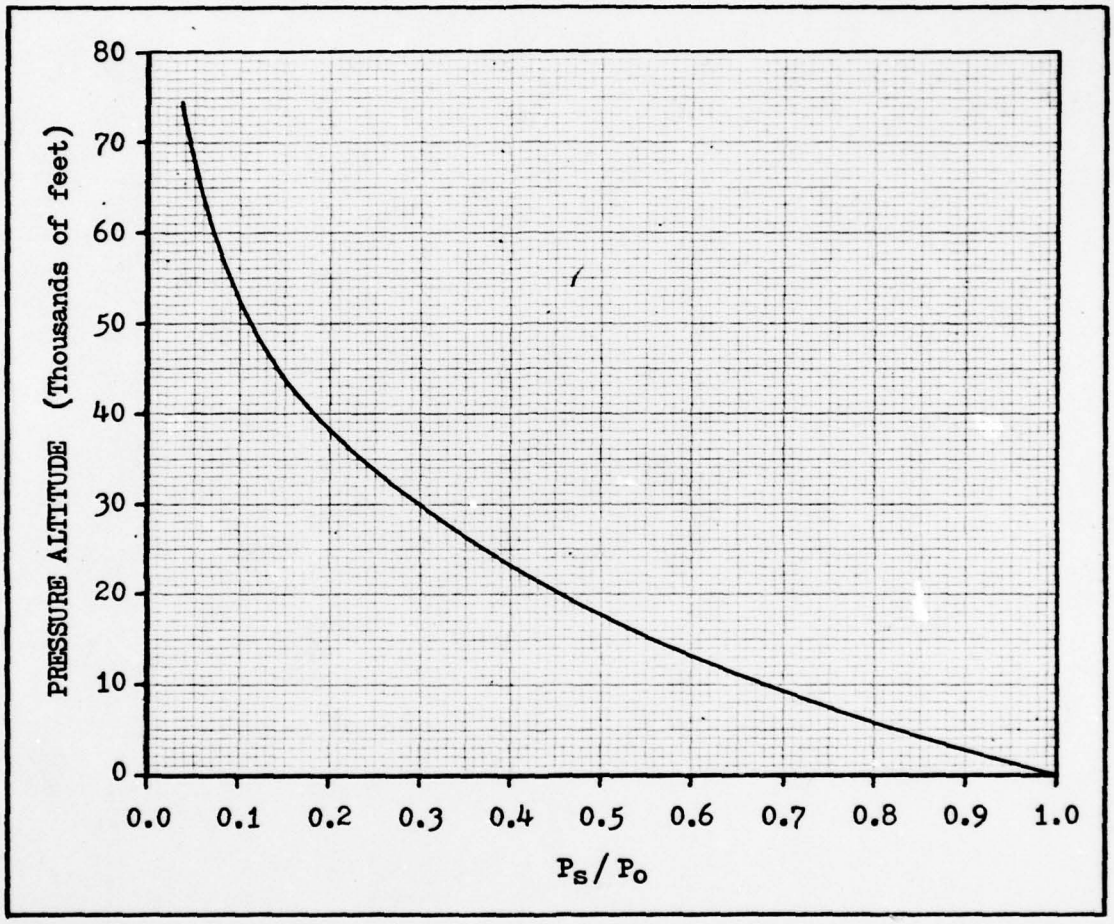
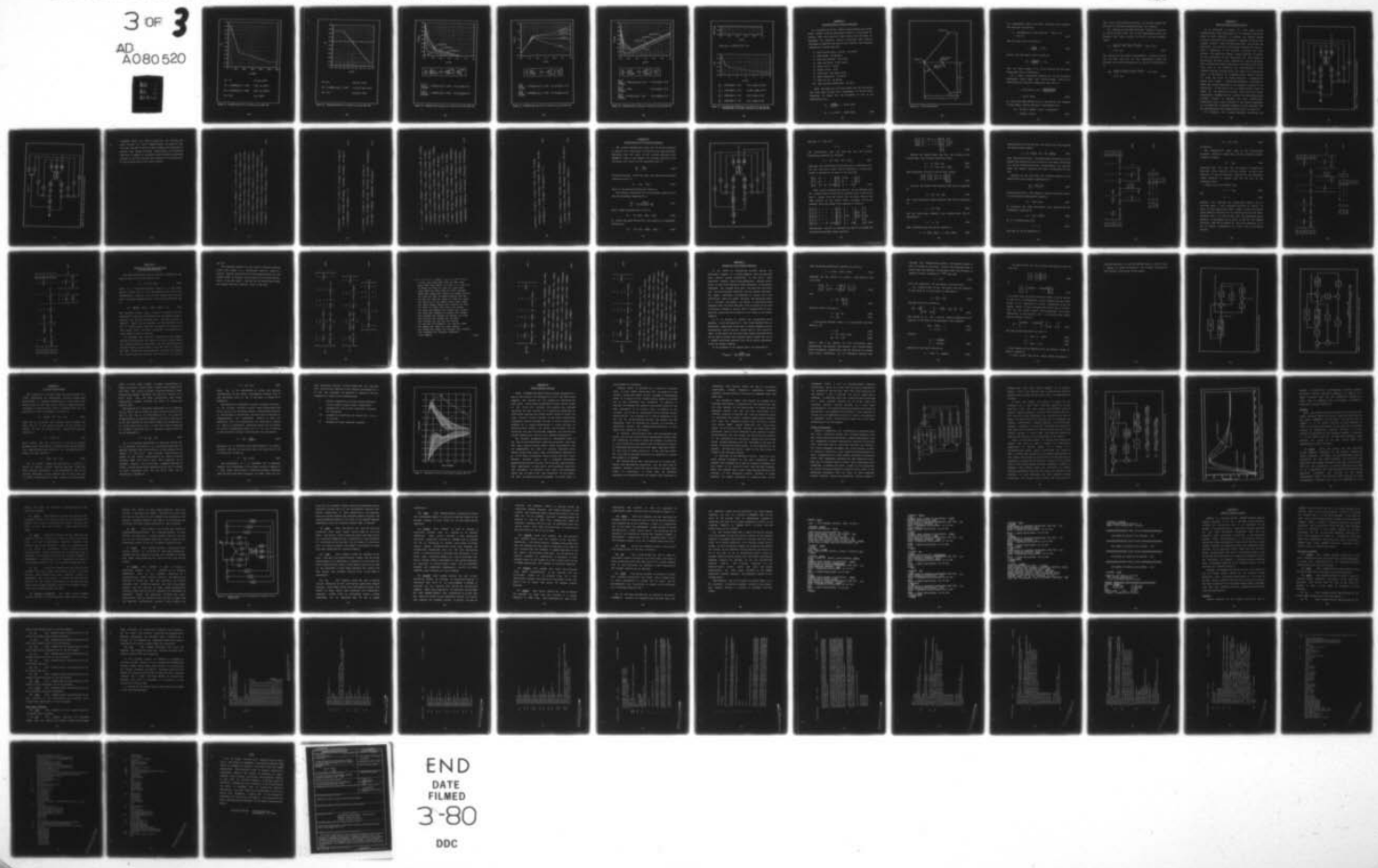


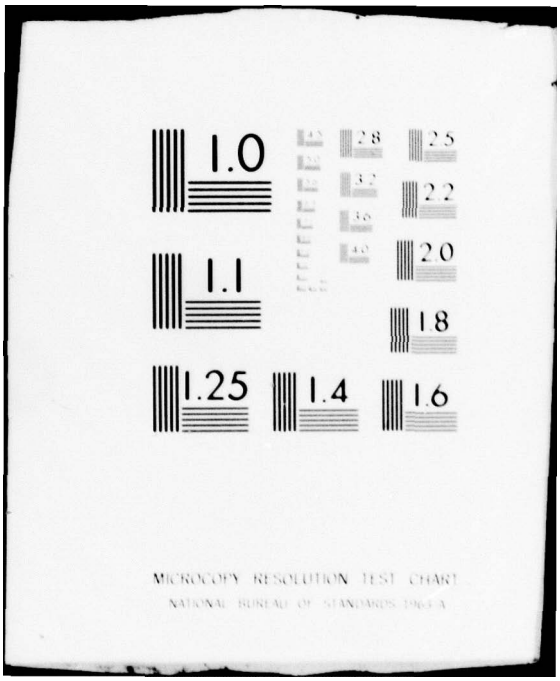
Figure 49. Ratio of static pressure at altitude to static pressure at Sea Level as a function of pressure altitude (Ref 10).

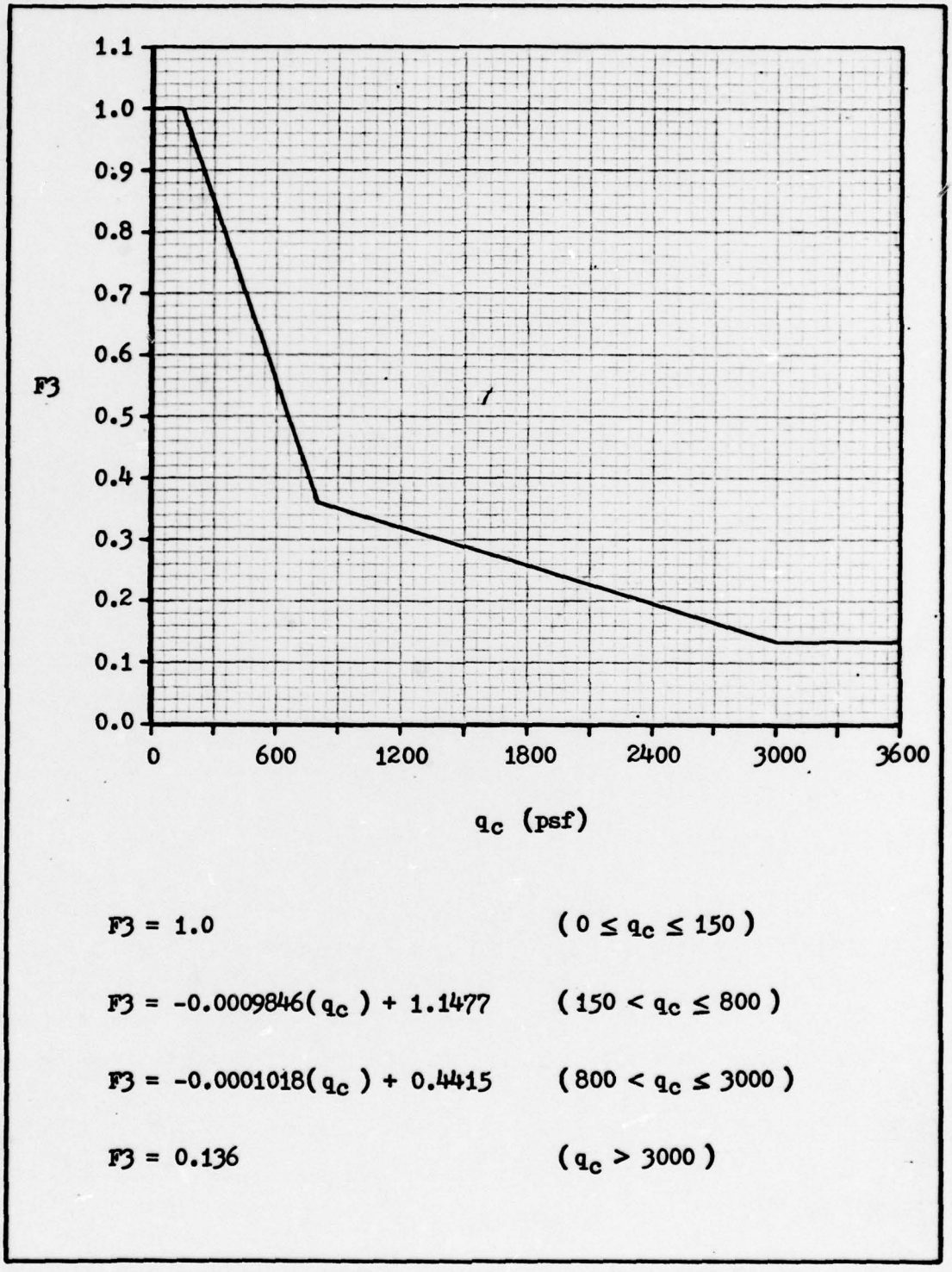
AD-A080 520 AIR FORCE INST OF TECH WRIGHT-PATTERSON AFB OH SCHOO--ETC F/G 1/3
USING VERTICAL GUST ALLEVIATION TO IMPROVE THE TARGET TRACKING --ETC(U)
AUG 79 E R MOLNER
UNCLASSIFIED AFIT/GGC/EE/79-5 NI

3 OF 3
AD A080 520



END
DATE FILMED
3-80
DDC


1.0
1.1
1.25
1.4
1.6
2.8
2.5
3.2
2.2
3.6
2.0
4.0
1.8
MICROCOPY RESOLUTION TEST CHART
NATIONAL BUREAU OF STANDARDS 1963-A



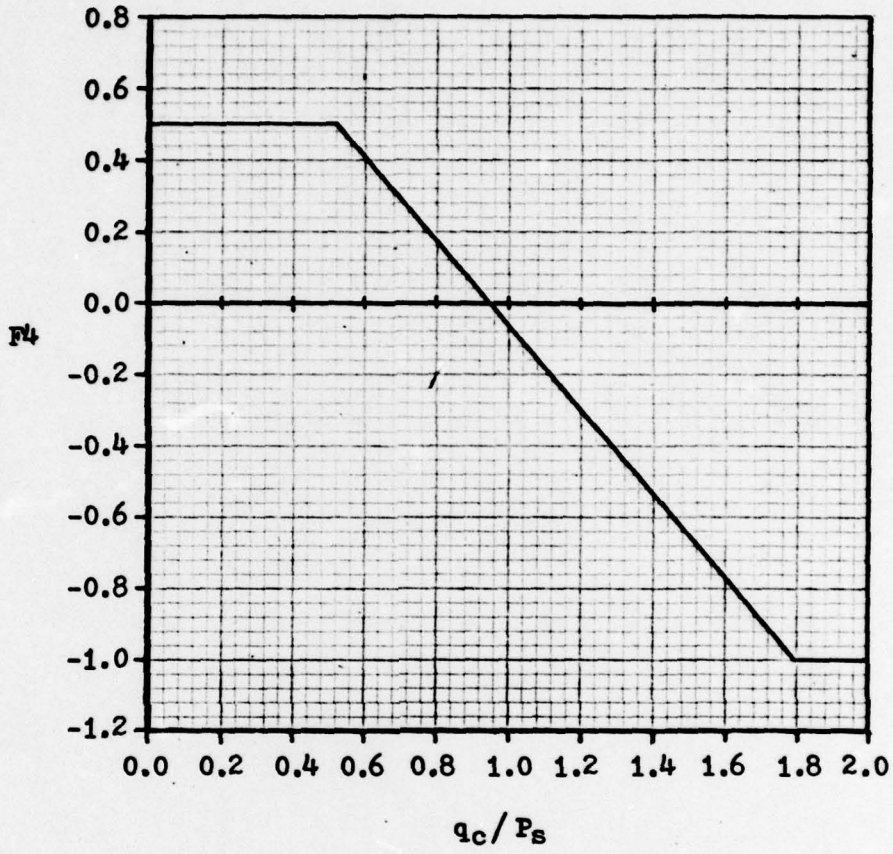
$F3 = 1.0$ $(0 \leq q_c \leq 150)$

$F3 = -0.0009846(q_c) + 1.1477$ $(150 < q_c \leq 800)$

$F3 = -0.0001018(q_c) + 0.4415$ $(800 < q_c \leq 3000)$

$F3 = 0.136$ $(q_c > 3000)$

Figure 50. Scheduled gain F3 as a function of q_c (Ref 10).

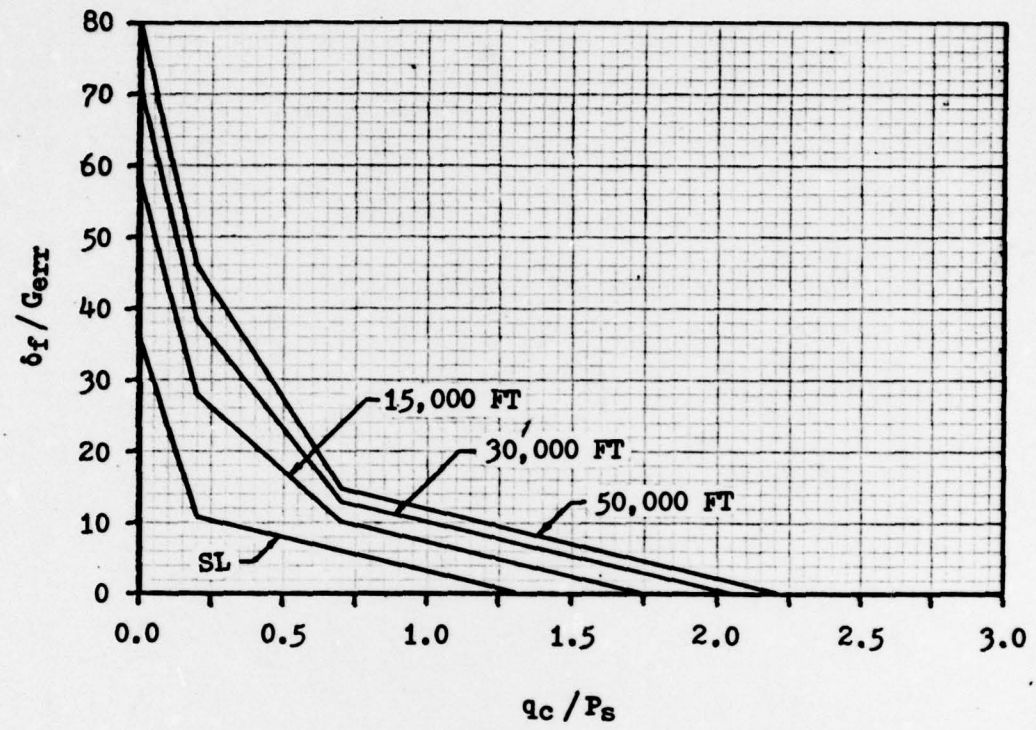


$F4 = 0.5$ $\quad (q_c / P_s < 0.53)$

$F4 = -1.1905(q_c / P_s) + 1.1310$ $\quad (.53 \leq q_c / P_s \leq 1.79)$

$F4 = -1.0$ $\quad (q_c / P_s > 1.79)$

Figure 51. Scheduled gain F4 as a function of q_c / P_s (Ref 10).

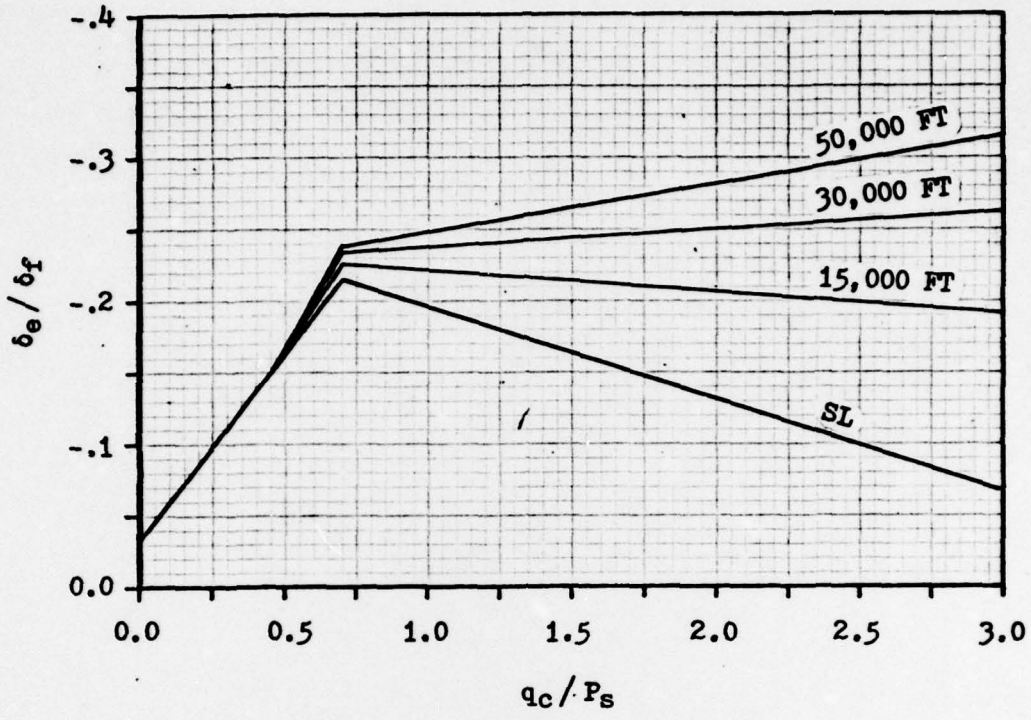


$$\frac{\delta_f}{G_{err}} = \left[\left[\frac{\delta_f}{G_{err}}\right]_{SL} + \left[52 - 60\frac{q_c}{P_s}\right]\Bigg|_{+10}^{+150}\left[1 - \frac{P_s}{P_o}\right]\right]_{0}^{+100}$$

$$\left[\frac{\delta_f}{G_{err}}\right]_{SL} = -122.5(q_c/P_s) + 35.00 \quad (0.0 \le q_c/P_s < 0.2)$$

$$\left[\frac{\delta_f}{G_{err}}\right]_{SL} = -9.545(q_c/P_s) + 12.41 \quad (0.2 \le q_c/P_s \le 1.3)$$

Figure 52. Scheduled gain δ_f / G_{err} as a function of q_c / P_s (Ref 10).

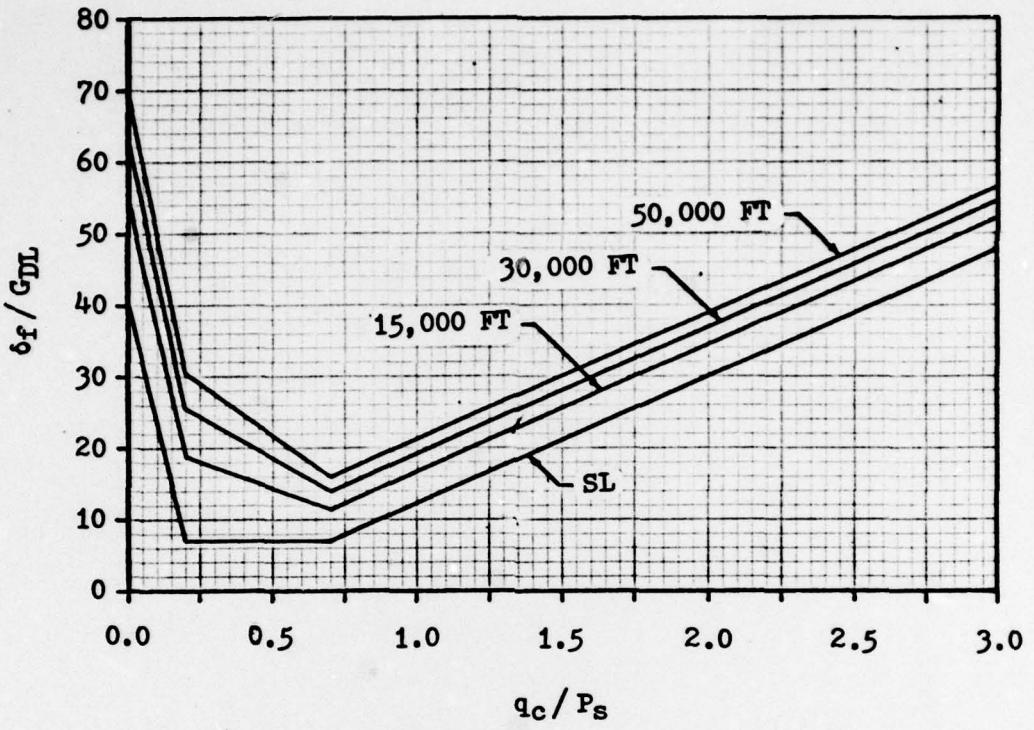


$$\frac{\delta_e}{\delta_f} = \left[\frac{\delta_e}{\delta_f}\right]_{SL} + \left[.05 - .11\frac{q_c}{P_s}\right]_{-\infty}^{0}\left[1 - \frac{P_s}{P_o}\right]$$

$$\left[\frac{\delta_e}{\delta_f}\right]_{SL} = -0.2571(q_c/P_s) - 0.035 \quad (0.0 \le q_c/P_s < 0.7)$$

$$\left[\frac{\delta_e}{\delta_f}\right]_{SL} = 0.06429(q_c/P_s) - 0.260 \quad (0.7 \le q_c/P_s \le 3.0)$$

Figure 53. Scheduled gain δ_e / δ_f as a function of q_c / P_s (Ref 10).



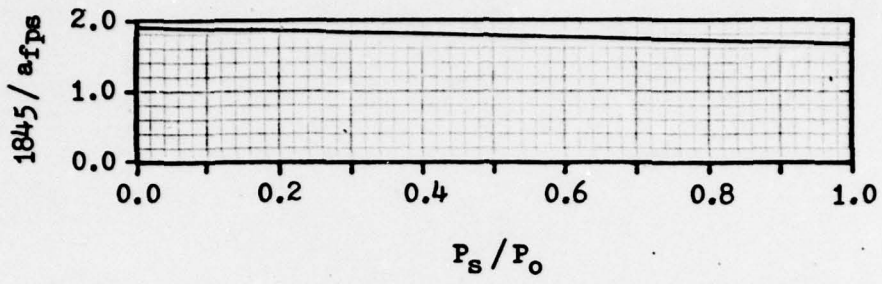
$$\frac{\delta_f}{G_{DL}} = \left[\frac{\delta_f}{G_{DL}}\right]_{SL} + 33\left[1 - \frac{q_c}{P_s}\right]\Bigg|_{+10}^{+\infty}\left[1 - \frac{P_s}{P_o}\right]$$

$$\left[\frac{\delta_f}{G_{DL}}\right]_{SL} = -165.0(q_c/P_s) + 40.0 \qquad (0.0 \le q_c/P_s < 0.2)$$

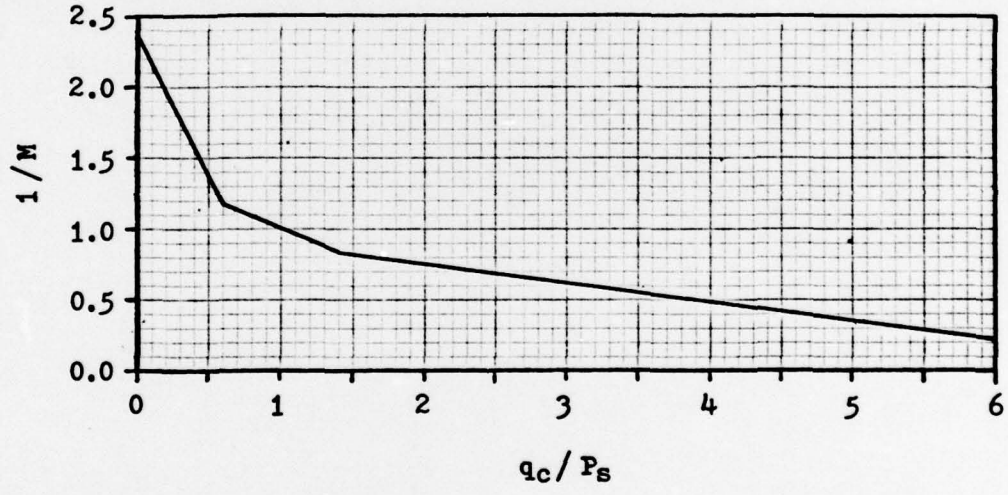
$$\left[\frac{\delta_f}{G_{DL}}\right]_{SL} = 7.000 \qquad (0.2 \le q_c/P_s < 0.7)$$

$$\left[\frac{\delta_f}{G_{DL}}\right]_{SL} = 17.71(q_c/P_s) - 5.40 \qquad (0.7 \le q_c/P_s \le 3.0)$$

Figure 54. Scheduled gain δ_f / G_{DL} as a function of q_c / P_s (Ref 10).



$$1845 / a_{fps} = -0.26(P_s / P_o) + 1.91$$



$$\frac{1}{M} = -2.00(q_c/P_s) + 2.35 \qquad (0.0 < q_c/P_s \leq 0.165)$$

$$\frac{1}{M} = -1.93(q_c/P_s) + 2.34 \qquad (0.165 < q_c/P_s \leq 0.6)$$

$$\frac{1}{M} = -.438(q_c/P_s) + 1.44 \qquad (0.6 < q_c/P_s \leq 1.4)$$

$$\frac{1}{M} = -.133(q_c/P_s) + 1.02 \qquad (1.4 < q_c/P_s \leq 6.0)$$

Figure 55. Scheduled gain $1845/a_{fps}$ as a function of P_s/P_o and determination of $1/M$ as a function of q_c/P_s (Ref 10).

Appendix E

Determination of Sensor Locations

As the position of the normal accelerometers and attack angle sensors must be determined relative to the center of gravity (CG), the location of the CG must first be known. To determine its location, certain structural data must be available to describe the wing of the aircraft. The following information is known (Ref 10):

1) Most forward point of wing: FS 218.80
2) Wing sweep: 40 degrees
3) Wing tip location: SS 173.90
4) Wing tip chord: 42.97 inches
5) Taper ratio: 0.2275
6) Aspect ratio: 3.00
7) Wing area: 280 square feet
8) Most forward CG: FS 319.70
9) Most aft CG: FS 326.20
10) Wing vertical centerline: WL 91.0

Since the wing tip is 173.90 inches from the centerline, the wing span is twice that measurement, or 347.80 inches. Referring to Figure 56, the distances d_1 and d_2 are determined to be

$$d_1 = \frac{173.90}{\tan(50°)} = 145.92 \text{ inches}$$

$$d_2 = d_1 + 42.97 = 188.89 \text{ inches} \qquad (116)$$

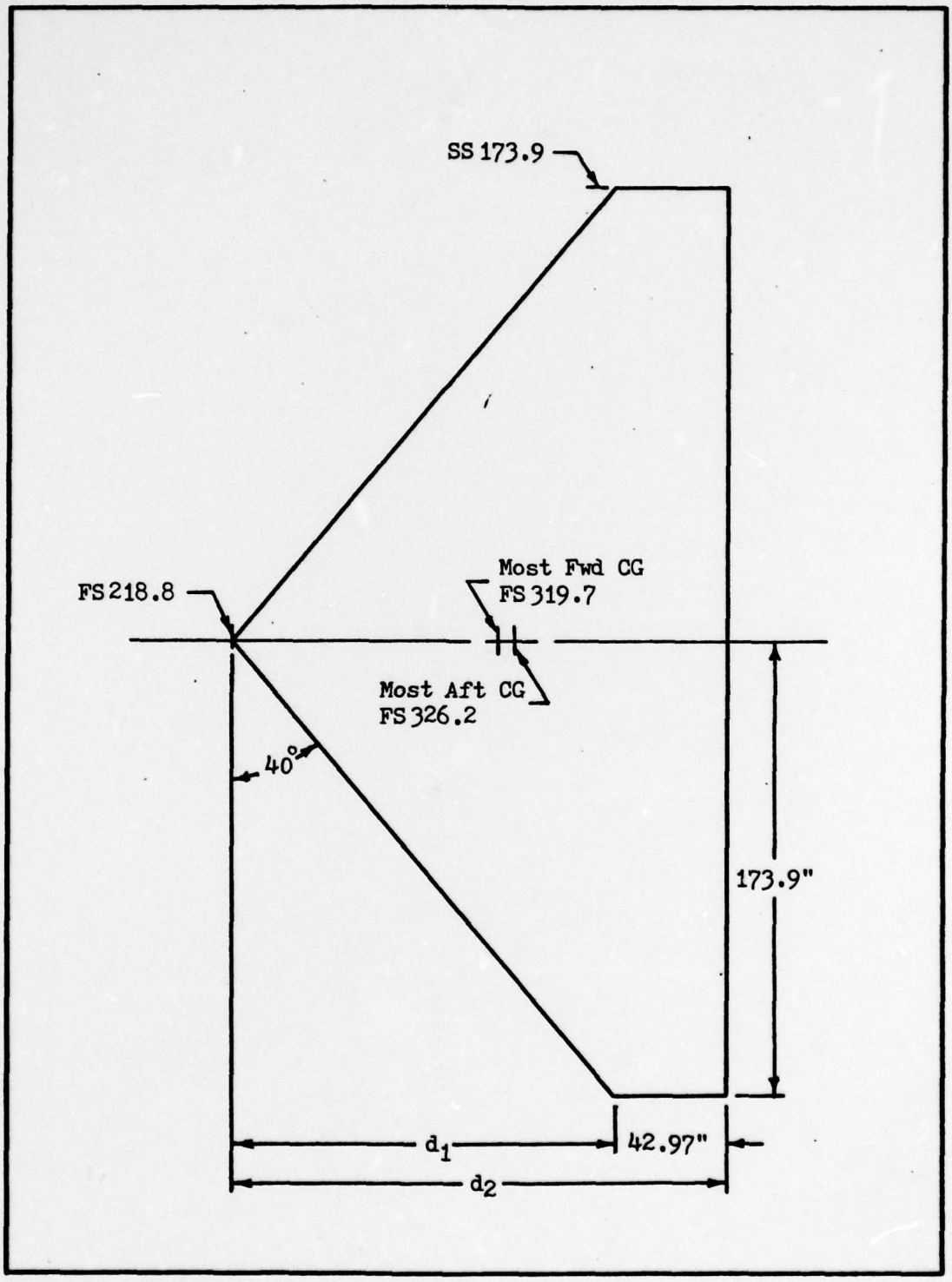


Figure 56. YF-16 wing planform.

For reassurance, some of the given data may now be checked. The wing area is given by

$$A = (145.92)(173.9) + (2)(42.97)(173.9) = 40320.5 \text{ in}^2$$
$$= 280 \text{ ft}^2 \quad (117)$$

The wing taper ratio is given by

$$T = \frac{42.97}{188.89} = 0.2275 \quad (118)$$

Lastly, the wing aspect ratio is given by

$$AR = \frac{(347.80)^2}{40320.5} = 3.00 \quad (119)$$

From the above checks, it is fairly certain that the given dimensional data is consistant.

As a final step before locating the CG, the wing Mean Aerodynamic Chord (MAC) must first be known. This can be determined from the known dimensional data (Ref 1):

$$c = (2/3)\ 188.89 + 42.97 - \frac{(188.89)(42.97)}{188.89 + 42.97}$$
$$= 131.24 \text{ inches} \quad (120)$$

As the CG has been defined to be at 35% MAC for the analysis in this thesis, the CG location is determined to be

$$CG = FS\ 218.8 + (188.89 - 131.24 + (.35)(131.24))$$
$$= FS\ 322.4\ ,\ WL\ 91.0 \quad (121)$$

This value falls within the limits of the most forward and most aft CG locations previously given, as it should.

The location of the angle-of-attack sensors is known to be FS 55, WL 88.51 (Ref 19). In the longitudinal plane, the distance from these sensors to the CG can now be readily found:

$$d_\alpha = \sqrt{(322.4 - 55)^2 + (91.0 - 88.51)^2} = 267.41 \text{ inches}$$

$$= 22.28 \text{ feet} \qquad (122)$$

The location of the normal accelerometers is known to be FS 167, WL 90.0 (Ref 19). In the longitudinal plane, the distance from these accelerometers to the CG is determined to be

$$d_{A_N} = \sqrt{(322.4 - 167.0)^2 + (91.0 - 90.0)^2} = 155.4 \text{ inches}$$

$$= 12.95 \text{ feet} \qquad (123)$$

Appendix F

Rejected System Configurations

As is mentioned in Chapter IV, three basic system configurations were investigated in an attempt to determine which is most effective in meeting the defined design criteria. Structured as G-command, C* command, and pitch rate command systems, these configurations make use of both the horizontal tail and the trailing-edge flaperons for control. From a comparison of the transfer functions for these systems, the pitch rate command system described in Chapter IV was determined to be potentially the most capable of controlling aircraft pitch responses to vertical gusting. This decision was based primarily on the form of the lowest order term in the numerator and the denominator of the transfer function relating pitch rate output to a disturbance input. In the case of the G-command system, shown in Figure 57, these two terms are almost identical - regardless of system gain levels - indicating absolutely no freedom to reduce the overall magnitude of the numerator relative to the denominator. In the case of the C* command system, shown in Figure 58, the addition of a pitch rate term to the normal acceleration feedback used to provide the controlled system variable results in improved, but still insufficient, flexibility. Only a small reduction in the relative magnitude of the numerator is possible compared to that available with the selected pitch rate command system shown in Figure 26.

For reference, the transfer functions derived for the

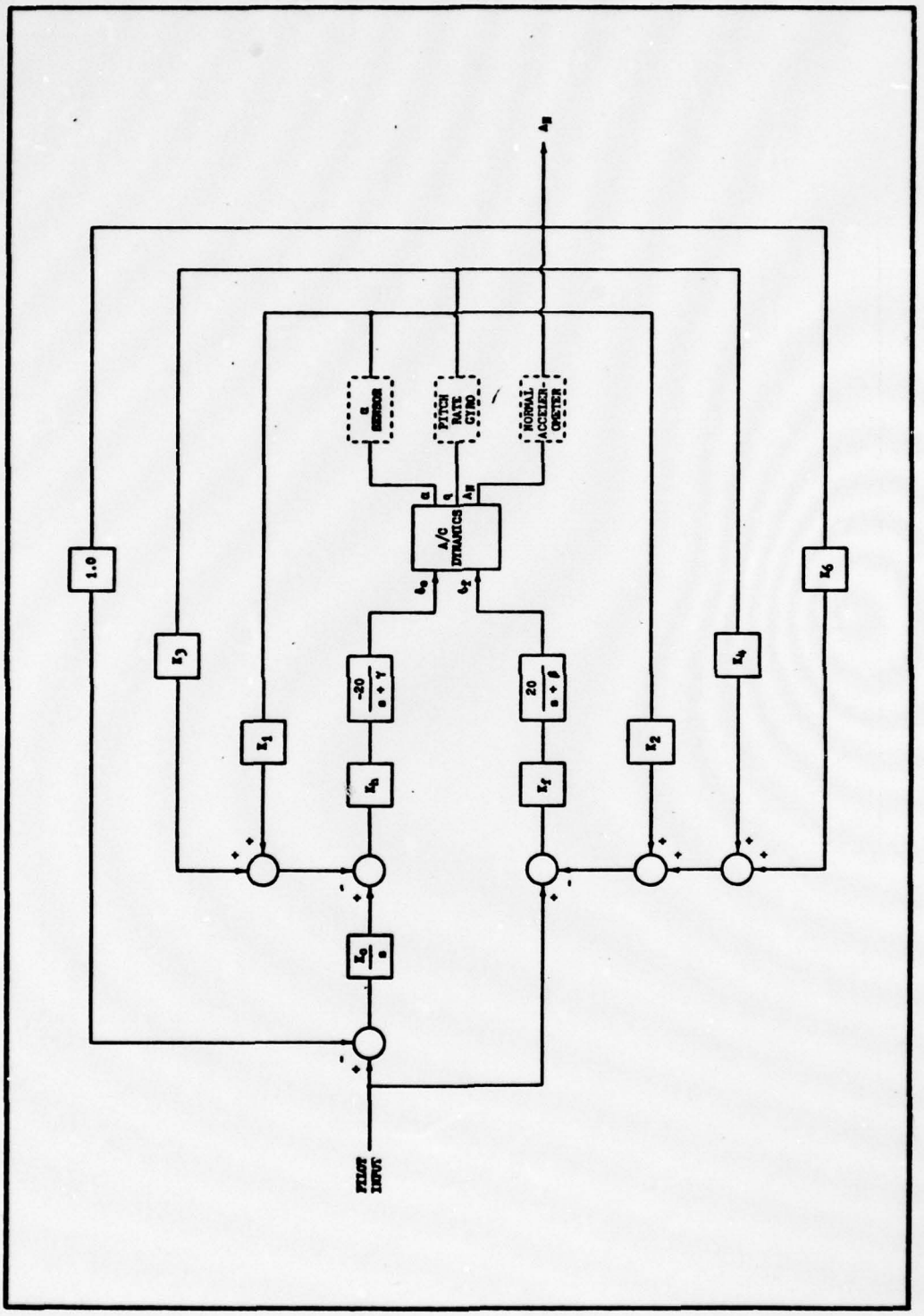


Figure 57. G-command flight control system configuration.

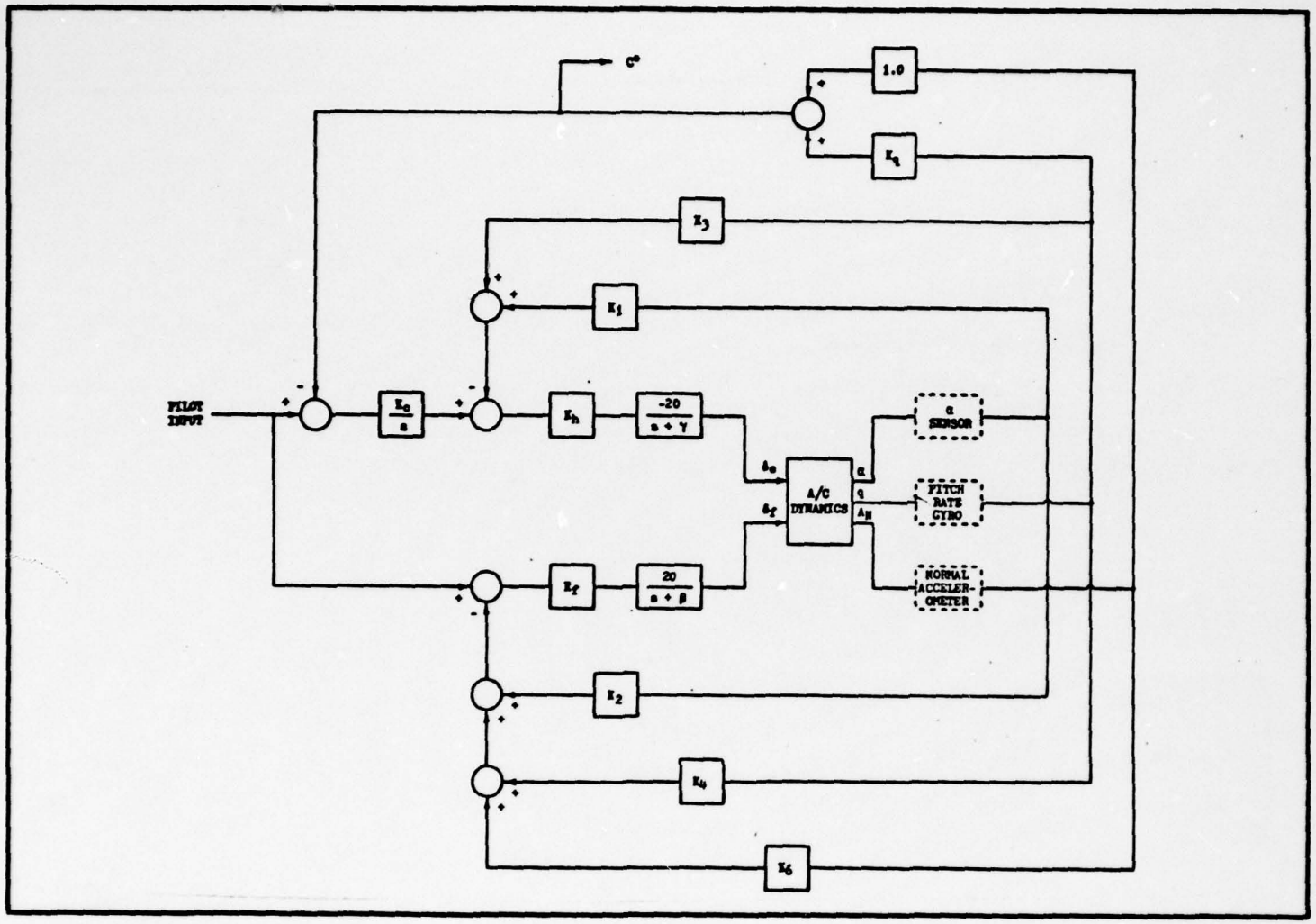


Figure 58. C* command flight control system configuration.

G-command system are given in Eqns 124, 125, and 126; and those derived for the C* command system are given in Eqns 127, 128, and 129. As both of these systems are configured to control some degree of normal acceleration, it is probable that each is capable of providing reduced normal acceleration response to vertical gusting when compared to the performance of the selected pitch rate control system.

$$
\begin{aligned}
CE = {} & s^5 + [\,5.0047 + \gamma + \beta - 2.664K_fK_6\,]s^4 + [\,-5.8622 + 5.0047(\gamma+\beta) - 4.9243K_fK_6 \\
& - 2.664\gamma K_fK_6 + 122.64K_fK_4 + 846.34K_hK_3 + 7.274K_fK_2 + 5.623K_hK_1 + 3.2198K_hK_c + \gamma\beta\,]s^3 \\
& + [\,-5.8622(\gamma+\beta) + 5.0047\gamma\beta + 193.25K_fK_6 - 4.9243\gamma K_fK_6 - 38.400K_hK_fK_6K_1 + 398.74K_fK_4 \\
& - 2649.5K_hK_fK_6K_3 + 122.64\gamma K_fK_4 + 2201.7K_hK_3 + 846.34\beta K_hK_3 + 138.58K_fK_2 + 7.274\gamma K_fK_2 \\
& + 845.55K_hK_1 + 5.623\beta K_hK_1 + 15.849K_hK_c + 3.2198\beta K_hK_c\,]s^2 + [\,-5.8622\gamma\beta + 193.25\gamma K_fK_6 \\
& - .33393K_hK_fK_6K_3 - 2649.5K_hK_fK_6K_1 + 398.74\gamma K_fK_4 - 5466.6K_hK_fK_4K_1 + 2649.5K_hK_fK_cK_4 \\
& + 5466.6K_hK_fK_3K_2 + 38.400K_hK_fK_cK_2 + 138.58\gamma K_fK_2 + 2201.7\beta K_hK_3 + 845.55\beta K_hK_1 + 1067.0K_hK_c \\
& + 15.849\beta K_hK_c\,]s + [\,.33393K_hK_fK_cK_4 + 2649.5K_hK_fK_cK_2 + 1067.0\beta K_hK_c\,] \qquad (124)
\end{aligned}
$$

$$q/\alpha_g \text{ Numerator} = [\ 12.339\ ]s^4 + [\ 12.339(\gamma + \beta) - 193.25K_fK_6 - 846.34K_hK_1 - 122.64K_fK_2\ ]s^3$$
$$+ [\ 12.339\gamma\beta - 193.25\gamma K_fK_6 + 2649.5K_hK_fK_6K_1 - 122.64\gamma K_fK_2 - 846.34\beta K_hK_1 - 1067.0K_hK_c\ ]s^2$$
$$+ [\ -2649.5K_hK_fK_cK_2 - 1067.0\beta K_hK_c\ ]s + [\ 0\ ] \qquad (125)$$

$$q/p \text{ Numerator} = [\ 122.64K_f\ ]s^3 + [\ 398.74K_f + 122.64\gamma K_f + 846.34K_hK_c\ ]s^2$$
$$+ [\ 398.74\gamma K_f + 846.34\beta K_hK_c + 2201.7K_hK_c - 5466.6K_hK_fK_1 + 2649.5K_hK_fK_c - 2649.5K_hK_fK_cK_6\ ]s$$
$$+ [\ 2201.7\beta K_hK_c + .33393K_hK_fK_c - .33393K_hK_fK_cK_6 + 5466.6K_hK_fK_cK_2\ ] \qquad (126)$$

$$
\begin{aligned}
CE = {} & s^5 + [5.0047 + \gamma + \beta - 2.664K_fK_6]s^4 + [-5.8622 + 5.0047\gamma + 5.0047\beta + \gamma\beta - 4.9243K_fK_6 \\
& - 2.664\gamma K_fK_6 + 122.64K_fK_4 + 846.34K_hK_3 + 7.274K_fK_2 - 3.066K_fK_2 + 5.623K_hK_1 - 21.16K_hK_1 \\
& + 3.2198K_hK_c]s^3 + [-5.8622(\gamma + \beta) + 5.0047\gamma\beta + 193.25K_fK_6 - 4.9243\gamma K_fK_6 + 398.74K_fK_4 \\
& + 122.64\gamma K_fK_4 + 2201.7K_hK_3 + 846.34\beta K_hK_3 + 138.58K_fK_2 - 9.969K_fK_2 + 7.274\gamma K_fK_2 - 3.066\gamma K_fK_2 \\
& + 845.55K_hK_1 - 55.04K_hK_1 + 5.623\beta K_hK_1 - 21.16\beta K_hK_1 + 15.849K_hK_c + 846.34K_qK_hK_c \\
& + 3.2198\beta K_hK_c - 2649.5K_hK_fK_3K_6 - 38.400K_hK_fK_6K_1 + 66.24K_hK_fK_6K_1]s^2 + [-5.8622\gamma\beta \\
& + 93.25\gamma K_fK_6 + 398.74\gamma K_fK_4 + 2201.7\beta K_hK_3 + 138.58\gamma K_fK_2 - 9.969\gamma K_fK_2 + 845.55\beta K_hK_1 \\
& - 55.04\beta K_hK_1 + 1067.0K_hK_c + 2201.7K_qK_hK_c + 15.849\beta K_hK_c + 846.34\beta K_qK_hK_c - .33393K_hK_fK_6K_3 \\
& - 2649.5K_hK_fK_6K_1 + .00835K_hK_fK_6K_1 - 5466.6K_hK_fK_4K_1 + 5466.6K_hK_fK_2K_3 - 2649.5K_qK_hK_fK_cK_6 \\
& + 2649.5K_hK_fK_cK_4 + 38.400K_hK_fK_cK_2 - 66.24K_hK_fK_cK_2]s + [1067\beta K_hK_c + 2201.7\beta K_qK_hK_c \\
& - .33393K_qK_hK_fK_cK_6 + .33393K_hK_fK_cK_4 + 2649.5K_hK_fK_cK_2 - .00835K_hK_fK_cK_2 + 5466.6K_qK_hK_fK_cK_2] \qquad (127)
\end{aligned}
$$

$$q/\alpha_g \text{ Numerator} = [12.339]s^4 + [12.339\gamma + 12.339\beta - 193.25K_fK_6 - 122.64K_fK_2 - 846.34K_hK_1]s^3 + [12.339\gamma\beta - 193.25\gamma K_fK_6 - 122.64\gamma K_fK_2 - 846.34\beta K_hK_\alpha - 1067.0K_hK_c + 2649.5K_hK_fK_6K_1]s^2 + [-1067.0\beta K_hK_c - 2649.5K_hK_fK_2K_1]s + [0] \quad (128)$$

$$q/p \text{ Numerator} = [122.64K_f]s^3 + [398.74K_f + 122.64\gamma K_f + 846.34K_hK_c]s^2 + [398.74\gamma K_f + 846.34\beta K_hK_c + 2201.7K_hK_c - 5466.6K_hK_fK_1 - 2649.5K_hK_fK_cK_6 + 2649.5K_hK_fK_c]s + [2201.7\beta K_hK_c - .33393K_hK_fK_cK_6 + 5466.6K_hK_fK_cK_2 + .33393K_hK_fK_c] \quad (129)$$

Appendix G

Determination of the System Equation

The system configuration chosen for the design presented in Chapter IV is shown again in Figure 59 for easy reference. Beginning with the input to the aircraft equations ("A/C DYNAMICS" block in the figure), the transfer function of the horizontal tail servo and the preceeding gain is

$$\frac{\delta_h}{e_h} = \frac{-20K_h}{s + \gamma} \tag{130}$$

Cross-multiplying, shuffling terms, and removing the Laplace notation results in

$$\dot{\delta}_h = -\gamma\delta_h - 20K_h e_h \tag{131}$$

which is the desired differential equation.

The transfer function of the trailing-edge flaperon servo and the preceeding compensation is

$$\frac{\delta_f}{e_f} = \frac{-20K_f s}{s^2 + (R + \beta)s + R\beta} \tag{132}$$

Again, simple manipulations result in

$$\ddot{\delta}_f = -(R + \beta)\dot{\delta}_f - R\beta\delta_f - 20K_f\dot{e}_f \tag{133}$$

To remove the input derivative, this equation is integrated, resulting in

$$\dot{\delta}_f = -(R + \beta)\delta_f - R\beta\int\delta_f - 20K_f e_f \tag{134}$$

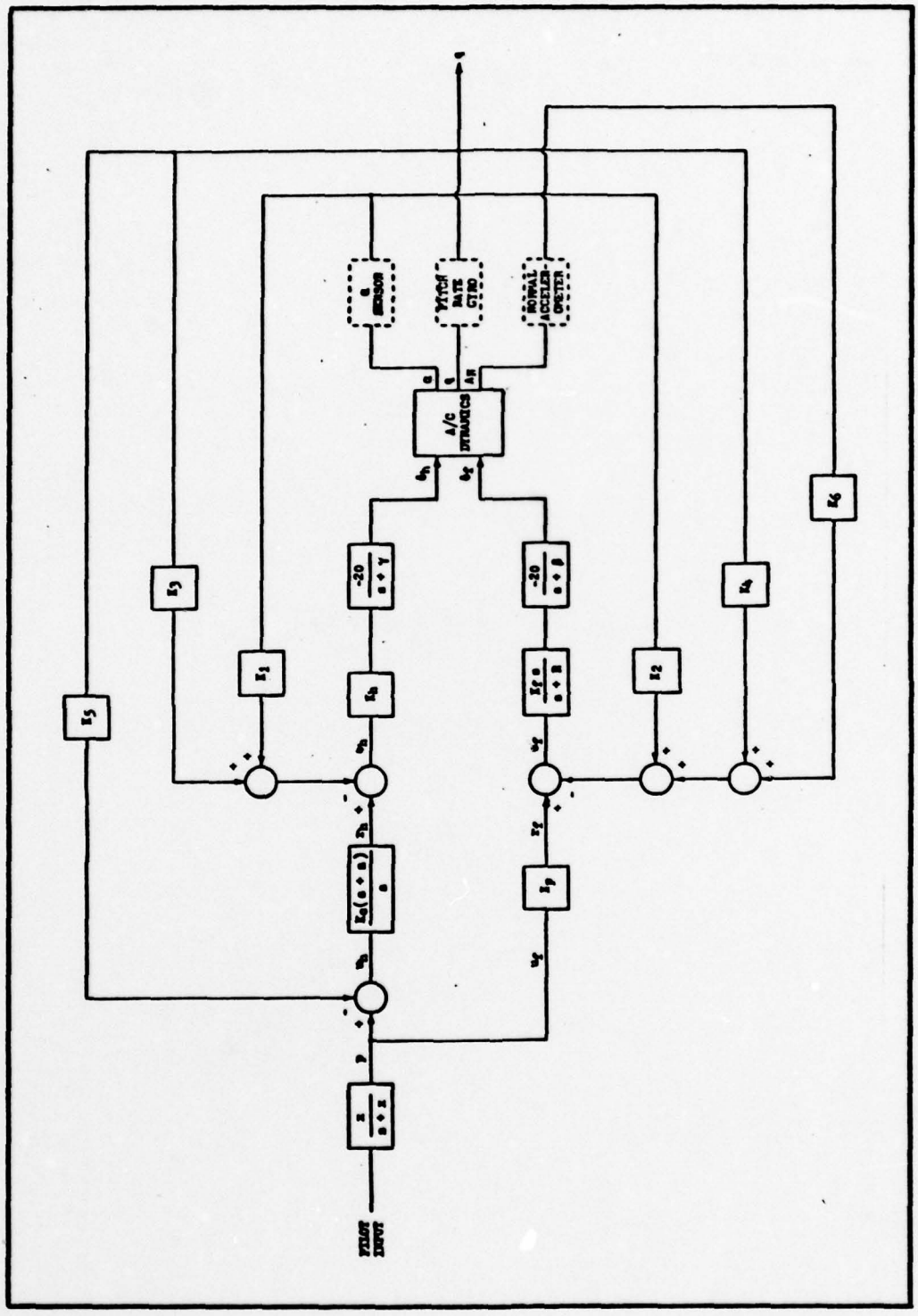


Figure 59. Selected pitch rate command flight control system configuration.

Defining '$\dot{x}$', such that

$$\dot{x} = \delta_f \tag{135}$$

and substituting Eqn 135 into Eqn 134, the desired differential equation is obtained:

$$\dot{\delta}_f = -(R + \beta)\delta_f - R\beta x - 20K_f e_f \tag{136}$$

Combining the differential equations given in Equations 131, 135 and 136 into a single matrix expression, a three-state system is obtained as an input to the aircraft:

$$\begin{bmatrix} \dot{\delta}_h \\ \dot{x} \\ \dot{\delta}_f \end{bmatrix} = \begin{bmatrix} -\gamma & 0 & 0 \\ 0 & 0 & 1 \\ 0 & -R\beta & -(R+\beta) \end{bmatrix} \begin{bmatrix} \delta_h \\ x \\ \delta_f \end{bmatrix} + \begin{bmatrix} -20K_h & 0 \\ 0 & 0 \\ 0 & -20K_f \end{bmatrix} \begin{bmatrix} e_h \\ e_f \end{bmatrix} \tag{137}$$

Using matrix augmentation, Eqn 137 can be combined with the aircraft Short Period matrix equation given in Eqn 38 to form a system with the e-vector as the input. This is the inner portion of the system shown in Figure 59 with no feedback. This new system state equation is given as

$$\begin{bmatrix} '\dot{\alpha} \\ \dot{q} \\ \dot{\delta}_h \\ \dot{x} \\ \dot{\delta}_f \end{bmatrix} = \begin{bmatrix} a & b & e & 0 & f \\ c & d & g & 0 & h \\ 0 & 0 & -\gamma & 0 & 0 \\ 0 & 0 & 0 & 0 & 1 \\ 0 & 0 & 0 & -R\beta & -(R+\beta) \end{bmatrix} \begin{bmatrix} '\alpha \\ q \\ \delta_h \\ x \\ \delta_f \end{bmatrix} + \begin{bmatrix} 0 & 0 \\ 0 & 0 \\ -20K_h & 0 \\ 0 & 0 \\ 0 & -20K_f \end{bmatrix} \begin{bmatrix} e_h \\ e_f \end{bmatrix} + \begin{bmatrix} i \\ m \\ 0 \\ 0 \\ 0 \end{bmatrix} \alpha_g \tag{138}$$

Additionally, Eqn 137 is combined with Eqn 39 to produce the new system measurable output equation

$$\begin{bmatrix} \alpha_s \\ q_s \\ A_{N_s} \end{bmatrix} = \begin{bmatrix} 1 & -.025 & 0 & 0 & 0 \\ 0 & 1 & 0 & 0 & 0 \\ n & p & u & 0 & v \end{bmatrix} \begin{bmatrix} \alpha \\ q \\ \delta_h \\ x \\ \delta_f \end{bmatrix} + \begin{bmatrix} 1 \\ 0 \\ x \end{bmatrix} \alpha_g \tag{139}$$

Backing up another step, such that the r-vector is the system input, the following equations result:

$$e_h = r_h - K_1\alpha_s - K_3 q_s \tag{140}$$

$$e_f = r_f - K_2\alpha_s - K_4 q_s - K_6 A_{N_s} \tag{141}$$

These equations, written in matrix form, become

$$\begin{bmatrix} e_h \\ e_f \end{bmatrix} = \begin{bmatrix} r_h \\ r_f \end{bmatrix} - \begin{bmatrix} K_1 & K_3 & 0 \\ K_2 & K_4 & K_6 \end{bmatrix} \begin{bmatrix} \alpha_s \\ q_s \\ A_{N_s} \end{bmatrix} \tag{142}$$

Letting the system state equation (Eqn 138) be expressed as

$$\dot{\underline{x}} = \underline{A}\underline{x} + \underline{B}\underline{e} + \underline{N}\alpha_g \tag{143}$$

the system measurable output equation (Eqn 139) be expressed as

$$\underline{y} = \underline{C}\underline{x} + \underline{M}\alpha_g \tag{144}$$

and the inner-stage feedback loop equation (Eqn 142) be expressed as

$$\underline{e} = \underline{r} - \underline{K}\underline{y} \tag{145}$$

Then, combining Eqns 144 and 145 results in

$$\underline{e} = \underline{r} - \underline{K}(\underline{C}\underline{x} + \underline{M}\alpha_g) = \underline{r} - \underline{K}\underline{C}\underline{x} - \underline{K}\underline{M}\alpha_g \tag{146}$$

Combining Eqn 143 with Eqn 146, and collecting terms provides the desired final result:

$$\dot{\underline{x}} = (\underline{A} - \underline{B}\underline{K}\,\underline{C})\underline{x} + \underline{B}\underline{r} + (\underline{N} - \underline{B}\underline{K}\,\underline{M})\alpha_g \qquad (147)$$

This expression allows a straightforward calculation of the closed-loop system with the r-vector as the input. Performing the matrix multiplications and manipulations, the resultant state and output equations are given as Equations 148 and 149.

Backing up the next step, the transfer function of the proportional plus integral compensation is

$$\frac{r_h}{u_h} = \frac{K_c(s + z)}{s} \qquad (150)$$

Cross-multiplication and removal of Laplace notation results in the following differential equation:

$$\dot{r}_h = K_c\dot{u}_h + zK_cu_h \qquad (151)$$

To eliminate the input derivative, this equation must be integrated, resulting in

$$r_h = K_cu_h + zK_c\int u_h \qquad (152)$$

If '$\dot{y}$' is defined such that

$$\dot{y} = u_h \qquad (153)$$

then Eqn 152 can be expressed as

$$\begin{bmatrix} \dot{\alpha}' \\ \dot{q} \\ \dot{\delta}_h \\ \dot{x} \\ \dot{\delta}_f \end{bmatrix} = \begin{bmatrix} a & b & e & 0 & f \\ c & d & g & 0 & h \\ 20K_1K_h & 20K_h(K_3 - .025K_1) & -\gamma & 0 & 0 \\ 0 & 0 & 0 & 0 & 1 \\ 20K_f(K_2 + nK_6) & 20K_f(K_4 - .025K_2 + pK_6) & 20uK_6K_f & -R\beta & -(R + \beta - 20vK_6K_f) \end{bmatrix} \begin{bmatrix} \alpha' \\ q \\ \delta_h \\ x \\ \delta_f \end{bmatrix}$$

$$+ \begin{bmatrix} 0 & 0 \\ 0 & 0 \\ -20K_h & 0 \\ 0 & 0 \\ 0 & -20K_f \end{bmatrix} \begin{bmatrix} r_h \\ r_f \end{bmatrix} + \begin{bmatrix} i \\ m \\ 20K_1K_h \\ 0 \\ 20K_f(K_2 + xK_6) \end{bmatrix} \alpha_g \qquad (148)$$

$$\begin{bmatrix} \alpha_s \\ q_s \\ A_{N_s} \end{bmatrix} = \begin{bmatrix} 1 & -.025 & 0 & 0 & 0 \\ 0 & 1 & 0 & 0 & 0 \\ n & p & u & 0 & v \end{bmatrix} \begin{bmatrix} \alpha' \\ q \\ \delta_h \\ x \\ \delta_f \end{bmatrix} + \begin{bmatrix} 1 \\ 0 \\ x \end{bmatrix} \alpha_g \qquad (149)$$

$$r_h = K_c u_h + zK_c y \tag{154}$$

as desired.

The proportional input path to the trailing-edge flaperons contains a simple gain, and the resultant transfer function is simply

$$r_f = K_p u_f \tag{155}$$

Equations 148, 153, 154, and 155 combine to produce the open-loop state equation with the u-vector as input. This equation is given in Eqn 156. Equation 157, the measurable output equation, is changed from Eqn 149 only by the additional state.

Closing the final feedback loop,

$$u_h = .p - K_5 q_s \tag{158}$$

and

$$u_f = p \tag{159}$$

Equation 147, defining the closed-loop system, may be utilized again - with different matrices, of course - to solve for the system with scalar input, P. The final system state equation, exclusive of the command prefilter and sensor dynamics only, is given in Eqn 160. The measurable output equation is unchanged, and is given as Eqn 157. The command prefilter need not be modeled in the matrix equation, as it can be easily incorporated at a later time in the design process.

$$\begin{bmatrix} \dot{'\alpha} \\ \dot{q} \\ \dot{\delta}_h \\ \dot{x} \\ \dot{\delta}_f \\ \dot{y} \end{bmatrix} = \begin{bmatrix} a & b & e & 0 & f & 0 \\ c & d & g & 0 & h & 0 \\ 20K_1K_h & 20K_h(K_3 - .025K_1) & -\gamma & 0 & 0 & -20zK_hK_c \\ 0 & 0 & 0 & 0 & 1 & 0 \\ 20K_f(K_2 + nK_6) & 20K_f(K_4 - .025K_2 + pK_6) & 20uK_6K_f & -R\beta & -(R + \beta - 20vK_6K_f) & 0 \\ 0 & 0 & 0 & 0 & 0 & 0 \end{bmatrix} \begin{bmatrix} '\alpha \\ q \\ \delta_h \\ x \\ \delta_f \\ y \end{bmatrix}$$

$$+ \begin{bmatrix} 0 & 0 \\ 0 & 0 \\ -20K_hK_c & 0 \\ 0 & 0 \\ 0 & -20K_fK_p \\ 1 & 0 \end{bmatrix} \begin{bmatrix} u_h \\ u_f \end{bmatrix} + \begin{bmatrix} i \\ m \\ 20K_1K_h \\ 0 \\ 20K_f(K_2 + xK_6) \\ 0 \end{bmatrix} \alpha_g \qquad (156)$$

$$\begin{bmatrix} \alpha_s \\ q_s \\ A_{N_s} \end{bmatrix} = \begin{bmatrix} 1 & -.025 & 0 & 0 & 0 & 0 \\ 0 & 1 & 0 & 0 & 0 & 0 \\ n & p & u & 0 & v & 0 \end{bmatrix} \begin{bmatrix} '\alpha \\ q \\ \delta_h \\ x \\ \delta_f \\ y \end{bmatrix} + \begin{bmatrix} 1 \\ 0 \\ x \end{bmatrix} \alpha_g \qquad (157)$$

$$\begin{bmatrix} \dot{\alpha}' \\ \dot{q} \\ \dot{\delta}_h \\ \dot{x} \\ \dot{\delta}_f \\ \dot{y} \end{bmatrix} = \begin{bmatrix} a & b & e & 0 & f & 0 \\ c & d & g & 0 & h & 0 \\ 20K_1K_h & 20K_h(K_cK_5 + K_3 - .025K_1) & -\gamma & 0 & 0 & -20zK_hK_c \\ 0 & 0 & 0 & 0 & 1 & 0 \\ 20K_f(K_2 + nK_6) & 20K_f(K_4 - .025K_2 + pK_6) & 20uK_6K_f & -R\beta & (20vK_6K_f - R - \beta) & 0 \\ 0 & -K_5 & 0 & 0 & 0 & 0 \end{bmatrix} \begin{bmatrix} \alpha' \\ q \\ \delta_h \\ x \\ \delta_f \\ y \end{bmatrix}$$

$$+ \begin{bmatrix} 0 \\ 0 \\ -20K_hK_c \\ 0 \\ -20K_fK_p \\ 1 \end{bmatrix} p + \begin{bmatrix} i \\ m \\ 20K_1K_h \\ 0 \\ 20K_f(K_2 + xK_6) \\ 0 \end{bmatrix} \alpha_g \qquad (160)$$

Appendix H

Solution of the System Equation for Transfer Functions

The closed-loop system equation derived in Appendix G and given as Eqn 160 is of the general form

$$\dot{\underline{x}} = \underline{A}\underline{x} + \underline{B}p + \underline{N}\alpha_g \tag{161}$$

where 'A' is the system dynamics matrix, 'B' is the system control matrix, and 'N' is the disturbance input matrix. The characteristic equation (CE) for the system can be derived from the system dynamics matrix using the relationship (Ref 6)

$$CE = \left|\underline{Q}(s)\right| = \left|\left[s\underline{I} - \underline{A}\right]\right| = \det\left[s\underline{I} - \underline{A}\right] \tag{162}$$

The resulting matrix, $\underline{Q}(s)$, is given in Equation 163. The determinant of $\underline{Q}(s)$ can be determined by expanding by minors. Choosing the entries in column four, rows four and five as "pivots", $\left|Q(s)\right|$ can be expressed as the difference of two two 5 x 5 terms given in Eqn 164. The process is continued in this manner until no further reductions are possible. The final result is given in Eqn 165.

To determine the numerator equation for the transfer function relating pitch rate output to a pilot command input, the system $\underline{B}$ vector is substituted for the second column in the $\underline{Q}(s)$ matrix, as per Cramer's Rule. The result is given in Eqn 166. Solving for the determinant of $\underline{Q}'(S)$ will produce the desired numerator equation. The final result is given in

Eqn 167.

The numerator equation for the transfer function relating pitch rate output to a disturbance input is found in a similar fashion. Substitution of the system $\underline{N}$ vector for the second column in the $\underline{Q}(s)$ matrix results in the matrix $\underline{Q}''(s)$, given in Eqn 168. Again, solving for the determinant yields the desired numerator equation, given in Eqn 169.

$$\underline{Q}(s) = \begin{bmatrix} s-a & -b & -e & 0 & -f & 0 \\ -c & s-d & -g & 0 & -h & 0 \\ -20K_1K_h & -20K_h(K_cK_5+K_3-.025K_1) & s+\gamma & 0 & 0 & 20zK_hK_c \\ 0 & 0 & 0 & s & -1 & 0 \\ -20K_f(K_2+nK_6) & -20K_f(K_4-.025K_2+pK_6) & -20uK_6K_f & R\beta & s-(20vK_6K_f-R-\beta) & 0 \\ 0 & K_5 & 0 & 0 & 0 & s \end{bmatrix} \tag{163}$$

$$CE = \begin{vmatrix} s-a & -b & -e & -f & 0 \\ -c & s-d & -g & -h & 0 \\ -20K_1K_h & -20K_h(K_cK_5+K_3-.025K_1) & s+\gamma & 0 & 20zK_hK_c \\ -20K_f(K_2+nK_6) & -20K_f(K_4-.025K_2+pK_6) & -20uK_6K_f & s+(R+\beta-20vK_6K_f) & 0 \\ 0 & K_5 & 0 & 0 & s \end{vmatrix} s$$

$$- \begin{vmatrix} s-a & -b & -e & -f & 0 \\ -c & s-d & -g & -h & 0 \\ -20K_1K_h & -20K_h(K_cK_5+K_3-.025K_1) & s+\gamma & 0 & 20zK_hK_c \\ 0 & 0 & -1 & -1 & 0 \\ 0 & K_5 & 0 & 0 & s \end{vmatrix} R\beta \tag{164}$$

$$
\begin{aligned}
CE = {} & s^6 + [-(a+d) + \beta + R + \gamma - 20vK_fK_6]s^5 + [(ad - bc) - (a+d)(\beta + R + \gamma) + R\beta + \beta\gamma \\
& + R\gamma - 20\,hK_fK_4 + .5hK_fK_2 - 20npK_fK_6 - 20fnK_fK_2 - 20fnK_fK_6 + 20(a+d)vK_fK_6 - 20v\gamma K_fK_6 \\
& - 20gK_hK_cK_5 - 20eK_hK_1 - 20gK_hK_3 + .5gK_hK_1]s^4 + [(ad - bc)(\beta + R + \gamma) - (a+d)(R\beta + \beta\gamma + R\gamma) \\
& + R\beta\gamma - 20gzK_hK_cK_5 - 20(cf - ah)K_fK_4 + .5(cf - ah)K_fK_2 - 20(cf - ah)pK_fK_6 - 20h\gamma K_fK_4 \\
& + .5h\gamma K_fK_2 - 20hp\gamma K_fK_6 + 20(df - bh)K_fK_2 - 20f\gamma K_fK_2 + 20(df - bh)nK_fK_6 - 400huK_hK_fK_cK_6K_5 \\
& - 20fn\gamma K_fK_6 + 400(gv - hu)K_hK_fK_6K_3 + 400(ev - fu)K_hK_fK_6K_1 + 10(hu - gv)K_hK_fK_6K_1 - 20e(\beta + R)K_hK_1 \\
& - 20(ad - bc)vK_fK_6 + 20(a+d)v\gamma K_fK_6 - 20(\beta + R)gK_hK_cK_5 + 400gvK_hK_fK_cK_6K_5 - 20g(\beta + R)K_hK_3 \\
& + .5g(\beta + R)K_hK_1 + 20(de - bg)K_hK_1 + 20(ag - ce)K_hK_cK_5 + .5(ce - ag)K_hK_1 + 20(ag - ce)K_hK_3]s^3 \\
& + [(ad - bc)(R\beta + \beta\gamma + R\gamma) - (a+d)R\beta\gamma - 20gR\beta K_hK_cK_5 - 20gR\beta K_hK_3 - 20eR\beta K_hK_1 + .5gR\beta K_hK_1 \\
& + 20(ag - ce)zK_hK_cK_5 - 20gz\beta K_hK_cK_5 - 20gRzK_hK_cK_5 + 400(gv - hu)zK_hK_fK_cK_6K_5 - 20(cf - ah)\gamma K_fK_4 \\
& + .5(cf - ah)\gamma K_fK_2 - 20(cf - ah)p\gamma K_fK_6 - 400(gf - eh)K_hK_fK_4K_1 - 400(gf - eh)pK_hK_fK_6K_1 \\
& + 20(df - bh)\gamma K_fK_2 + 400(gf - eh)K_hK_fK_cK_5K_2 + 400(gf - eh)K_hK_fK_3K_2 + 400(gf - eh)nK_hK_fK_cK_6K_5 \\
& + 20(df - bh)n\gamma K_fK_6 + 400(gf - eh)nK_hK_fK_6K_3 + 10(eh - gf)nK_hK_fK_6K_1 + 400(df - bh)uK_hK_fK_6K_1 \\
& + 400(ah - cf)uK_hK_fK_cK_6K_5 + 400(ah - cf)uK_hK_fK_6K_3 + 10(cf - ah)uK_hK_fK_6K_1 - 20(ad - bc)v\gamma K_fK_6 \\
& + 20(de - bg)(\beta + R)K_hK_1 - 400(de - bg)vK_hK_fK_6K_1 + 20(ag - ce)(\beta + R)K_hK_cK_5 \\
& - 400(ag - ce)vK_hK_fK_cK_6K_5 + 20(ag - ce)(\beta + R)K_hK_3 - 400(ag - ce)vK_hK_fK_6K_3 \\
& + .5(ce - ag)(\beta + R)K_hK_1 - 10(ce - ag)vK_hK_fK_6K_1]s^2 + [(ad - bc)R\beta\gamma + 20(de - bg)R\beta K_hK_1 \\
& + 20(ag - ce)R\beta K_hK_cK_5 + 20(ag - ce)R\beta K_hK_3 + .5(ce - ag)R\beta K_hK_1 - 20gRz\beta K_hK_cK_5 \\
& + 20(ag - ce)z\beta K_hK_cK_5 + 20(ag - ce)RzK_hK_cK_5 + 400(gf - eh)zK_hK_fK_cK_5K_2 + 400(gf - eh)nzK_hK_fK_cK_6K_5 \\
& + 400(ah - cf)uzK_hK_fK_cK_6K_5 + 400(ce - ag)vzK_hK_fK_cK_6K_5 - 400gvzK_hK_fK_cK_6K_5]s \\
& + [20(ag - ce)zR\beta K_hK_cK_5]
\end{aligned}
\tag{165}
$$

$$\left|\underline{Q}'(s)\right| = \begin{vmatrix} s-a & 0 & -e & 0 & -f & 0 \\ -c & 0 & -g & 0 & -h & 0 \\ -20K_1K_h & -20K_hK_c & s+\gamma & 0 & 0 & 20zK_hK_c \\ 0 & 0 & 0 & s & -1 & 0 \\ -20K_f(K_2+nK_6) & -20K_fK_p & -20uK_fK_6 & R\beta & s+(\beta+R-20vK_fK_6) & 0 \\ 0 & 1 & 0 & 0 & 0 & s \end{vmatrix} \tag{166}$$

$$\begin{aligned} = {} & [-20hK_fK_p - 20gK_hK_c]s^4 + [-20h\gamma K_fK_p + 20(ah-cf)K_fK_p - 400huK_hK_fK_6K_c - 20g(\beta+R)K_hK_c \\ & + 400gvK_hK_fK_cK_6 - 20gzK_hK_c + 20(ag-ce)K_hK_c]s^3 + [400(gf-eh)K_hK_fK_cK_2 \\ & + 400(gf-eh)nK_hK_fK_cK_6 - 400(hu-gv)zK_hK_fK_cK_6 + 400(ah-cf)uK_hK_fK_cK_6 + 20(ah-cf)\gamma K_fK_p \\ & - 400(ag-ce)vK_hK_fK_cK_6 - 20gz(\beta+R)K_hK_c + 20(ag-ce)(\beta+R)K_hK_c + 20(ag-ce)zK_hK_c \\ & - 20gR\beta K_hK_c + 400(eh-gf)K_hK_fK_pK_1]s^2 + [400(gf-eh)zK_hK_fK_cK_2 + 400(gf-eh)nzK_hK_fK_cK_6 \\ & + 400(ah-cf)uzK_hK_fK_cK_6 + 400(ce-ag)vzK_hK_fK_cK_6 + 20(ag-ce)(\beta+R)zK_hK_c - 20gzR\beta K_hK_c \\ & + 20(ag-ce)R\beta K_hK_c]s + [20(ag-ce)zR\beta K_hK_c] \end{aligned} \tag{167}$$

$$\left|\underline{Q}''(s)\right| = \begin{vmatrix} s-a & i & -e & 0 & -f & 0 \\ -c & m & -g & 0 & -h & 0 \\ -20K_1K_h & 20K_1K_h & s+\gamma & 0 & 0 & 20zK_hK_c \\ & 0 & 0 & s & -1 & 0 \\ -20K_f(K_2+nK_6) & 20K_f(K_2+xK_6) & -20uK_fK_6 & R\beta & s+(\beta+R-20vK_fK_6) & 0 \\ 0 & 0 & 0 & 0 & 0 & s \end{vmatrix} \tag{168}$$

$$\begin{aligned} &= [m(\beta+R+\gamma) + 20gK_hK_1 - 20mvK_fK_6 + 20hK_fK_2 + 20hxK_fK_6 + (ci-am)]s^4 \\ &+ [m(R\beta+\beta\gamma+R\gamma) + (ci-am)\gamma - 20(ci-am)vK_fK_6 + (ci-am)(\beta+R) - 20mv\gamma K_fK_6 \\ &+ 20g(\beta+R)K_hK_1 + 400(hu-gv)K_hK_fK_6K_1 + 20(ce-ag)K_hK_1 + 20(gi-em)K_hK_1 + 20h\gamma K_fK_2 \\ &+ 20hx\gamma K_fK_6 + 20(cf-ah)K_fK_2 + 20(cf-ah)xK_fK_6 + 20(hi-fm)K_fK_2 + 20(hi-fm)nK_fK_6]s^3 \\ &+ [mR\beta\gamma + (ci-am)(R\beta+\beta\gamma+R\gamma) - 20(ci-am)v\gamma K_fK_6 + 20gR\beta K_hK_1 + 20(ce-ag)(\beta+R)K_hK_1 \\ &- 400(ce-ag)vK_hK_fK_6K_1 + 400(cf-ah)uK_hK_fK_6K_1 + 20(gi-em)(\beta+R)K_hK_1 + 20(cf-ah)\gamma K_fK_2 \\ &- 400(gi-em)vK_hK_fK_6K_1 + 20(cf-ah)x\gamma K_fK_6 + 400(hi-fm)uK_hK_fK_6K_1 + 20(hi-fm)\gamma K_fK_2 \\ &+ 20(hi-fm)n\gamma K_fK_6 + 400(gf-eh)xK_hK_fK_6K_1 + 400(eh-gf)nK_hK_fK_6K_1]s^2 \\ &+ [20(gi-em)R\beta K_hK_1 + 20(ce-ag)R\beta K_hK_1 + (ci-am)R\beta\gamma]s + [0] \end{aligned} \tag{169}$$

Appendix I

Design of a First-Order Observer

To be useful in controlling aircraft motion, the electrical outputs of a flight computer must be converted into control surface deflections. In the YF-16, these electrical signals drive electromechanical command servos, which in turn drive hydraulic power actuators. As previously discussed, the command servo used with both the horizontal tail and trailing-edge flaperons has two outputs available. One output, obviously, is mechanical in nature, and is the controlling input to a power actuator. The remaining output is a variable resistance, the amount of resistance being dependent upon the servo position. Such an output can be used to provide a voltage or current that is proportional to servo position, permitting servo position to be input to the flight computer.

If it is desired to include the second-order servo dynamics in the derivation of a full state feedback FCS, an additional output must be derived to allow feedback signals representing each of the two states (Ref 6). The electrical input to the servo and the electrical output described above can be used to derive this required output through the use of a simple first-order observer that can be easily implemented within the flight computer.

If the dynamics of the command servo are expressed as

$$TF_{(Servo)} = \frac{2704}{s^2 + 72.8s + 2704} \qquad (170)$$

then the system differential equation is given by

$$\ddot{y} = -72.8\dot{y} - 2704y + 2704z \tag{171}$$

Defining the two states as x_1 and x_2, such that $x_1 = y$ and $x_2 = \dot{y}$, then

$$\begin{bmatrix} \dot{x}_1 \\ \dot{x}_2 \end{bmatrix} = \begin{bmatrix} 0 & 1 \\ -2704 & -72.8 \end{bmatrix} \begin{bmatrix} x_1 \\ x_2 \end{bmatrix} + \begin{bmatrix} 0 \\ 2704 \end{bmatrix} z \tag{172}$$

and

$$\underline{y} = \begin{bmatrix} 1 & 0 \end{bmatrix} \begin{bmatrix} x_1 \\ x_2 \end{bmatrix} \tag{173}$$

which can also be written as

$$\dot{\underline{x}} = \underline{A}\underline{x} + \underline{B}z \tag{174}$$

$$\underline{y} = \underline{C}^T\underline{x} \tag{175}$$

A first-order observer state, w, is now defined such that (Refs 12, 15)

$$w = \underline{T}\underline{x} \tag{176}$$

$$\dot{w} = Dw + E\underline{C}^T\underline{x} + \underline{T}\underline{B}z \tag{177}$$

$$\underline{T}\underline{A} - D\underline{T} = E\underline{C}^T \tag{178}$$

where D and E are scalars (in this first-order case) representing the observer time constant and a system output matrix multiplier, respectively, and the vector $\underline{T}$ is a system state matrix multiplier. As the definable observer time

constant will determine how readily the observer output is able to settle to the actual value of the observed state, a fairly fast time constant is desirable. This time constant is chosen to allow a response of e^{-100t}, and thus

$$D = -100 \tag{179}$$

Also, for simplicity, "E" may assume a value of unity.

All values in Eqn 177 are now known, with the exception of the vector $\underline{T}$. If this vector is expressed as

$$\underline{T} = \begin{bmatrix} t_1 & t_2 \end{bmatrix} \tag{180}$$

then Eqn 178 can be written as

$$\begin{bmatrix} t_1 & t_2 \end{bmatrix} \begin{bmatrix} 0 & 1 \\ -2704 & -72.8 \end{bmatrix} + 100 \begin{bmatrix} t_1 & t_2 \end{bmatrix} = \begin{bmatrix} 1 & 0 \end{bmatrix} \tag{181}$$

The values of t_1 and t_2 can be found by expressing this equation in the form of two equations in two unknowns:

$$100 t_1 - 2704 t_2 = 1 \tag{182}$$

$$t_1 + 27.2 t_2 = 0 \tag{183}$$

Solving,

$$t_1 = -.000184366$$

$$t_2 = .00501475 \tag{184}$$

Equation 177 can now be written as

$$\dot{w} = -100w + y - 0.49853z \tag{185}$$

An output vector can now be formed from Eqns 175 and 176, such that

$$\begin{bmatrix} w \\ \hline y \end{bmatrix} = \begin{bmatrix} \underline{T} \\ \hline \underline{C}^T \end{bmatrix} \begin{bmatrix} x_1 \\ \hline x_2 \end{bmatrix} \tag{186}$$

or

$$\begin{bmatrix} w \\ y \end{bmatrix} = \begin{bmatrix} .00501475 & -.000184366 \\ 1 & 0 \end{bmatrix} \begin{bmatrix} x_1 \\ x_2 \end{bmatrix} \tag{187}$$

It is clear that the two-by-two matrix made up of the vectors $\underline{T}$ and $\underline{C}^T$ is a transformation matrix allowing the new output vector to be expressed as a linear combination of the two system states. If this transformation matrix has an inverse, then the two system states can be expressed as a linear combination of the outputs w and y . This matrix does indeed have an inverse, which is

$$\underline{F}^{-1} = \begin{bmatrix} .00501475 & -.000184366 \\ 1 & 0 \end{bmatrix}^{-1} = \begin{bmatrix} 0 & 1 \\ -5424 & 27.2 \end{bmatrix} \tag{188}$$

The final system equations are given by

$$\dot{w} = -100w + y - .49853 \tag{185}$$

$$x_1 = y \tag{189}$$

$$x_2 = -5424w + 27.2y \tag{190}$$

A block diagram of the complete servo and observer system is shown in Figure 60.

A total system may now be easily formed introducing a

forward-loop gain, K_x, and two feedback gains K_1 and K_2. Such a system is shown in Figure 61. The transfer function for this system is also given in the figure.

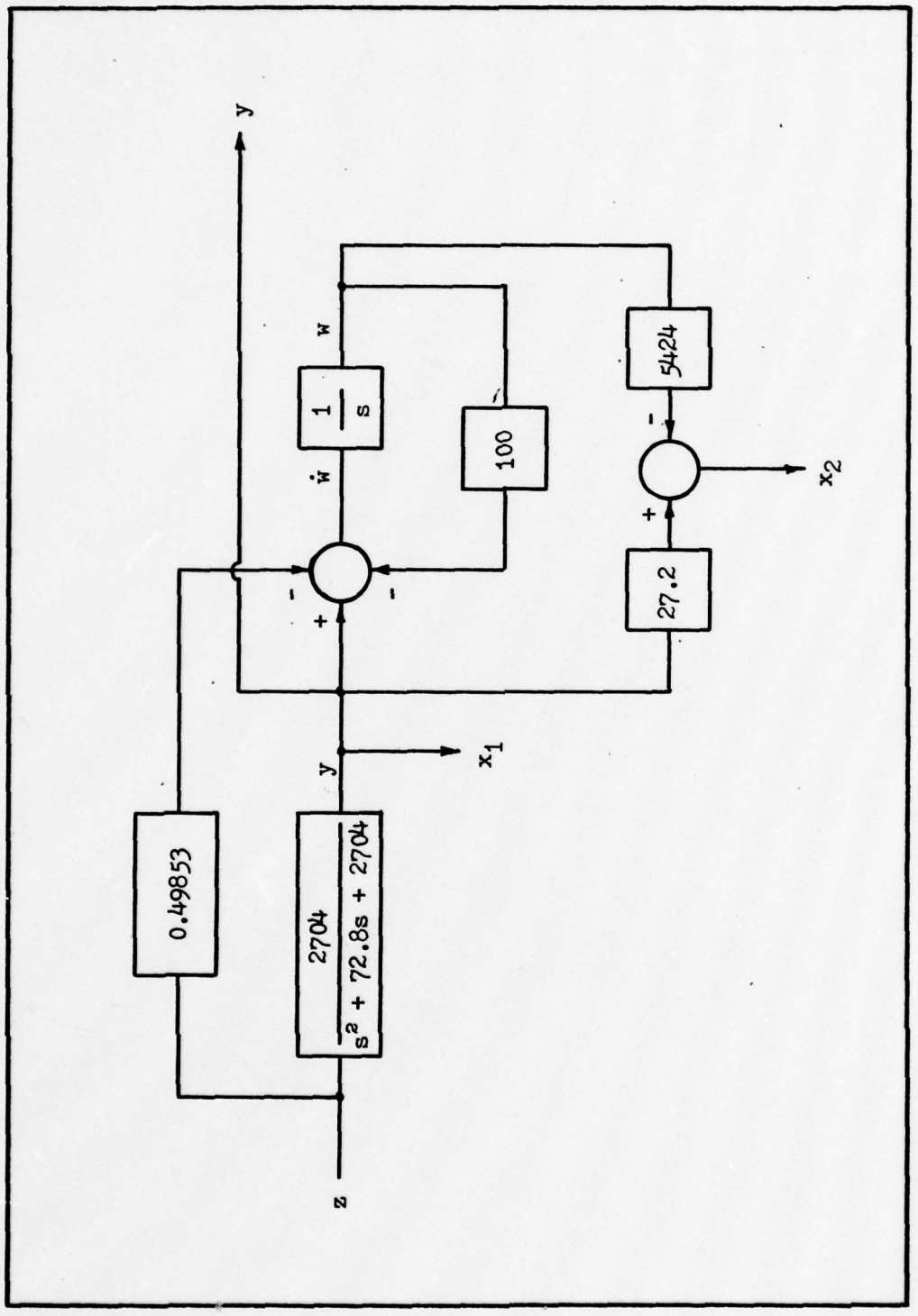


Figure 60. Servo and first-order observer.

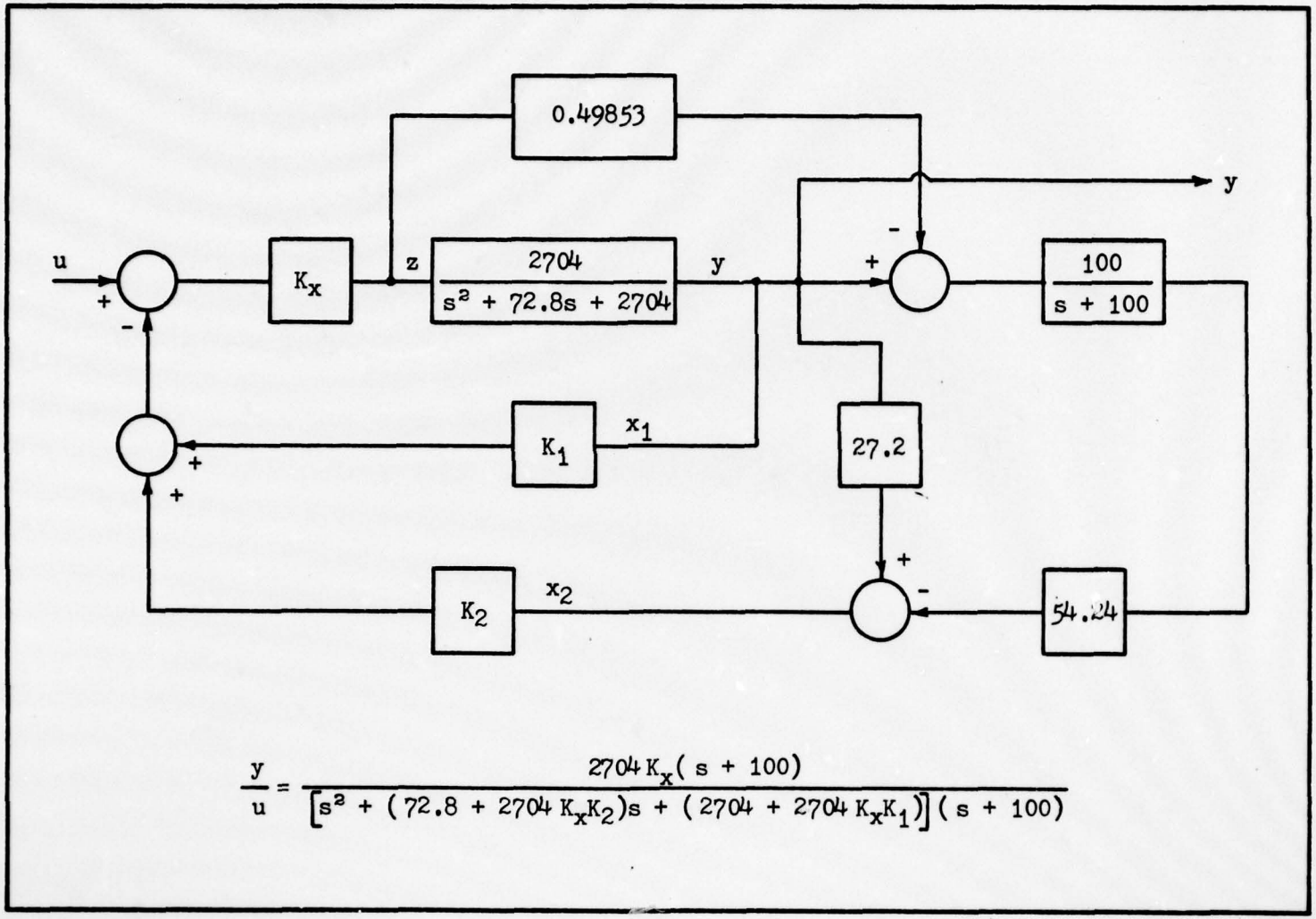


Figure 61. Servo / observer system with state variable feedback.

Appendix J

C* Control Derivation

The concept of C* is based upon the active control of a linear combination of longitudinal aircraft states; more specifically, a weighted combination of pitch rate, pitch acceleration, and the time rate of change of angle-of-attack. Introduced in 1966 by Tobie, Elliot, and Malcom (Ref 22), one definition of the C* performance criterion is

$$C^* = K_N U_o(q - \dot{\alpha}) + K_q q + K_{\dot{q}} \dot{q} \tag{191}$$

where K_N, K_q, and $K_{\dot{q}}$ are gain constants used to weight each term, and U_o is the forward velocity of the aircraft. In Chapter IV, Eqn 28 defines normal acceleration, positive downward, as

$$A_z = U_o(\dot{\alpha} - q) \tag{28}$$

which reveals that the first term in Eqn 191 is actually weighted normal acceleration, defined positive upward. Making this substitution, and letting $A_N = -A_z$, the definition of C* looks a bit more familiar:

$$C^* = K_N A_N + K_q q + K_{\dot{q}} \dot{q} \tag{192}$$

The C* control concept was conceived as a result of a desire to improve aircraft handling qualities based upon pilot sensory perception. It was hypothesized that at low aircraft velocities, a pilot responds more to pitch cues than to normal acceleration, as large changes in pitch attitude

result in only small changes in normal acceleration. At higher velocities, a pilot tends to sense normal acceleration cues more than pitch, as slight pitching results in large acceleration changes. Therefore, the idea of C* control is to blend pitch rate and pitch acceleration with normal acceleration, thereby allowing the pilot to control the dominant mode.

The quantity C* is generally dimensioned in G's, implying that K_q and $K_{\dot{q}}$ must be chosen in such a way as to permit each term in Eqn 192 to be dimensioned in G's. As a means of standardization, K_N normally assumes a unit value, and K_q and $K_{\dot{q}}$ are then selected on that basis. Making this assumption is in no way restrictive, as it is only the relative weighting of feedback quantities that is important. Equation 192 can now be expressed as

$$C^* = A_N + K_q q + K_{\dot{q}} \dot{q} \qquad (193)$$

As it is pitching acceleration at the pilot station that is of interest, the value of $K_{\dot{q}}$ is selected based upon the physical distance from the aircraft CG to the location of the cockpit. In the YF-16, these pitching accelerations are sensed by the normal accelerometers, as they are located directly under the pilot's seat. This occurance is no accident, however, as the YF-16 has a somewhat modified C* flight control system using washed-out pitch rate to respond to pitch transients only. For the YF-16 then, the C* definition is reduced to

$$C^* = A_{N_S} + K_q q \tag{194}$$

where A_{N_S} is the combination of normal and pitching accelerations at the normal accelerometer location. This is the definition used in the C* FCS shown in Figure 58 in Appendix F.

The quantity K_q represents a chosen "crossover velocity", or the aircraft velocity at which normal acceleration and pitch rate will be controlled equally. Assuming that velocity is dimensioned in feet/second, and pitch rate is measured in degrees/second, the dimensional product of these two quantities will be ft-deg/sec-sec. As described in Chapter IV, Eqn 32, a dimensional conversion factor must be applied to permit a dimensional product of G's. If "V_{co}" is defined as the crossover velocity in feet/second, Eqn 194 becomes

$$C^* = A_{N_S} + \frac{V_{co}}{1843.6} q \tag{195}$$

Typically, V_{co} is selected as 400 feet/second for jet fighter aircraft (Ref 22). For the YF-16 then, the final form of the C* definition is given as

$$C^* = A_{N_S} + 0.217q \tag{196}$$

The performance of a C* commanded FCS is generally assumed to be acceptable if the system transient response to a step input falls within a specified envelope, depending upon the particular mode (category) of flight. There are four

such categories defined in MIL-F-8785B (Ref 13), and they have been directly applied to the transient performance of a C* FCS. The envelopes are depicted in Figure 62, and the categories of flight are as defined below.

I Optimal response for critical flying conditions (aerial combat, ground attack, penetration).

II Response for less critical conditions (cruising, air refueling).

III Response for conditions not covered by I, II, or IV (loiter).

IV Response for power approach (landing).

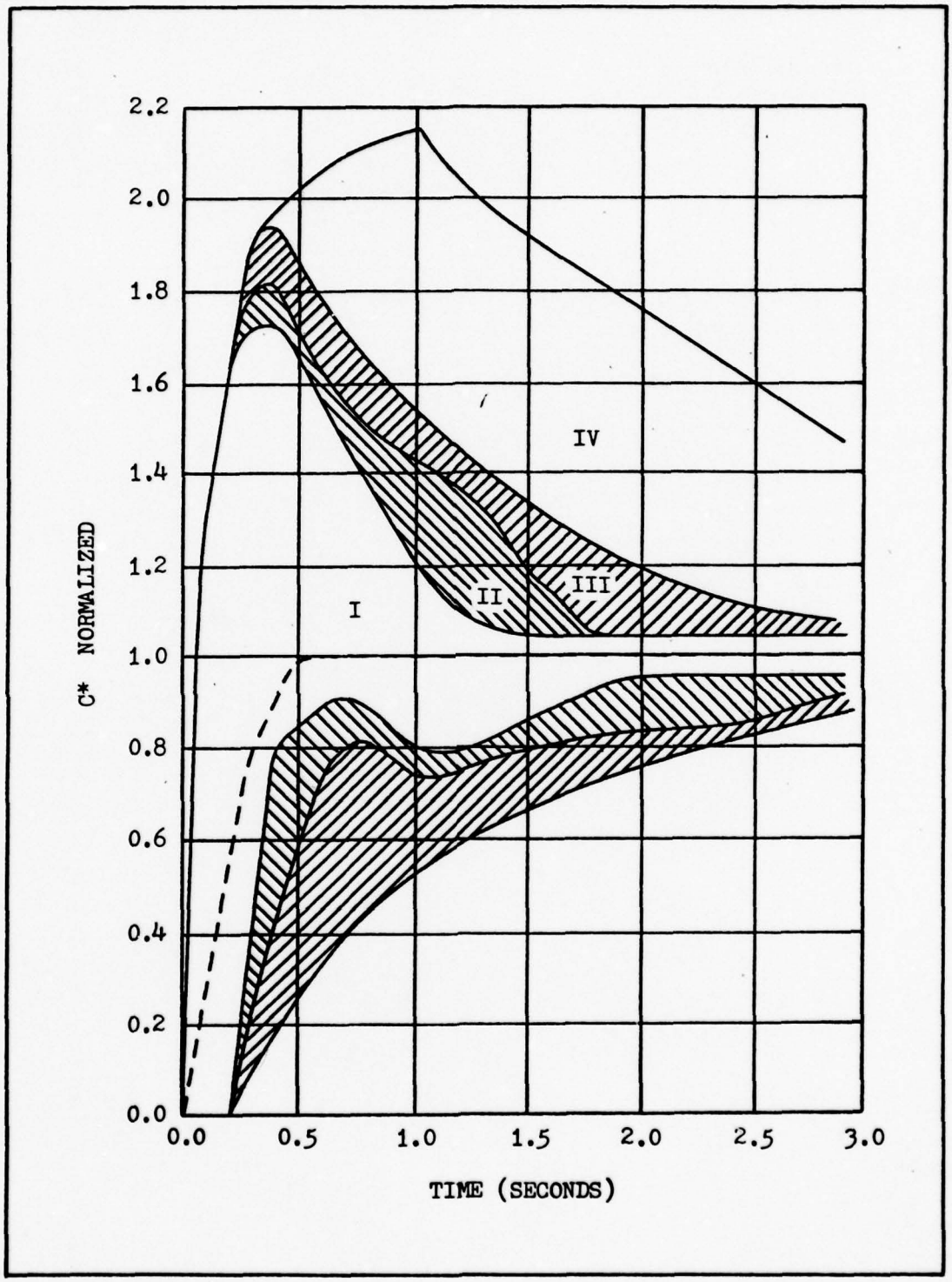


Figure 62. Definition of the C* time history envelopes (Ref 11).

Appendix K

YFCCV Computer Program

YFCCV, a FORTRAN Extended software package developed as a part of this thesis, and designed to run on a CDC 6600 series computer, was created for the purpose of simulating the multi-input, multi-output longitudinal flight control system of the YF-16 CCV. Although the program was designed especially for this aircraft, it is capable of simulating the longitudinal dynamics and flight control system of almost any other aircraft having a maximum of two active longitudinal aerodynamic control surfaces. The user is free to specify the dynamics of a normal accelerometer, a pitch rate gyro, an angle-of-attack sensor, the servos and actuators for the horizontal tail and trailing-edge flaperons, two forward-loop cascade compensators, and up to six feedback compensators.

The aircraft aerodynamic data is conveniently input in the form of non-dimensional stability derivatives. The pitch rate gyro, angle-of-attack sensor, normal accelerometer, and all compensators are input as transfer functions. Pilot inputs include step, pulse, ramp, and polynomial functions of up to 5th order. Disturbance inputs include step and "1-cos" discrete vertical gusts, and a uniformly distributed pseudo-random vertical gusting. The magnitudes (and duration, where applicable) of both pilot and disturbance inputs are user definable. In addition, both pilot and disturbance inputs may be used in the same simulation. In this manner, the user can observe aircraft response to a pilot input in

the presence of turbulence.

Program output is available as a listing or in plotted form. In most cases, output data will be routed to a line printer. Using this output device, listings of measurements taken at 21 points in the flight control system are printed out at user definable time increments. In addition, if desired, the program will generate line printer plots for the same simulation to be printed with, or instead of, the listings. Any of the 21 measurements can be plotted (scaled automatically), but a maximum of 15 may be requested in any one run. As an alternative, the user may request that the measurement data be formatted for routing to a Calcomp (or equivalent) plotter. The computer-generated plots in this report were created in this manner.

If desired, the horizontal tail and trailing-edge flap servos may be rate limited and/or displacement limited. When the deflection of either of these two surfaces is plotted as a line printer plot, the maximum rate of deflection achieved is calculated and printed out on the upper right-hand corner of the plot. If either limiter is in use, the flag "LIMIT, ON" will also be printed. Saturation is specified in degrees per second or in degrees.

The program may be used interactively or in batch mode. Having been designed for interactive use, all data input is prompted. However, a data file may be used if the same input format is maintained. In either mode, all specified parameters are retained within the program until execution is

terminated. This feature allows the user to run several simulations, perhaps changing a compensator eigenvalue location, without having to re-enter the unchanged input data each time.

All simulation output data (except for Calcomp use as mentioned previously) is formatted for the line printer. This was done because of the large volume of output generally produced. However, the user may view this output at an intercom terminal if desired. The flow of simulation output is controlled by a switch command. Simply typing "COPY,ON" will cause all simulation output to be written to a local file called "COPY". Typing "COPY,OFF" will cause future output to be written to the terminal. All output other than simulation data is still connected to the terminal in either switch position. For this reason, the switch may be turned on at the beginning of an interactive session and still allow normal program operation with the advantage of the user not having to watch data being listed. At the conclusion of the session, the COPY file may be routed to the line printer or viewed at the intercom terminal.

In addition to the simulation routine, there are a few other options available to the user. Originally, these options were intended to be used for program de-bugging, but were found to be useful in other ways and thus retained. Since the program uses a state space representation of the aircraft in its simulation process, printout of these matrices (in either continuous or discrete form) can be

requested. Given a set of non-dimensional stability derivatives, the A, B, F, and G matrices may be obtained for the dynamics of any aircraft. Also, the F and G matrices for any general A and B matrices (up to 5th order) may be obtained. In addition, the F and G matrices may be obtained for a given transfer function of up to 5th order. The remaining options include setting up a state space representation of aircraft dynamics generated from stability derivatives, the capability to "convert" a root location in s-plane to a corresponding location in z-plane, and executing a polynomial curve fitting routine using up to 10th order polynomials to fit data points.

Theory of Operation

During a simulation, all integration is performed using the state transition method. The aircraft dynamics, pitch rate gyro, angle-of-attack sensor, normal accelerometer, and all compensator transfer functions are converted to discrete state space form (Ref 2). With each iteration, the values of the states propagate throughout the entire system, as shown in Figure 63. Since the state transition method performs an exact integration of a linear system, accuracy is maintained within each "subsystem" (allowing for some round-off error). Some loss of accuracy occurs, however, when interfacing these subsystems to produce the entire system. As the integration of states is being performed in separate parts, there is the underlying assumption that the input to each subsystem remains constant during the integration process. Except in

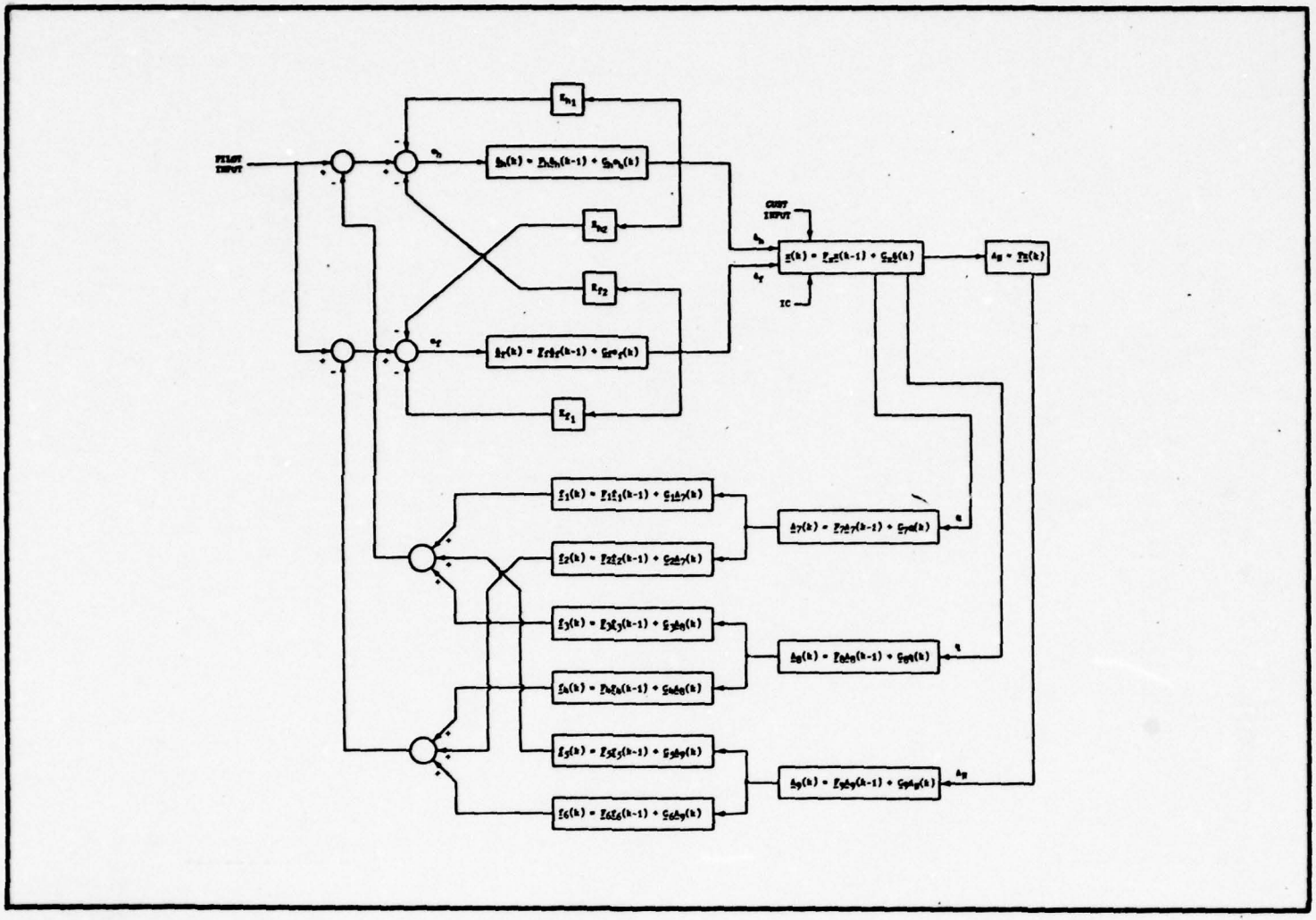
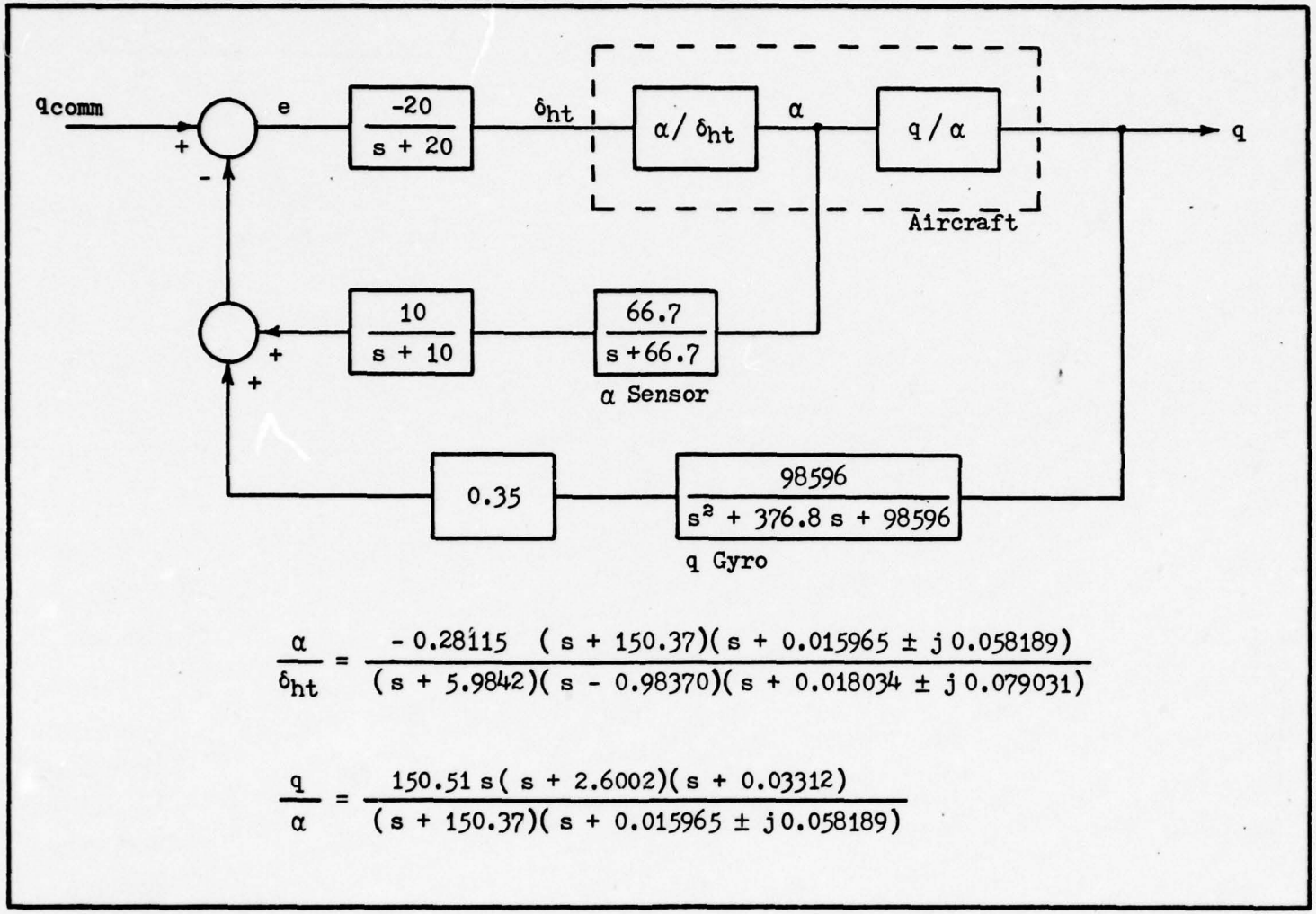


Figure 63. Basic functional YFCCV Computer Program block diagram showing propagation of subsystem states.

steady-state, this never truely happens. It is assumed, however, that if the iteration rate is much greater than the maximum rate of change of any system state, the approximation is valid.

To test this scheme, the system in Figure 64 was simulated for a step input using the program at various iteration rates. The same system was simulated using an inverse Laplace technique, or actual time function (Ref 23). The results of these simulations are plotted on one axis in Figure 65. Note that as the iteration rate is increased, the discrete approximation rapidly converges to the continuous response. Although a rate of 200 iterations per second has been found to be suitable for simulating most aircraft flight control systems, a rate of 2000 iterations per second was used for the majority of the simulations in this thesis.

There are two main reasons for chosing this integration scheme. The first is that it allows the simultaneous application of several inputs to a system in a straightforward manner (matrix operations). The second is that it allows each subsystem to be changed independently of the others, and avoids the alternative of reconstructing and processing a system matrix that may contain up to 59 states (this is the maximum number of states available in YFCCV). In addition, this method allows the simulation of certain digital controllers. Since the FCS signals are applied to the aircraft at each iteration, and held constant between iterations, the program operates using the zero-order hold



$$\frac{\alpha}{\delta_{ht}} = \frac{-0.28115\ (s + 150.37)(s + 0.015965 \pm j\,0.058189)}{(s + 5.9842)(s - 0.98370)(s + 0.018034 \pm j\,0.079031)}$$

$$\frac{q}{\alpha} = \frac{150.51\, s(s + 2.6002)(s + 0.03312)}{(s + 150.37)(s + 0.015965 \pm j\,0.058189)}$$

Figure 64. Simplified pitch rate FCS for the YF-16 at 0.8 Mach at SL.

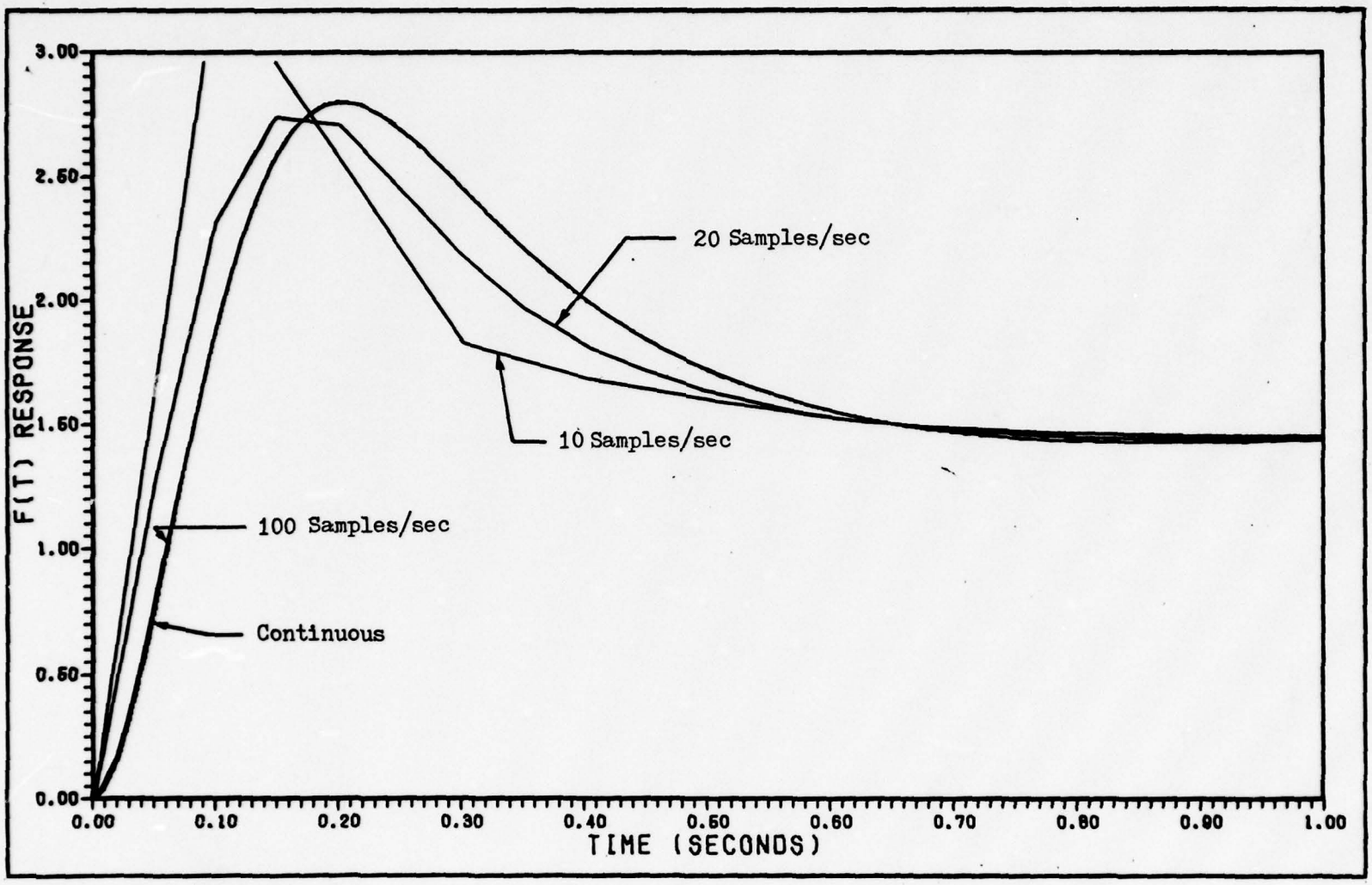


Figure 65. Continuous vs discrete system time responses for selected iteration rates.

concept. By allowing the servo/actuator, aircraft, and gyro subsystems (having continuous dynamics) to operate at a faster iteration rate, and the feedback to operate at a slower rate (a sampling rate), the program is capable of simulating a digital controller.

Commands

After the program has been attached for interactive use, simply entering "YFCCV" will begin execution, and result in the prompt "<COMMAND>". At this point, the user may enter a command, a "?" to obtain a listing of valid commands, or "STOP" to terminate the program. At any time that the program requests an alphabetical response, entering a "?" will provide an explanation of the requested response. In addition to "?" and "STOP", there are 21 other valid commands. These commands are listed on the next several pages with explanations of their functions.

(1) ACDAT Using this option, the user specifies certain physical properties of the aircraft, defines the flight condition, and inputs the non-dimensional stability derivatives for that flight condition. For the YF-16, some quantities are defined internally (wing area, aircraft mass, MAC, etc), and in addition, if a flight condition of 0.8 Mach at SL is specified, the required stability derivatives are specified internally. The location of the normal accelerometer ("AZL", the distance in feet from the CG to the accelerometer location) must also be specified in this

option. The input of this data is necessary prior to any simulation attempt.

(2) ACSTM This command will cause the aircraft state transition matrix and input matrices to be calculated and printed out. Before requesting this option, the user must enter aircraft data and specify a flight condition using ACDAT.

(3) ALPHA Using this command, the user specifies the feedback from the attack angle sensor to the HT (horizontal tail) and TEF (trailing-edge flaperon) channels. Each feedback may be zero (default), a gain, or a compensator (up to 5th order). To accommodate a wider variety of system configurations, either attack angle or its derivative may be specified for feedback by entering the responses "NORMAL" or "DERIVATIVE", respectively, at the requested time. Input of this feedback element is for use in GENSIM simulations only.

(4) AN Using this command, the user specifies the feedback from the normal accelerometer to the HT and TEF channels. Each feedback may be zero (default), a gain, or a compensator (up to 5th order). It should be noted that the position of the normal accelerometer is specified by data input using the ACDAT command. Input of this feedback element is for use in GENSIM simulations only.

(5) COPY,ON or COPY,OFF The COPY switch command controls the file to which simulation output data is written.

Turning this switch on will cause simulation data to be written to the local file "COPY". Turning it off will cause the data to be written to the "OUTPUT" file connected at the intercom terminal (default). The status of this switch does not affect any other program operation or user prompting.

(6) CSA This command is an acronym that stands for Compensator/Servo/Actuator. The combined dynamics of these devices are entered as a single transfer function (one each for HT and TEF channels) using this option. Input of this feedforward element is for use in GENSIM simulations only.

(7) CURVE This command executes a polynomial curve fitting routine. It is limited to 10th order polynomials. Calcomp plots and numerical listings are available to display both input data points and the result of the curve fitting process.

(8) GENSIM This command is used to initiate a simulation process that is referred to as "GENeral SIMulation". This is the standard simulation of a continuous-time flight control system of the general form depicted in Figure 66. The user specifies the desired iteration rate (0.0005 is typical), the form of the output desired, and the location at which normal acceleration, velocity, and/or position will be measured (if measurement is requested) during the simulation. Although the normal acceleration used for feedback within the FCS is always from the specified accelerometer location (using ACDAT), this

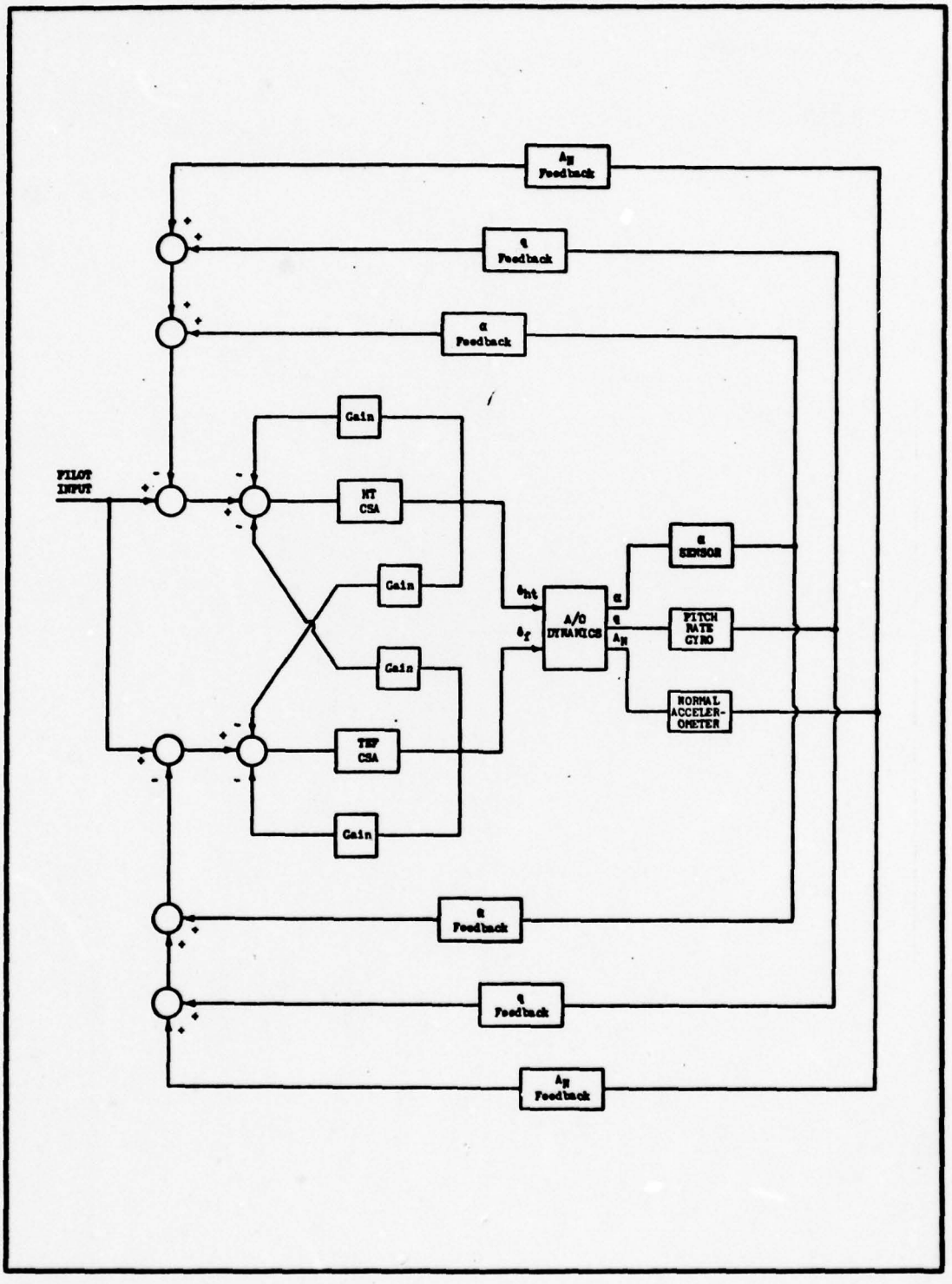


Figure 66. General form of the FCS configuration simulated by the GFNSIM option.

state and its integrals (normal velocity and position) may be measured at either the CG or the accelerometer location. This permits observation of these quantities at one location, while the system feedback may represent another location. The actual simulation begins at the close of the command sequence immediately after the requested command "RUN" is entered.

(9) GSTM With this option, the user may input any continuous state space system (matrix form) of up to 5th order, and obtain a state transition matrix and input matrix for a specified sampling rate. In addition, a time simulation of the system can be obtained for any number of iterations, with any state as output. This output is available in listed form only (formatted for intercom display).

(10) GYRO This command allows the dynamics of the pitch rate gyro, the angle-of-attack sensor, and the normal accelerometer to be specified. A minimum of a first-order lag must be specified for each of these devices that will be used in the simulation, or zero output (default) will result from that device. Any transfer function of up to 5th order is permissible.

(11) IC This command allows the user to specify initial conditions on (the perturbation quantities) forward velocity, pitch angle, pitch rate, and angle-of-attack. This option is often useful when designing and simulating a regulator without pilot or disturbance inputs. Initial conditions can be specified only for use in GENSIM

simulations.

(12) INPUT This command permits definition of pilot and disturbance inputs. If either of these two inputs is not defined, default is zero. Either one or both inputs may be specified.

(13) OPTSIM This command is used to initiate a simulation process that is referred to as "OPTimal SIMulation". This option provides a more specialized simulation capability (relative to GENSIM), and is intended for use in simulating an optimal servo class of flight control system configurations using gain feedback and forward-loop integration (Ref 11). The user may specify either a continuous-time or discrete-time controller. In the latter case, controller sample rate must be provided. This option further differs from GENSIM in that system parameters are specified in matrix format, rather than as individual feedback and feedforward compensators. As with all YFCCV commands, input requests are fully prompted.

(14) PLOTTER This command permits the user to plot simulation results on a Calcomp (or equivalent) plotter. A simulation must first be run (using GENSIM or OPTSIM) to calculate all the required data points. By entering the response "TAPE" when prompted by the question, "DO YOU WANT ANY LINE PRINTER PLOTS?", this information is written into the local file "COPY" by the simulation routine, in a format that enables the PLOTTER routine to extract the data as

required. The response, "TAPE", is entered during the simulation command sequence, and simply indicates to the routine that simulation output should be written to the file COPY for use by PLOTTER. Each plot requested causes the program to read the COPY file, reformat and insert the necessary labeling, and write into an additional local file called "PLOT". This PLOT file must then be routed to the particular plotter that is to be used.

(15) SERVOFB Using this command, the user specifies four feedback gains from the outputs of the two CSA's. Essentially, this option permits a feedback loop around each CSA, and feedback from the output of each CSA to the input of the alternate CSA. The feedback is summed negatively at the CSA inputs, and therefore these gains will be positive for negative feedback. No compensation is available in these feedback paths. As the concept of a CSA is valid only for use in GENSIM simulations, this feedback is otherwise undefined.

(16) STSPACE This command will cause the continuous state space representation of the aircraft with two first-order servos to be printed. Also, for a more specialized problem, this option will calculate a state cost matrix from an output cost matrix for optimal control problems.

(17) TARGET This option permits the user to specify the distance (in feet) from the aircraft to a target (defaults to 6000 feet). This information is used in the

calculation and printout or plot (if requested) of longitudinal target tracking error as defined in Chapter II.

(18) THDOT Using this command, the user specifies the feedback from the pitch rate gyro to the HT and TEF channels. Each feedback may be zero (default), a gain, or a compensator (up to 5th order). To accommodate a wider variety of system configurations, either pitch rate or its derivative may be specified for feedback by entering the responses "NORMAL" or "DERIVATIVE", respectively, at the requested time. Input of this feedback element is for use in GENSIM simulations only.

(19) TIME Use of this command results in the current time being printed at the user's terminal.

(20) TRF This option allows the user to input any realizable transfer function of up to 5th order, and obtain a state transition matrix and input matrix for a given sampling rate (F and G matrices). In addition, a time simulation of the transfer function may be obtained.

(21) ZROOT This option performs an s-plane to z-plane root location "conversion". Any single root or complex pair of roots represented in s-plane can be input, and the corresponding root location(s) in z-plane will be obtained for a specified sampling rate.

Any of the above commands may be entered at the prompt "<COMMAND>". Whenever all requested data has been input, and

any requested output has been generated in a given command sequence, the user is returned to <COMMAND> mode. At any point in the program where an alphabetical response is requested, the entry of an invalid command will result in the response, "WHAT??", or "PARDON ME??", at which time the proper entry can be re-typed.

The next several pages show a sample interactive session with the program. During the session, several of the commands required for GENSIM simulations are utilized. The end result would be an actual simulation of an aircraft flight control system. In this particular example, no stability derivatives are entered, as all required aircraft data for the YF-16 at a FC of 0.8 Mach at SL is permanently stored within the program. Angle-of-attack, pitch rate, and normal acceleration feedback elements are defined, as are the forward-loop dynamics (CSA's). The transfer functions of the angle-of-attack sensor, pitch rate gyro, and normal accelerometer are then input, followed by the GENSIM simulation command sequence. The requested output is four Calcomp plots.

Unfortunately, due to the length of program YFCCV, it is not practical to include a program listing in this thesis. Upon request, however, a listing is available from the author.

```
COMMAND- YFCCV

 TYPE '?' FOR <COMMAND> OPTIONS, 'STOP' TO STOP...

 <COMMAND>  ACDAT
 AIRCRAFT DESIGNATION:  YF-16

 ENTER INITIAL ALTITUDE,MACH NO.:  0 .8
 SERVO DISPLACEMENT LIMITERS (ON OR OFF):  OFF
 SERVO RATE LIMITERS (ON OR OFF):  ON
 ENTER HT SERVO LIMITING RATE (DEG/SEC):  60
 ENTER TEF SERVO LIMITING RATE (DEG/SEC):  56
 ENTER TYPE OF ANALYSIS (LINEAR OR NON-LINEAR): LINEAR
 DO YOU WISH TO INPUT STABILITY DERIVATIVES?  NO

 <COMMAND>  INPUT
 >>>WIND
 WIND INPUT = 1-COS
 ENTER VERTICAL GUST VELOCITY (FT/SEC), DURATION: 50 1
 >>>EXIT

 <COMMAND>  ALPHA
 SELECT 'STATE' OR 'SENSOR' ALPHA FEEDBACK: SENSOR
 >>>HT
 FEEDBACK STATE (NORMAL OR DERIVATIVE):  DERIV
 FEEDBACK SPECIFICATION =COMPENSATOR
 ENTER ORDERS OF NUMERATOR,DENOMINATOR (MAX 5TH):  1 1
 ENTER NUMERATOR CONSTANT:  .035
 ENTER  2 NUMERATOR COEFFICIENTS...HI TO LOW:
 1 8
 ENTER  2 DENOM COEFFICIENTS...HI TO LOW:
 1 5
 >>>TEF
 FEEDBACK STATE (NORMAL OR DERIVATIVE):  DERIV
 FEEDBACK SPECIFICATION =COMP
 ENTER ORDERS OF NUMERATOR,DENOMINATOR (MAX 5TH):  1 1
 ENTER NUMERATOR CONSTANT:  -1.875
 ENTER  2 NUMERATOR COEFFICIENTS...HI TO LOW:
 1 8
 ENTER  2 DENOM COEFFICIENTS...HI TO LOW:
 1 0
 >>>EXIT
```

```
<COMMAND>  THDOT
>>>HT
FEEDBACK STATE (NORMAL OR DERIVATIVE):  DERIV
FEEDBACK SPECIFICATION =COMP
ENTER ORDERS OF NUMERATOR,DENOMINATOR (MAX 5TH):  2 2
ENTER NUMERATOR CONSTANT:  1
ENTER  3 NUMERATOR COEFFICIENTS...HI TO LOW:
.075  1.225  5
ENTER  3 DENOM COEFFICIENTS...HI TO LOW:
1  5  0
>>>TEF
FEEDBACK STATE (NORMAL OR DERIVATIVE):  DERIV
FEEDBACK SPECIFICATION = COMP
ENTER ORDERS OF NUMERATOR,DENOMINATOR (MAX 5TH):  1 1
ENTER NUMERATOR CONSTANT:  -.875
ENTER  2 NUMERATOR COEFFICIENTS...HI TO LOW:
1  8
ENTER  2 DENOM COEFFICIENTS...HI TO LOW:
1  0
>>>EXIT

<COMMAND>  AN
>>>TEF
FEEDBACK SPECIFICATION = COMPENSATOR
ENTER ORDERS OF NUMERATOR,DENOMINATOR (MAX 5TH):  1 1
ENTER NUMERATOR CONSTANT:  187.5
ENTER  2 NUMERATOR COEFFICIENTS...HI TO LOW:
1 8
ENTER  2 DENOM COEFFICIENTS...HI TO LOW:
1 100
>>>EXIT

<COMMAND>  CSA
>>>HT
ENTER ORDERS OF NUMERATOR,DENOMINATOR (MAX 5TH):  1 3
ENTER NUMERATOR COEFFICIENT:  -160
ENTER  2 NUMERATOR COEFFICIENTS...HI TO LOW:
1 5
ENTER  4 DENOM COEFFICIENTS...HI TO LOW:
1 28 160 0
>>>TEF
ENTER ORDERS OF NUMERATOR,DENOMINATOR (MAX 5TH):  1 3
ENTER NUMERATOR COEFFICIENT:  -320
ENTER  2 NUMERATOR COEFFICIENTS...HI TO LOW:
1 0
ENTER  4 DENOM COEFFICIENTS...HI TO LOW:
1 43 580 2400
>>>EXIT
```

```
<COMMAND>  GYRO
>>>ALPHA
ENTER ORDERS OF NUMERATOR,DENOMINATOR (MAX 5TH):  0 1
ENTER NUMERATOR CONSTANT: 66.7
ENTER  1 NUMERATOR COEFFICIENTS...HI TO LOW:
1
ENTER  2 DENOM COEFFICIENTS...HI TO LOW:
1 66.7
>>>THDOT
ENTER ORDERS OF NUMERATOR,DENOMINATOR (MAX 5TH):  0 2
ENTER NUMERATOR CONSTANT:  1
ENTER  1 NUMERATOR COEFFICIENTS...HI TO LOW:
98596
ENTER  3 DENOM COEFFICIENTS...HI TO LOW:
1 376.8 98596
>>>AN
ENTER ORDERS OF NUMERATOR,DENOMINATOR (MAX 5TH):  0 2
ENTER NUMERATOR CONSTANT:  98596
ENTER  1 NUMERATOR COEFFICIENTS...HI TO LOW:
1
ENTER  3 DENOM COEFFICIENTS...HI TO LOW:
1 376.8 98596
>>>EXIT

<COMMAND>  GENSIM
ENTER SYSTEM ITERATION TIME.  IT=.0005
ENTER PRINTOUT TIME INCREMENT, SIMULATION DURATION: .005 4
DO YOU WANT ANY LINE PRINTER PLOTS?  TAPE
ENTER CROSSOVER VELOCITY (FT/SEC).  VCO= 400
NORMAL POSITION, VELOCITY, AND ACCELERATION CAN BE
MEASURED AT THE CENTER OF GRAVITY OR AT THE PILOT
STATION. ENTER 'CG' OR 'PS' (DEFAULT, PS): PS
TYPE 'RUN' TO SIMULATE, 'EXIT' TO RETURN TO <COMMAND>: RUN
```

```
<COMMAND> PLOTTER
ENTER NUMBER OF PLOTS DESIRED: 4
ENTER  4 PLOT IDENTIFIERS: 2 4 5 6

#################### DRAWZ CALLED ####################

     THE NUMBER OF POINTS TO BE PLOTTED =  800

#################### DRAWZ CALLED ####################

     THE NUMBER OF POINTS TO BE PLOTTED =  800

#################### DRAWZ CALLED ####################

     THE NUMBER OF POINTS TO BE PLOTTED =  800

#################### DRAWZ CALLED ####################

     THE NUMBER OF POINTS TO BE PLOTTED =  800

<COMMAND> STOP

GOOD-BYE. THE TIME IS  13.34.36
 STOP  NORMAL TERMINATION
  5.201 CP SECONDS EXECUTION TIME

COMMAND- ROUTE,PLOT,DC=PT,TID=BB,FID=YA037,ST=CSB
COMMAND- LOGOUT
CPA      34.053 SEC.       14.782 ADJ.
IO       34.861 SEC.       17.440 ADJ.
CRUS                       43.695
CONNECT TIME    0 HRS.   16 MIN.
 01/04/79  LOGGED OUT AT 13.36.54
      <
```

Appendix L

YFSOLVE Computer Program

YFSOLVE is a special purpose FORTRAN Extended computer program designed to run on a CDC 6600 series computer. Intended for interactive use, it was developed for the purpose of providing certain closed-loop transfer functions for the Pitch Performance Enhancement (PPE) FCS from specified input parameters. In addition, as the simulation program, YFCCV (see Appendix K), is not directly suited to simulating system configurations such as the PPE FCS, program YFSOLVE provides the required feedback and feedforward (CSA) dynamics for an equivalent system model that fits the YFCCV system configuration. The use of an equivalent model is due to the PPE FCS requirement for summation of feedback twice in the horizontal tail channel, a forward-loop gain occurring prior to feedback summation in the flaperon channel, and the inclusion of a command prefilter.

Although the program was written to aid in the design of the PPE flight control system for the selected flight condition, minor alterations could enable it to be used to provide similar transfer functions for a variety of systems. The basic architecture of the program would remain unchanged, with only the statements defining polynomial coefficients requiring modification.

Commands

Initial execution of the program places the user in

command mode, at which time one of 19 valid commands can be entered. Entry of an invalid command results in a response of, "PARDON ME??". Of the valid commands, 15 are used for data entry, three produce program output, and the remaining command, "STOP", is used to terminate execution. All system parameters must be specified (using the data input commands) prior to executing a data output command. If all input parameters are not so specified, attempted execution of a data output command will result in a response of, "HAVE YOU INPUT ALL VARIABLES?", after which the user is returned to command mode. Valid commands, and their functions, are as follows (given in alphabetical order):

Data Entry Commands

(1) FILTER This command permits definition of the pilot command prefilter first-order lag. As this compensator is unity gain, specification of the eigenvalue location automatically sets the gain constant.

(2) HPOLE This command permits specification of the HT (horizontal tail) first-order lag servo eigenvalue.

(3) INPUT This command permits the user to input all required system parameters (variables) at the same time. Generally, this option would be used at the start of a session, or when a large number of variables is to be modified.

(4) K1 This command permits specification of the attack angle feedback gain to the HT channel.

(5) K2 This command permits specification of the

attack angle feedback gain to the TEF channel.

(6) K3 This command permits specification of the pitch rate feedback gain to the HT channel.

(7) K4 This command permits specification of the pitch rate feedback gain to the TEF channel.

(8) K6 This command permits specification of the normal acceleration feedback gain to the TEF channel.

(9) KC This command permits specification of the command forward-loop gain in the HT channel.

(10) KF This command permits specification of the TEF forward-loop gain.

(11) KH This command permits specification of the HT forward-loop gain.

(12) KP This command permits specification of the command forward-loop gain in the TEF channel.

(13) POLE This command permits specification of the washout circuit eigenvalue in the TEF channel.

(14) TPOLE This command permits specification of the TEF first-order lag servo eigenvalue.

(15) ZERO This command permits specification of the zero location in the proportional plus integral (P+I) forward-loop compensation in the HT channel.

Data Output Commands

(16) LIST This command lists the current values of the system input variables.

(17) RUN This command generates all available output from the routine. The current values of the system

input variables are listed first, followed by a listing of the two pitch rate numerator equations and characteristic equation (polynomial and factored form), followed by a listing of the feedback and feedforward gains and transfer functions to be used by program YFCCV for simulation.

(18) SIM This command calculates and lists the feedback and feedforward gains and transfer functions to be used by program YFCCV for simulation.

As the intended purpose of YFSOLVE is to support an iterative design process, it was assumed that considerable program output could result while zeroing in on values for the system variables. To enable a permanent record of this output, the program writes output to both the user's intercom terminal and a local file named "STUFF". At the end of a session, this file is available to be routed to a line printer for a "hard" copy.

A listing of the source code for the program is provided on the next several pages.

```
      PROGRAM SOLVE(INPUT,OUTPUT,STUFF,TAPE2=STUFF)
      INTEGER INFLAG(12)
      REAL K1,K2,K3,K4,K5,KH,KF,KC,KP
      REAL ROOTR(10),ROOTI(10),CPOLY(10)
      COMMON/EXPCOM/ROOTR,ROOTI,CPOLY,NF
      K5=KF=1.0
      FILT=8.0
      D=.02494
1     PRINT 10
10    FORMAT(/,5X,"COMMAND>  ")
13    READ 11,ANS
11    FORMAT(A5)
      IF(ANS.EQ."INPUT")GO TO 20
      IF(ANS.EQ."POLE")GO TO 24
      IF(ANS.EQ."ZERO")GO TO 26
      IF(ANS.EQ."K1")GO TO 30
      IF(ANS.EQ."K2")GO TO 40
      IF(ANS.EQ."K3")GO TO 50
      IF(ANS.EQ."K4")GO TO 60
      IF(ANS.EQ."K6")GO TO 70
      IF(ANS.EQ."KC")GO TO 80
      IF(ANS.EQ."KH")GO TO 90
      IF(ANS.EQ."KF")GO TO 100
      IF(ANS.EQ."KP")GO TO 105
      IF(ANS.EQ."HPOLE")GO TO 110
      IF(ANS.EQ."TPOLE")GO TO 120
      IF(ANS.EQ."FILT")GO TO 125
      IF(ANS.EQ."LIST")GO TO 130
      IF(ANS.EQ."RUN")GO TO 140
      IF(ANS.EQ."SIM")GO TO 160
      IF(ANS.EQ."STOP")GO TO 999
```


THIS PAGE IS BEST QUALITY PRACTICABLE
FROM COPY FURNISHED TO DDC

```
      PRINT 12
12    FORMAT(5X,"PARDON ME??? ")
      GO TO 13
20    DO 21 I=1,12
      INFLAG(I)=1
21    CONTINUE
      PRINT 22
22    FORMAT(5X,"INPUT THE FOLLOWING:",//,5X,
     +"K1, K2, K3, K4, K5, KC, KH, KF, KP, HPOLE, TPOLE, ZERO, POLE",//)
      READ*,K1,K2,K3,K4,K5,KC,KH,KF,KP,HPOLE,TPOLE,ZERO,POLE
      GO TO 1
24    INFLAG(11)=1
      PRINT 25
25    FORMAT(5X,"POLE= ")
      READ*,POLE
      GO TO 1
26    INFLAG(12)=1
      PRINT 27
27    FORMAT(5X,"ZERO= ")
      READ*,ZERO
      GO TO 1
30    INFLAG(1)=1
      PRINT 31
31    FORMAT(5X,"K1= ")
      READ*,K1
      GO TO 1
```


THIS PAGE IS BEST QUALITY PRACTICABLE
FROM COPY FURNISHED TO DDC

```
40    INFLAG(2)=1
      PRINT 41
41    FORMAT(5X,"K2= ")
      READ*,K2
      GO TO 1
50    INFLAG(3)=1
      PRINT 51
51    FORMAT(5X,"K3= ")
      READ*,K3
      GO TO 1
60    INFLAG(4)=1
      PRINT 61
61    FORMAT(5X,"K4= ")
      READ*,K4
      GO TO 1
70    INFLAG(5)=1
      PRINT 71
71    FORMAT(5X,"K6= ")
      READ*,K6
      GO TO 1
80    INFLAG(6)=1
      PRINT 81
81    FORMAT(5X,"KC= ")
      READ*,KC
      GO TO 1
90    INFLAG(7)=1
```


THIS PAGE IS BEST QUALITY PRACTICABLE
FROM COPY FURNISHED TO DDC

```
      PRINT 91
91    FORMAT(5X,"KH= ")
      READ*,KH
      GO TO 1
100   INFLAG(8)=1
      PRINT 101
101   FORMAT(5X,"KF= ")
      READ*,KF
      GO TO 1
105   PRINT 106
106   FORMAT(5X,"KP= ")
      READ*,KP
      GO TO 1
110   INFLAG(9)=1
      PRINT 111
111   FORMAT(5X,"HPOLE= ")
      READ*,HPOLE
      GO TO 1
120   INFLAG(10)=1
      PRINT 121
121   FORMAT(5X,"TPOLE= ")
      READ*,TPOLE
      GO TO 1
125   PRINT 126
126   FORMAT(5X,"ENTER PILOT PREFILTER 1ST ORDER LAG, S + ")
      READ*,FILT
      GO TO 1
130   PRINT 132,K1,KC,K2,KH,K3,KF,K4,HPOLE,K6,TPOLE,KP,ZERO,POLE
132   FORMAT(/,5X,"K1= ",F10.6,10X,"KC= ",F10.6,
     +/,5X,"K2= ",F10.6,10X,"KH= ",F10.6,
     +/,5X,"K3= ",F10.6,10X,"KF= ",F10.6,
```


THIS PAGE IS BEST QUALITY PRACTICABLE
FROM COPY FURNISHED TO DDC

```
     +/,5X,"K4= ",F10.5,10X,"HPOLE= ",F10.5,
     +/,5X,"K5= ",F10.5,10X,"TPOLE= ",F10.5,
     +/,5X,"KP= ",F10.5,10X,"ZERO=  ",F10.6,
     +/,29X,"POLE=  ",F10.5,/)
      GO TO 1
200   PRINT 201
201   FORMAT(5X,"HAVE YOU INPUT ALL VARIABLES?")
      GO TO 1
140   J=0
      DO 141 I=1,12
      J=J+INFLAG(I)
141   CONTINUE
      IF(J.NE.12)GO TO 201
      PRINT(2,132)K1,KC,K2,KH,K3,KF,K4,HPOLE,K5,TPOLE,KP,ZERO,POLE
C
      GZ=KP*KF
C
      P4=846.34*KH*KC-122.64*GZ
C
      P3=2201.70*KH*KC+846.34*ZERO*KH*KC+846.34*(POLE+TPOLE)*KH*KC+2649.
     #5*KH*KF*KC*K6-398.74*GZ-122.64*HPOLE*GZ
C
      P2=2201.70*ZERO*KH*KC+2201.70*(POLE+TPOLE)*KH*KC+846.34*ZERO*(POLE
     #+TPOLE)*KH*KC+846.34*POLE*TPOLE*KH*KC+.33333*KH*KF*KC*K6+2649.5*ZE
     #RO*KH*KF*KC*K5-5466.6*KH*KF*KC*K2+5466.5*KH*GZ*K1-398.74*HPOLE*GZ
C
      P1=2201.7*(POLE*TPOLE+POLE*ZERO+TPOLE*ZERO)*KH*KC+846.34*ZERO*POLE
     #*TPOLE*KH*KC+.33333*ZERO*KH*KF*KC*K5-5466.5*ZERO*KH*KF*KC*K2
```


THIS PAGE IS BEST QUALITY PRACTICABLE
FROM COPY FURNISHED TO DDC

```
C
      P0=2201.7*ZERO*POLE*TPOLE*KH*KC
C
      W5=12.339
C
      W4=12.339*(TPOLE+POLE+HPOLE)+193.25*KF*K3+122.64*KF*K2-846.34*KH*K
     #1
C
      W3=12.339*(POLE*TPOLE+TPOLE*HPOLE+HPOLE*POLE)+193.25*HPOLE*KF*K6+1
     #22.64*HPOLE*KF*K2-2349.5*KH*KF*K3*K1-846.34*(TPOLE+POLE)*KH*K1
C
      W2=12.339*POLE*TPOLE*HPOLE-846.34*POLE*TPOLE*KH*K1
C
      W1=0.
C
      W0=0.
C
      S6=1.
C
      S5=5.0047+TPOLE+HPOLE+POLE+2.664*KF*K6
C
      S4=-5.8622+5.0047*(HPOLE+TPOLE+POLE)+TPOLE*HPOLE+TPOLE*POLE+HPOLE*
     #POLE+4.9243*KF*K3+2.664*HPOLE*KF*K5+346.34*KH*KC*K5-122.64*KF*K4+8
     #46.34*KH*K3-7.27*KF*K2+122.64*ZERO*KF*K2+5.523*KH*K1-846.34*ZERO*KH*K1
C
      S3=-5.8622*(TPOLE+HPOLE+POLE)+5.0047*(TPOLE*HPOLE+TPOLE*POLE+HPOLE
     #*POLE)+POLE*TPOLE*HPOLE-193.25*KF*K3+4.9243*HPOLE*KF*K6+2201.7*KH*
     #KC*K5+846.34*ZERO*KH*KC*K5+846.34*(TPOLE+POLE)*KH*KC*K5-398.74*KF*
     #K4-122.64*HPOLE*KF*K4+2201.7*KH*K3-138.55*KF*K2+846.34*(TPOLE+POLE
```


THIS PAGE IS BEST QUALITY PRACTICABLE
FROM COPY FURNISHED TO DDC

```
     #)*KH*K3+378.74*D*KF*K2-7.274*HPOLE*KF*K2+122.64*D*HPOLE*KF*K2+845.
     #55*KH*K1-2201.7*D*KH*K1+5.623*(TPOLE+POLE)*KH*K1-846.34*D*(TPOLE+P
     #OLE)*KH*K1+2649.5*KH*KF*KC*K6*K5+2649.5*(1.-KF*K6*K3+38.4*KH*KF*K6*
     #K1-2649.5*D*KH*KF*K6*K1
C
      S2=-5.8622*(TPOLE*HPOLE+TPOLE*POLE+HPOLE*POLE)+5.0047*POLE*TPOLE*H
     #POLE-193.25*HPOLE*KF*KF+2201.7*ZERO*(H*KC*(5+846.34*(POLE*TPOLE+ZE
     #RO*TPOLE+POLE*ZERO)*KH*KC*K5-378.74*HPOLE*(F*K2+846.34*POLE*TPOLE*
     #KH*K3+2201.7*(TPOLE+POLE)*KH*K3-133.58*HPOLE*KF*K2+5.623*POLE*TPOL
     #E*KH*K1-846.34*D*POLE*TPOLE*KH*K1+378.74*D*HPOLE*KF*K2+2201.7*(TPO
     #LE+POLE)*KC*KH*K5+845.55*(TPOLE+POLE)*KH*(1-2201.7*D*(TPOLE+POLE)*
     #KH*K1+.33393*KH*KF*KC*K6*K5+2649.5*ZERO*(1.*KF*KC*K6*K5+.33393*KH*K
     #F*K6*K3+2649.5*KH*KF*KF*K1-.33393*D*(H*KF*(6*K1-5466.6*KH*KF*KC*K5
     #*K2+5466.6*KH*KF*K4*K1-5466.6*KH*(F*(3*K2
C
      S1=-5.8622*POLE*TPOLE*HPOLE+2201.7*(POLE*TPOLE+ZERO*TPOLE+POLE*ZER
     #O)*KH*KC*K5+846.34*POLE*TPOLE*ZERO*(H*KC*(5+2201.7*POLE*TPOLE*KH*K
     #3+845.55*POLE*TPOLE*KH*K1-2201.7*D*POLE*TPOLE*KH*K1+.33393*ZERO*KH
     #*KF*KC*K6*K5-5466.6*ZERO*KH*KF*KC*K5*K2
C
      S0=2201.7*ZERO*POLE*TPOLE*KH*KC*(5
C
      CPOLY(1)=P4
      CPOLY(2)=P3
      CPOLY(3)=P2
      CPOLY(4)=P1
      CPOLY(5)=P0
```


THIS PAGE IS BEST QUALITY PRACTICABLE
FROM COPY FURNISHED TO DDC

```
      NF=4
      CALL FACTOR
      DO 150 I=1,4
      IF(ROOTI(I).EQ.0.)GO TO 150
      IF(ABS(ROOTI(I)).LE.1.0E-6)ROOTI(I)=0.0
  150 CONTINUE
      PRINT(2,151)
      PRINT(2,152)P4,ROOTR(1),ROOTI(1),P3,ROOTR(2),ROOTI(2),P2,ROOTR(3),
     +ROOTI(3),P1,ROOTR(4),ROOTI(4),P0
      PRINT 151
  151 FORMAT(/,5X,"THE 3/2 NUMERATOR EQUATION IS:")
      PRINT 152,P4,ROOTR(1),ROOTI(1),P3,ROOTR(2),ROOTI(2),P2,ROOTR(3),RO
     +OTI(3),P1,ROOTR(4),ROOTI(4),P0
  152 FORMAT(/,5X,E14.8,3X,"S**4",10X,"(",E14.8,") +J(",E14.8,")",
     +/,5X,E14.8,3X,"S**3",10X,"(",E14.8,") +J(",E14.8,")",
     +/,5X,E14.8,3X,"S**2",10X,"(",E14.8,") +J(",E14.8,")",
     +/,5X,E14.8,3X,"S**1",10X,"(",E14.8,") +J(",E14.8,")",
     +/,5X,E14.8,3X,"S**0",/)
      CPOLY(1)=W5
      CPOLY(2)=W4
      CPOLY(3)=W3
      CPOLY(4)=W2
      CPOLY(5)=W1
      CPOLY(6)=W0
      NF=5
      CALL FACTOR
      DO 153 I=1,5
      IF(ROOTI(I).EQ.0.)GO TO 153
      IF(ABS(ROOTI(I)).LE.1.0E-6)ROOTI(I)=0.0
  153 CONTINUE
```


THIS PAGE IS BEST QUALITY PRACTICABLE
FROM COPY FURNISHED TO DDC

```
      PRINT(2,154)
      PRINT(2,155)W5,ROOTR(1),ROOTI(1),W4,ROOTR(2),ROOTI(2),W3,ROOTR(3),
     +ROOTI(3),W2,ROOTR(4),ROOTI(4),W1,ROOTR(5),ROOTI(5),W0
      PRINT 154
  154 FORMAT(5X,"THE Q/W NUMERATOR EQUATION IS:")
      PRINT 155,W5,ROOTR(1),ROOTI(1),W4,ROOTR(2),ROOTI(2),W3,ROOTR(3),RO
     +OTI(3),W2,ROOTR(4),ROOTI(4),W1,ROOTR(5),ROOTI(5),W0
  155 FORMAT(/,5X,E14.8,3X,"S**5",10X,"(",E14.8,") +J(",E14.8,")",
     +/,5X,E14.8,3X,"S**4",10X,"(",E14.8,") +J(",E14.8,")",
     +/,5X,E14.8,3X,"S**3",10X,"(",E14.8,") +J(",E14.8,")",
     +/,5X,E14.8,3X,"S**2",10X,"(",E14.8,") +J(",E14.8,")",
     +/,5X,E14.8,3X,"S**1",10X,"(",E14.8,") +J(",E14.8,")",
     +/,5X,E14.8,3X,"S**0",/)
      CPOLY(1)=S6
      CPOLY(2)=S5
      CPOLY(3)=S4
      CPOLY(4)=S3
      CPOLY(5)=S2
      CPOLY(6)=S1
      CPOLY(7)=S0
      NF=6
      CALL FACTOR
      DO 156 I=1,6
      IF(ROOTI(I).EQ.0.)GO TO 156
      IF(ABS(ROOTI(I)).LE.1.0E-6)ROOTI(I)=0.0
  156 CONTINUE
```


THIS PAGE IS BEST QUALITY PRACTICABLE
FROM COPY FURNISHED TO DDC

```
      PRINT(2,157)
      PRINT(2,158)S5,ROOTR(1),ROOTI(1),S5,ROOTR(2),ROOTI(2),S4,ROOTR(3),
     +ROOTI(3),S3,ROOTR(4),ROOTI(4),S2,ROOTR(5),ROOTI(5),S1,ROOTR(6),ROO
     +TI(6),S0
      PRINT 157
157   FORMAT(5X,"THE CHARACTERISTIC EQUATION IS:")
      PRINT 158,S5,ROOTR(1),ROOTI(1),S5,ROOTR(2),ROOTI(2),S4,ROOTR(3),RO
     +OTI(3),S3,ROOTR(4),ROOTI(4),S2,ROOTR(5),ROOTI(5),S1,ROOTR(6),ROOTI
     +(6),S0
158   FORMAT(/,5X,E14.8,3X,"S**6",10X,"(",E14.3,") +J(",E14.8,")",
     +/,5X,E14.8,3X,"S**5",10X,"(",E14.3,")  +J(",E14.8,")",
     +/,5X,E14.8,3X,"S**4",10X,"(",E14.3,")  +J(",E14.8,")",
     +/,5X,E14.8,3X,"S**3",10X,"(",E14.3,")  +J(",E14.8,")",
     +/,5X,E14.8,3X,"S**2",10X,"(",E14.3,")  +J(",E14.8,")",
     +/,5X,E14.8,3X,"S**1",10X,"(",E14.3,")  +J(",E14.8,")",
     +/,5X,E14.8,3X,"S**0",//)
      GO TO 1
160   HG=-20*FILT*KH*KC
      HP2=FILT+HPOLE
      HP1=FILT*HPOLE
      TG=-20*FILT*KP*KF
      TP2=FILT+POLE+TPOLE
      TP1=FILT*TPOLE+POLE*TPOLE+FILT*POLE
      TP0=FILT*TPOLE*POLE
      IF(KC.NE.0.)GO TO 161
      HA=HQ2=HQ1=HQ0=0.
      GO TO 162
161   HA=K1/(FILT*KC)
      HQ2=(K3+KC*KF)/(FILT*KC)
      HQ1=(FILT*K3+FILT*KC*KF+ZERO*KC*K5)/(FILT*KC)
      HQ0=ZERO*K5
```


THIS PAGE IS BEST QUALITY PRACTICABLE
FROM COPY FURNISHED TO DDC

```
162   IF(KP.NE.0.)GO TO 163
      TA=TO=TZ=0.
      GO TO 164
163   TA=K2/(FILT*KP)
      TO=K4/(FILT*KP)
      TZ=K6/(FILT*KP)
164   PRINT(2,165)HG,ZERO,HP2,HP1,TG,TP2,TP1,TP0,HA,FILT,ZERO,TA,FILT,HO
     +2,HO1,HO0,ZERO,TO,FILT,TZ,FILT
      PRINT 165,HG,ZERO,HP2,HP1,TG,TP2,TP1,TP0,HA,FILT,ZERO,TA,FILT,HO2,
     +HO1,HO0,ZERO,TO,FILT,TZ,FILT
165   FORMAT(//,5X,"THE HT CSA TRANSFER FUNCTION IS:",//,10X,F8.3,
     +"(S + ",F5.1,") / (S**3 + ",F5.1,"S**2 + ",F6.1,"S + 0.0)",//,5X,
     +"THE TEF CSA TRANSFER FUNCTION IS:",//,10X,F8.3,"S / (S**3 + ",
     +F5.1,"S**2 + ",F5.1,"S + ",F7.1,")",//,5X,
     +"THE HT ALPHA FEEDBACK TRANSFER FUNCTION IS:",//,11X,F8.4,
     +"(S**2 + ",F5.1,"S + 0.0) / (S + ",F5.1,")",//,5X,
     +"THE TEF ALPHA FEEDBACK TRANSFER FUNCTION IS:",//,11X,F8.4,
     +"(S + ",F5.1,")",//,5X,"THE HT THDOT FEEDBACK TRANSFER",
     +" FUNCTION IS:",//,11X,F8.4,"S**2 + ",F8.4,"S + ",F8.4,
     +" / (S + ",F5.1,")",//,5X,"THE TEF THDOT FEEDBACK TRANSFER",
     +" FUNCTION IS:",//,11X,F8.4,"(S + ",F5.1,")",//,5X,
     +"THE TEF AN FEEDBACK TRANSFER FUNCTION IS:",//,11X,F8.4,
     +"(S + ",F5.1,")",///)
      GO TO 1
999   STOP   "NORMAL TERMINATION"
      END
```


THIS PAGE IS BEST QUALITY PRACTICABLE
FROM COPY FURNISHED TO DDC

```
C
C
C*****
C
      SUBROUTINE FACTOR
      REAL ROOTR(10),ROOTI(10),CPOLY(10)
      COMMON/EXPCOM/ROOTR,ROOTI,CPOLY,NF
      N4=0
      I=NF+1
1     IF (CPOLY(I)) 3,2,3
2     N4=N4+1
      ROOTR(N4)=0.0
      ROOTI(N4)=0.0
      I=I-1
      IF (N4-NF) 1,20,1
3     CONTINUE
4     AXR=0.8
      AXI=0.0
      L=1
      N3=1
      ALP1R=AXR
      ALP1I=AXI
      M=1
      GO TO 26
5     BET1R=TEMR
      BET1I=TEMI
      AXR=0.85
      ALP2R=AXR
      ALP2I=AXI
      M=2
      GO TO 25
6     BET2R=TEMR
      BET2I=TEMI
      AXR=0.9
      ALP3R=AXR
      ALP3I=AXI
      M=3
      GO TO 25
7     BET3R=TEMR
      BET3I=TEMI
8     TE1=ALP1R-ALP3R
      TE2=ALP1I-ALP3I
      TE5=ALP3R-ALP2R
      TE6=ALP3I-ALP2I
      TEM=TE5*TE5+TE6*TE6
      TE3=(TE1*TE5+TE2*TE6)/TEM
      TE4=(TE2*TE5-TE1*TE6)/TEM
      TE7=TE3+1.0
      TE9=TE3*TE3-TE4*TE4
      TE10=2.0*TE3*TE4
      DE15=TE7*BET3R-TE4*BET3I
```

THIS PAGE IS BEST QUALITY PRACTICABLE
FROM COPY FURNISHED TO DDC

```
      DE16=TE7*BET3I+TE4*BET3R
      TE11=TE3*BET2R-TE4*BET2I+BET1R-DE15
      TE12=TE3*BET2I+TE4*BET2R+BET1I-DE15
      TE7=TE9-1.0
      TE1=TE9*BET2R-TE10*BET2I
      TE2=TE9*BET2I+TE10*BET2R
      TE13=TE1-BET1R-TE7*BET3R+TE10*BET3I
      TE14=TE2-BET1I-TE7*BET3I-TE10*BET3R
      TE15=DE15*TE3-DE15*TE4
      TE16=DE15*TE4+DE15*TE3
      TE1=TE13*TE13-TE14*TE14-4.0*(TE11*TE15-TE12*TE16)
      TE2=2.0*TE13*TE14-4.0*(TE12*TE15+TE11*TE16)
      TEM=SQRT(TE1*TE1+TE2*TE2)
      IF (TE1) 9,9,10
    9 TE4=SQRT(0.5*(TEM-TE1))
      TE3=0.5*TE2/TE4
      GO TO 13
   10 TE3=SQRT(0.5*(TEM+TE1))
      IF (TE2) 11,12,12
   11 TE3=-TE3
   12 TE4=0.5*TE2/TE3
   13 TE7=TE13+TE3
      TE8=TE14+TE4
      TE9=TE13-TE3
      TE10=TE14-TE4
      TE1=2.0*TE15
      TE2=2.0*TE16
      IF (TE7*TE7+TE8*TE8-TE9*TE9-TE10*TE10) 14,14,15
   14 TE7=TE9
      TE8=TE10
   15 TEM=TE7*TE7+TE8*TE8
      TE3=(TE1*TE7+TE2*TE8)/TEM
      TE4=(TE2*TE7-TE1*TE8)/TEM
      AXR=ALP3R*TE3*TE5-TE4*TE6
      AXI=ALP3I*TE3*TE5+TE4*TE5
      ALP4R=AXR
      ALP4I=AXI
      N=4
      GO TO 26
   16 IF (ABS(HELL)+ABS(BELL)-1.0E-20) 13,19,17
   17 TE7=ABS(ALP3R-AXR)+ABS(ALP3I-AXI)
      IF (TE7/(ABS(AXR)+ABS(AXI))-1.0E-7) 19,13,18
   18 N3=N3+1
      ALP1R=ALP2R
      ALP1I=ALP2I
      ALP2R=ALP3R
      ALP2I=ALP3I
      ALP3R=ALP4R
      ALP3I=ALP4I
      BET1R=BET2R
      BET1I=BET2I
      BET2R=BET3R
      BET2I=BET3I
```


THIS PAGE IS BEST QUALITY PRACTICABLE
FROM COPY FURNISHED TO DDC

```
      BET3R=TEMR
      BET3I=TEMI
      IF (N3-100) 8,13,19
13    N4=N4+1
      ROOTR(N4)=ALP4R
      ROOTI(N4)=ALP4I
      N3=0
      IF (N4-NF) 21,20,20
20    RETURN
21    IF (ABS(ROOTI(N4))-1.0E-5) 4,4,22
22    IF(L.EQ.2) GO TO 4
23    AXR=ALP1R
      AXI=-ALP1I
      ALP1I=-ALP1I
      M=1
      GO TO 26
24    BET1R=TEMR
      BET1I=TEMI
      AXR=ALP2R
      AXI=-ALP2I
      ALP2I=-ALP2I
      M=2
      GO TO 26
25    BET2R=TEMR
      BET2I=TEMI
      AXR=ALP3R
      AXI=-ALP3I
      ALP3I=-ALP3I
      L=2
      M=3
26    TEMR=CPOLY(1)
      TEMI=0.0
      DO 27 I=1,NF
      TE1=TEMR*AXR-TEMI*AXI
      TEMI=TEMI*AXR+TEMR*AXI
27    TEMR=TE1+CPOLY(I+1)
      HELL=TEMR
      BELL=TEMI
      IF (N4) 28,30,28
28    DO 29 I=1,N4
      TEM1=AXR-ROOTR(I)
      TEM2=AXI-ROOTI(I)
      TE1=TEM1*TEM1+TEM2*TEM2
      TE2=(TEMR*TEM1+TEMI*TEM2)/TE1
      TEMI=(TEMI*TEM1-TEMR*TEM2)/TE1
29    TEMR=TE2
30    GO TO (5,6,7,16,24,25), M
      END
```

THIS PAGE IS BEST QUALITY PRACTICABLE
FROM COPY FURNISHED TO DDC

Vita

Eric R. Molner was born on 14 February 1954 in Somers Point, New Jersey. He graduated from Mainland Regional High School in Linwood, New Jersey in 1972 with a four year AFROTC scholarship. After spending a year at Steven's Institute of Technology, Hoboken, New Jersey, he completed his undergraduate work at Purdue University, West Lafayette, Indiana in May 1976. He received a Bachelor of Science Degree in Electrical Engineering and a commission in the United States Air Force. In September 1976, he entered the School of Engineering, Air Force Institute of Technology, as his first active duty assignment. In April 1978, he was assigned to Vandenberg Air Force Base, California, as an Electronic and Data Processing Systems Engineer for the Space Transportation System.

Permanent Address: 1038 Oakwood Trail
Indianapolis, IN 46260

UNCLASSIFIED

SECURITY CLASSIFICATION OF THIS PAGE (When Data Entered)

REPORT DOCUMENTATION PAGE

READ INSTRUCTIONS BEFORE COMPLETING FORM

1. REPORT NUMBER: AFIT/GGC/EE/79-5	2. GOVT ACCESSION NO.
3. RECIPIENT'S CATALOG NUMBER	
4. TITLE (and Subtitle): Using Vertical Gust Alleviation To Improve The Target Tracking Capability Of The Control Configured YF-16	5. TYPE OF REPORT & PERIOD COVERED: MS THESIS
	6. PERFORMING ORG. REPORT NUMBER
7. AUTHOR(s): Eric R. Molner, 1Lt USAF	8. CONTRACT OR GRANT NUMBER(s)
9. PERFORMING ORGANIZATION NAME AND ADDRESS: Air Force Institute of Technology (AFIT/EN) Wright-Patterson AFB, Ohio 45433	10. PROGRAM ELEMENT, PROJECT, TASK AREA & WORK UNIT NUMBERS
11. CONTROLLING OFFICE NAME AND ADDRESS: Air Force Flight Dynamics Lab (AFFDL/FGX) Wright-Patterson AFB, Ohio 45433	12. REPORT DATE: August 1979
	13. NUMBER OF PAGES: 275
14. MONITORING AGENCY NAME & ADDRESS (if different from Controlling Office)	15. SECURITY CLASS. (of this report): UNCLASSIFIED
	15a. DECLASSIFICATION/DOWNGRADING SCHEDULE

16. DISTRIBUTION STATEMENT (of this Report)

Approved for public release; distribution unlimited.

17. DISTRIBUTION STATEMENT (of the abstract entered in Block 20, if different from Report)

18. SUPPLEMENTARY NOTES

Approved for public release; IAW AFR 190-17
JOSEPH P. HIPPS, Maj, USAF
Director of Public Affairs

19. KEY WORDS (Continue on reverse side if necessary and identify by block number)

Control Configured Vehicle, Flight Control System, Disturbance Rejection, F-16, YF-16, Fighter CCV, CCV

20. ABSTRACT (Continue on reverse side if necessary and identify by block number)

This thesis investigates the use of multiple aerodynamic control surfaces as a part of a flight control system configured to reduce aircraft pitch response to atmospheric disturbances. Coordinated deflection of two surfaces provides the desired gust alleviation with no decrease in system damping. At the same time, the commanded aircraft performance is improved relative to the performance of the baseline flight control system using a single control surface.

DD FORM 1 JAN 73 1473 EDITION OF 1 NOV 65 IS OBSOLETE

UNCLASSIFIED

SECURITY CLASSIFICATION OF THIS PAGE (When Data Entered)